Cytokine Engineering through Ligand/Receptor Dynamics: a Study on Granulocyte Colony-Stimulating Factor

by

Casim Ali Sarkar

B.S., Chemical Engineering
The University of Texas at Austin, 1997

SUBMITTED TO THE DEPARTMENT OF CHEMICAL ENGINEERING IN PARTIAL FULFILLMENT OF THE REQUIREMENTS FOR THE DEGREE OF

DOCTOR OF PHILOSOPHY IN CHEMICAL ENGINEERING
AT THE
MASSACHUSETTS INSTITUTE OF TECHNOLOGY

SEPTEMBER 2002

Signature of Author: _____
Department of Chemical Engineering
July 30, 2002

Certified by: _____
Douglas A. Lauffenburger
Professor of Chemical Engineering
Thesis Supervisor

Accepted by: _____
Daniel Blankschtein
Professor of Chemical Engineering
Chairman, Committee for Graduate Students

Cytokine Engineering through Ligand/Receptor Dynamics: A Study on Granulocyte Colony-Stimulating Factor

by

Casim Ali Sarkar

Submitted to the Department of Chemical Engineering
on July 30, 2002 in Partial Fulfillment of the
Requirements for the Degree of Doctor of Philosophy in
Chemical Engineering

ABSTRACT

Granulocyte colony-stimulating factor (GCSF) is a cytokine of great clinical importance, with application to elevate neutrophil counts in cancer patients undergoing chemotherapy. GCSF binds to its specific receptor (GCSFR) on bone marrow precursor cells and generates intracellular signals that cause these cells to proliferate and differentiate into mature neutrophils. However, for such cytokines that act as agonists for cell-surface receptors, these complexes undergo trafficking processes that often attenuate the intracellular signals through internalization and degradation. Additionally for GCSF, the bloodstream neutrophils represent a further negative feedback mechanism that limits the potency of the drug, as they also express GCSFR and degrade the drug through receptor-mediated endocytosis.

Using the GCSF/GCSFR system, we have developed an effective method for deconvoluting the effects of binding affinity on ligand potency, and this analysis successfully predicts the half-life ranking of combinatorially generated GCSF analogs in culture. Protein structural studies and equilibrium denaturation experiments unexpectedly revealed that GCSF becomes more stable as the pH decreases from 7 to 4 (coincident with the pH range experienced along the endocytic trafficking pathway); however, similar experiments performed on analogs from the deconvolution analysis were consistent with a proposed correlation between decreased structural stability at endosomal pH and enhanced ligand half-life.

We also propose a new method for the rational design of more effective analogs by identifying amino acid substitutions that should reduce receptor binding affinity in intracellular endosomal compartments to yield enhanced sorting to recycling and consequently longer lifetimes in extracellular medium. We successfully demonstrate this approach, which we term 'histidine switching,' for GCSF, employing computationally predicted histidine substitutions to switch protonation states between cell-surface and endosomal pH. Finally, we integrate a cell-level model of GCSF/GCSFR dynamics into an existing pharmacokinetic/pharmacodyamic model to elucidate the relationship between molecular and pharmacological properties of GCSF. The work presented here may provide general principles for cytokine design.

Thesis Supervisor: Douglas A. Lauffenburger
Title: Professor of Chemical Engineering, Biological Engineering, and Biology

Acknowledgements

I am indebted to my advisor, Doug Lauffenburger, who was my mentor throughout this intellectual journey. His wholehearted support of my ideas allowed me to grow as a scientist, and this thesis, which resulted from the evolution and integration of these ideas, would not have been possible without him. I also warmly thank Bruce Tidor, a member of my thesis committee, who served essentially as a co-advisor on a large portion of this work. I am grateful to Harvey Lodish for sharing his expertise in this area of research with me, and I thank him, along with Bob Langer, for serving on my thesis committee. Dane Wittrup and I also had many interesting discussions. In addition, I would like to express my appreciation to David Brems and Margaret Ricci, who were always willing to lend a helping hand and who hosted me for a summer at Amgen.

I must acknowledge several people who provided technical expertise and assistance for this work. Tom Horan at Amgen provided all of the analogs that were studied, and Ky Lowenhaupt in our lab performed the surface plasmon resonance experiments described herein. Justin Caravella, Erik Kangas, David Wu, and, in particular, Eric Fallon, were all extremely helpful in showing me techniques and tools that were indispensable for my research. Peggy Wang was a talented undergraduate who helped me with many laboratory experiments.

I wish to thank all of the Lauffenburger and Griffith lab members, past and present, for making these five years a fun and memorable learning experience; in particular, I would like to thank Lily Koo, Eric Fallon, Anand Asthagiri, Jenny Fujii, Ann DeWitt, Chase Orsello, Jason Haugh, Doug Osborne, Mark Powers, and Michael Lässle for their friendships and generally sunny dispositions.

This work was funded by a graduate fellowship from the Fannie and John Hertz Foundation and a grant from the Amgen/MIT partnership.

بسم الله الرحمن الرحيم

To my parents, Husain and Durriya

Table of Contents

Chapter 1: Introduction and Background

Transmembrane receptors of a mammalian cell can serve as its windows to the world, allowing transmission of molecules or information from the complex extracellular environment to the inside of the cell. This transmission often occurs through exquisite molecular recognition between the membrane proteins and their respective extracellular ligands. Thus, receptors can play vital roles in nutrient uptake either through direct interaction or via carrier proteins, cell adhesion and migration through formation and spatial organization of bonds with insoluble matrix proteins, and chemotaxis by gradient perception. Furthermore, growth factor receptors interact with soluble ligands, often with high affinity and specificity, to regulate a variety of cellular behaviors, including proliferation, differentiation, and apoptosis. It may therefore be possible to tune the cellular functions regulated by a particular growth factor receptor by altering the directions encoded within its cognate ligand.

An important subset of these growth factors is the cytokine superfamily, which regulates hematopoiesis and lymphopoiesis as well as the behaviors of the resulting mature blood and immune cells. Recombinant cytokines have shown great promise for therapeutic use, and some are already of great clinical importance, including granulocyte colony-stimulating factor (GCSF). The work presented in this thesis attempts to establish some guiding principles for cytokine engineering, primarily in the context of ligand/receptor dynamics, using GCSF as a model system.

GRANULOCYTE COLONY-STIMULATING FACTOR (GCSF)

Granulocyte colony-stimulating factor (GCSF) is a cytokine that specifically induces the differentiation of precursor cells committed to the neutrophilic granulocyte lineage, although there is some evidence that GCSF, in synergy with other cytokines, also acts as far back as hematopoietic stem cells (Morstyn *et al.*, 1998). For clinical use, Amgen markets Filgrastim (r-metHuGCSF), which has been shown to have activity comparable to that of naturally produced human GCSF. Filgrastim is a 175 amino-acid protein with a molecular weight of approximately 18.8 kiloDaltons (kDa); naturally produced human GCSF is *O*-glycosylated, which contributes an additional 0.8 kDa to its molecular weight. Filgrastim

contains five cysteine residues. Two disulfide bridges (Cys37–Cys43 and Cys65–Cys75) are necessary for biological activity; the free cysteine residue at position 18 is not critical for biological activity (Lu *et al.*, 1989).

GCSF shares its four-α-helical-bundle structure (see Figure 1.1) with growth hormone (GH), interleukin-2 (IL-2), and granulocyte-macrophage colony-stimulating factor (GMCSF), to name a few. The four helices (A, B, C, and D) are connected by three loops (AB, BC, CD). In addition, GCSF also contains a small helical region within the AB loop that adopts a 3_{10} helix conformation. Epitope mapping studies have shown that residues 35 through 50 play a significant role in ligand binding to the receptor. The fact that Lys41, His44, Glu46, and Glu47 also play an important role in binding suggests that charge interactions are also substantial (Morstyn *et al.*, 1998).

Unlike many cytokines of the hematopoietic system which are pleiotropic differentiation agents, GCSF has marked specificity for the lineage of neutrophilic granulocytes (Demetri and Griffin, 1991). GMCSF is less specific, inducing differentiation of precursor cells along both the granulocyte and macrophage lineages. At the opposite extreme from GCSF, interleukin-3 (IL-3) appears to stimulate non-specific differentiation of hematopoietic stem cells and precursor cells, thus leading to a gamut of differentiated cells (Park *et al.*, 1989). The specificity of GCSF for the neutrophil lineage makes it an ideal pharmaceutical agent for elevation of neutrophil counts *in vivo*, and Filgrastim was approved in 1991 to ameliorate chemotherapy-induced neutropenia. It has since found many other clinical applications.

GRANULOCYTE COLONY-STIMULATING FACTOR RECEPTOR (GCSFR)

On cells of the neutrophilic granulocyte lineage, it was shown that GCSF bound to receptors on these cells with high specificity and affinity (Morstyn *et al.*, 1998), and that binding was saturable (Nicola and Metcalf, 1984; Demetri and Griffin, 1991). This receptor for GCSF (GCSFR) has also been found on non-hematopoietic cells, such as placental trophoblastic cells (Uzumaki *et al.*, 1989), but its function in these settings is not well understood. It has been observed that GCSFR number increases with cell maturity along the neutrophilic lineage; thus, mature neutrophils have the greatest number of receptors per cell (Demetri and Griffin, 1991). However, even for mature neutrophils, this number typically

does not exceed a few thousand receptors per cell (Morstyn *et al.*, 1998; Demetri and Griffin, 1991). The regulation of GCSFR expression has been poorly characterized (Demetri and Griffin, 1991).

The mature form of the human GCSF receptor, with approximately nine *N*-linked glycosylations, has a molecular weight of about 84.0 kDa (Haniu *et al.*, 1996). The receptor for GCSF contains several well-characterized domains (see Figure 1.2). The extracellular domain contains an immunoglobulin G-like domain (IgG), a WSXWS motif characteristic of the cytokine receptor superfamily, and three fibronectin type-3 domains (FNIII) (Haniu *et al.*, 1995). The cytoplasmic domain contains different signaling regions for proliferation and differentiation (Fukunaga *et al.*, 1993). It is believed that homodimerization of the receptor is necessary for the signal to be transduced (Watowich *et al.*, 1996; de Koning *et al.*, 1998).

GCSF/GCSFR BINDING AND TRAFFICKING

There has been much uncertainty over the stoichiometry and molecular recognition in GCSF/GCSFR binding. Initial results indicated that a single GCSF molecule bound two receptors (Hiraoka *et al.*, 1995), which is consistent with data for growth hormone (GH). The GH paradigm suggests that there are two binding sites on the ligand, a high affinity site and a low affinity site, each of which binds a distinct receptor (Cunningham *et al.*, 1991). This interaction dimerizes two receptors via the ligand, a complex which is believed to be sufficient for signaling. This model has been corroborated by the co-crystal structure of GH and its receptor in a 1:2 ligand:receptor complex (de Vos *et al.*, 1992), and a similar result was found for erythropoietin (Syed *et al.*, 1998). An initial study for GCSF, however, was not as convincing; a 1:2 ligand:receptor complex was found using a subdivided cytokine receptor homology (CRH) domain, with the ligand binding to each fragment of the CRH domain – a 1:1:1 complex (Hiraoka *et al.*, 1995).

Subsequent experiments, with the CRH domain left intact, suggested a 2:2 GCSF:GCSFR complex (Horan *et al.*, 1996; Horan *et al.*, 1997). This result was rationalized by realizing that the two potential binding sites on the ligand could associate with the *same* CRH domain, rather than CRH domains on two different receptors. This could not be distinguished in the earlier study since the CRH domain was split, and therefore led to a 1:1:1 complex. One explanation for how this complex was formed is that GCSF binds

monovalently to its receptor, and then complexes with a second receptor and then a second ligand; or, that two 1:1 complexes interact to form a 2:2 complex. This is more clearly illustrated in Figure 1.3. It was shown that the electrostatic interaction between GCSF and its receptor is significantly different than the interaction between GH and GHR, suggesting that there was a different mechanism for GCSF binding to its receptor (Demchuk *et al.*, 1994).

Recently, the co-crystal structure of GCSF complexed with the CRH domain of its receptor was solved. The result suggested a novel cytokine recognition scheme, where the complex does indeed have a 2:2 stoichiometry of ligand and receptor. However, each ligand also interacts with both receptors, resulting in two major and two minor binding interfaces. The crystal structure complex is shown in Figure 1.4.

Receptor-mediated trafficking processes (see Figure 1.5) can be well quantified by kinetic modeling of these cellular events (Lauffenburger and Linderman, 1993). Although such studies have been extensively performed on other ligand/receptor systems, there is a scarce amount of information available for the GCSF/GCSFR system (Kuwabara *et al.*, 1996). Thus, more extensive quantitative characterization of these phenomena would be of great interest in understanding and improving a therapeutically important ligand.

Since GCSFR numbers are typically very low, it has been difficult to quantify the binding and trafficking properties of this system. Literature data for various cell lines report a wide range of dissociation constants for GCSF/GCSFR binding, ranging from 20 to 400 pM (Watanabe *et al.*, 1990; El-Sonbaty *et al.*, 1995; Uzumaki *et al.*, 1989). Some of the kinetic parameters in GCSF/GCSFR trafficking have been elucidated (Kuwabara *et al.*, 1996), but a full cell-level model for these dynamics has not been reported.

GCSF/GCSFR SIGNALING

GCSFR has no intrinsic tyrosine kinase activity, but GCSFR homodimerization is believed to be necessary to activate downstream signals (Watowich *et al.*, 1996; de Koning *et al.*, 1998). The cytoplasmic domain of the receptor contains different signaling regions for proliferation and differentiation. The membrane-proximal region of the cytoplasmic domain is sufficient for transducing the proliferation signaling cascade; the membrane-distal region is critical for the neutrophilic differentiation signal (Fukunaga *et al.*, 1993).

Very little is known about the intracellular signaling cascades for the GCSF/GCSFR system, though the Janus kinases (Jaks) and signal transducers and activators of transcription (STATs) are implicated; activated Jaks lead to phosphorylated STATs, which then dimerize and translocate into the nucleus to activate specific genes. It has been shown through coimmunoprecipitation studies that the tyrosine kinase Jak1 is associated with the receptor, even before stimulation with GCSF (Nicholson *et al.*, 1994). More recent data suggest that Jaks associated with the membrane-proximal region become activated upon ligand-induced receptor dimerization and thereby initiate the Jak/STAT pathway; Jak1, Jak2, STAT1, STAT3, and STAT5 are believed to be activated through GCSF binding (de Koning *et al.*, 1998). Other findings indicate that the kinase Tyk2 is also activated by GCSF but, in fact, Jak2 is the predominantly activated kinase (Parganas *et al.*, 1998).

Cell stimulation through ligand binding is usually accompanied by marked changes in intracellular calcium or hydrogen ion concentration. However, data suggest that GCSF binding to its receptor on neutrophils does not lead to changes in intracellular free Ca^{2+} or intracellular pH (Demetri and Griffin, 1991).

SIGNIFICANCE

GCSF is of great clinical importance. It is routinely administered to cancer patients who have undergone chemotherapy, since these patients are often severely immuno-compromised after treatment. It is also being used extensively in the treatment of chronic neutropenia, a condition in which the patient has severely depressed levels of circulating neutrophils. More recently, GCSF is being used in Australia, Japan, and India to treat neutropenia and neutrophil dysfunction in HIV-infected patients (Morstyn *et al.*, 1998). GCSF is indicated in almost all therapies which require rapid repopulation of these infection-fighting neutrophils.

Amgen produces Filgrastim (r-metHuGCSF) to serve these crucial clinical needs, generating in excess of $1 billion in revenue each year. The drug is intended to target the bone marrow, where GCSF binds to its cognate receptor on precursor cells, initiating intracellular signals that cause these cells to proliferate and differentiate into mature neutrophils. These mature neutrophils then enter the bloodstream. However, clinical studies reveal that this drug is then largely cleared by peripheral blood neutrophils (see Figure 1.6).

Thus, the potency of GCSF is not only limited by local receptor-mediated trafficking and degradation by precursor cells in the bone marrow, but also by a more global negative feedback loop (*i.e.*, clearance by peripheral neutrophils through receptor-mediated uptake). An improved understanding of the binding and trafficking dynamics of GCSF may lead to the design of new analogs with more desirable pharmacokinetic and pharmacodynamic properties, which in turn would improve the treatment of patients. The results on GCSF presented here may elucidate more general cytokine design principles in the context of cell-level dynamics, for both *in vitro* and *in vivo* applications.

REFERENCES

Berman, H.M., Westbrook, J., Feng, Z., Gilliland, G., Bhat, T.N., Weissig, H., Shindyalov, I.N. and Bourne, P.E. (2000). The Protein Data Bank. *Nucleic Acids Research.* **28:** 235-242.

Cunningham, B.C., Ultsch, M., de Vos, A.M., Mulkerrin, M.G., Clauser, K.R. and Wells, J.A. (1991). Dimerization of the extracellular domain of the human growth hormone receptor by a single hormone molecule. *Science.* **254:** 821-825.

de Koning, J.P., Soede-Bobok, A.A., Schelen, A.M., Smith, L., van Leeuwen, D., Santini, V., Burgering, B.M.T., Bos, J.L., Lowenberg, B. and Touw, I.P. (1998). Proliferation signaling and activation of Shc, p21Ras, and myc via tyrosine 764 of human granulocyte colony-stimulating factor receptor. *Blood.* **91:** 1924-1933.

de Vos, A.M., Ultsch, M. and Kossiakoff, A.A. (1992). Human growth hormone and extracellular domain of its receptor: crystal structure of the complex. *Science.* **255:** 306-312.

Demchuk, E., Mueller, T., Oschkinat, H., Sebald, W. and Wade, R.C. (1994). Receptor binding properties of four-helix-bundle growth factors deduced from electrostatic analysis. *Protein Science.* **3:** 920-935.

Demetri, G.D. and Griffin, J.D. (1991). Granulocyte colony-stimulating factor and its receptor. *Blood.* **78:** 2791-2808.

El-Sonbaty, S.S., Hochito, K., Yamaguchi, K., Matsuda, I. and Tsuchiya, H. (1995). Exogenously expressed granulocyte colony-stimulating factor (G-CSF) receptor on K562 cells can transduce G-CSF-triggered growth and differentiation signals. *International Journal of Hematology.* **61:** 61-68.

Fukunaga, R., Ishizaka-Ikeda, E. and Nagata, S. (1993). Growth and differentiation signals mediated by different regions in the cytoplasmic domain of granulocyte colony-stimulating factor receptor. *Cell.* **74:** 1079-1087.

Haniu, M., Horan, T., Arakawa, T., Le, J., Katta, V., Hara, S. and Rohde, M.F. (1996). Disulfide structure and N-glycosylation sites of an extracellular domain of granulocyte-colony stimulating factor receptor. *Biochemistry.* **35:** 13040-13046.

Haniu, M., Horan, T., Arakawa, T., Le, J., Katta, V. and Rohde, M.F. (1995). Extracellular domain of granulocyte-colony stimulating factor receptor. *Archives of Biochemistry and Biophysics.* **324:** 344-356.

Hiraoka, O., Anaguchi, H., Asakura, A. and Ota, Y. (1995). Requirement for the immunoglobulin-like domain of granulocyte colony-stimulating factor receptor in formation of a 2:1 receptor-ligand complex. *Journal of Biological Chemistry.* **270:** 25928-25934.

Horan, T., Wen, J., Narhi, L., Parker, V., Garcia, A., Arakawa, T. and Philo, J. (1996). Dimerization of the extracellular domain of granulocyte-colony stimulating factor receptor by ligand binding: a monovalent ligand induces 2:2 complexes. *Biochemistry.* **35:** 4886-4896.

Horan, T.P., Martin, F., Simonet, L., Arakawa, T. and Philo, J.S. (1997). Dimerization of granulocyte-colony stimulating factor receptor: the Ig plus CRH construct of granulocyte-colony stimulating factor receptor forms a 2:2 complex with a ligand. *Journal of Biochemistry.* **121:** 370-375.

Kuwabara, T., Kobayashi, S. and Sugiyama, Y. (1996). Kinetic analysis of receptor-mediated endocytosis of G-CSF derivative, nartograstim, in rat bone marrow cells. *American Journal of Physiology-Endocrinology and Metabolism*. **34:** E73-E84.

Lauffenburger, D.A. and Linderman, J.J. (1993). *Receptors: Models for Binding, Trafficking, and Signaling*. Oxford University Press, New York.

Layton, J.E., Hockman, H., Sheridan, W.P. and Morstyn, G. (1989). Evidence for a novel in vivo control mechanism of granulopoiesis: mature cell-related control of a regulatory growth factor. *Blood*. **74:** 1303-1307.

Lu, H.S., Boone, T.C., Souza, L.M. and Lai, P. (1989). Disulfide and secondary structures of recombinant human granulocyte colony stimulating factor. *Archives of Biochemistry and Biophysics*. **268:** 81-92.

Morstyn, G., Dexter, T.M. and Foote, M. (1998). *Filgrastim (r-metHuG-CSF) in Clinical Practice*. Marcel Dekker, New York.

Nicholson, S.E., Oates, A.C., Harpur, A.G., Ziemiecki, A., Wilks, A.F. and Layton, J.E. (1994). Tyrosine kinase JAK1 is associated with the granulocyte-colony-stimulating factor receptor and both become tyrosine-phosphorylated after receptor activation. *Proceedings of the National Academy of Sciences USA*. **91:** 2985-2988.

Nicola, N.A. and Metcalf, D. (1984). Binding of the differentiation-inducer, granulocyte-colony-stimulating factor, to responsive but not unresponsive leukemic cell lines. *Proceedings of the National Academy of Sciences USA*. **81:** 3765-3769.

Parganas, E., Wang, D., Stravopodis, D., Topham, D.J., Marine, J.-C., Teglund, S., Vanin, E.F., Bodner, S., Colamonici, O.R., van Deursen, J.M., Grosveld, G. and Ihle, J.N. (1998). Jak2 is essential for signaling through a variety of cytokine receptors. *Cell*. **93:** 385-395.

Park, L.S., Waldron, P.E., Friend, D., Sassenfeld, H.M., Price, V., Anderson, D., Cosman, D., Andrews, R.G., Bernstein, I.D. and Urdal, D.L. (1989). Interleukin-3, GM-CSF, and G-CSF receptor expression on cell lines and primary leukemia cells: Receptor heterogeneity and relationship to growth factor responsiveness. *Blood*. **74:** 56-65.

Syed, R.S., Reid, S.W., Li, C.W., Cheetham, J.C., Aoki, K.H., Liu, B.S., Zhan, H.J., Osslund, T.D., Chirino, A.J., Zhang, J.D., Finer-Moore, J., Elliott, S., Sitney, K., Katz, B.A., Matthews, D.J., Wendoloski, J.J., Egrie, J. and Stroud, R.M. (1998). Efficiency of signalling through cytokine receptors depends critically on receptor orientation. *Nature*. **395:** 511-516.

Uzumaki, H., Okabe, T., Sasaki, N., Hagiwara, K., Takaku, F., Tobita, M., Yasukawa, K., Ito, S. and Umezawa, Y. (1989). Identification and characterization of receptors for granulocyte colony-stimulating factor on human placenta and trophoblastic cells. *Proceedings of the National Academy of Sciences USA*. **86:** 9323-9326.

Watanabe, M., Fukamachi, H., Uzumaki, H., Kabaya, K., Tsumura, H., Ishikawa, M., Matsuki, S. and Kusaka, M. (1990). Mutant protein of recombinant human granulocyte colony-stimulating factor for receptor binding assay. *Analytical Biochemistry*. **195:** 38-44.

Watowich, S.S., Wu, H., Socolovsky, M., Klingmuller, U., Constantinescu, S.N. and Lodish, H.F. (1996). Cytokine receptor signal transduction and the control of hematopoietic cell development. *Annual Review of Cell and Developmental Biology*. **12:** 91-128.

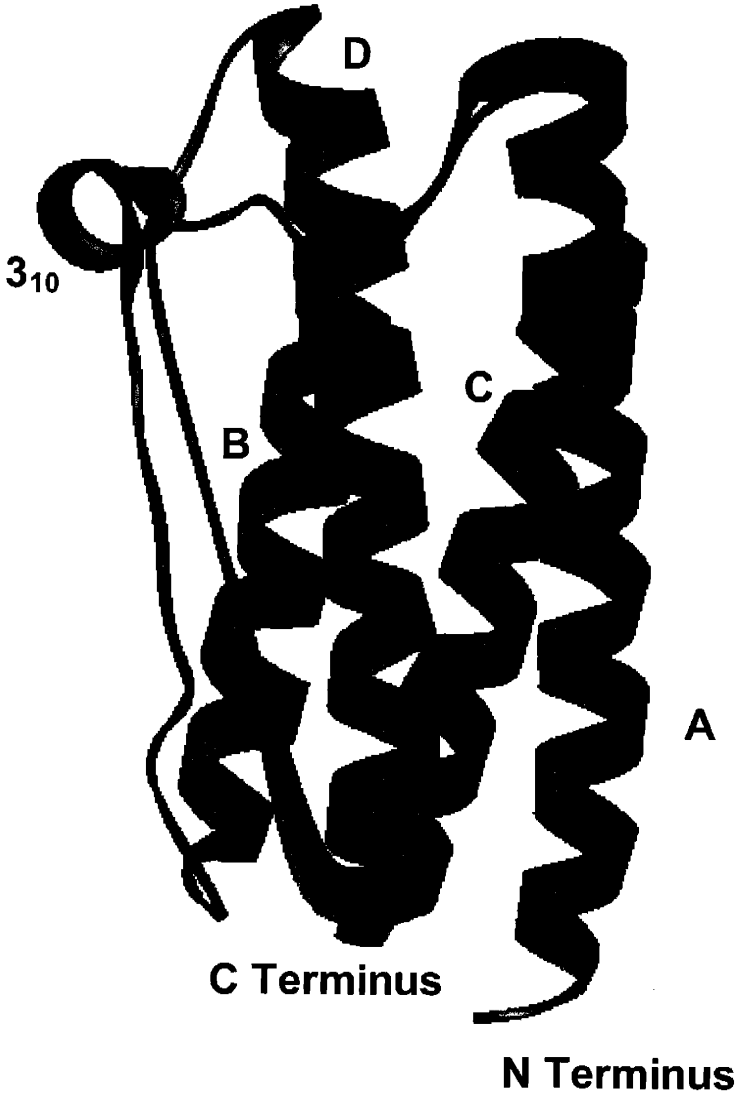

Figure 1.1: Structure of granulocyte colony-stimulating factor (adapted from Protein Data Bank, entry 1RHG) (Berman *et al.*, 2000). The four major α helices are each denoted by a single letter (A, B, C, and D); the minor helix is referred to as the 3_{10} helix.

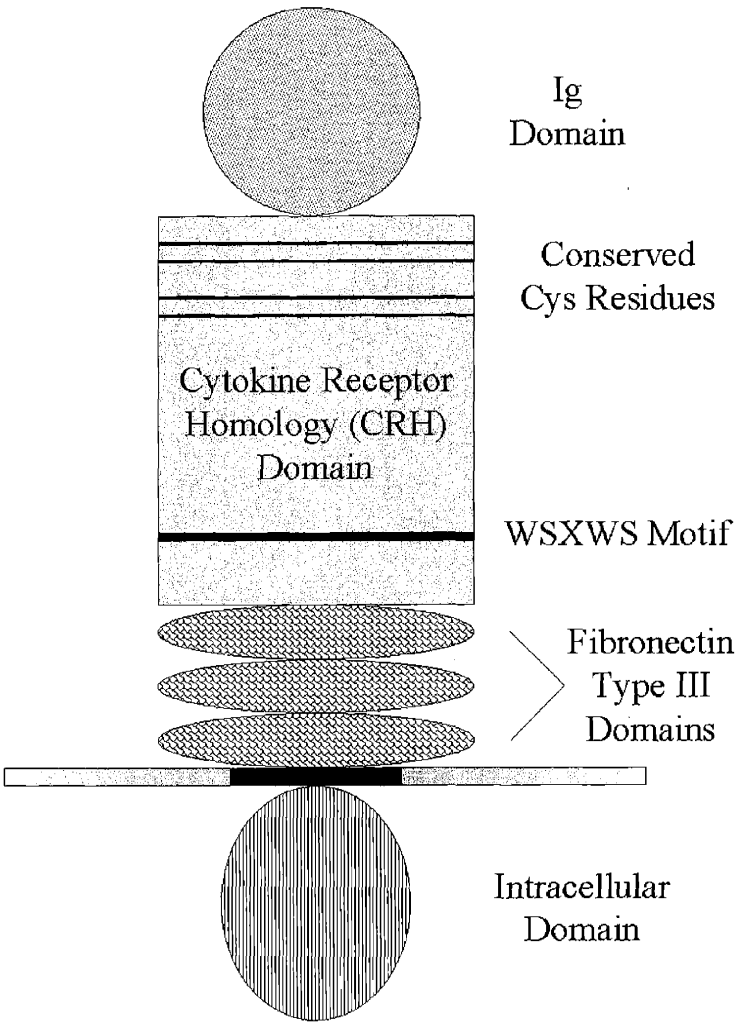

Figure 1.2A: Structural domains of the receptor for granulocyte colony-stimulating factor (adapted from Morstyn *et al.*, 1998).

Figure 1.2B: Structure of the CRH domain of GCSFR (adapted from Protein Data Bank, entry 1CD9) (Berman *et al.*, 2000).

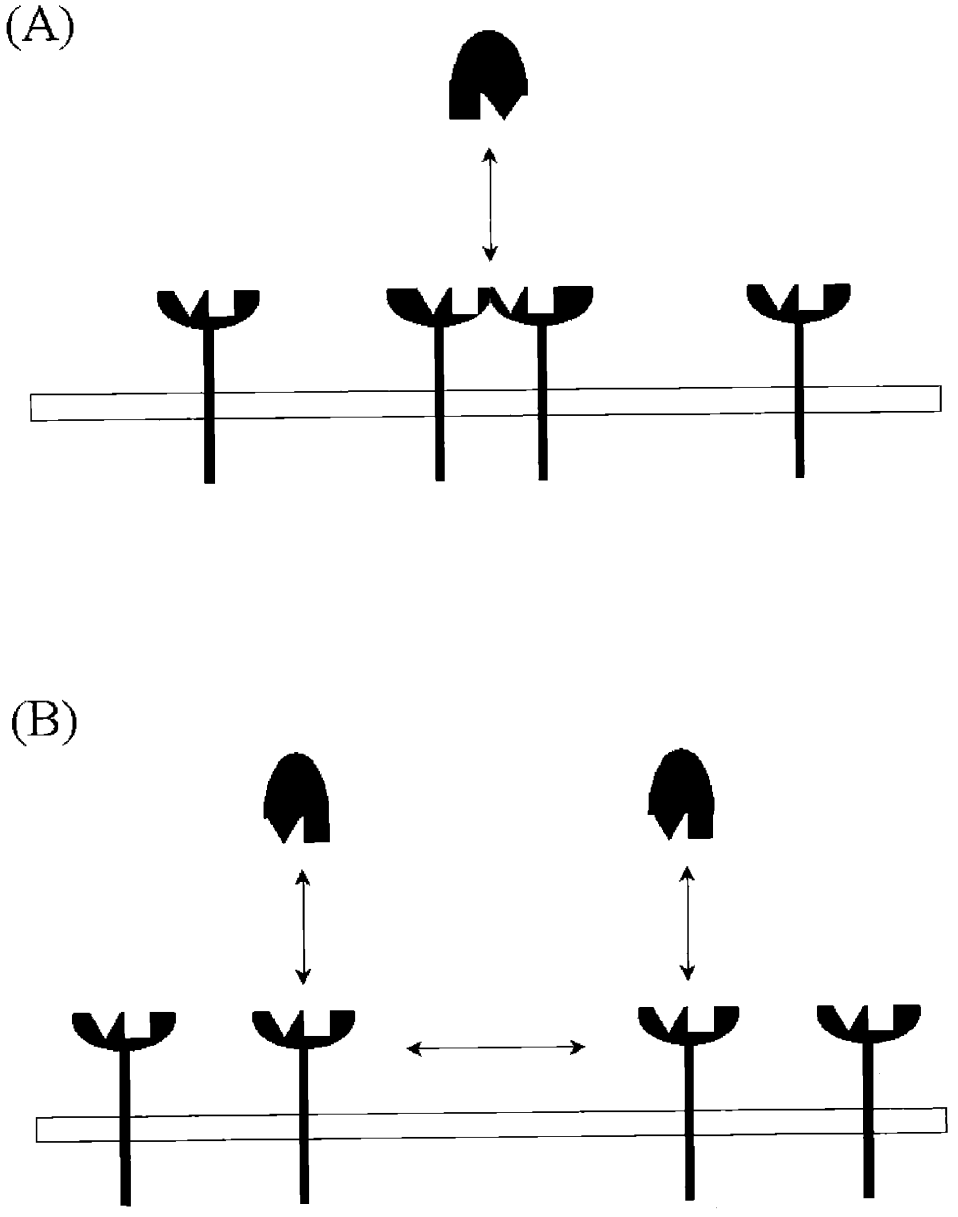

Figure 1.3: Two earlier models for GCSF/GCSFR complex formation on the surface of a cell. (A) A single ligand, with two distinct binding domains, binds to (and therefore dimerizes) two receptors, possibly at a distinct site within each receptor (Hiraoka *et al.*, 1995), thus forming a 1:2 ligand:receptor complex. (B) A single ligand, possibly with two binding domains, binds to a single receptor. This complex then initially binds a second receptor and then a second ligand molecule to form a 2:2 complex; or, two 1:1 complexes bind to form the 2:2 complex (Horan *et al.*, 1996; Horan *et al.*, 1997).

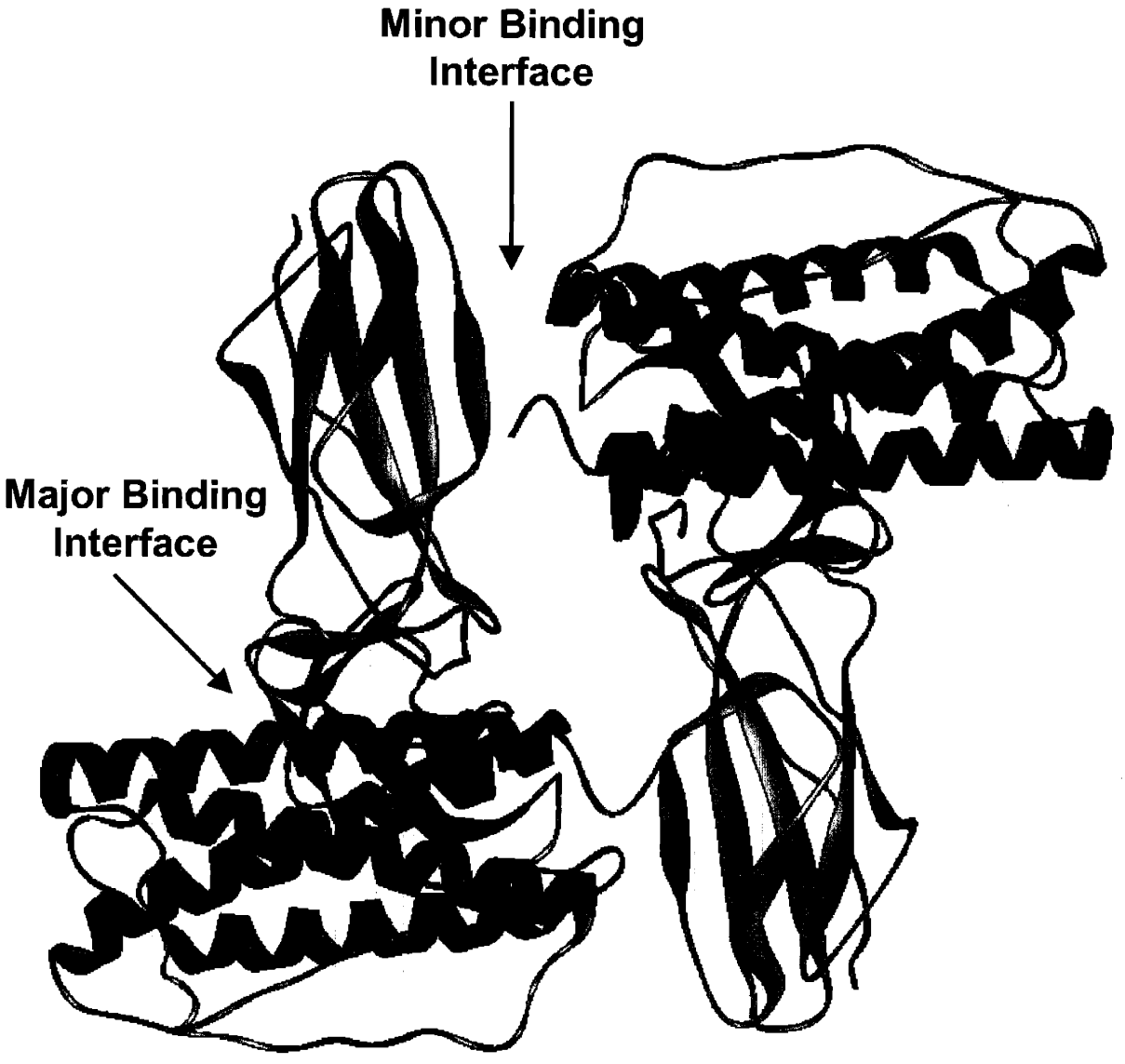

Figure 1.4: Crystal structure of GCSF complexed with the CRH domain of GCSFR reveals a 2:2 stoichiometry, with two major binding interfaces and two minor binding interfaces (adapted from Protein Data Bank, entry 1CD9) (Berman *et al.*, 2000).

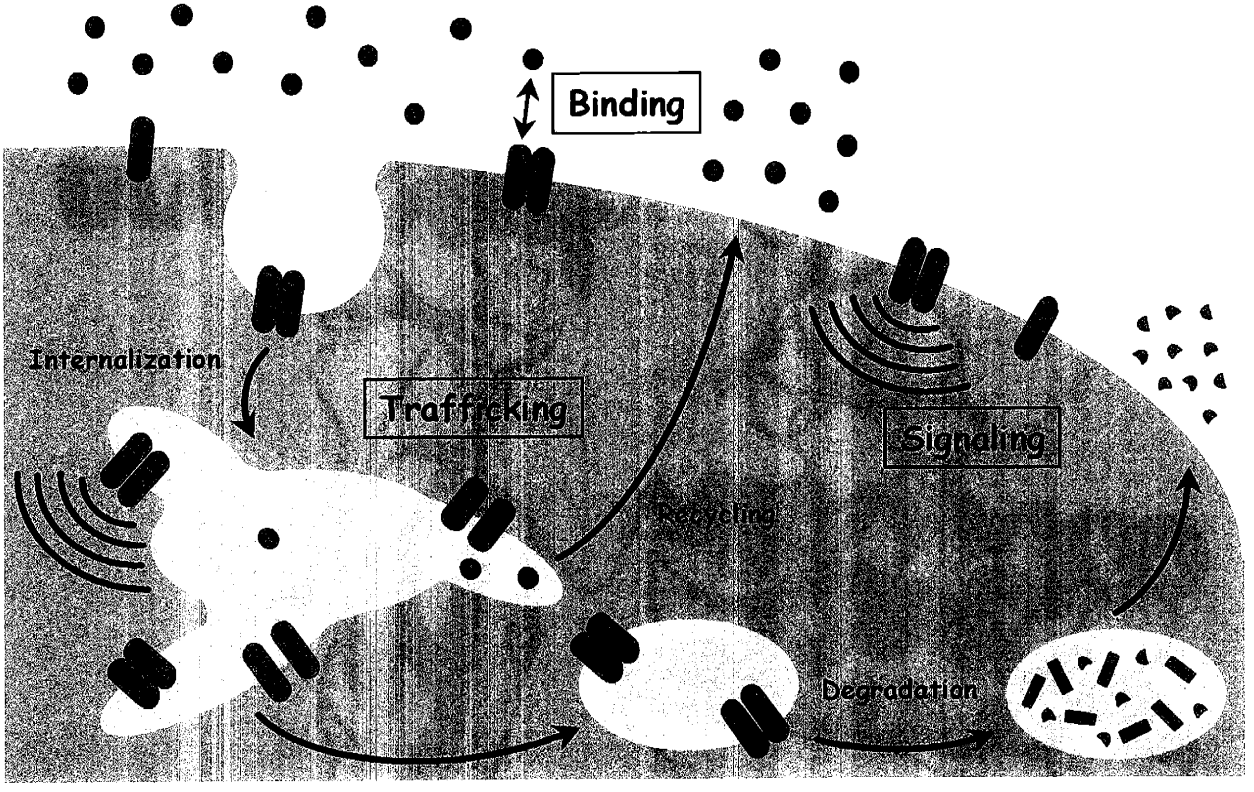

Figure 1.5: Binding and trafficking schematic for the GCSF/GCSFR system.

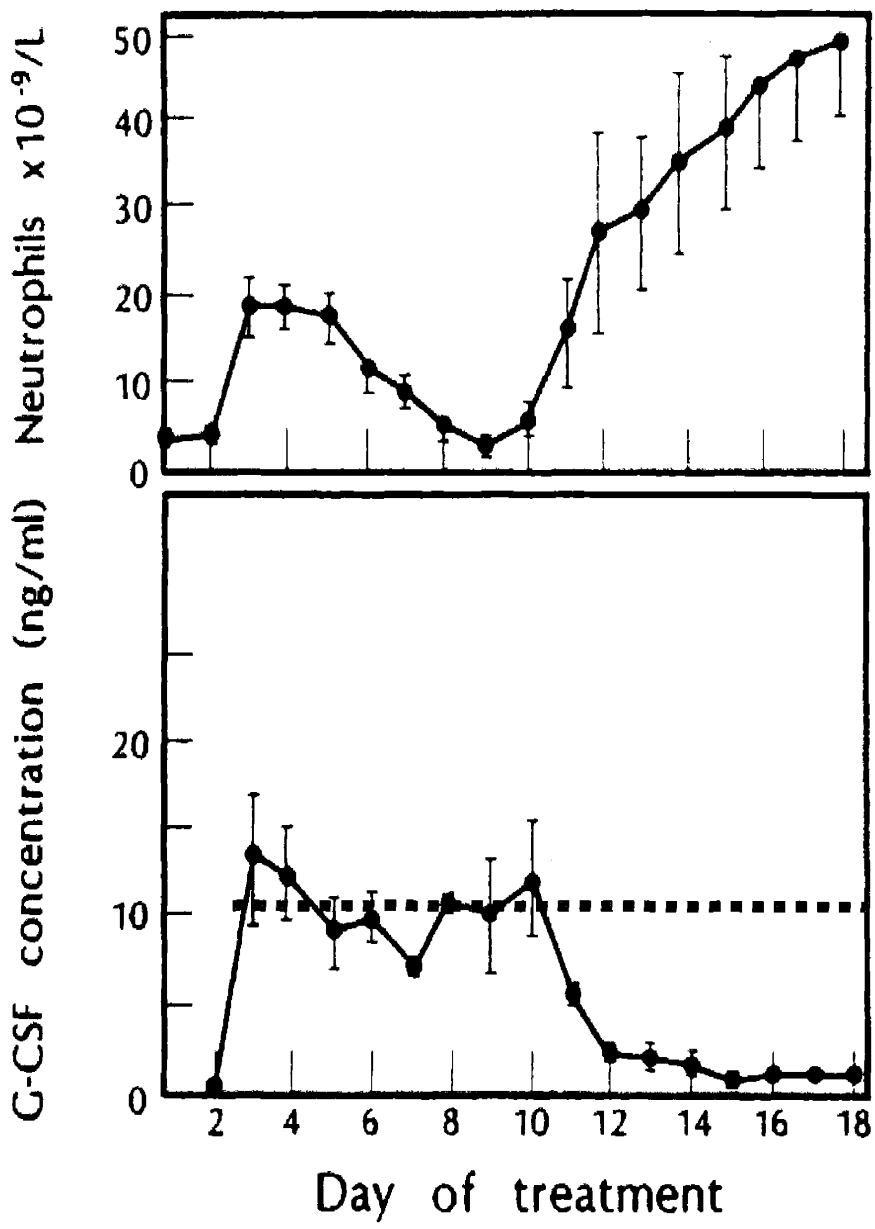

Figure 1.6: Relationship between peripheral blood neutrophils and GCSF concentration for patients receiving a continuous infusion of GCSF (10 μg/kg/day) (adapted from Layton *et al.*, 1989). The data indicate that peripheral neutrophil recovery leads to clearance of GCSF after approximately 10 days, despite continuous infusion of GCSF up to day 18.

Chapter 2: Pharmacodynamic Quadrant Plot Analysis of Cytokine Potency

The pharmacodynamic potency of a therapeutic cytokine interacting with a cell-surface receptor can be attributed primarily to three central properties: [1] cytokine/receptor binding affinity, [2] cytokine/receptor endocytic trafficking dynamics, and [3] cytokine /receptor signaling. Thus, engineering novel or second-generation cytokines requires an understanding of the contribution of each of these for the overall cell response. We describe here an efficient method toward this goal in demonstrated application to the clinically important cytokine granulocyte colony-stimulating factor (GCSF) with a chemical analog and a number of amino acid mutants. Using a combination of simple receptor-binding and dose-response proliferation assays we construct an appropriately scaled plot of relative mitogenic potency *versus* ligand concentration normalized to binding affinity, which partitions ligand analog behavior into four distinct quadrants. This 'pharmacodynamic quadrant plot' (PDQP) analysis conveniently indicates which of the cytokine properties – binding, trafficking, and/or signaling – are contributing substantially to altered potency effects. For the GCSF analogs studied here, two point mutations as well as a polyethylene glycol chemical conjugate were found to have increased potency despite similar affinity, and trafficking was predicted to be the responsible mechanism. A third point mutant exhibiting comparable binding affinity but reduced potency was predicted to have unchanged trafficking properties. Additionally, a mutant possessing order-of-magnitude weaker binding affinity displayed enhanced potency, and increased ligand half-life was predicted to be responsible for this net beneficial effect. Each of these predictions was successfully demonstrated by subsequent measurements of depletion of these five analogs from cell culture medium. Thus, for the GCSF system we find that ligand trafficking dynamics can play a major role in regulating mitogenic potency. More generally, our approach demonstrates that cytokine analogs can exhibit pharmacodynamic behaviors across a diverse spectrum of 'binding-potency space' and that the PDQP analysis can efficiently elucidate hypotheses for the underlying mechanisms for further dedicated testing.

INTRODUCTION

Therapeutic cytokines are capable of eliciting favorable cell responses such as proliferation, differentiation, or migration, through specific, high-affinity interactions with cell-surface receptors. However, cytokine/receptor binding is only an initial step in the sequence of events ultimately leading to the cell response, as it is consequently carried out via intracellular signaling cascades, and often with attenuation due to endocytosis of the signaling complexes accompanied to some degree by subsequent lysosomal degradation of these molecules. This endocytic trafficking can deplete the extracellular ligand concentration over time as well as desensitize the cell to further stimulation by downregulating the number of cell-surface receptors. Therefore, the pharmacodynamic cell response does not necessarily correlate with binding affinity alone, but instead can be strongly influenced by associated mechanisms governing signal transduction and cytokine/receptor trafficking (see Figure 1.5) (Lauffenburger *et al.*, 1998).

Many cytokines, including interferons, interleukins, and colony-stimulating factors, show great therapeutic promise (Tossing, 2001; Tompkins, 1999; Aulitzky *et al.*, 1994; Costello, 1993; Morstyn *et al.*, 1998; Vose and Armitage, 1995). These soluble proteins play roles in such phenomena as natural immunity (Kaser and Tilg, 2001), lymphocyte activation (Smith, 1988), and various aspects of hematopoiesis (Broudy, 1997; Wendling, 1999; Souza *et al.*, 1986). One cytokine of particular current importance is granulocyte colony-stimulating factor (GCSF), which stimulates elevation of neutrophil counts in patients presenting congenital neutropenia or in cancer patients undergoing chemotherapy (Trilletlenoir *et al.*, 1993).

GCSF is a 19-kDa member of the Group I cytokine superfamily, which is characterized by an antiparallel 4-α-helical-bundle structure and includes other therapeutically important proteins such as erythropoietin and growth hormone (Nicola, 1994). The target tissue for GCSF is bone marrow, where it binds with high affinity to the GCSF receptor (GCSFR) on neutrophilic precursor cells, inducing them to proliferate and differentiate into infection-fighting neutrophils (Fukunaga *et al.*, 1993). While this cytokine is an effective therapeutic agent, it suffers from an unusually short lifespan *in vivo*, due in large part to receptor-mediated endocytosis and degradation by circulating neutrophils that express GCSFR (Morstyn *et al.*, 1998; Layton *et al.*, 1989). Thus, the efficacy of the drug is

attenuated by this negative feedback mechanism, and consequently GCSF is commonly administered daily to maintain an adequate concentration *in vivo* (Morstyn *et al.*, 1998). Many efforts in therapeutic drug design focus on maximizing the affinity of the drug for its intended target, but this may not necessarily be the optimal design criterion. In the case of re-engineering GCSF, this strategy may actually be counterproductive, as it may augment receptor-mediated clearance of the drug by circulating neutrophils (Layton *et al.*, 1989; Morstyn *et al.*, 1998).

An alternative – or complementary – protein engineering approach that can directly affect the potency of a cytokine for local cell response (along with, in the particular case of GCSF, systemic pharmacokinetics by influencing receptor-mediated clearance) is the modification of ligand binding or trafficking in order to reduce receptor-mediated endocytosis and degradation. This modification could be an increased complex dissociation rate, a decreased complex internalization rate, or increased endosomal recycling of ligand molecules.

Two methods commonly utilized in modifying therapeutic proteins are the chemical conjugation of polymers such as polyethylene glycol (PEG) (Delgado *et al.*, 1992; Katre, 1993), and the substitution of amino acid residues in the protein. The attachment of PEG moieties to therapeutic proteins is expected to reduce renal clearance, as well as mask proteolytic cleavage sites, thus enhancing pharmacokinetic properties *in vivo* (Molineux *et al.*, 1999). A GCSF analog conjugated with PEG, termed SD/01, was found to require significantly less frequent dosing, yet was at least as efficacious (Molineux *et al.*, 1999; Johnston *et al.*, 2000).

As a previous example, work on epidermal growth factor receptor (EGFR) has shown human epidermal growth factor (EGF) and human transforming growth factor α (TGFα) to exhibit similar extracellular binding affinities for EGFR but different cellular trafficking properties and mitogenic potencies (French *et al.*, 1995). TGFα is largely dissociated from EGFR in the endosomes, and is effectively recycled (French *et al.*, 1995). In contrast, EGF binding does not exhibit as great a pH sensitivity, and the higher retention of endosomal complexes leads to greater degradation (French *et al.*, 1995). These differences in trafficking result in altered mitogenic potencies for the two ligands. This may be a direct result of the amino acid composition of these two growth factors. TGFα contains more histidine residues,

which may make binding this protein more sensitive to receptor binding in the endosomal environment (Groenen *et al.*, 1994). Interestingly, a mutant of EGF (Y13G) with lower receptor binding affinity has been shown to have enhanced mitogenic potency relative to both EGF and TGFα, suggesting that the trafficking properties of this mutant may be improved (Reddy *et al.*, 1996).

As a second example, a study of the cellular trafficking properties of interleukin-2 (IL-2) revealed that a double mutant of this cytokine (L18M/L19S) had an increased recycling fraction (~ 50%) relative to wild type (~ 30%) (Fallon *et al.*, 2000). This enhanced the potency of the mutant, despite similar extracellular receptor binding affinities and complex internalization rates for the two ligands. This finding demonstrates that only increasing the recycling fraction can significantly improve ligand potency.

These results for EGF and IL-2 suggest that, while amino acid substitutions can predictably modulate the binding affinity of a ligand for its receptor, an increased, decreased, or unchanged affinity does not necessarily directly correlate to superagonism, partial agonism, or full agonism, respectively (Lauffenburger *et al.*, 1998). As noted in these examples, even mutations which result in no observable difference in receptor binding affinity can still impact trafficking in a manner different from wild type, which in turn can alter pharmacodynamic response.

Our interest here is in analyzing the contributions of receptor-mediated properties (binding, signaling, and trafficking) of ligand analogs on pharmacodynamic cell response for the case of GCSF, the SD/01 chemical analog, and amino acid mutants which sample a diverse range of pharmacodynamic behaviors, as measured by dose-response cell proliferation assays. In conjunction with receptor-binding experiments, we use this proliferation data to generate a scaled plot of relative mitogenic potency *versus* normalized ligand concentration. This methodology conveniently partitions the various ligand analogs into four different graphical quadrants: weaker affinity than wild type and reduced potency; comparable affinity to wild type but reduced potency; comparable affinity to wild type but enhanced potency; and weaker affinity than wild type but enhanced potency. Not only is the inadequacy of binding affinity as a reliable predictor of potency clear from this methodology, but the resulting 'pharmacodynamic quadrant plot' (PDQP) can be further employed to generate testable hypotheses concerning which cell-level properties are significantly

modulating the potency of each analog. For the GCSF analogs studied here, the PDQP analysis generates specific predictions regarding the trafficking properties of five of these ligands, and subsequent ligand depletion experiments for these mutants confirmed these PDQP-guided inferences. Thus, the PDQP may serve as a generally useful diagnostic tool for deconvoluting binding, signaling, and trafficking processes, and for indicating which of these processes are significantly contributing to altered ligand potency.

In particular, we surprisingly find that SD/01 has a better pharmacodynamic response than wild type, despite a 3-fold lower receptor binding affinity. The PDQP predicts that this enhanced response is due to improved trafficking properties, and ligand depletion experiments reveal that SD/01 indeed has a 5-fold longer half-life than wild type. Thus, the PEG moiety on SD/01 not only improves the drug pharmacokinetics *in vivo* (Molineux *et al.*, 1999), but also appears to enhance its pharmacodynamic response through longer ligand half-life locally at the cell level. Additionally, using the PDQP analysis, we identify three mutants with even greater pharmacodynamic responses than SD/01 and successfully predict that reduced receptor-mediated depletion is likewise responsible for the improved potency of each.

MATERIALS AND METHODS

Preparation of GCSF analogs

Both mutant and wild-type GCSF were refolded from inclusion bodies and purified as previously described (Lu *et al.*, 1992). Additionally, to remove any trace of GCSF dimer, all samples were subjected to gel filtration on a 35/600 Superdex 75 column (Pharmacia) run in 25 mM sodium acetate, 100 mM sodium chloride, pH 5.0. SD/01 was prepared as described (Kinstler *et al.*, 1996). The entire extracellular domain of the GCSF receptor was expressed in Chinese hamster ovary cells and purified from conditioned medium as previously reported (Horan *et al.*, 1996).

Cell line and culture

The GCSF-dependent suspension cell line OCI/AML1, a generous gift from Ernest A. McCulloch (University of Toronto), was used for all experiments. Minimum essential medium alpha (MEMα), L-glutamine, penicillin-streptomycin, fetal bovine serum (FBS), and

phosphate-buffered saline were obtained from Life Technologies (Frederick, MD). Isotonic solution for the Coulter counter (ISOTON II, Coulter Diagnostics, Hialeah, FL) was obtained from Curtin Matheson Scientific (Houston, TX). Every 3 to 4 days, cells were diluted to 10^5/mL in MEMα supplemented with 20% FBS, 200 mM L-glutamine, 100 units/mL penicillin, 100 μg/mL streptomycin, and 270 pM GCSF, and incubated in a humidified atmosphere with 5% CO_2 at 37°C.

Binding experiments

The interaction between GCSF and GCSFR was studied using the BIAcore™ 2000 (BIAcore, Uppsala, Sweden). Wild-type GCSF, modified to include a $(His)_6$-tag was coupled to the BIAcore™ NTA chip in the presence of nickel. Binding of GCSFR to coupled GCSF was measured directly in eluent buffer (10 mM HEPES, 0.15 M NaCl, 50 μM EDTA, 0.005% Surfactant P-20 (BIAcore, Uppsala, Sweden), pH 7.4). Varying concentrations of GCSFR were passed over a surface with 300 relative units (RU) of GCSF attached. It was not possible to dissociate GCSFR from GCSF without denaturing both components; therefore, the surface was stripped with 0.35 M EDTA and fresh $(His)_6$-GCSF was bound between each concentration of receptor. Binding was measured at a flow rate of 20 μL/min for 5 min, followed by a 50 min dissociation phase. The binding curve was analyzed by BIAeval™ version 3.0 (BIAcore, Uppsala, Sweden), using a Langmuir binding model with sloping baseline. All experiments were performed in triplicate.

The equilibrium binding constants for wild-type GCSF and the various analogs were determined using the concentration of free receptor in equilibrium mixtures of GCSF and GCSFR. Under conditions where binding is limited by mass transport, the rate of binding is proportional to the concentration of analyte. The rate of binding for various concentrations of GCSFR was determined in NTA buffer at a flow rate of 5 μL/min, with 1000 RU of $(His)_6$-GCSF attached to the surface. A fresh surface was prepared for each data point. The standard curve of receptor concentration *versus* binding was used to determine the concentration of free GCSFR. Mixtures of GCSF or an analog with 2 nM GCSFR were equilibrated at room temperature for at least 30 min, and tested as described for GCSFR. Comparison of samples equilibrated for 30 min or up to 24 h showed no systematic variation.

All samples were analyzed three times and all experiments were carried out in triplicate. K_D values were determined using BIAeval™ version 3.0.

Cell proliferation experiments

Cells were passaged into supplemented MEMα medium without GCSF 24 h prior to the initiation of the cell proliferation experiments, at which point parallel plates of cells at a density of 10^5/mL were incubated in supplemented MEMα medium with a known concentration of wild-type GCSF or analog (L_0 = 125, 250, 500, 1000 pM). For each experiment, duplicate plates were prepared for each sample, and the plates were stored in a humidified atmosphere with 5% CO_2 at 37°C. After 3 days, one plate of each sample was diluted 1:15 in isotonic solution and counted using a Coulter counter to determine cell density. This procedure was repeated for the second set of samples after 7 days. The error bars for all plots represent the standard deviations from at least two independent experiments.

Ligand depletion experiments

Cells were passaged into supplemented MEMα medium without GCSF 24 h prior to the initiation of the ligand depletion experiments, at which point parallel flasks of cells at a density of 10^5/mL were incubated in supplemented MEMα medium with 270 pM wild-type GCSF or analog. After 3 h and 6 h, an aliquot of each medium supernatant, obtained after centrifugation to pellet cellular debris, was stored at –20°C for later analysis. After 24 h from the start of an experiment, the cell density in each flask was monitored using a Coulter counter and an aliquot of each medium supernatant was stored at –20°C for later analysis. This was repeated every 24 h for 6 to 8 days. The concentration in each medium supernatant sample was quantitated using enzyme-linked immunosorbent assay (ELISA) kits obtained from R&D Systems (Minneapolis, MN). The half-life of each ligand was determined by fitting each data set to an exponential decay equation. Wild-type GCSF depletion experiments performed using the YT-2C2 suspension cell line, which is GCSF-independent and does not express GCSFR, revealed nearly 80% intact ligand after six days (data not shown); therefore, ligand depletion from the medium indeed appears to be driven by receptor-mediated trafficking and not by differences in extracellular ligand stability.

RESULTS

Equilibrium binding affinities for wild type and analogs

Since SD/01 is more efficacious than wild-type GCSF *in vivo* (Molineux *et al.*, 1999; Johnston *et al.*, 2000), we wanted to see whether, and if so how, this efficacy manifested itself at the cellular level. Additionally, several amino acids known to contribute to receptor binding were considered for mutagenesis. Positions of the five native amino acid residues on GCSF that were mutated in this study are shown in Figure 2.1. The crystal structure of the GCSF:GCSFR complex (Aritomi *et al.*, 1999) reveals that Glu20, Gly27, and Glu34 lie at the major binding interface and that Glu47 and Leu51 lie at the minor binding interface. These residues were mutated as follows: E20A, G27L, E34A, E47A, and L51E. An important determinant in assessing the potency of a therapeutic analog *in vivo* is the equilibrium binding affinity of the ligand for its receptor. The GCSF receptor is present on the surface of (at least) two classes of cells: neutrophilic precursor cells in the bone marrow and circulating mature neutrophils in the bloodstream (Demetri and Griffin, 1991). Binding of GCSF to GCSFR on precursor cells initiates intracellular signaling cascades, causing proliferation and differentiation of these cells into mature neutrophils, which then enter the bloodstream (Fukunaga *et al.*, 1993). However, GCSF binding to GCSFR on the mature neutrophils largely serves to deplete GCSF from the bloodstream through receptor-mediated endocytosis (Layton *et al.*, 1989; Morstyn *et al.*, 1998). It has been reported that the binding affinity of growth hormone for its receptor may exceed that which is necessary to elicit a sufficient response (Pearce *et al.*, 1999). If this is also the case for GCSF, then reducing the binding affinity may actually reap the benefits of reduced cellular clearance, without the drawbacks of diminished potency. Thus, there may exist an optimal binding affinity for the ligand that largely maintains the neutrophilic proliferation desired by the therapy, but reduces the depletion of the drug mediated by this neutrophilic proliferation as a consequence of binding. Such an altered binding affinity, in conjunction with improved trafficking properties, may thus have significant impact on GCSF pharmacokinetics.

The equilibrium dissociation constant (K_D = inverse equilibrium affinity constant) for each protein was determined by surface plasmon resonance measurements (data for wild type shown in Figure 2.2). The K_D values for the analogs, normalized to wild type, are given in order of increasing binding affinity from left to right in Figure 2.3. Interestingly, SD/01 was

found to have a 3-fold lower affinity than wild type. Thus, it appears that the PEG moiety reduces the receptor binding affinity of SD/01, but this does not appear to impact its clinical efficacy (Molineux *et al.*, 1999). In addition to reduced renal clearance and masking of potential proteolytic cleavage sites, it is possible that the PEG moiety on SD/01 is of further benefit by lowering receptor-binding affinity to reduce consequent endocytic trafficking and degradation of the drug by mature neutrophils. The K_D values for the mutant analogs range from more than 360-fold lower affinity to slightly higher affinity than wild type. If increased binding affinity correlated positively with increased potency, we would expect to see, in a cell proliferation assay using each mutant in Figure 2.3, a monotonic increase in cell density going from E20A to G27L.

Cell proliferation of wild type and analogs

To determine how modulation of the receptor binding affinity affects mitogenicity *in vitro*, we tested wild-type GCSF and the analogs in a dose-response cell proliferation assay with the GCSF-dependent cell line OCI/AML1. Using initial ligand concentrations of 125, 250, 500, and 1000 pM with no replenishment, we incubated cells at an initial density of 10^5/mL. The resulting cell densities for wild type after 3 and 7 days are given in Figure 2.4A. The cell densities for the analogs, normalized to corresponding wild-type values at the same initial ligand concentration, are given in Figures 2.4B (t = 3 days) and 2.4C (t = 7 days). The order of the mutants is the same as in Figure 2.3 (increasing binding affinity from left to right); however, it is especially clear from Figure 2.4C that mitogenicity does not positively correlate with binding affinity.

Most surprisingly, L51E binds with much lower affinity than wild type (Figure 2.3), but elicits a pharmacodynamic response essentially equal to wild type at 3 days (Figure 2.4B), and greater than wild type at 7 days (Figure 2.4C). Conversely, E47A binds with similar affinity to wild type (and with much higher affinity than L51E), yet is less potent than expected at both time points (Figures 2.4B and 2.4C). An initial dose of 125 pM E34A, which has a receptor binding affinity similar to wild type, elicits a cellular response greater than 2-fold that achieved with the same dose of wild type after 7 days (Figure 2.4C).

No difference in cell density was observed between wild type and SD/01 after 3 days at any of the concentrations. In fact, if we extend the time point to 7 days, we find that the

cell density for each sample treated with SD/01 was greater than that treated with an equivalent concentration of wild type (Figure 2.4C). These results suggest that a 3-fold reduction in binding affinity does not affect the mitogenic potency of SD/01.

These counterintuitive results suggest that other processes, namely trafficking and signaling, are significantly affecting the pharmacodynamic potency, since the results of these dose-response proliferation assays cannot be explained by binding affinity alone. Using both the binding affinity and proliferation results, we generated a scaled plot to help assess the contributions of these other processes to the overall pharmacodynamic response.

Generation of the pharmacodynamic quadrant plot (PDQP)

For each analog, the cell proliferation experiments were performed with the same initial ligand concentrations (L_0 = 125, 250, 500, 1000 pM). However, these values are not the best indicators of the concentrations "seen" by the cells; a cell senses the ligand concentration through the number of complexes formed with its surface receptors. Since the analogs have a range of K_D values, a better estimate of the ligand concentration is the nondimensionalized L_0/K_D. Thus, although the same initial ligand concentrations were used for each analog (an 8-fold span between 125 pM and 1000 pM), the value for L_0/K_D ranges from 0.002 to 12 (a 6000-fold span). The normalization used for pharmacodynamic potency is the cell density of the analog at a given time point (t = 3 or 7 days) divided by the corresponding cell density of wild type at the equivalent initial ligand concentration. We then generate a 4-point curve for each analog, plotting the nondimensional potency (ρ/ρ_{WT} where ρ is cell density) *versus* the logarithmically scaled nondimensional ligand concentration (L_0/K_D). This pharmacodynamic quadrant plot (PDQP) for the 3-day results is given in Figure 2.5A, and that for the 7-day results in Figure 2.5B.

Following each curve from left to right in the 3-day PDQP (Figure 2.5A), the four data points represent initial ligand concentrations of 125, 250, 500, and 1000 pM, but the spread along the x-axis results from the wide range of K_D values for the analogs. There is not much spread along the y-axis for this 3-day time point except for the E20A and E47A mutants, which are less potent (below $\rho/\rho_{WT} = 1$). If we now look at the 7-day PDQP (Figure 2.5B), when ligand depletion effects are more significant, marked changes in comparison to the 3-day PDQP are apparent. We see a much more pronounced spread along the y-axis. In

particular, several analogs are well above the solid horizontal line at $\rho/\rho_{WT} = 1$, which positions the mutants more potent than wild type above it and those less potent below. The mutants that bind with orders-of-magnitude lower affinities than wild type fall to the left of the dashed vertical line, and those with comparable affinities (on a logarithmic scale) lie to the right. For the 7-day time point, the mutants have partitioned into four distinct quadrants, whose boundaries are delineated by the solid horizontal line and the dashed vertical line. The bottom left quadrant contains the E20A mutant, which binds over 360-fold more weakly than wild type, and is predictably less potent. The bottom right quadrant contains E47A, which binds comparably to wild type, yet is only roughly half as potent. The top right quadrant contains the chemical analog SD/01 as well as mutants E34A and G27L, which bind comparably to wild type and are more potent than wild type. Finally, the top left quadrant, which is perhaps the most unexpected quadrant to find occupied, contains the L51E mutant, which binds over 60-fold more weakly than wild type, yet is more potent.

Given the three processes that can impact ligand potency, the quadrant plot suggests further details about some of the mutants. In examining the top right quadrant of the PDQP in Figure 2.5B, note that the curves for the two mutants, E34A and G27L, have pronounced slopes. The improved potency of these two mutants does not appear to be due to differences in binding affinity, since these mutants and wild type all lie in the right half of the PDQP. Additionally, at an L_0/K_D value near 10, ligand concentration is in relative excess and we do not expect trafficking and depletion of the ligand to play a significant role; thus, by process of elimination, we attribute any differences in potency at this value of L_0/K_D to signaling. Differences in potencies between these mutants and wild type are small at this point, suggesting that the mutants are not significantly superior signal transducers upon receptor binding. Conversely, at an L_0/K_D value near 1, trafficking and depletion of the ligand can greatly affect potency, and at this concentration the mutants are twice as potent as wild type. Since we have already inferred that the enhanced potency is not due to differences in binding affinity or signaling, we can hypothesize that this superagonism is a consequence of improved trafficking, which results in a longer ligand half-life. Through this reasoning, we conjecture that mutants with such negative sloping curves have improved trafficking properties. Thus, we also expect to see a trafficking improvement for SD/01, which also lies in the top right quadrant of the PDQP, although perhaps not as great of an enhancement.

By contrast, E47A in the bottom right quadrant of Figure 2.5B is essentially horizontal. Again, the reduced potency does not seem to result from differences in binding affinity, since this mutant also lies in the right half of the PDQP. This analog, unlike those in the top right quadrant, does not show a concentration dependence on potency, suggesting that its trafficking properties are macroscopically no different from those of wild type. Otherwise, we would expect to see a significant change in potency between high L_0/K_D (where trafficking effects are masked) and low L_0/K_D (where trafficking effects are important). This analysis then leads us to the conclusion that E47A simply signals more poorly than wild type.

The mutants to the left of the dashed vertical line are more difficult to analyze, since we can no longer rule out differences in binding affinity in explaining altered potencies (these mutants share no common L_0/K_D value with wild type for comparison purposes). The E20A mutant in the bottom left quadrant is perhaps a predictable result, with such a large reduction in binding affinity leading to insufficient proliferative signals. The binding and proliferation results here are consistent with other findings that confirm that Glu20 is critical for receptor recognition and ligand function (Layton *et al.*, 1999; Reidhaar-Olson *et al.*, 1996).

The L51E mutant in the top left quadrant has a 60-fold worse affinity than wild type. Given this significantly lower binding affinity, we expect that a much smaller fraction of L51E molecules will be subjected to receptor-mediated endocytosis and degradation in comparison to wild type. Therefore, we expect this ligand to have a significantly longer half-life, resulting from its reduced binding affinity, improved trafficking properties, or some combination of these processes. At earlier times, when trafficking effects are not as prominent, the important processes are likely to be binding affinity and signaling. This mutant maintains almost comparable potency to wild type after 3 days (Figure 2.5A); since there are fewer surface complexes formed at this reduced affinity, it is possible that there is enhanced signaling to account for the almost complete agonism, but this cannot be inferred from the PDQP. An alternative explanation is that wild-type GCSF binding affinity could exceed that which is necessary (Pearce *et al.*, 1999), and therefore this mutant generates enough normal signals despite its lower binding affinity. At later times (Figure 2.5B), L51E shifts into the top left quadrant, likely due to the predicted long ligand half-life.

This analysis of the 7-day PDQP compares the pharmacodynamic response of the analogs relative to wild type at a given initial ligand concentration for each data point. While this is the proper pharmacodynamic comparison, we can examine the two right-hand quadrants of the 7-day PDQP more rigorously by comparing the pharmacodynamic response of the analogs relative to wild type at a given initial L_0/K_D. In order to do this, we fit the 7-day data from Figure 2.4A to the equation $\rho_{WT} = m*\log(L_0/K_D) + b$ ($r^2 = 0.999$). For each data point in Figure 2.5B with an x-coordinate that lies in the wild-type range of L_0/K_D (0.8 to 6.4), the corresponding y-coordinate for each such data point was normalized to the ρ_{WT} value calculated from this equation using the same x-coordinate value. This modified plot is shown in Figure 2.5C. The dashed lines and open circles represent extrapolations outside of the wild-type L_0/K_D range, and therefore may not necessarily be quantitatively precise, but are included to show all four points in each curve. This method of normalizing the y-axis should fully cancel out any contributions of binding affinity, although a comparison of Figures 2.5B and 2.5C shows that the results are still qualitatively the same. Thus, we expect the analogs above $\rho/\rho_{WT} = 1$, with similar values to wild type at high L_0/K_D and negative slopes, to have improved trafficking properties, resulting in longer ligand lifetimes. We expect the mutant below this line, with almost no slope, to have decreased signaling capacity but largely unchanged trafficking properties. In summary, the PDQP analysis suggests the analogs will have roughly the following order of half-lives: L51E > E34A ~ G27L > SD/01 > E47A ~ wild type.

Ligand depletion and half-life calculations for GCSF mutants

To test trafficking predictions made through analysis of the PDQP, ligand depletion experiments using enzyme-linked immunosorbent assays were performed. The half-lives for wild type and analogs with interesting properties are shown in Figure 2.6. Consistent with the predictions, L51E had the longest half-life, likely because of its lower receptor binding affinity (reducing uptake from the medium) but additionally due to enhanced trafficking properties (reducing degradation following uptake). The predictions for the mutants in the right half of the plot were also corroborated. E47A was predicted to have macroscopically similar trafficking properties to wild type, and this manifested itself in comparable half-lives for this mutant and wild type. E34A and G27L were expected to have improved trafficking

properties, and their half-lives were measured to be 14- and 16-fold, respectively, that of wild type. Finally, SD/01 was also found to have a 5-fold longer half-life than wild type. Based on our findings, it is likely that SD/01 has diminished cellular uptake and depletion by circulating neutrophils in comparison to wild type. Thus, it is possible that both nonspecific and specific clearance mechanisms of GCSF are reduced by the addition of this PEG moiety, resulting in the longer half-life of SD/01 *in vivo* (Molineux *et al.*, 1999).

DISCUSSION

Increased efficiency in evaluation of therapeutic protein analogs – whether the modifications be chemical or genetic in nature and whether they be generated by rational design, directed evolution, combinatorial screening, or trial-and-error – is desirable across a spectrum of required properties including pharmacokinetics, pharmacodynamics, and toxicity. For the case of GCSF, a highly important example clinically, a new chemical analog (SD/01) has been demonstrated to exhibit increased effectiveness *in vivo* (Molineux *et al.*, 1999), with the enhancement attributed to improved pharmacokinetic behavior – specifically, longer half-life in the systemic circulation. It is not clear, however, what underlying cell-level mechanism is responsible for this longer half-life. Both the actual target cell-type for GCSF action, neutrophilic precursor cells in the bone marrow, and the resulting mature neutrophils circulating in the bloodstream, express surface GCSFR that can bind the ligand leading to its endocytic degradation (Layton *et al.*, 1989; Morstyn *et al.*, 1998). Thus, the enhanced effectiveness could be due to a combination of improvements in both pharmacodynamic as well as pharmacokinetic behaviors. We were accordingly motivated to quantitatively analyze pharmacodynamic properties of SD/01 along with analogs generated by amino acid substitution.

We find here that SD/01 binds with lower affinity to GCSFR than wild type (Figure 2.3); however, this does not appear to impact mitogenic potency at short times (3 days) and, in fact, yields greater potency at later times (7 days). The explanation for this improved pharmacodynamic behavior is a longer half-life of SD/01 even in cell culture (Figure 2.6). These findings suggest that the greater *in vivo* effectiveness of SD/01 may be due to improved pharmacodynamics as well as the enhanced pharmacokinetics previously considered. Moreover, this result presents the possibility that analogs of GCSF – as well as

other therapeutic cytokines – exhibiting superior pharmacodynamic properties might be engineered more generally, by appropriate influence of at least one of three central properties: [1] cytokine/receptor binding affinity, [2] cytokine/receptor endocytic trafficking dynamics, and [3] cytokine/receptor complex signaling (see Figure 1.5). Since quantitative information connecting signaling metrics with cell responses is essentially unavailable at the present time, and since increasing binding affinity may rarely be a productive avenue for providing greater cell response (Pearce *et al.*, 1999), manipulation of endocytic trafficking offers an exceptionally promising direction toward this objective (Lauffenburger *et al.*, 1998).

Thus, with a convenient methodology for analyzing how these three mechanisms may contribute to some observed cellular potency metric in response to cytokine stimulation, we were interested in probing a 'binding-potency space' of GCSF analogs. The theoretical binding-potency space for a ligand and its analogs would look like the sextant plot in Figure 2.7 (with binding affinity effectively normalized), and significantly tighter binding and weaker binding analogs occupying the two rightmost and two leftmost regions, respectively. Examples in the top, middle region are: equivalent signaling, improved trafficking (square symbols, negative slope); improved signaling, equivalent trafficking (diamonds, zero slope); and, improved signaling, worsened trafficking (triangles, positive slope). The examples in the bottom, middle region follow the same principles. It is also conceivable that the normalized curve for an analog could cross the wild-type curve and lie partially in this top region and partially in this bottom region. Once binding affinity has been normalized on this plot, the two remaining properties to assess are trafficking and signaling. The overall paradigm in determining the contributions of these parameters is analogous to determining the slope and intercept of linear x-y data. Here, the "intercept" is the relative potency of the analog at high L_0/K_D and suggests the contribution of changes in signaling to the overall pharmacodynamic response of the analog; the steepness of the analog curve is the "slope" (not necessarily positive or constant) and is indicative of modifications in the trafficking properties relative to wild type. These features of the analog curves become more pronounced at later time points, since these processes are magnified over time.

In our analysis, the x-axis was scaled logarithmically; thus, mutants occupying the rightmost regions in Figure 2.7 bind with at least an order-of-magnitude higher affinity than

wild type. However, finding such mutants may be difficult, or even impossible, especially for many cytokines with naturally high affinities for their respective receptors. Since wild-type GCSF and GCSFR form a high affinity complex containing two ligands and two receptors (Horan *et al.*, 1996; Horan *et al.*, 1997), it is unlikely that single mutants of GCSF would be found to bind substantially tighter. Indeed, we did not find any such mutants, and our binding-potency space was reduced to a four-region 'pharmacodynamic quadrant plot' (PDQP); actual examples of this PDQP are shown in Figures 2.5A and 2.5B for the GCSF analogs studied explicitly here. As we have shown through analysis of the features of the curves in this plot, we can deconvolute the processes of binding, signaling, and trafficking and suggest which of these are contributing substantially to altered ligand potency. We did this, in part, by analyzing the "intercepts" and "slopes" of some of the mutant curves. We were able to generate hypotheses from the plot and we then successfully tested our predictions using ligand depletion experiments, which demonstrated either the presence (L51E, E34A, G27L, SD/01) or absence (E47A) of beneficial endocytic trafficking effects. Thus, this methodology may serve as a useful diagnostic for screening ligands, not just by binding affinity and potency – which we have shown not to correlate well here – but also by inference of some trafficking and signaling properties. Testing of a hypothesis indicated by the PDQP that signaling would be affected by a ligand mutation, either positively or negatively, requires that an intracellular signal quantitatively determining the cell behavioral response of interest be identified and validated. For the case of GCSF this information has not been clearly elucidated, thus precluding direct testing of any signaling effect hypothesis had one been indicated for a mutant from the PDQP.

Using the PDQP framework, the double mutant of IL-2 (L18M/L19S), which has improved trafficking properties as a result of enhanced ligand recycling (Fallon *et al.*, 2000), would lie in the top right quadrant of Figure 2.5B. Additionally, the lower binding affinity EGF mutant (Y13G) with improved trafficking properties (Reddy *et al.*, 1996) would lie in the top left quadrant. The compatibility of the quadrant plot with these other mutants suggests that the results presented here are not limited to the particular mutants or system chosen, but are generalizable.

Interestingly, while SD/01 is more potent than wild type and has a longer half-life, we see from Figures 2.5 and 2.6 that three mutants (L51E, E34A, and G27L) are actually more

potent than SD/01, with longer half-lives as well. Thus, these mutants may reduce the receptor-mediated clearance mechanisms experienced *in vivo* to an even greater extent than SD/01. To gain the benefits of the PEG moiety with respect to renal clearance mechanisms and masking of proteolytic cleavage sites, our findings suggest that the addition of the PEG moiety to these three mutants may result in even more effective therapeutic agents.

REFERENCES

Aritomi, M., Kunishima, N., Okamoto, T., Kuroki, R., Ota, Y. and Morikawa, K. (1999). Atomic structure of the GCSF-receptor complex showing a new cytokine-receptor recognition scheme. *Nature*. **401:** 713-717.

Aulitzky, W.E., Schuler, M., Peschel, C. and Huber, C. (1994). Interleukins: clinical pharmacology and therapeutic use. *Drugs*. **48:** 667-677.

Berman, H.M., Westbrook, J., Feng, Z., Gilliland, G., Bhat, T.N., Weissig, H., Shindyalov, I.N. and Bourne, P.E. (2000). The Protein Data Bank. *Nucleic Acids Research*. **28:** 235-242.

Broudy, V.C. (1997). Stem cell factor and hematopoiesis. *Blood*. **90:** 1345-1364.

Costello, R.T. (1993). Therapeutic use of granulocyte-macrophage colony-stimulating factor (GM-CSF): a review of recent experience. *Acta Oncologica*. **32:** 403-408.

Delgado, C., Francis, G.E. and Fisher, D. (1992). The uses and properties of PEG-linked proteins. *Critical Reviews in Therapeutic Drug Carrier Systems*. **9:** 249-304.

Demetri, G.D. and Griffin, J.D. (1991). Granulocyte colony-stimulating factor and its receptor. *Blood*. **78:** 2791-2808.

Fallon, E.M., Liparoto, S.F., Lee, K.J., Ciardelli, T.L. and Lauffenburger, D.A. (2000). Increased endosomal sorting of ligand to recycling enhances potency of an interleukin-2 analog. *Journal of Biological Chemistry*. **275:** 6790-6797.

French, A.R., Tadaki, D.K., Niyogi, S.K. and Lauffenburger, D.A. (1995). Intracellular trafficking of epidermal growth factor family ligands is directly influenced by the pH sensitivity of the receptor/ligand interaction. *Journal of Biological Chemistry*. **270:** 4334-4340.

Fukunaga, R., Ishizaka-Ikeda, E. and Nagata, S. (1993). Growth and differentiation signals mediated by different regions in the cytoplasmic domain of granulocyte colony-stimulating factor receptor. *Cell*. **74:** 1079-1087.

Groenen, L.C., Nice, E.C. and Burgess, A.W. (1994). Structure-function relationships for the EGF/TGFα family of mitogens. *Growth Factors*. **11:** 235-257.

Horan, T., Wen, J., Narhi, L., Parker, V., Garcia, A., Arakawa, T. and Philo, J. (1996). Dimerization of the extracellular domain of granulocyte-colony stimulating factor receptor by ligand binding: a monovalent ligand induces 2:2 complexes. *Biochemistry*. **35:** 4886-4896.

Horan, T.P., Martin, F., Simonet, L., Arakawa, T. and Philo, J.S. (1997). Dimerization of granulocyte-colony stimulating factor receptor: the Ig plus CRH construct of granulocyte-colony stimulating factor receptor forms a 2:2 complex with a ligand. *Journal of Biochemistry*. **121:** 370-375.

Johnston, E., Crawford, J., Blackwell, S., Bjurstrom, T., Lockbaum, P., Roskos, L., Yang, B.B., Gardner, S., Miller-Messana, M.A., Shoemaker, D., Garst, J. and Schwab, G. (2000). Randomized, dose-escalation study of SD/01 compared with daily Filgrastim in patients receiving chemotherapy. *Journal of Clinical Oncology*. **18:** 2522-2528.

Kaser, A. and Tilg, H. (2001). Interferon-α in inflammation and immunity. *Cellular and Molecular Biology*. **47:** 609-617.

Katre, N.V. (1993). The conjugation of proteins with polyethylene glycol and other polymers: altering properties of proteins to enhance their therapeutic potential. *Advanced Drug Delivery Reviews*. **10:** 91-114.

Kinstler, O.B., Brems, D.N., Lauren, S.L., Paige, A.G., Hamburger, J.B. and Treuheit, M.J. (1996). Characterization and stability of N-terminally PEGylated rhG-CSF. *Pharmaceutical Research.* **13:** 996-1002.

Lauffenburger, D.A., Fallon, E.M. and Haugh, J.M. (1998). Scratching the (cell) surface: cytokine engineering for improved ligand/receptor trafficking dynamics. *Chemistry & Biology.* **5:** R257-R263.

Layton, J.E., Hockman, H., Sheridan, W.P. and Morstyn, G. (1989). Evidence for a novel in vivo control mechanism of granulopoiesis: mature cell-related control of a regulatory growth factor. *Blood.* **74:** 1303-1307.

Layton, J.E., Shimamoto, G., Osslund, T., Hammacher, A., Smith, D.K., Treutlein, H.R. and Boone, T. (1999). Interaction of granulocyte colony-stimulating factor (G-CSF) with its receptor: evidence that Glu^{19} of G-CSF interacts with Arg^{288} of the receptor. *Journal of Biological Chemistry.* **274:** 17445-17451.

Lu, H.S., Clogston, C.L., Narhi, L.O., Merewether, L.A., Pearl, W.R. and Boone, T.C. (1992). Folding and oxidation of recombinant human granulocyte colony stimulating factor produced in *Escherichia coli. Journal of Biological Chemistry.* **267:** 8770-8777.

Molineux, G., Kinstler, O., Briddell, B., Hartley, C., McElroy, P., Kerzic, P., Sutherland, W., Stoney, G., Kern, B., Fletcher, F.A., Cohen, A., Korach, E., Ulich, T., McNiece, I., Lockbaum, P., Miller-Messana, M.A., Gardner, S., Hunt, T. and Schwab, G. (1999). A new form of Filgrastim with sustained duration in vivo and enhanced ability to mobilize PBPC in both mice and humans. *Experimental Hematology.* **27:** 1724-1734.

Morstyn, G., Dexter, T.M. and Foote, M. (1998). *Filgrastim (r-metHuG-CSF) in Clinical Practice.* Marcel Dekker, New York.

Nicola, N.A. (1994). *Guidebook to Cytokines and Their Receptors.* Oxford University Press, New York.

Pearce, K.H., Cunningham, B.C., Fuh, G., Teeri, T. and Wells, J.A. (1999). Growth hormone binding affinity for its receptor surpasses the requirements for cellular activity. *Biochemistry.* **38:** 81-89.

Reddy, C.C., Niyogi, S.K., Wells, A., Wiley, H.S. and Lauffenburger, D.A. (1996). Engineering epidermal growth factor for enhanced mitogenic potency. *Nature Biotechnology.* **14:** 1696-1699.

Reidhaar-Olson, J.F., De Souza-Hart, J.A. and Selick, H.E. (1996). Identification of residues critical to the activity of human granulocyte colony-stimulating factor. *Biochemistry.* **35:** 9034-9041.

Smith, K.A. (1988). Interleukin-2: inception, impact, and implications. *Science.* **240:** 1169-1176.

Souza, L.M., Boone, T.C., Gabrilove, J., Lai, P.H., Zsebo, K.M., Murdock, D.C., Chazin, V.R., Bruszewski, J., Lu, H., Chen, K.K., Barendt, J., Platzer, E., Moore, M.A.S., Mertelsmann, R. and Welte, K. (1986). Recombinant human granulocyte colony-stimulating factor: effects on normal and leukemic myeloid cells. *Science.* **232:** 61-65.

Tompkins, W.A. (1999). Immunomodulation and therapeutic effects of the oral use of interferon-α: mechanism of action. *Journal of Interferon and Cytokine Research.* **19:** 817-828.

Tossing, G. (2001). New developments in interferon therapy. *European Journal of Medical Research*. **6:** 47-65.

Trilletlenoir, V., Green, J., Manegold, C., Vonpawel, J., Gatzemeier, U., Lebeau, B., Depierre, A., Johnson, P., Decoster, G., Tomita, D. and Ewen, C. (1993). Recombinant granulocyte colony-stimulating factor reduces the infectious complications of cytotoxic chemotherapy. *European Journal of Cancer*. **29A:** 319-324.

Vose, J.M. and Armitage, J.O. (1995). Clinical applications of hematopoietic growth factors. *Journal of Clinical Oncology*. **13:** 1023-1035.

Wendling, F. (1999). Thrombopoietin: its role from early hematopoiesis to platelet production. *Haematologica*. **84:** 158-166.

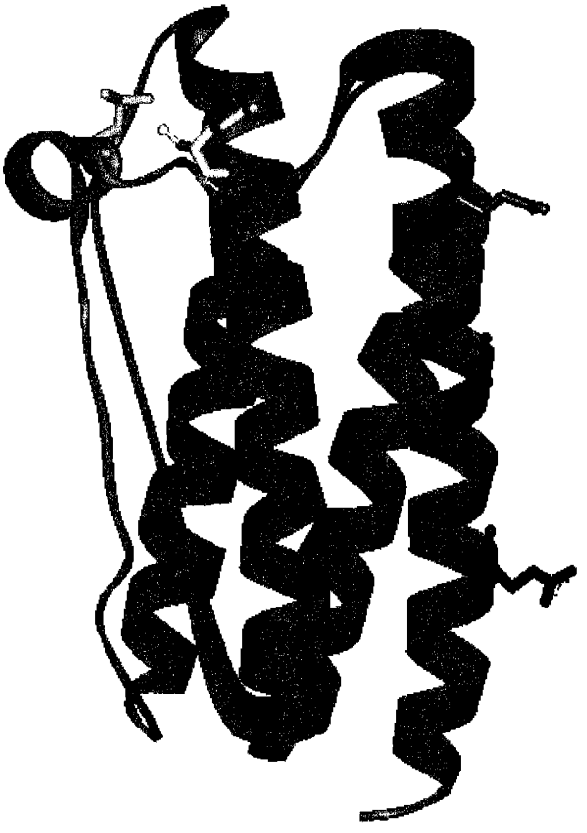

Figure 2.1: Amino acid sites considered for substitution. The native amino acid residues are Glu20 (blue), Gly27 (red), and Glu34 (orange), which lie at the major binding interface, and Glu47 (yellow) and Leu51 (green), which lie at the minor binding interface. The single mutants generated were E20A, G27L, E34A, E47A, and L51E. The structure of GCSF (entry 1RHG) was obtained from the Protein Data Bank (Berman *et al.*, 2000).

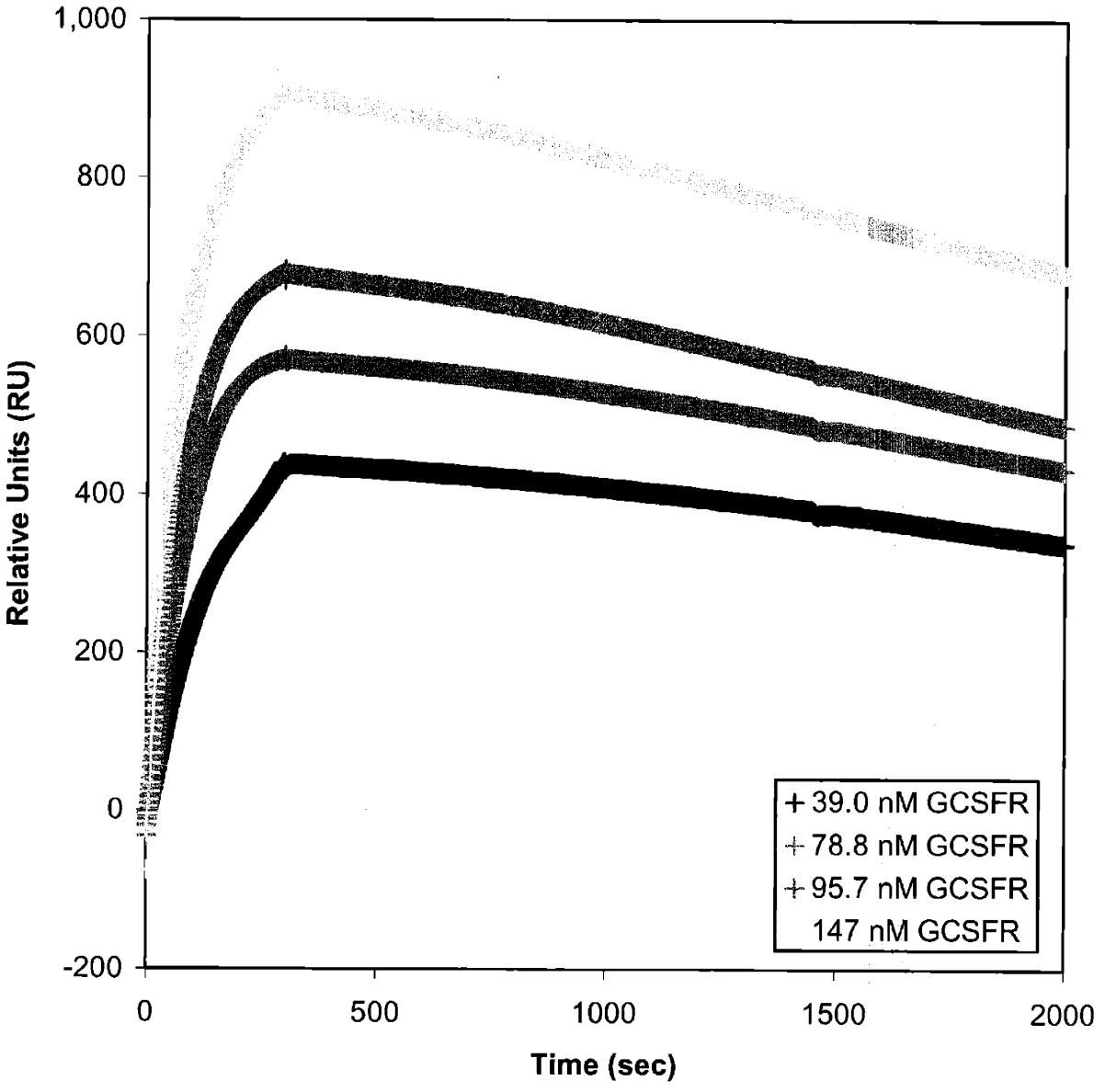

Figure 2.2: Surface plasmon resonance data for determining the effective K_D of wild type GCSF. Real time measurements of binding of GCSFR to $(His)_6$-GCSF were performed as described. 39.0 nM (teal), 78.8 nM (rose), 95.7 nM (gray) and 147 nM (beige) GCSFR were passed over a surface modified with $(His)_6$-GCSF. These representative data show a K_D of 130 pM.

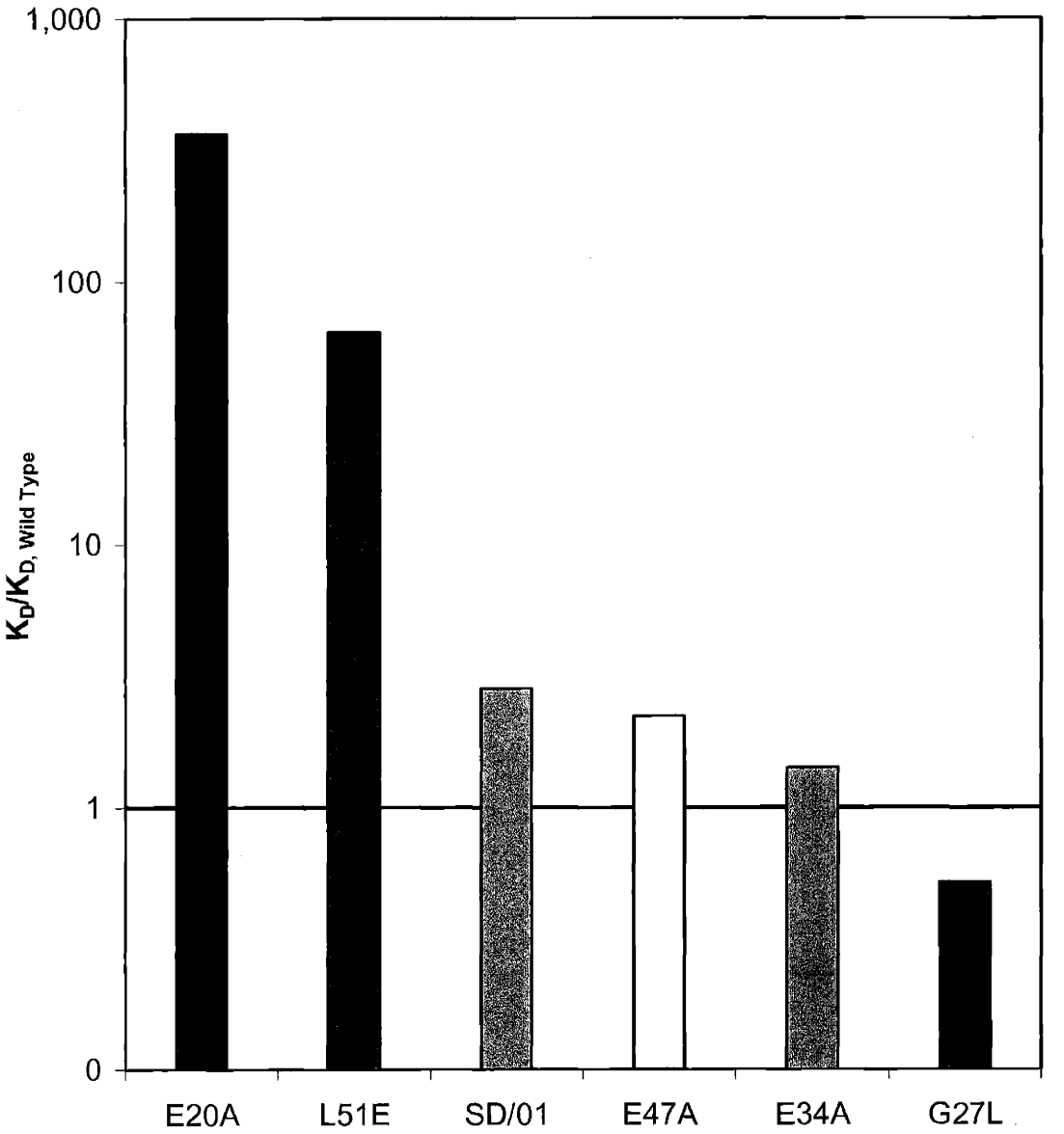

Figure 2.3: Effective K_D data for all GCSF analogs, normalized to wild type. Analogs are arranged in order of increased binding affinity from left to right. Color coding: E20A (blue), L51E (green), SD/01 (purple), E47A (yellow), E34A (orange), and G27L (red).

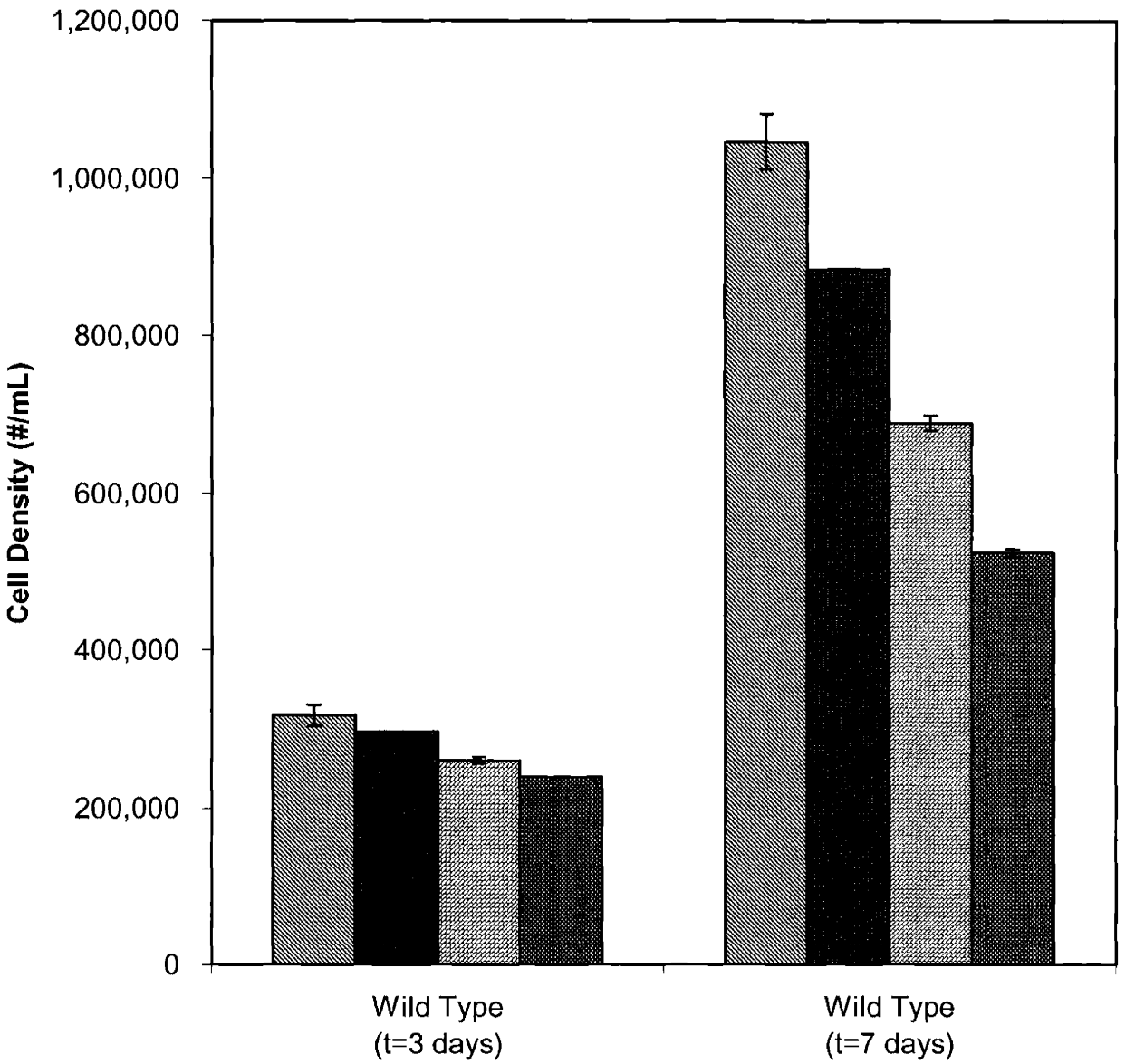

Figure 2.4A: Cell proliferation data for wild type (t = 3 and 7 days). The initial cell density for all samples was 10^5/mL, and initial ligand concentrations used were 1000 pM (diagonal lines), 500 pM (wavy lines), 250 pM (diagonal bricks), and 125 pM (spheres).

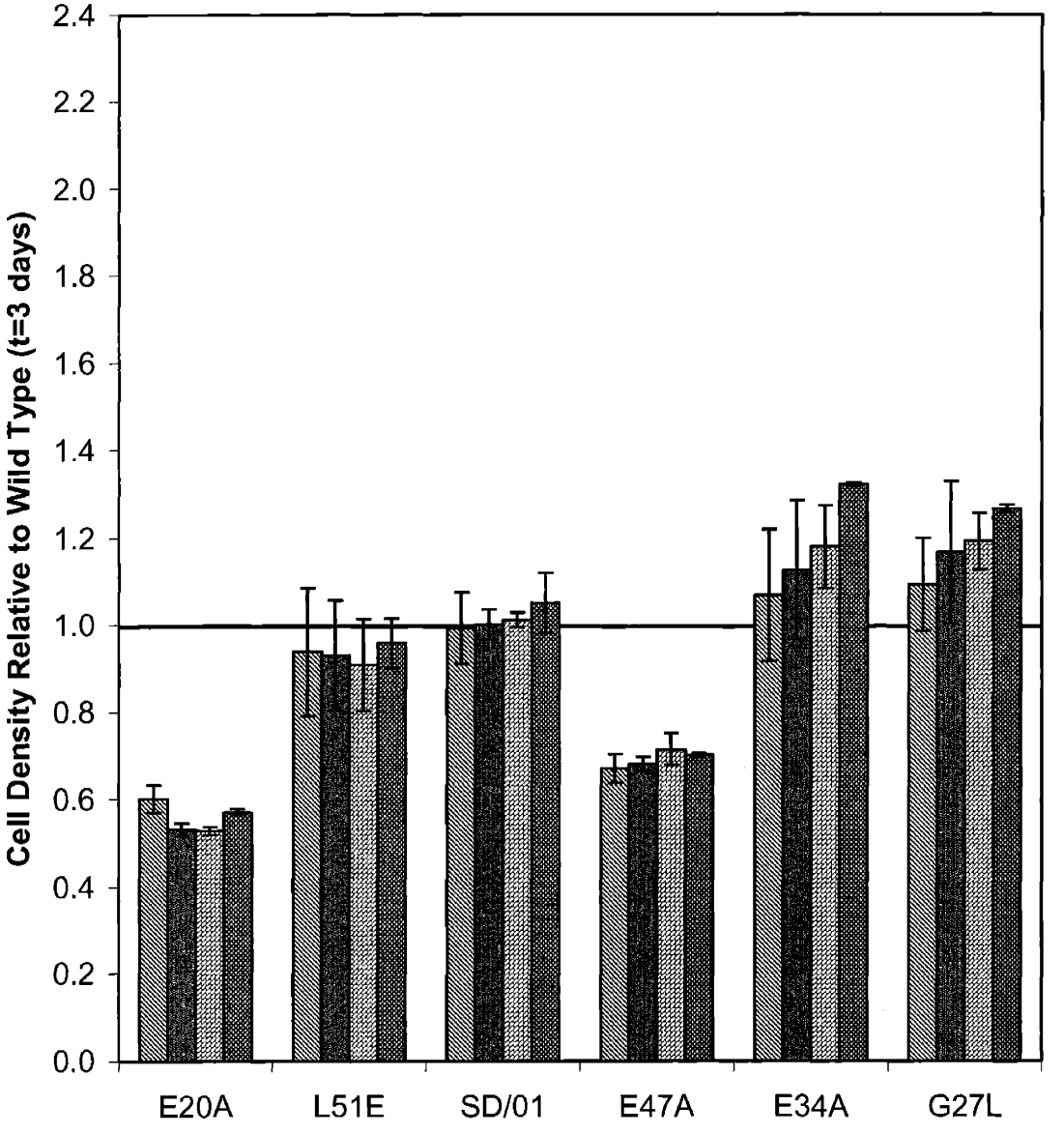

Figure 2.4B: Cell proliferation data for analogs normalized to wild type (t = 3 days). The initial cell density for all samples was 10^5/mL, and initial ligand concentrations used were 1000 pM (diagonal lines), 500 pM (wavy lines), 250 pM (diagonal bricks), and 125 pM (spheres).

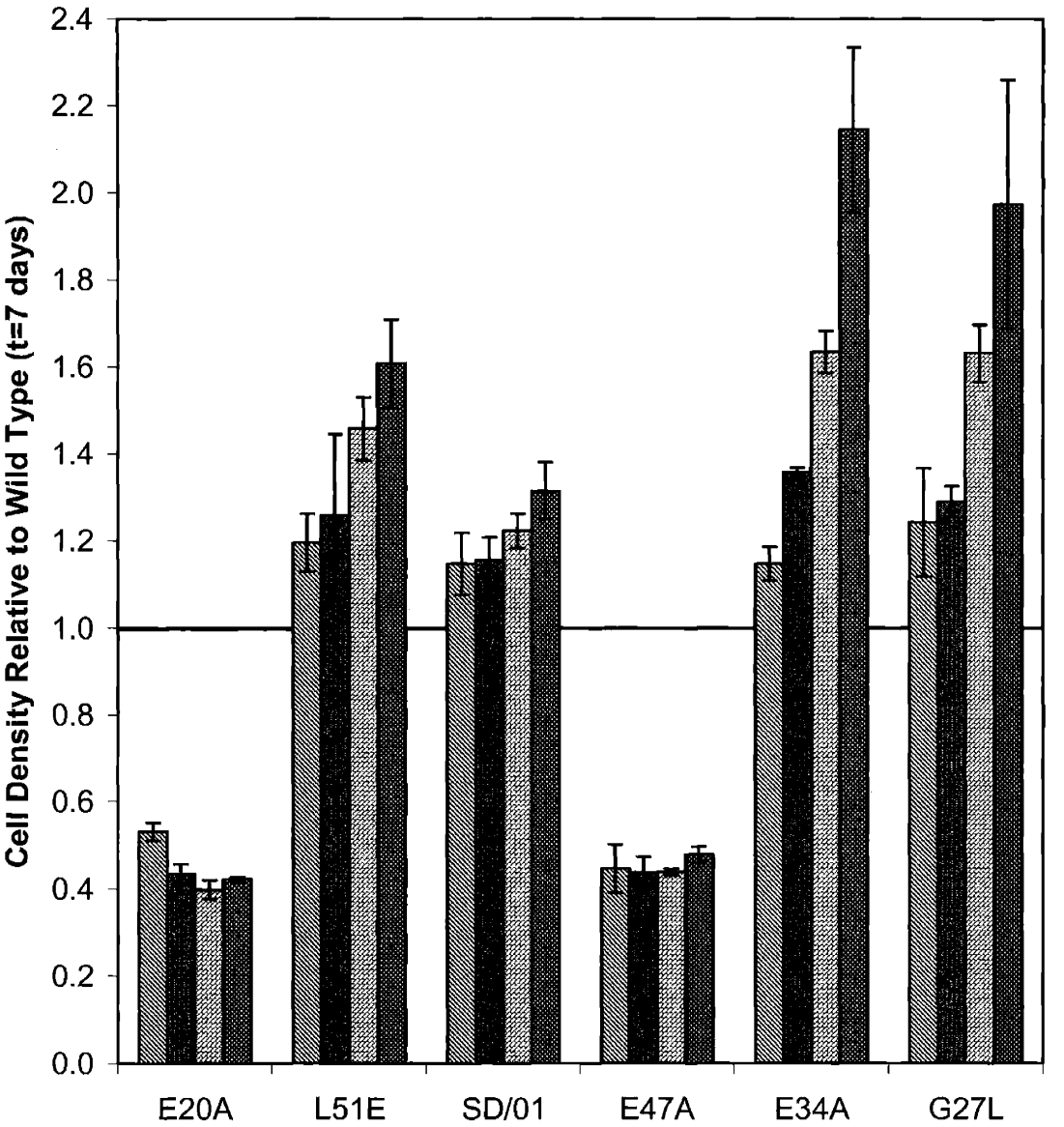

Figure 2.4C: Cell proliferation data for analogs normalized to wild type (t = 7 days). The initial cell density for all samples was 10^5/mL, and initial ligand concentrations used were 1000 pM (diagonal lines), 500 pM (wavy lines), 250 pM (diagonal bricks), and 125 pM (spheres).

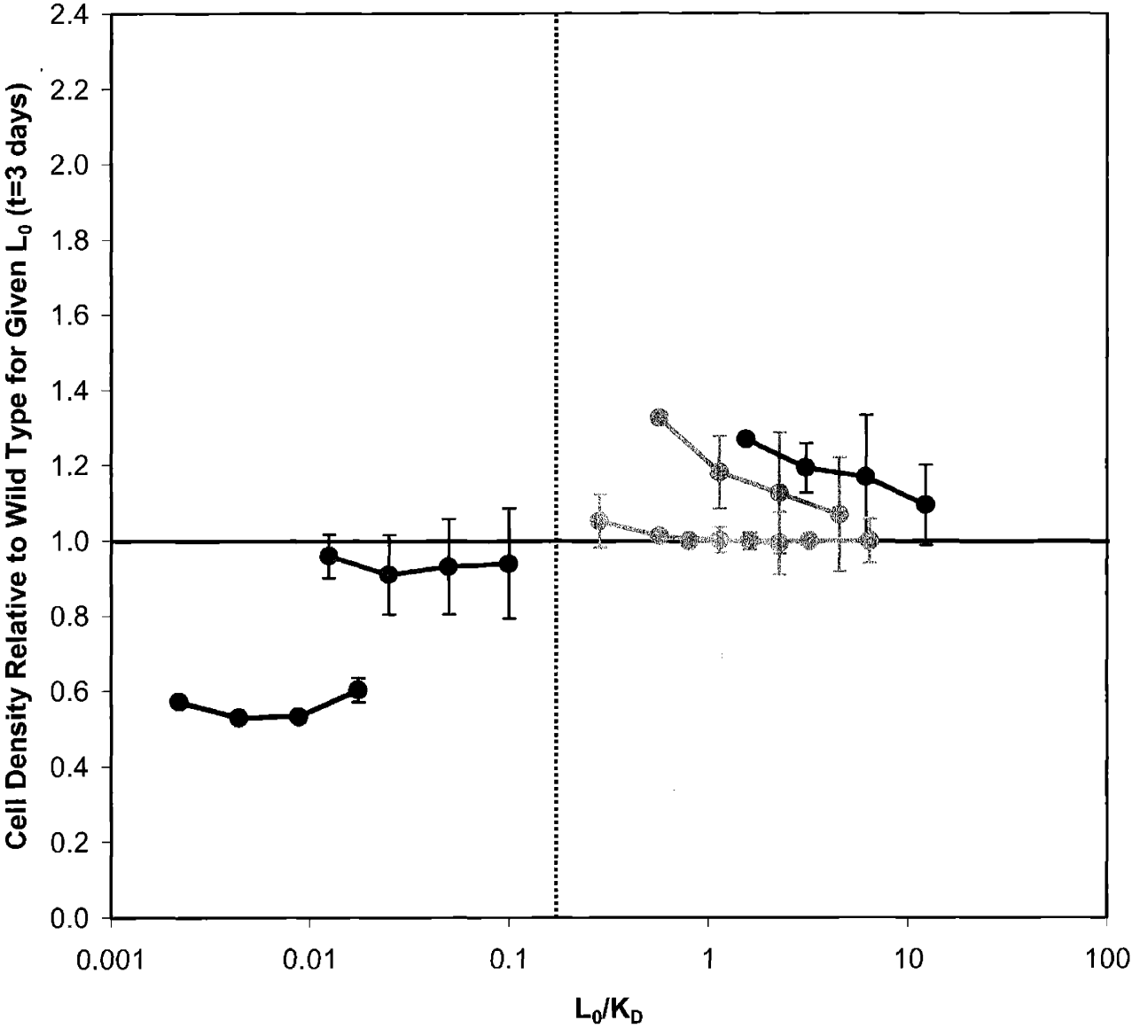

Figure 2.5A: Pharmacodynamic quadrant plot (PDQP) for t = 3 days. The PDQP is generated by normalizing the pharmacodynamic response of the analog by that of wild type at the same initial ligand concentration and plotting this *versus* the initial ligand concentration normalized by the K_D of the analog. These plots can be used to infer additional properties of the mutants, as described in the Results section. Color coding: E20A (blue), L51E (green), SD/01 (purple), E47A (yellow), E34A (orange), and G27L (red).

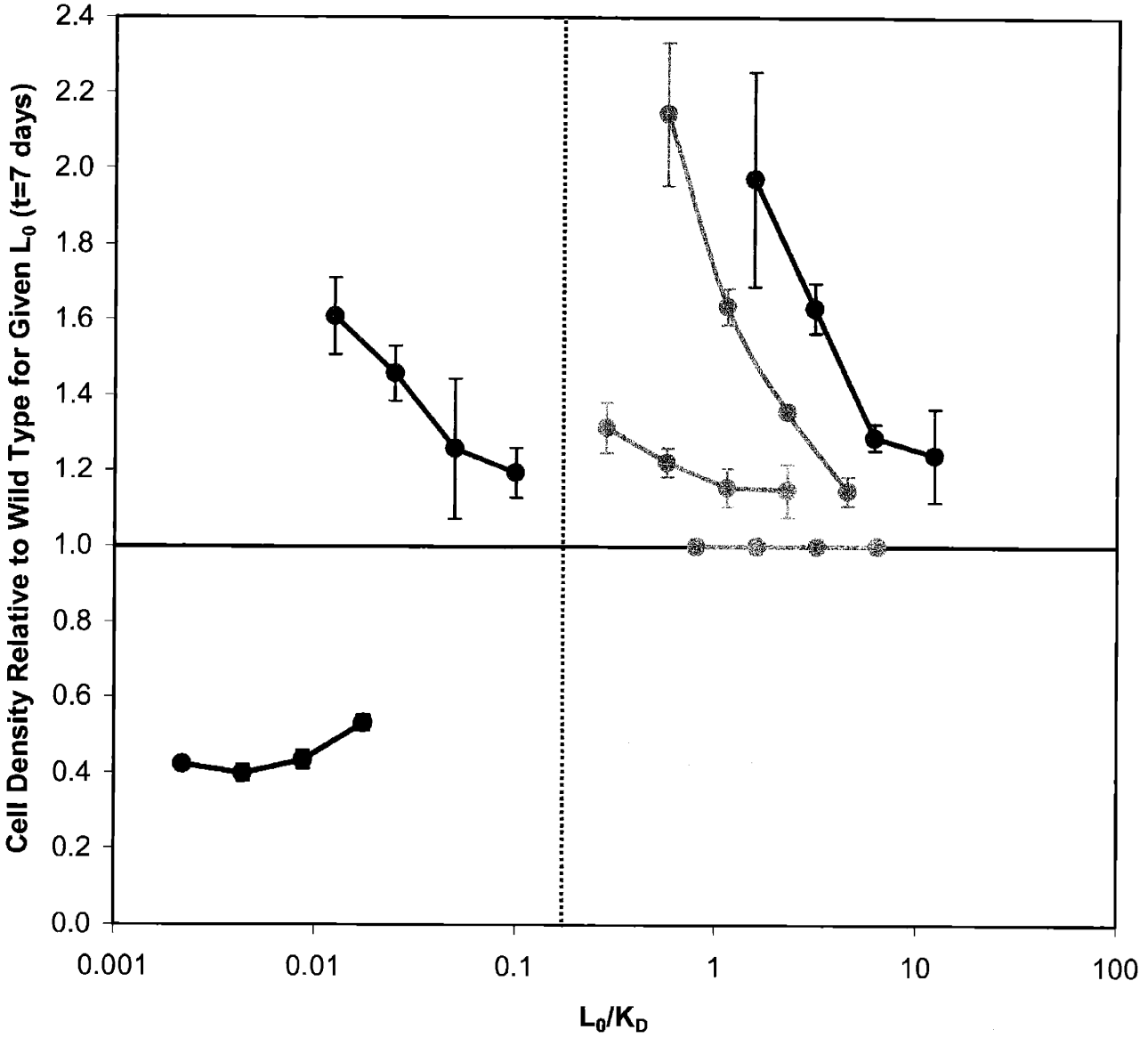

Figure 2.5B: Pharmacodynamic quadrant plot (PDQP) for t = 7 days. The PDQP is generated by normalizing the pharmacodynamic response of the analog by that of wild type at the same initial ligand concentration and plotting this *versus* the initial ligand concentration normalized by the K_D of the analog. These plots can be used to infer additional properties of the mutants, as described in the Results section. Color coding: E20A (blue), L51E (green), SD/01 (purple), E47A (yellow), E34A (orange), and G27L (red).

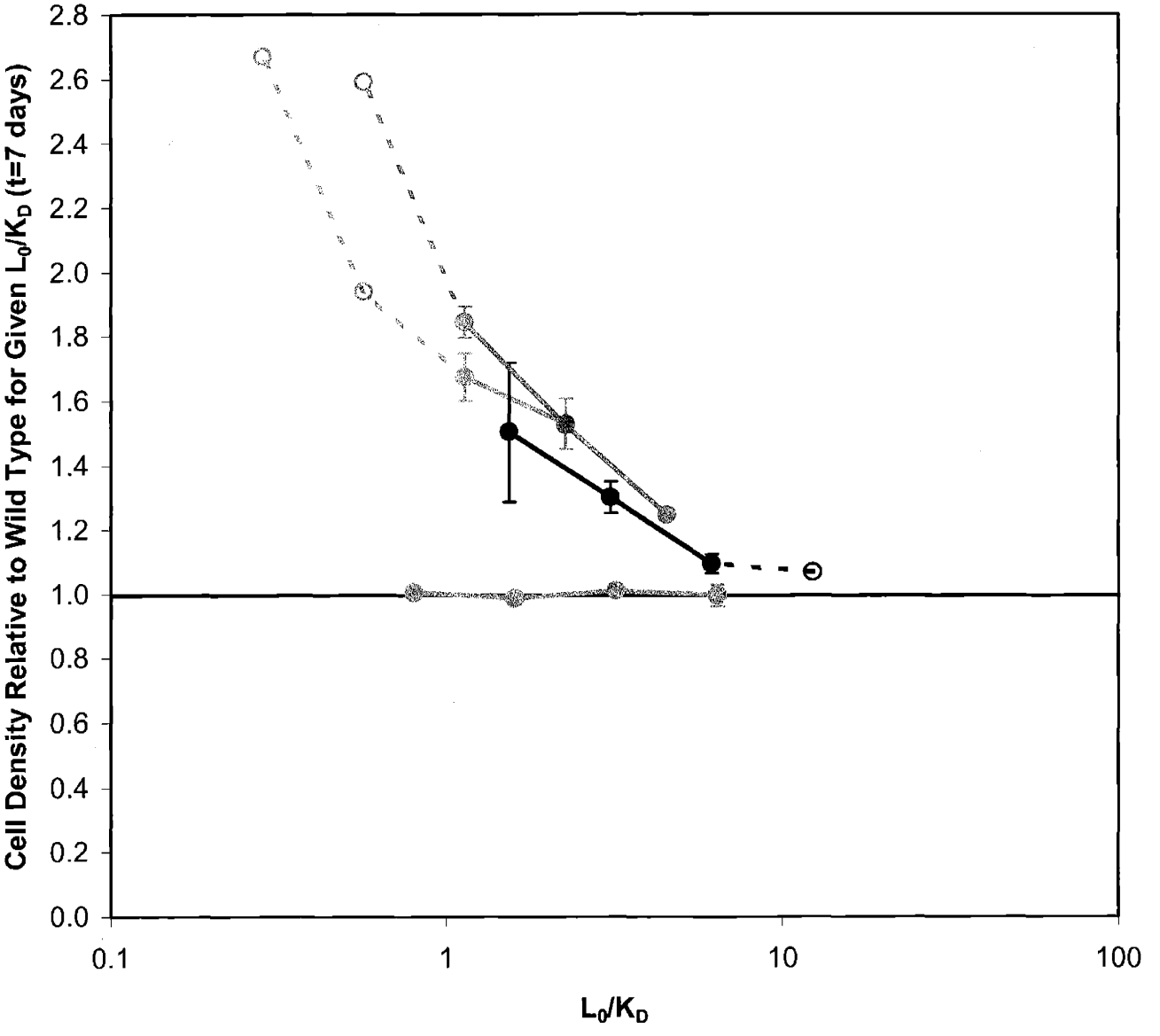

Figure 2.5C: Renormalized *y*-axis for right two quadrants in Figure 2.5B, comparing pharmacodynamic response at equivalent L_0/K_D values. These plots can be used to infer additional properties of the mutants, as described in the Results section. Color coding: E20A (blue), L51E (green), SD/01 (purple), E47A (yellow), E34A (orange), and G27L (red).

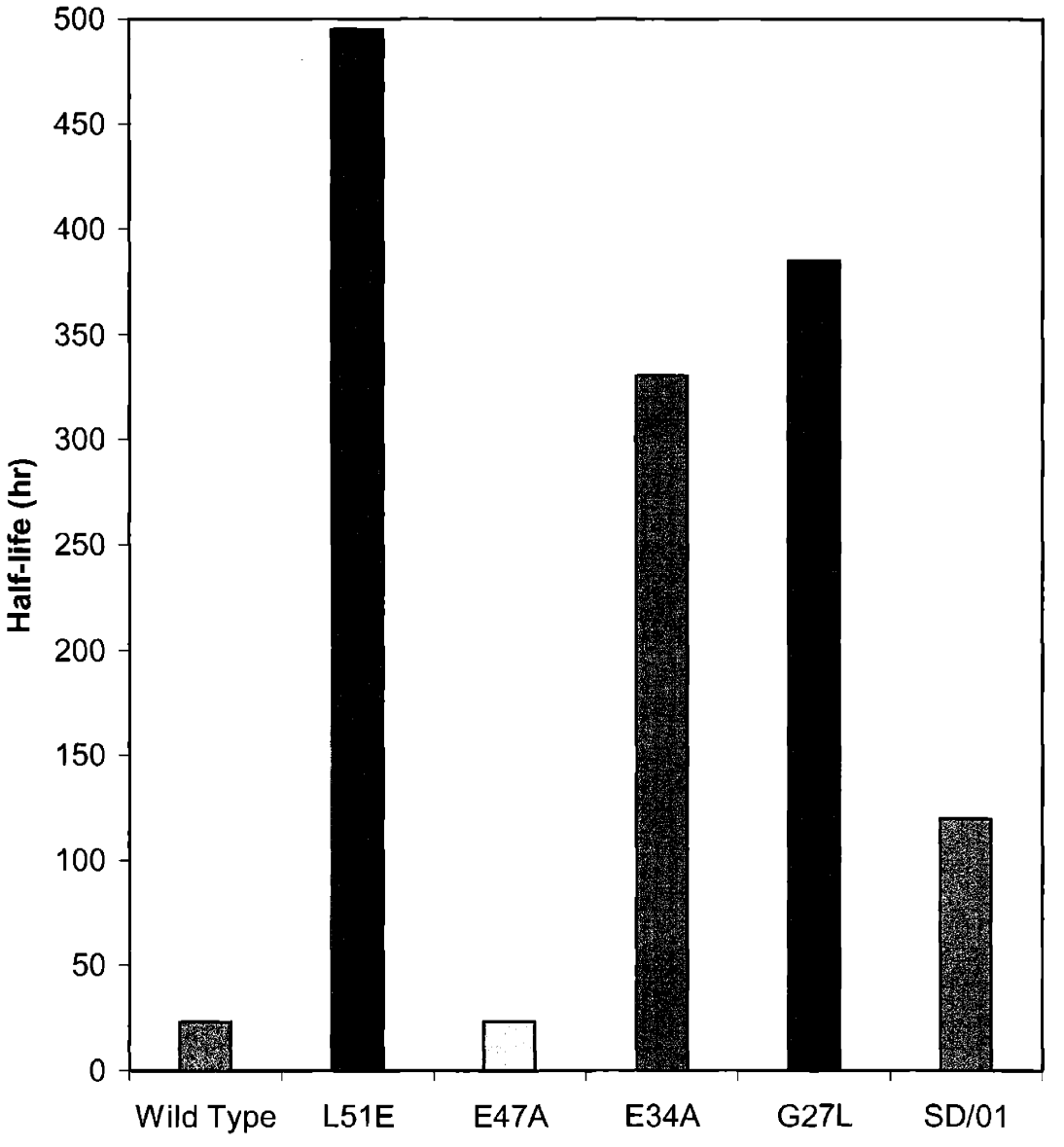

Figure 2.6: Half-life values for wild type and mutants. The initial cell density for all samples was 10^5/mL, and the initial ligand concentration was 270 pM. Color coding: L51E (green), E47A (yellow), E34A (orange), G27L (red), and SD/01 (purple).

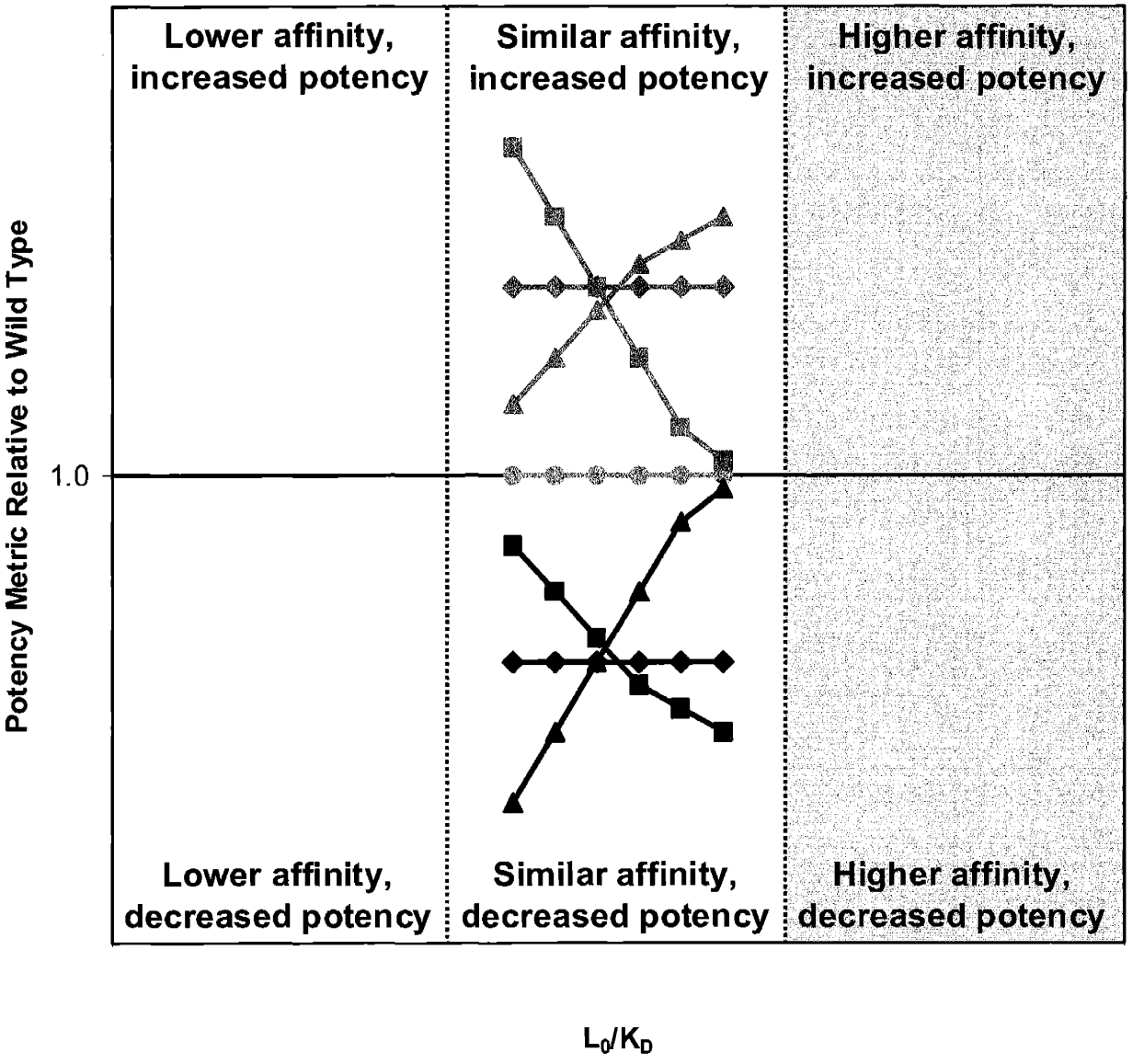

Figure 2.7: Theoretical 'binding-potency space' with examples. This general methodology can be used to deconvolute the contributions of binding, trafficking, and signaling in a manner that allows the guided generation of hypotheses for a large spectrum of ligand analogs (see Discussion). This can be used to screen for ligands with specific pharmacodynamic properties, and these predictions can be more rigorously tested by signaling and trafficking assays.

Chapter 3: Structural Stability of Granulocyte Colony-Stimulating Factor

After a cytokine binds its receptor at the cell surface (pH ~ 7), the complex is internalized into acidic endosomal compartments (pH ~ 5–6), where partially unfolded intermediates can form, and is then degraded in the lysosomes (pH ~ 4). The nature of potential pH-dependent structural transitions was studied for granulocyte colony-stimulating factor (GCSF). Tertiary structural perturbations in GCSF suggest the presence of an intermediate state, a common feature of this structural family of four-helical-bundle proteins. Unexpectedly, GCSF displays a monotonic increase in stability as the pH is decreased from 7 to 4. We hypothesize that cytokines such as GCSF with cell-based clearance mechanisms *in vivo* may have evolved to help stabilize endosomal complexes for sorting to lysosomal degradation. We show that mutants of GCSF have differential stabilities to their wild-type counterpart as a function of pH, and that these differences may explain the observed variations in ligand trafficking and depletion. Further understanding of the contributions of cytokine makeup and environmental factors on structural stability may help guide cytokine design not only with respect to physical stability and formulation, but also ligand binding, endocytic trafficking, and, consequently, therapeutic efficacy.

INTRODUCTION

Granulocyte colony-stimulating factor (GCSF) is a member of the four-helical-bundle family of proteins, having a structure similar to that of interleukin-2 (IL-2), human growth hormone (hGH), megakaryocyte growth and development factor (MGDF), erythropoietin, leptin, and many other cytokines (Brandhuber *et al.*, 1987; Hill *et al.*, 1993). One of the challenges in utilizing some of these cytokines as therapeutic agents is the difficulty in storing the products for long periods of time, since the stability of these proteins is often pH- and temperature-sensitive. Thus, additional costs for buffer formulation and product refrigeration or freezing are incurred. Multiple studies have examined the precipitation and loss of these cytokines during refolding, purification, storage, or delivery (Tzannis *et al.*, 1996; Vlasveld *et al.*, 1993; Prestrelski *et al.*, 1995; Marston, 1986; Brems, 1988; Schein, 1990; DeYoung *et al.*, 1993), and GCSF itself is known to aggregate at neutral pH,

particularly at high concentrations. Furthermore, conformational studies of GCSF as a function of pH and denaturant concentration have shown the presence of folding intermediates (Narhi *et al.*, 1991; DeFelippis *et al.*, 1993; Hamburger *et al.*, 1998). These intermediates have also been observed for other cytokines, including hGH and MGDF (Narhi *et al.*, 1991; Hamburger *et al.*, 1998). A mechanistic understanding of the roles of molecular composition of the cytokine and environmental conditions on structural stability may increase the physical stability of the formulation and may therefore lead to less stringent purification and storage criteria. We further hypothesize that structural stability of the cytokine may influence both extracellular and intracellular receptor-binding properties, and therefore lead to changes in ligand depletion.

The endocytic trafficking properties of IL-2 and a double mutant of this cytokine (L18M/L19S) have been previously studied in cells expressing the heterotrimeric IL-2 receptor (Fallon *et al.*, 2000). The α subunit of this receptor is constitutively recycled, whereas the βγ-subunit complex is constitutively degraded (Hemar *et al.*, 1995). It was determined that, while both ligands bind the extracellular receptor with similar affinity and both complexes internalize at the same rate, the double mutant recycled to a greater extent than wild type and, consequently, the mutant was depleted to a lesser extent in culture (Fallon *et al.*, 2000). Since this might be achieved by reducing the affinity of the ligand for the βγ-subunit complex in the endosomal compartments, or by increasing the affinity for the α subunit, these affinities were measured and it was confirmed that the selectivity of the mutant for the α subunit over the βγ-subunit complex is greater than that for wild-type IL-2. Subsequent structural studies revealed that the secondary and tertiary stabilities of the two ligands are similar at pH 7, but that the mutant becomes less stable as the pH is decreased to that seen under endosomal conditions (Fallon, 2000). Thus, there appears to be an inverse relationship between low-pH structural stability and ligand recycling (and half-life).

Our goal was to determine the structural stability of wild-type GCSF as a function of the endocytic trafficking pH-range and to further examine whether the inverse correlation between low-pH structural stability and ligand half-life seen for IL-2 would hold for some of the GCSF analogs studied in Chapter 2. Previous conformational studies of GCSF have shown that the molecule undergoes structural changes induced by pH, heat, and guanidine hydrochloride (Narhi *et al.*, 1991; Kolvenbach *et al.*, 1993; Kolvenbach *et al.*, 1997). GCSF

maintains its native-like helical structure over a large, acidic pH range, from 2 to 7. Although the tertiary structure differs at pH 2, 4, and 7, the maintenance of a distinct tertiary structure and the compactness at pH 2 suggest that the molecule does not adopt a partially unfolded 'A' state in acid (Kolvenbach *et al.*, 1997). At pH 4 and 7, GCSF loses its secondary and tertiary structures at the same point during thermal denaturation, whereas at pH 2 the helical structure unravels slightly before the cooperative unfolding of the remaining secondary structure and tertiary structure.

Several mutational studies have identified certain amino acids in GCSF that are involved in receptor binding and dimerization, as well as overall bioactivity (Reidhaar-Olson *et al.*, 1996; Young *et al.*, 1997; Li *et al.*, 1997). Some of these mutants have different binding and trafficking properties from wild type, resulting in altered potencies *in vitro*. As detailed in Chapter 2, an L51E mutant binds the GCSF receptor with lower affinity than wild-type GCSF, yet elicits a better cellular response and much greater half-life, possibly through reduced endocytic flux or increased endosomal recycling or some combination of these processes. Another mutant, E47A, binds the receptor with roughly the same affinity as wild-type GCSF, yet elicits a significantly worse cellular response, acting as a partial agonist. Conversely, E34A also has a similar K_D to wild type and elicits roughly the same cellular response at high ligand concentrations, yet elicits a 2-fold increase in cellular response at ligand concentrations near the K_D, which suggests enhanced endocytic trafficking properties of this mutant. E34A is located in the N-terminal helix A, and E47A and L51E are in the 3_{10}-helix segment in the long AB loop just after helix A (see Figure 1.1). The 3_{10}-helix segment is also thought to be involved in receptor binding (Li *et al.*, 1997).

Previous work in evaluating the thermodynamic stability of GCSF at neutral pH was performed to identify mutations with enhanced stability (Bishop *et al.*, 2001). The present series of equilibrium denaturation experiments investigates the unfolding transitions of GCSF as a function of pH in order to characterize structural and stability properties that may influence ligand trafficking within the pH range encountered in cellular compartments.

EXPERIMENTAL PROCEDURES

Materials

Recombinant human GCSF was produced in *Escherichia coli* at Amgen. The GCSF mutants that were studied included E34A, E47A, and L51E. Purified wild-type GCSF was stored in 0.58 mM HCl, pH 3.0, and the GCSF mutants were in a buffer of 10 mM sodium acetate, 100 mM NaCl, pH 5.0.

The buffer for the full circular dichroism scans was 1 mM sodium citrate, 1 mM sodium phosphate, 1 mM sodium borate, pH 4 through 7. For the denaturation studies, the buffer was 50 mM Tris-HCl, 20 mM sodium acetate, 20 mM MES, pH 4 through 7. Ultra pure guanidine hydrochloride (GuHCl) was obtained from ICN and Pierce.

Circular dichroism

Circular dichroism (CD) in the far-UV region was performed using an Aviv CD spectrometer (model 62A DS) with a titrator (Microlab 500 series). The far-UV signal was measured at 222 nm, and the full spectrum was recorded between 300 nm and 180 nm. The equilibrium denaturation studies were performed by preparing stock protein solutions at 0.025 mg/mL in 50 mM Tris-HCl, 20 mM sodium acetate, 20 mM MES with 0 M or > 6 M GuHCl at each pH. After each CD measurement, the titration apparatus removed a set volume of sample from the cuvette and injected an equivalent volume of denatured protein, increasing the concentration of GuHCl by 0.1 M each time. After each injection, the sample was stirred and equilibrated before the next measurement was made.

Near-UV CD measurements were made on a Jasco spectropolarimeter (model J-720). Full wavelength scans were recorded between 320 nm and 250 nm using 0.5 mg/mL protein solutions, and the near-UV signals at 291 nm and 280 nm are reported as measures of tertiary structure at each pH.

Fluorescence

For the fluorescence studies, an Aviv automated titrating differential/ratio spectrofluorometer (model ATF105) with a titrator was used, and equilibrium denaturation studies were performed by preparing stock protein solutions at 0.025 mg/mL in 50 mM Tris-HCl, 20 mM sodium acetate, 20 mM MES with 0 M or > 6 M GuHCl at each pH. Samples

were excited at either 280 nm or 295 nm, and full emission scans were recorded from 400 nm to 300 nm. Manual pH titrations for wild type and the mutants were performed from pH 7 to pH 3, and emission scans were recorded at each pH value to monitor tertiary structural changes as a function of pH.

Equilibrium denaturation studies using fluorescence were performed similarly to those described for CD. Each sample was excited at 280 nm and the fluorescence signal was monitored at 350 nm (the emission maximum). The titrator then removed an aliquot from the cuvette and injected an equivalent volume of denatured protein, increasing the concentration of GuHCl by 0.1 M each time. The sample was mixed and equilibrated before the next reading was made.

RESULTS

Upon binding to GCSFR at cell surface pH (~ 7), GCSF is internalized into vesicles that eventually fuse with endosomal compartments, which are acidified to pH ~ 5–6 by proton pumps. Here, the molecular components can either by recycled intact or degraded in lysosomal compartments (pH ~ 4). We examined the structure and stability of wild-type GCSF and several mutants as a function of this pH range. Changes in tertiary structure as a function of pH were monitored by both intrinsic fluorescence and near-UV circular dichroism (CD). Equilibrium denaturation studies provided information on ligand stability as a function of pH; far-UV CD was used to probe secondary structure (helical content) and intrinsic fluorescence was used to monitor tertiary structure (local tryptophan environment). These results may help determine whether the properties of GCSF are altered by the various pH environments to which the molecule is exposed during extracellular binding and endocytic trafficking.

Structural analysis of wild-type GCSF as a function of pH

The secondary structure of wild-type GCSF was monitored by far-UV CD across a pH range from 7 to 4. These data indicate that the proteins displayed similar helical content (as assessed by the CD signal at 222 nm), with no changes in secondary structure in this range (Figure 3.1). Additionally, intrinsic fluorescence of tryptophan (and tyrosine) residues was used to probe tertiary structural changes as a function of pH. In contrast to the results

for secondary structure, wild-type GCSF displayed a significant decrease in intrinsic fluorescence as the environment became more acidic (Figure 3.2). This pH-induced change in intrinsic fluorescence is accompanied by increased near-UV CD signals at 291 nm and 280 nm as a function of pH (Figure 3.3). This structural change could be due to local charge changes near the tryptophan residues as the neighboring histidine residues are titrated (His157–Trp59, His80–Trp119). In addition, slight tertiary conformational changes may contribute to the altered fluorescence and near-UV CD signals as a function of pH (Bishop *et al.*, 2001; Narhi *et al.*, 1991; Kolvenbach *et al.*, 1993).

Secondary and tertiary structural stabilities of wild-type GCSF

Equilibrium denaturation studies were performed on GCSF from pH 7 to 4 to test for structural stability. Secondary structural transitions, monitored by far-UV CD signal at 222 nm to detect loss of helicity, are shown for each pH in Figure 3.4. As in previous studies with IL-2, GCSF displays increased stability under acidic conditions.

Figure 3.5 shows the intrinsic fluorescence data for the equilibrium denaturation transitions for this pH range. Measurements at pH 7 were difficult to make because of protein instability that resulted in baseline artifacts in generating the two-state unfolding curves. Measurements at pH 6 were not possible because the emission spectra for native and denatured GCSF were almost indistinguishable. Nonetheless, similar to the results for secondary structure, the data suggest that the tertiary structure of GCSF is more stable at acidic pH. The noncoincidence in CD and fluorescence transitions (Figure 3.6) was minor and within the error of the measurement. Generally, the denaturation midpoint by fluorescence was slightly lower but within 0.05M GuHCl units of the CD denaturation midpoint.

Structural properties of GCSF mutants compared to wild type

Secondary and tertiary structural stability studies were also performed on several GCSF mutants, including E34A, E47A, and L51E. These analogs all display structural properties similar to wild type: no change in secondary structure across the pH range for cellular trafficking, pH-dependent change in tertiary structure, increases in secondary and

tertiary structural stabilities as pH decreases from 7 to 4, and negligible noncoincidences in CD and fluorescence transitions.

We can use the unfolding information to calculate the free energy of unfolding for each ligand in a two-state model:

$$\Delta G_{unfolding} = -RT \ln\left(\frac{f_U}{1-f_U}\right) \tag{3.1}$$

where f_U is the fraction of protein unfolded. We can also look at the relative change in the free energy of unfolding

$$\Delta\Delta G_{unfolding} = \Delta G_{unfolding} - \Delta G_{unfolding,WT} \tag{3.2}$$

for each mutant over the pH range for cell trafficking. Using Equations 3.1 and 3.2, these relative changes are given in Figure 3.7. With the exception of E47A, the mutants are more stable than wild-type GCSF at pH 7. All of the mutants are less stable than wild type in conditions representative of the endosomal environment (pH 5–6), and mostly so in lysosomal conditions (pH 4).

DISCUSSION

Role of intermediates in protein folding

For many recombinantly produced small globular proteins, the molecules are often secreted as aggregates in inclusion bodies, necessitating denaturation and refolding to obtain native-like product. The kinetic process of refolding involves the rapid burial of hydrophobic amino acids into the core of the protein, minimizing the thermodynamic penalty for exposing such residues to the aqueous environment (Kim and Baldwin, 1990). Our equilibrium denaturation studies provide essentially the reverse analogy for this refolding process. Each increment along the unfolding pathway in our experiments can represent a kinetic or thermodynamic intermediate in refolding, depending on how the refolding is carried out.

Structural studies on cytokines have frequently identified a molten globule intermediate with partial disruption of tertiary structure and intact native-like secondary structure (Hamburger *et al.*, 1998; Ptitsyn *et al.*, 1990; Brems and Havel, 1989). For GCSF, there are two tryptophan residues that can serve as spectral markers for monitoring such

tertiary structural transitions. However, each of these residues is in close proximity to a histidine (His 156–Trp 58, His 79–Trp 118); therefore, observed changes in the intrinsic fluorescence and near-UV signatures may actually result from local charge changes due to histidine titration or from subtle tertiary structural changes (Figures 3.2 and 3.3).

Proposed role of acid stability in cellular trafficking

Enhanced stability at low pH is an unusual property for small monomeric proteins. In fact, many small monomeric proteins undergo conformational destabilization under acidic conditions. Previous studies of about 20 monomeric proteins have indicated that these proteins fall in distinct categories displaying certain acid unfolding transitions that depend on the type of protein and the buffer conditions (Fink *et al.*, 1994). In particular, a partially unfolded conformer may exist at pH 3–4, and lower pH values may populate the acid unfolded 'A' state, which is less compact than the molten globule state. The populations of these conformers and the nature of the acid denaturation transitions are affected by denaturant, salt, and temperature.

Surprisingly, both GCSF and IL-2 display increased stability at low pH. In contrast, this increase in stability is not observed for hGH, which suggests that this phenomenon is not a common feature of 4-helical-bundle cytokines. Both GCSF and IL-2 have significant clearance mechanisms *in vivo* by the very cell populations that they induce to expand (neutrophils for GCSF and T-lymphocytes for IL-2). These negative feedback mechanisms are crucial in regulating bloodstream levels of GCSF/neutrophils and IL-2/T-lymphocytes. Therefore, we conjecture that these cytokines may have evolved to have increased structural stability at low pH to ensure that they remain bound to their respective lysosomally targeted receptors (GCSF receptor or βγ-subunit complex of the IL-2 receptor) within the acidic endosomal environment. The ligand therefore gets degraded in the lysosomes as part of an optimized cell-based clearance mechanism. By contrast, hGH does not have a dominant cell-based clearance mechanism *in vivo*.

However, for applications as therapeutic proteins, the native ligands may be improved by engineering for superior endocytic trafficking properties (Lauffenburger *et al.*, 1998). Ligand/receptor trafficking can depend substantially on the variations in extracellular and intracellular environments, including the differences in pH. This is true not only for

complexes with cytokine receptors but also for those formed with transport receptors such as the transferrin receptor (Hopkins and Trowbridge, 1983). The pH-sensitivity of the ligand/receptor interaction can impact endosomal sorting, thereby regulating the fractions of ligand and receptor that are recycled, degraded, and transcytosed (Maier and Steverding, 1996). These processes are contingent upon exquisite recognition between the ligand and receptor, and even slight differences in conformational stability may have significant effects on endocytic trafficking. For cytokines that have primarily cell-based clearance mechanisms, the extent of endosomal ligand sorting to recycling versus degradation may be controlled by structural or stability properties at low pH.

Possible role for structural stability in altering endocytic trafficking

Specific amino acid substitutions can have large effects on protein folding and stability (Ptitsyn *et al.*, 1990; Brems and Havel, 1989) and thus alter the steps involved in product purification and formulation. Additionally, such mutations in a cytokine can alter its conformational stability at low pH and thereby impact its endocytic trafficking properties. In a system where the number of ligands per cell is not limiting (French and Lauffenburger, 1997), mutants with lower stability relative to wild type may dissociate from the receptor complex or from certain receptor subunits under acidic conditions, and thereby reduce exposure to the lysosomal proteases and enhance recycling to the extracellular space.

Previous studies with IL-2 support an inverse correlation between low-pH structural stability and ligand recycling (and half-life). A double mutant of IL-2 (L18M/L19S) was found to recycle to a greater extent than wild type, resulting in a longer half-life (Fallon *et al.*, 2000). This could have been achieved by reducing the affinity of the ligand for the constitutively degraded $\beta\gamma$-subunit complex in the endosomal compartments, or by increasing the affinity for the constitutively recycled α subunit. Indeed, the mutant displayed enhanced selectivity for the α subunit over the $\beta\gamma$-subunit complex in comparison to wild type (Fallon *et al.*, 2000). Structural studies on these two ligands revealed that the secondary and tertiary stabilities of the two ligands are similar at pH 7, but that the mutant becomes less stable as the pH is decreased to that experienced in endosomal compartments (Fallon, 2000). This decrease in conformational stability could alter the dynamic between the ligand and the receptor subunits, contributing to the observed changes in endocytic trafficking.

To determine whether this relationship between low-pH structural stability and ligand half-life might apply to the analogous GCSF/GCSFR system, we also measured the structural stabilities of GCSF mutants studied in Chapter 2: E34A, E47A, and L51E. Detailed endocytic trafficking measurements of these mutants are beyond the scope of this work, but half-life measurements were performed (see Figure 2.6). Thus, we could see whether this phenomenological comparison is consistent with what was observed for IL-2.

From Figure 3.7, all of the mutants are more stable than wild type at pH 7, with the exception of E47A. Furthermore, E34A is less stable than wild type at endosomal pH (5–6), suggesting that this mutant may have enhanced recycling in comparison to wild type. The L51E analog appears to be the least stable of all ligands at pH 5–6, indicating that it may have an even greater ligand recycling fraction. Finally, E47A is less stable than wild-type GCSF at pH 7, which suggests that it may be more prone to neutral-pH aggregation than the native protein, although this may be balanced by enhanced endosomal recycling. Thus, the predictions of half-life based solely on the pH-structural stability data presented in Figure 3.7 are: L51E > E34A > E47A ~ wild type. This trend is consistent with experimentally determined half-life values (Figure 2.6).

Thus, for cytokines that have substantial cell-based clearance mechanisms, the extent of endosomal ligand sorting to recycling versus degradation may be controlled by structural or stability properties at low pH. The overall increase in stability at low pH (see Figures 3.4 and 3.5) may allow sufficient structural stability to preserve binding to the receptor leading to degradation in the lyososomes. If acid unfolding were to occur, disruption of the ligand/receptor complex may result in the free ligand being recycled to the cell surface. For proteins that have primarily cell-based clearance mechanisms, the wild-type molecule may be designed for optimal lysosomal degradation. In addition to differences in ligand/receptor dynamics, structural perturbations at low pH may also affect the susceptibility to proteolysis in the lysosomes. Since L51E and E34A are less stable than wild type molecules at low pH, one would expect the variants to be more susceptible to proteolysis. However, data indicate that these analogs elicit reduced degradation of ligand compared to wild type (Figure 2.6). Thus, a possible explanation is that the enhanced recycling of the less stable molecules outweighs (or occurs prior to) the susceptibility to proteolytic degradation.

In general, amino acid mutagenesis may be a useful strategy for improving the physical stability of therapeutic proteins for purification, refolding, formulation, and long-term storage. Additionally, mutants that tweak the balance between recycling and lysosomal degradation may display significant improvements in overall local pharmacokinetics, and result in more effective therapeutics.

REFERENCES

Bishop, B., Koay, D.C., Sartorelli, A.C. and Regan, L. (2001). Reengineering granulocyte colony-stimulating factor for enhanced stability. *Journal of Biological Chemistry.* **276:** 33465-33470.

Brandhuber, B.J., Boone, T., Kenney, W.C. and McKay, D.B. (1987). 3-dimensional structure of interleukin-2. *Science.* **238:** 1707-1709.

Brems, D.N. (1988). Solubility of different folding conformers of bovine growth hormone. *Biochemistry.* **27:** 4541-4546.

Brems, D.N. and Havel, H.A. (1989). Folding of bovine growth hormone is consistent with the molten globule hypothesis. *Proteins: Structure, Function, and Genetics.* **5:** 93-95.

DeFelippis, M.R., Alter, L.A., Pekar, A.H., Havel, H.A. and Brems, D.N. (1993). Evidence for a self-associating equilibrium intermediate during folding of human growth hormone. *Biochemistry.* **32:** 1555-1562.

DeYoung, L.R., Fink, A.L. and Dill, K.A. (1993). Aggregation of globular proteins. *Accounts of Chemical Research.* **26:** 614-620.

Fallon, E.M. (2000). Analysis of trafficking dynamics and cellular response in the interleukin-2 ligand/receptor system. Ph.D. Thesis, Chemical Engineering, Massachusetts Institute of Technology, Cambridge, MA.

Fallon, E.M., Liparoto, S.F., Lee, K.J., Ciardelli, T.L. and Lauffenburger, D.A. (2000). Increased endosomal sorting of ligand to recycling enhances potency of an interleukin-2 analog. *Journal of Biological Chemistry.* **275:** 6790-6797.

Fink, A.L., Calciano, L.J., Goto, Y., Kurotsu, T. and Palleros, D.R. (1994). Classification of acid denaturation of proteins: intermediates and unfolded states. *Biochemistry.* **33:** 12504-12511.

French, A.R. and Lauffenburger, D.A. (1997). Controlling receptor/ligand trafficking: effects of cellular and molecular properties on endosomal sorting. *Annals of Biomedical Engineering.* **25:** 690-707.

Hamburger, J.B., Chen, E., Narhi, L.O., Wu, G.M. and Brems, D.N. (1998). Multiple conformational states of a new hematopoietic cytokine (megakaryocyte growth and development factor): pH- and urea- induced denaturation. *Proteins: Structure, Function, and Genetics.* **32:** 495-503.

Hemar, A., Subtil, A., Lieb, M., Morelon, E., Hellio, R. and Dautryvarsat, A. (1995). Endocytosis of interleukin-2 receptors in human T lymphocytes: distinct intracellular localization and fate of the receptor α-chain, β-chain, and γ-chain. *Journal of Cell Biology.* **129:** 55-64.

Hill, C.P., Osslund, T.D. and Eisenberg, D. (1993). The structure of granulocyte colony-stimulating factor and Its relationship to other growth factors. *Proceedings of the National Academy of Sciences USA.* **90:** 5167-5171.

Hopkins, C.R. and Trowbridge, I.S. (1983). Internalization and processing of transferrin and the transferrin receptor in human carcinoma A431 cells. *Journal of Cell Biology.* **97:** 508-521.

Kim, P.S. and Baldwin, R.L. (1990). Intermediates in the folding reactions of small proteins. *Annual Review of Biochemistry.* **59:** 631-660.

Kolvenbach, C.G., Elliott, S., Sachdev, R., Arakawa, T. and Narhi, L.O. (1993). Characterization of two fluorescent tryptophans in recombinant human granulocyte

colony-stimulating factor: comparison of native sequence protein and tryptophan-deficient mutants. *Journal of Protein Chemistry*. **12:** 229-236.

Kolvenbach, C.G., Narhi, L.O., Philo, J.S., Li, T.S., Zhang, M. and Arakawa, T. (1997). Granulocyte colony-stimulating factor maintains a thermally stable, compact, partially folded structure at pH 2. *Journal of Peptide Research*. **50:** 310-318.

Lauffenburger, D.A., Fallon, E.M. and Haugh, J.M. (1998). Scratching the (cell) surface: cytokine engineering for improved ligand/receptor trafficking dynamics. *Chemistry & Biology*. **5:** R257-R263.

Li, T.S., Horan, T., Osslund, T., Stearns, G. and Arakawa, T. (1997). Conformational changes in G-CSF/receptor complex as investigated by isotope-edited FTIR spectroscopy. *Biochemistry*. **36:** 8849-8857.

Maier, A. and Steverding, D. (1996). Low affinity of Trypanosoma brucei transferrin receptor to apotransferrin at pH 5 explains the fate of the ligand during endocytosis. *FEBS Letters*. **396:** 87-89.

Marston, F.A.O. (1986). The purification of eukaryotic polypeptides synthesized in *Escherichia coli*. *Biochemical Journal*. **240:** 1-12.

Narhi, L.O., Kenney, W.C. and Arakawa, T. (1991). Conformational changes of recombinant human granulocyte colony-stimulating factor induced by pH and guanidine hydrochloride. *Journal of Protein Chemistry*. **10:** 359-367.

Prestrelski, S.J., Pikal, K.A. and Arakawa, T. (1995). Optimization of lyophilization conditions for recombinant human interleukin-2 by dried-state conformational analysis using Fourier transform infrared spectroscopy. *Pharmaceutical Research*. **12:** 1250-1259.

Ptitsyn, O.B., Pain, R.H., Semisotnov, G.V., Zerovnik, E. and Razgulyaev, O.I. (1990). Evidence for a molten globule state as a general intermediate in protein folding. *FEBS Letters*. **262:** 20-24.

Reidhaar-Olson, J.F., De Souza-Hart, J.A. and Selick, H.E. (1996). Identification of residues critical to the activity of human granulocyte colony-stimulating factor. *Biochemistry*. **35:** 9034-9041.

Schein, C.H. (1990). Solubility as a function of protein structure and solvent components. *Bio/Technology*. **8:** 308-315.

Tzannis, S.T., Hrushesky, W.J.M., Wood, P.A. and Przybycien, T.M. (1996). Irreversible inactivation of interleukin 2 in a pump-based delivery environment. *Proceedings of the National Academy of Sciences USA*. **93:** 5460-5465.

Vlasveld, L.T., Beijnen, J.H., Sein, J.J., Rankin, E.M., Melief, C.J.M. and Hekman, A. (1993). Reconstitution of recombinant interleukin-2 (rIL-2): a comparative study of various rIL-2 muteins. *European Journal of Cancer*. **29A:** 1977-1979.

Young, D.C., Zhan, H.J., Cheng, Q.L., Hou, J.Z. and Matthews, D.J. (1997). Characterization of the receptor binding determinants of granulocyte colony stimulating factor. *Protein Science*. **6:** 1228-1236.

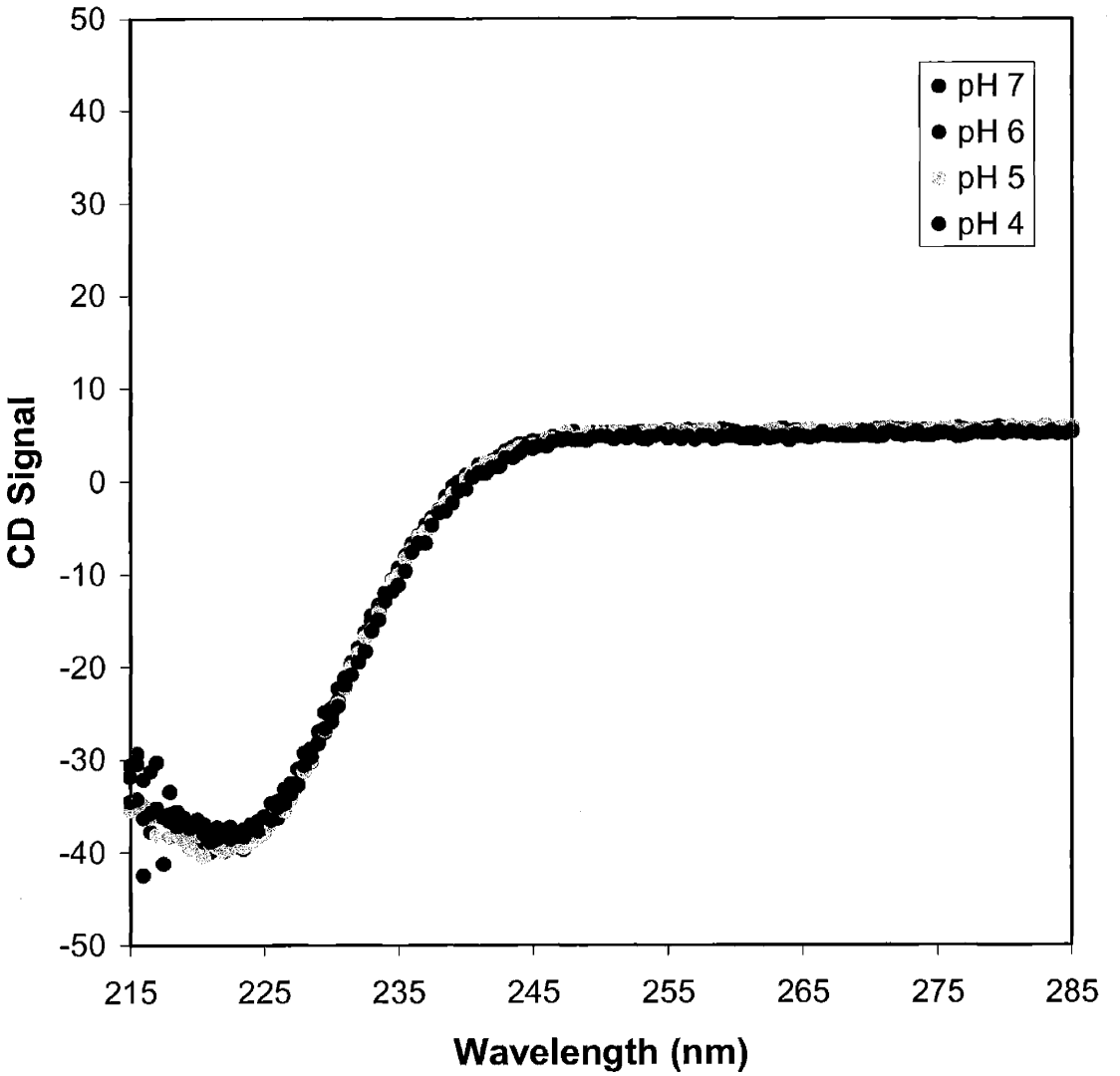

Figure 3.1: Far-UV CD scans of GCSF from pH 7 to 4. Scans are performed between 300 nm and 180 nm, with the degree of helicity measured at 222 nm.

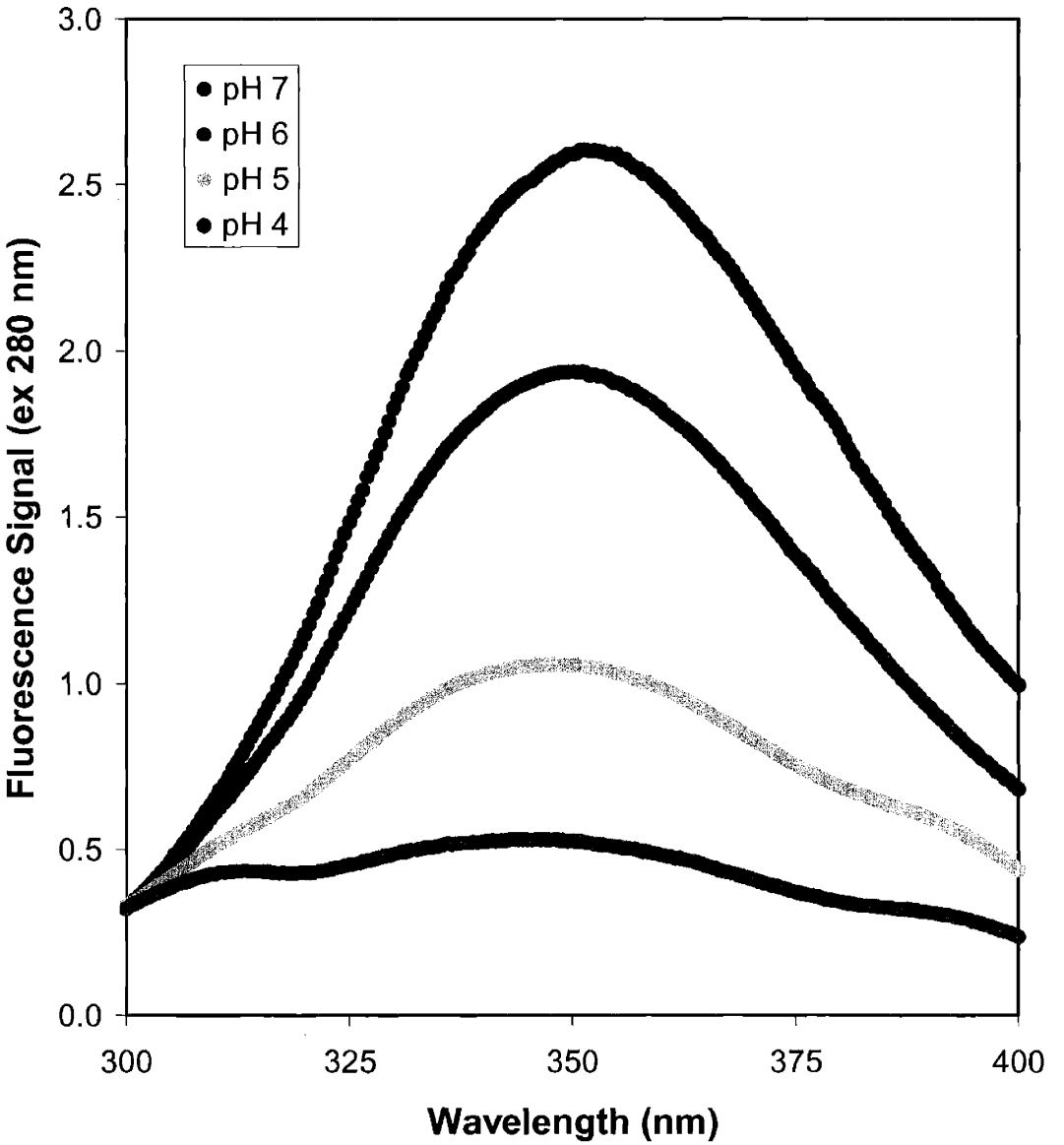

Figure 3.2: Emission scans of GCSF from pH 7 to 4. Scans are performed between 400 nm and 300 nm with an excitation of 280 nm, with an emission maximum of 350 nm used in equilibrium denaturation studies.

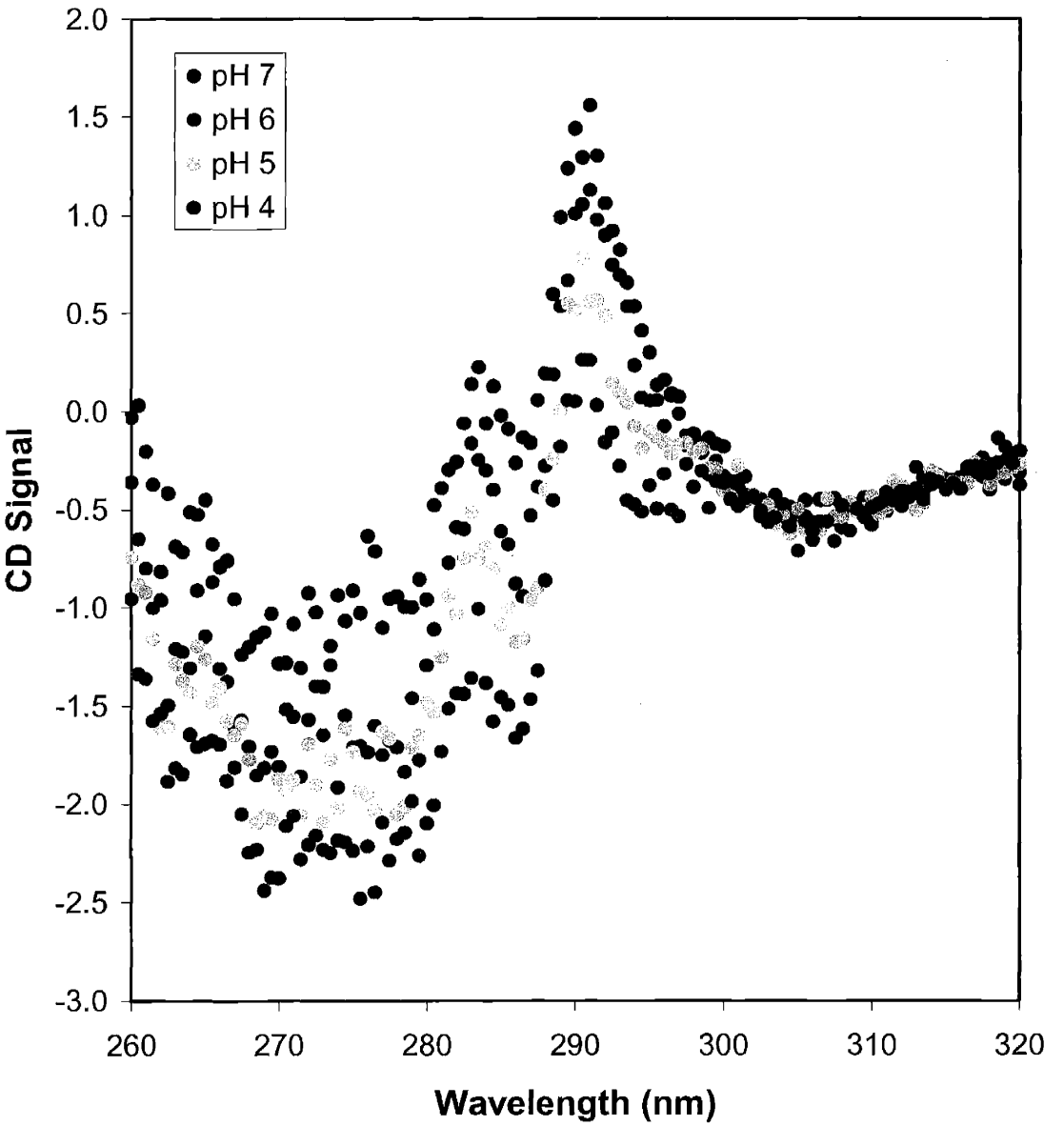

Figure 3.3: Near-UV scans of GCSF from pH 7 to 4. Scans are performed between 320 nm and 260 nm, with structural changes monitored at 291 nm and 280 nm.

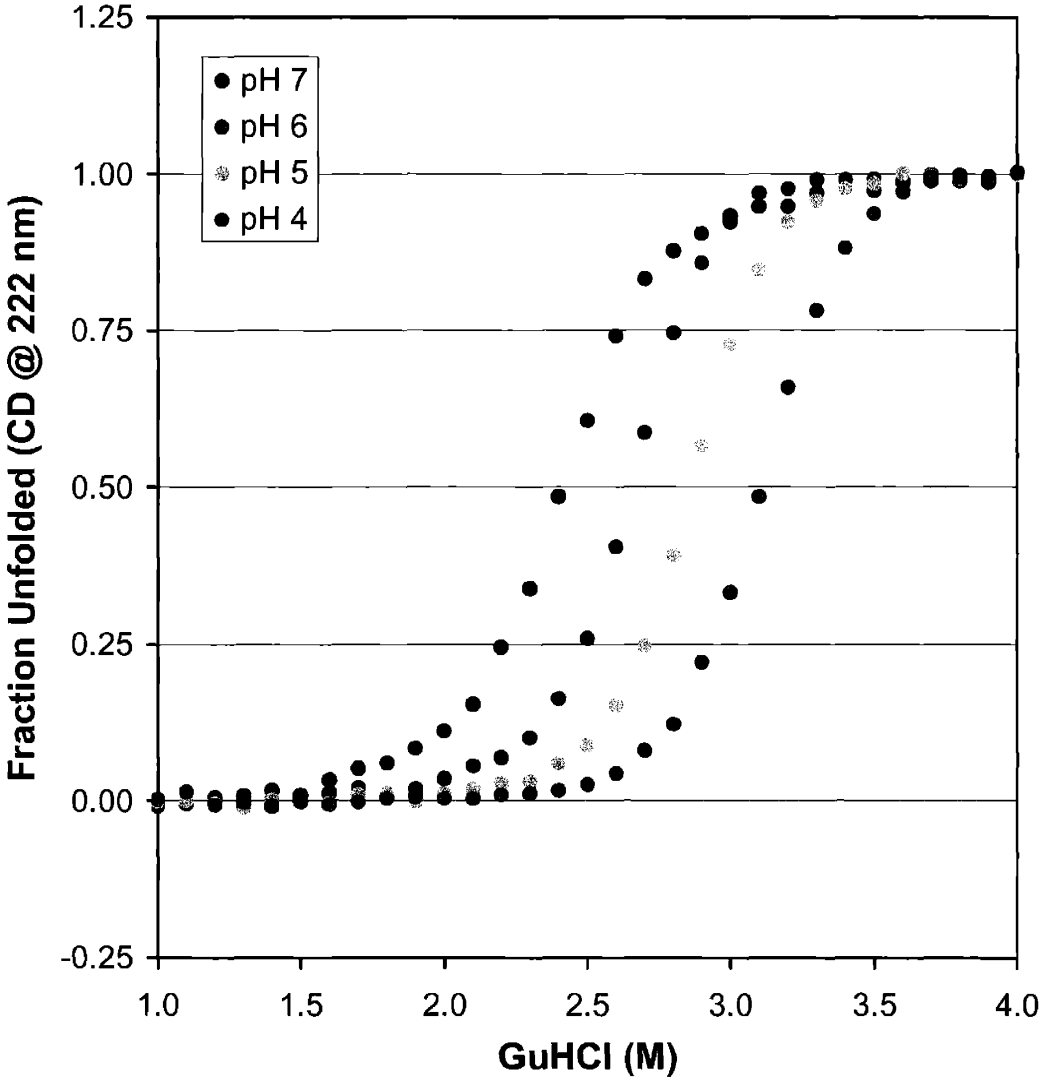

Figure 3.4: CD equilibrium denaturation studies of GCSF from pH 7 to 4.

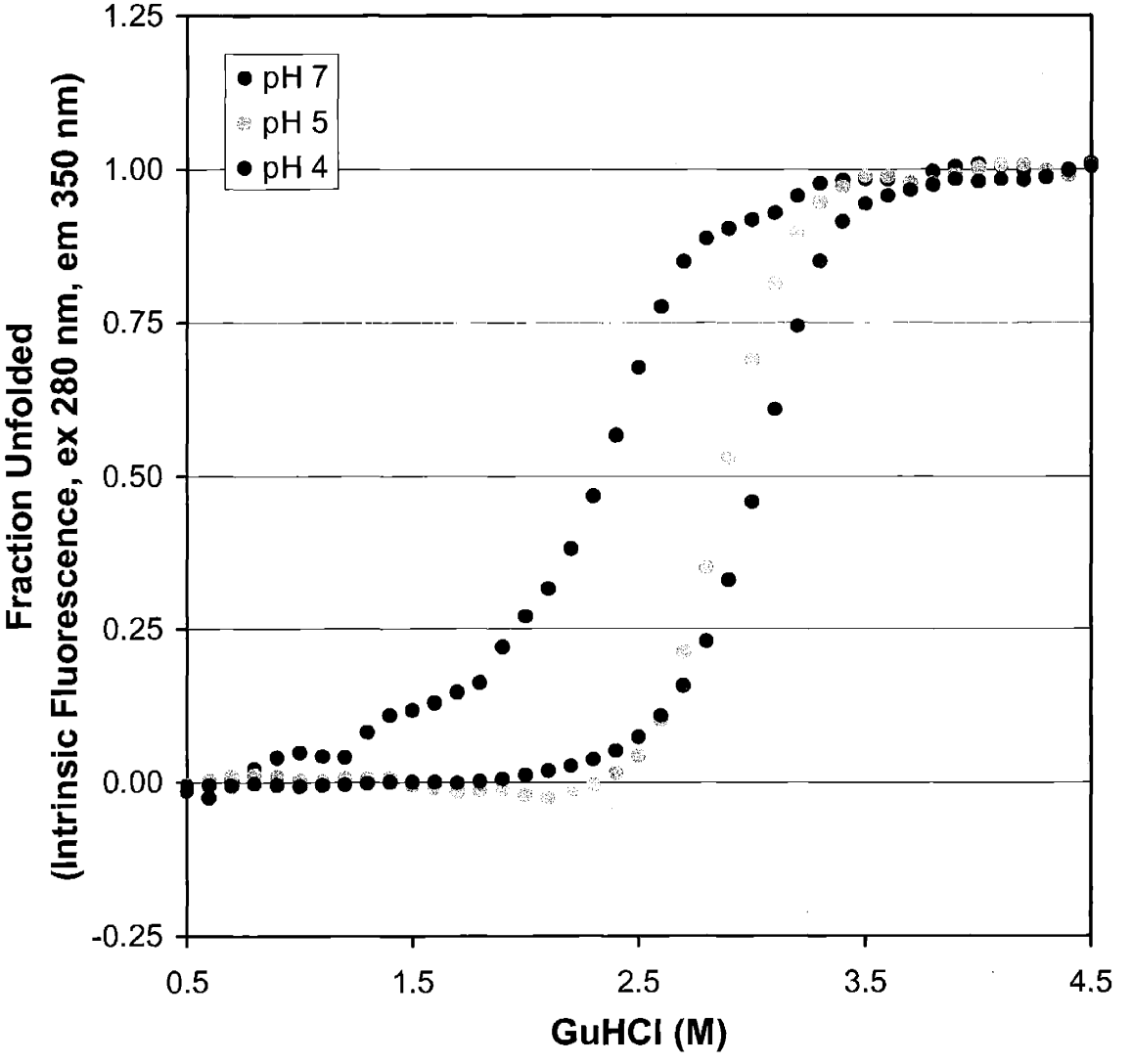

Figure 3.5: Fluorescence equilibrium denaturation studies of GCSF from pH 7 to 4.

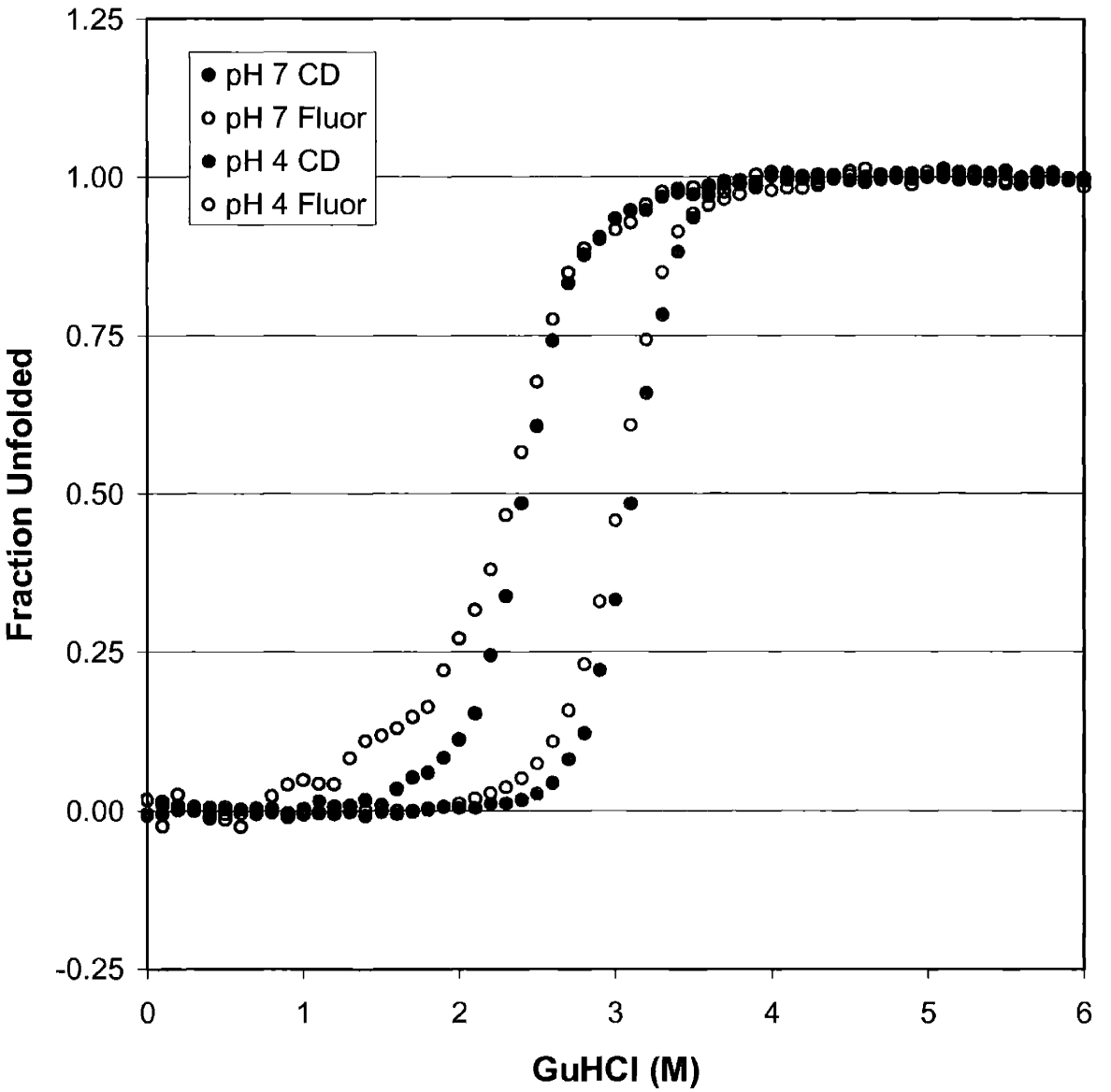

Figure 3.6: Overlay of secondary and tertiary structural transitions.

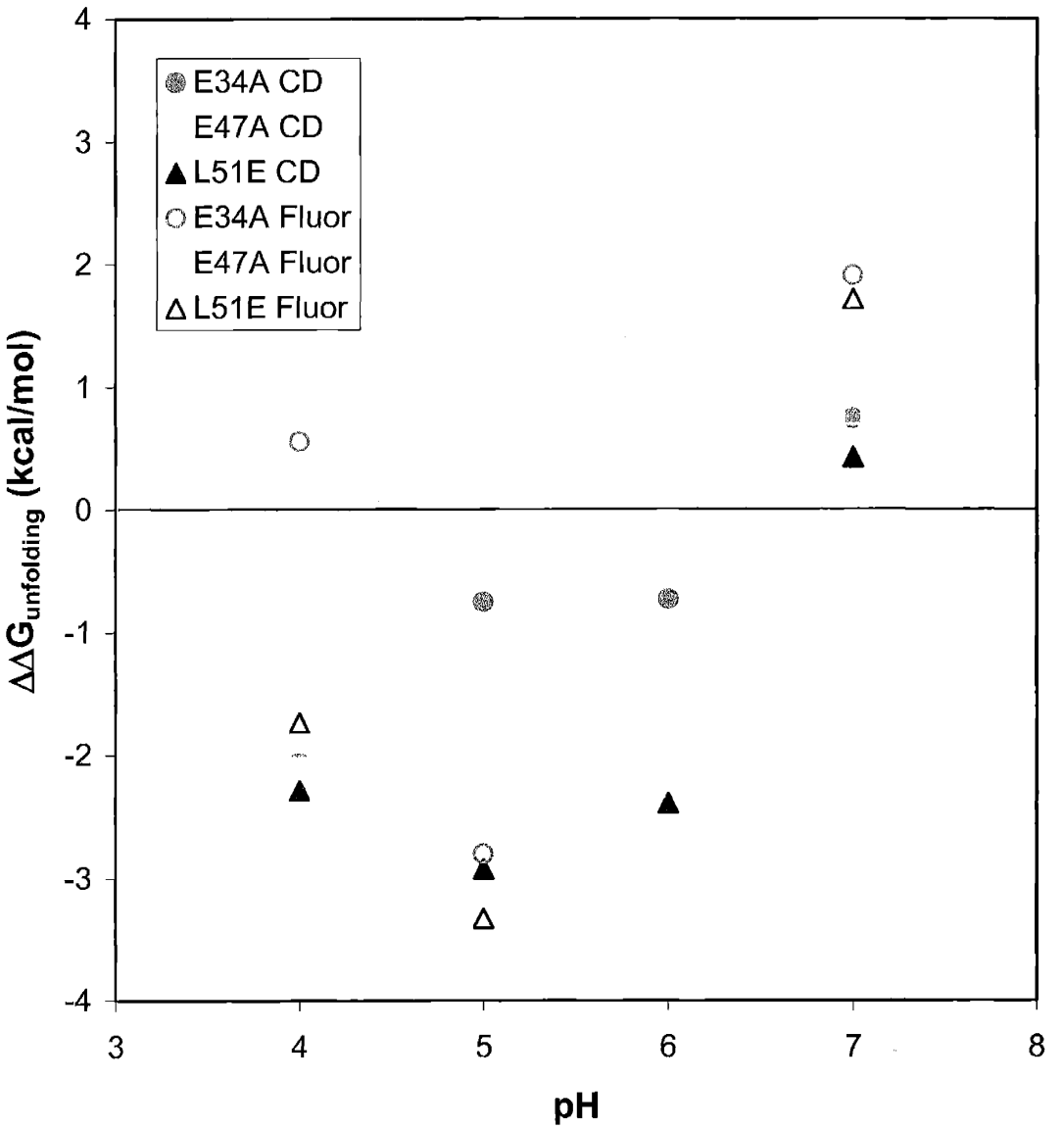

Figure 3.7: Free energy of unfolding of mutants relative to wild-type GCSF.

Chapter 4: Molecular Modeling of GCSF/GCSFR Interaction: 'Histidine Switching'

Therapeutic proteins can interact with cell-surface receptors and elicit cellular responses. The overall potency of such therapeutic ligands depends not only on the strength and nature of the binding interaction at the cell surface; potency is also strongly affected by subsequent cellular trafficking, which can lead to receptor downregulation and ligand depletion. We propose a framework for rationally modulating the outcome of endocytic trafficking events using single substitutions to histidine in the ligand. Our intention is to use the decreased pH of endosomal compartments relative to the extracellular medium to trigger a reduction in the endosomal ligand/receptor affinity, since the dissociated components may recycle to a greater extent than the intact complex. We present a computational approach for identifying candidate ligand residues for histidine substitution, and we illustrate the approach using granulocyte colony-stimulating factor (GCSF), finding locations at which histidine substitution is computed to be tolerated at neutral but not acidic pH. These results demonstrate principles and a methodology for redesigning therapeutic ligands to alter their endocytic trafficking for enhanced potency.

INTRODUCTION

Drug design is typically focused on the ability of a ligand to bind tightly and specifically to its intended target. However, if the drug is a protein and the target a cell-surface receptor, there are additional issues to consider from a systems-level analysis. When therapeutic ligands bind to receptors on the surface of a cell, an intracellular signaling cascade is initiated that ultimately results in an appropriate cellular response. Additionally, modulation – generally attenuation – of these signals begins almost immediately by cellular trafficking of the ligand/receptor complexes. The complexes on the surface of the cell are internalized into vesicles that fuse with endosomal compartments. From endosomes, the molecules can either be routed to degradation in lysosomes or be recycled to the cell surface intact, where free and ligand-bound receptor are redisplayed and free ligand is released to the extracellular medium. Recent evidence suggests the outcome of this sorting decision for complexes involving growth factors or cytokines often is related to the endosomal affinity

constant for the ligand/receptor interaction: complexes that remain bound are readily degraded while those that dissociate are recycled (Lauffenburger *et al.*, 1998). In general, dissociation of complexes in endosomes appears to enhance receptor recycling because it results in altered interactions between the receptors and lysosomal targeting components. Additionally, for cytokine/receptor systems in which complex numbers are relatively low, cell-level computational models indicate that decreasing the complex affinity in endosomes can enhance ligand recycling (French and Lauffenburger, 1997). Thus, if a ligand could be designed to enhance endosomal dissociation after binding to its cell-surface receptor and generating signals within its target cell, the drug might reduce receptor downregulation so that cells would be more responsive to further ligand stimulation. The lifetime and effectiveness of the drug itself might also be enhanced if ligand recycling were augmented by endosomal dissociation. This contrasts with the conventional approach of attempting to improve ligand potency through enhanced affinity. If extracellular affinity enhancements extend to endosomes, such attempts might actually be counterproductive because they increase receptor downregulation and possibly ligand depletion. Thus, cellular trafficking may be a bottleneck in enhancing ligand potency, particularly in cases where degradation through receptor-mediated endocytosis is substantial.

Previous work with epidermal growth factor receptor (EGFR) has shown distinct differences between human epidermal growth factor (EGF) and transforming growth factor α (TGFα) in their interactions with EGFR. These two ligands exhibit similar extracellular receptor-binding affinities but different cellular trafficking properties and mitogenic potencies (French *et al.*, 1995). TGFα is largely dissociated from EGFR in low-pH endosomes and is effectively recycled (French *et al.*, 1995); EGF binding, however, does not exhibit as great a pH sensitivity, and the higher retention of endosomal complexes leads to greater degradation, particularly when the number of intracellular complexes is low (French *et al.*, 1995). Consistent with this view, a mutant of EGF (Y13G) with lower receptor binding affinity has been shown to have improved mitogenic potency relative to both EGF and TGFα (Reddy *et al.*, 1996).

Likewise, a study on the cellular trafficking properties of interleukin-2 (IL-2) revealed that a double mutant of this cytokine (L18M/L19S), isolated from a random library of analogs, was found to be more potent than wild-type IL-2 (Berndt *et al.*, 1994).

Subsequent trafficking experiments revealed that this analog has a similar extracellular affinity and complex internalization rate to the native ligand, yet an increased recycling fraction (~ 50%) relative to wild type (~ 30%) (Fallon *et al.*, 2000). This result suggests that increasing the recycling fraction alone can significantly improve ligand potency.

A system in which the optimization of cellular trafficking properties could have a profound impact on potency is that of granulocyte colony-stimulating factor (GCSF) and its receptor (GCSFR). GCSF is a 19-kDa cytokine that specifically stimulates the proliferation and differentiation of neutrophilic precursor cells into mature neutrophils (Fukunaga *et al.*, 1993). Like IL-2, it is a member of the Group I superfamily of cytokines, which is characterized by a 4-α-helical-bundle structure and includes other therapeutically important drugs such as erythropoietin and growth hormone. GCSF binds specifically and with high effective affinity to GCSFR, resulting in a ligand:receptor complex with a 2:2 stoichiometry (Horan *et al.*, 1997; Horan *et al.*, 1996). The extracellular region of GCSFR contains the ligand-binding cytokine receptor homology (CRH) domain (Fukunaga *et al.*, 1991), and the crystal structure of GCSF complexed with the CRH domain of GCSFR shows the expected 2:2 ligand:receptor stoichiometry (Aritomi *et al.*, 1999). The major binding interface between one ligand molecule and one receptor molecule is shown in Figure 4.1.

GCSF is indicated for a range of important clinical applications, including administration to patients with neutropenia or cancer patients undergoing chemotherapy, and is intended to elevate neutrophil counts in the blood. However, GCSF is rapidly cleared through receptor-mediated endocytosis by bloodstream neutrophils expressing GCSFR (Layton *et al.*, 1989; Morstyn *et al.*, 1998). Thus, the potency of the drug is reduced by this negative feedback mechanism. Since cells naturally express GCSFR in low numbers, decreasing the endosomal affinity of the complex may not only reduce receptor downregulation but may also enhance ligand recycling, as predicted by modeling (French and Lauffenburger, 1997). The goal of our work is to develop a rational strategy for improving potency by increasing the lifetimes of protein therapeutics whose efficacies are limited by receptor-mediated clearance mechanisms in the body, and we have used GCSF as a model system.

Upon ligand/receptor binding, the pH decreases from a value of roughly 7 at the cell surface to between 5 and 6 in the endosomes, to 4 in the lysosomes. Given these pH

changes, we seek to manipulate the strength of the complex interaction through *in silico* mutagenesis of the ligand to affect the pH-dependent electrostatic contribution to binding. Specifically, we are interested in making mutations that largely maintain (or improve) the electrostatic interactions at extracellular pH but worsen the interaction at endosomal pH, since cell-level modeling predicts that this could enhance ligand recycling. The pK_a of histidine on the surface of free ligand (~ 6.4) (Tanokura, 1983) suggests that protonation of this amino acid could result in large pH-dependent effects on binding between extracellular and endosomal environments, up to a 10-fold lower affinity at pH 5.4; this effect is limited by the cost of deprotonating histidine in unbound GCSF (Yang and Honig, 1993). Although other residues may also be appropriate, given the appropriate local protein environment, here the analysis was limited to histidine. Calculations are used to identify candidate locations for histidine substitution. Preferred locations are those for which the computed binding affinity is strong for neutral histidine and weak for positively charged histidine. In this chapter, we propose a general framework for improving drug potency through designed improvements in trafficking, describe a computational scheme capable of identifying appropriate design changes, and apply the approach to GCSF using ligand mutations to histidine that function as pH-activated switches.

MATERIALS AND METHODS

Structure preparation

The X-ray crystal structure of GCSF in 2:2 complex with the ligand-binding domain of GCSFR has been solved using data to 2.8 Å from crystals grown and maintained at pH 7.5 (Aritomi *et al.*, 1999). The coordinates of the crystal structure were obtained from the Protein Data Bank (http://www.rcsb.org/pdb/), entry 1CD9 (Berman *et al.*, 2000). Only rigid docking of segments 'A' and 'B' was considered, which represents formation of the major binding interface between one GCSF molecule and one CRH domain of GCSFR (see Figure 4.1).

While recent work has elucidated the interaction sites between GCSF and its receptor more completely (Layton *et al.*, 2001), this particular binding interface in the X-ray crystal structure (Aritomi *et al.*, 1999) is very similar to site II in a newly proposed model (Layton *et al.*, 2001). Most of the available mutagenesis data on GCSF suggest that, while the site III

interface is necessary for dimerization and activity, the interactions at the site II interface contribute most of the binding free energy (Layton *et al.*, 2001; Layton *et al.*, 1997). In fact, it can readily be shown through thermodynamic cycle analysis that our framework is independent of the relative strengths of the site II and III interactions, and does not require full knowledge of site III:

$$\Delta\Delta G_{binding}^{pH\sim7.4} = \Delta G_{binding}^{mut,pH\sim7.4} - \Delta G_{binding}^{WT,pH\sim7.4} \tag{4.1}$$

$$\Delta\Delta G_{binding}^{pH\sim7.4} = \Delta G_{mutation}^{bound,pH\sim7.4} - \Delta G_{mutation}^{unbound,pH\sim7.4} \tag{4.2}$$

$$\Delta\Delta G_{binding}^{pH\sim5.5} = \Delta G_{binding}^{mut,pH\sim5.5} - \Delta G_{binding}^{WT,pH\sim5.5} \tag{4.3}$$

$$\Delta\Delta G_{binding}^{pH\sim5.5} = \Delta G_{mutation}^{bound,pH\sim5.5} - \Delta G_{mutation}^{unbound,pH\sim5.5} \tag{4.4}$$

The $\Delta\Delta G$ value computed corresponds to the relative binding free energy of a mutant compared to wild type. While this is normally thought of as the difference in receptor-binding affinity between mutant and wild type (Equations 4.1 and 4.3), through a thermodynamic cycle analysis each is equal to a difference in free energy for mutating from wild type to mutant in the bound and unbound states (Equations 4.2 and 4.4). This thermodynamic cycle analysis is standard in the field of protein energetics and avoids the need to compute the entire binding free energy and to know details of the site III interaction. All that is required is that mutation to histidine at site II does not affect interactions at site III, which is a very good assumption based on the distance between the sites and the accommodation of the histidine mutations in the absence of global motion. Thus, the lack of a high-resolution structural model of the site III interaction does not limit the calculations of site II contacts. Moreover, the relative values reported throughout this chapter do not depend on whether the site III interactions are stronger or weaker than those in site II, because they are the same in wild type and mutant. If a structure including site III interactions were available, we could perform calculations at that interface to attempt to locate additional sites with the desirable properties. However, this in no way limits the strength of the results presented here, in which all of the side chains considered for mutation lie directly in the site II interface.

The coordinates for the 'A' and 'B' segments were extracted from the coordinate file and polar and aromatic hydrogen-atom positions, as well as a small number of missing heavy-atom positions, were built using CHARMM (Brünger and Karplus, 1988; Brooks *et al.*, 1983). Titratable side chains at the interface in the wild-type complex, none of which were histidine, were all treated as being in their standard neutral-pH titration states based on an examination of their local environments. Mutations to histidine were analyzed as both neutral tautomers (protonated at either the δ or ε nitrogen, indicated as His_{δ}^{0} or His_{ε}^{0}, respectively) and positively charged histidine (His^{+}).

Candidate histidine mutations were identified by a three-part procedure *in silico*. First, the nature of electrostatic binding interactions was quantified using a method that explicitly accounts for ligand desolvation and interaction and locates regions at the interface that are somewhat too negative or too positive for optimal binding (Kangas and Tidor, 1998). Second, trial histidine mutants (both neutral and positively charged) were constructed and their energies minimized. Third, the electrostatic binding free energy of each was computed.

Electrostatic binding free energy calculations

Continuum electrostatic calculations were performed with a locally modified version of the DelPhi computer program, which solves the linearized Poisson-Boltzmann equation

$$\nabla \cdot (\varepsilon_i(\mathbf{x}) \nabla \phi_i(\mathbf{x})) - \varepsilon_s \kappa_i^2(\mathbf{x}) \phi_i(\mathbf{x}) = -4\pi Q_i(\mathbf{x}) \tag{4.5}$$

using finite difference methods (Nicholls and Honig, 1991; Gilson *et al.*, 1988). Here, $\phi_i(\mathbf{x})$ represents the electrostatic potential; $\varepsilon_i(\mathbf{x})$ represents the dielectric constant of either the protein interior (ε_m) or the solvent (ε_s), depending on the position, $\mathbf{x}$. The parameter $\kappa_i(\mathbf{x})$, which is the inverse of the Debye length, λ, is a function of the ionic strength of the bulk solution, $I_i(\mathbf{x})$:

$$\kappa_i(\mathbf{x}) = \frac{1}{\lambda} = \left[\frac{8\pi e^2 I_i(\mathbf{x})}{\varepsilon_s kT} \right]^{1/2}, \text{ where } I_i(\mathbf{x}) = \tfrac{1}{2} \sum_j z_j^2 c_j^b \tag{4.6}$$

where z_j and c^b_j are the charge valency and bulk concentration of ionic species j, respectively. $Q_i(\mathbf{x})$ describes the electrostatic charge density in the system. If no salts are present in the bulk solution, then $\kappa_i(\mathbf{x})$ is identically zero and Equation 4.5 reduces to the Poisson equation.

Potentials were calculated on a molecular surface described using a 1.4-Å probe sphere. A value of four was used for ε_m and 80 for ε_s; the bulk ionic strength was chosen to be 145 mM with a Stern layer of 2 Å. Calculation of the electrostatic free energy of binding, ΔG_{elec}, was determined using

$$\Delta G_{elec} = G_{complex} - (G_{ligand} + G_{receptor}), \text{ where } G_i = \tfrac{1}{2}\sum_i q_i(\mathbf{x})\phi_i(\mathbf{x}) \tag{4.7}$$

where $q_i(\mathbf{x})$ is the partial atomic charge at position $\mathbf{x}$ in state i (Sharp and Honig, 1990). Because the terms on the right-hand side of Equation 4.7 each actually represent the change in free energy between the real state and its equivalent hydrophobic isostere (a theoretically identical state that is purely hydrophobic), each term should technically be expressed as a ΔG; however, we omit the additional delta symbols for simplicity of notation. This procedure was employed for the wild-type complexes, complexes with hydrophobic isosteres of the side chains, complexes containing single unprotonated histidine mutations, and complexes containing single protonated histidine mutations. The complexes involving protonated histidines were used to predict and isolate the effect that the mutation would have on the electrostatics at endosomal pH.

Calculations were performed using a two-step focusing procedure first with 23% and then with 92% fill. For visualization of electrostatic potentials, a cubic lattice of 65×65×65 grid units was used. For electrostatic binding free energy calculations a 191×191×191 grid was used (final grid spacing 0.476 Å) and each value given is the average of 10 offsets of the molecule relative to the grid.

Characterization of electrostatic complementarity

Molecular surface potentials were visualized using GRASP (Nicholls *et al.*, 1991). More quantitatively, the following measure was used to determine the complementarity of electrostatic potentials at the interfacial surface:

$$\beta = \sum_{\substack{\text{interfacial} \\ \text{surface}}} \frac{(\phi_L(\mathbf{x}) + \phi_R(\mathbf{x}))^2}{\phi_L^2(\mathbf{x}) + \phi_R^2(\mathbf{x})} \tag{4.8}$$

where $\phi_L(\mathbf{x})$ is the electrostatic potential of the ligand and $\phi_R(\mathbf{x})$ is the electrostatic potential of the receptor, both calculated from DelPhi using a 191×191×191 grid. A β equal to zero suggests ideal electrostatic complementarity; a β of one is equivalent to orthogonality; and, a β equal to two implies that the ligand and receptor have equal electrostatic potentials. While electrostatic binding free energy calculations are expected to provide the most direct measure of ligand/receptor affinity, we wanted to quantify how close these electrostatic complementarities are to ideality. The following metrics were used to compare the effectiveness of the histidine mutations. The ratio of β to wild-type β (β/β_{WT}) gives a measure of similarity to wild type, where $\beta/\beta_{WT} > 1$ implies that the mutation has disrupted electrostatic complementarity. Ideally, β/β_{WT} is approximately equal to (or less than) one for an unprotonated histidine mutant. Another measure to quantify the effect of endosomal protonation on electrostatic complementarity is $\beta_{His^+}/\beta_{His_\delta^0}$ or $\beta_{His^+}/\beta_{His_\varepsilon^0}$, where His^+ represents a protonated histidine mutant and the unprotonated histidine tautomer mutants are given by His_δ^0 and His_ε^0. Here, $\beta_{His^+}/\beta_{His_\delta^0} > 1$ or $\beta_{His^+}/\beta_{His_\varepsilon^0} > 1$ is desirable to enhance endosomal recycling.

In silico mutagenesis of GCSF

Mutagenesis of wild-type amino acids to histidine was performed using Quanta (Molecular Simulations, San Diego, CA). The residues on the ligand that were mutated – Glu20, Gln21, Asp110, Asp113, Thr117, and Gln120 – were selected because each contributed negative net electrostatic potential, as visualized by GRASP. Only single histidine mutations were considered. Conformations of all ligand and receptor side chains within 10 Å of the mutation, including the mutation itself, were repacked onto a rigid backbone using a standard rotamer library (Dunbrack and Karplus, 1993). The complex energies were calculated using an energy function incorporating van der Waals interactions and electrostatic interactions with a distance-dependent dielectric ($\varepsilon = 4r$), as implemented in CHARMM PARAM19 (Brooks *et al.*, 1983), extended to include PARSE partial atomic charges (Sitkoff *et al.*, 1994). Energy-minimized complexes were found using a combination of the dead-end elimination and A* algorithms (Leach and Lemon, 1998; Desmet *et al.*, 1992; Goldstein, 1994; Hart *et al.*, 1968). All complexes within 10 kcal/mol of the minimum

were retained and analyzed, with the minimum used in further calculations. This optimization was performed for substitutions to both neutral histidine tautomers as well as the positively charged histidine. Controls were performed to check whether this strategy would rebuild the wild-type structure by allowing the side chains within 10 Å of the chosen mutation site to rearrange, without making the actual mutation. The above procedure was applied to calculate ΔG_{elec} and β values for each complex.

RESULTS

Electrostatic complementarity in the wild-type complex

The desolvation, interaction, and net electrostatic potentials on the ligand and receptor for the wild-type complex were visualized on the molecular surfaces using GRASP (Figure 4.2). Desolvation of the ligand reveals three significant regions of electrostatic potential: an intense region of negative electrostatic potential localized at Glu20, a lesser and more broad area of negative electrostatic potential around Asp113, and a region of positive electrostatic potential near Lys17. Interaction with the receptor reveals three regions of almost equal but opposite electrostatic potential, resulting in a diffuse negative electrostatic potential upon summation of the desolvation and interaction potentials. This negative net electrostatic potential on the surface of GCSF is mostly contributed by six amino acids: Glu20, Gln21, Asp110, Asp113, Thr117, and Gln120. The location of each of these residues on the molecular surface and in the context of the helical structure of GCSF is given in Figure 4.3. In an attempt to manipulate the electrostatic interactions between GCSF and its receptor, these six residues were considered for mutagenesis to histidine.

Generation and minimization of histidine mutants

In addition to studying the wild-type GCSF/GCSFR complex, six positions on the ligand – Glu20, Gln21, Asp110, Asp113, Thr117, and Gln120 – were singly mutated to histidine *in silico*. Each position was substituted with an unprotonated histidine tautomer (either His_{δ}^{0} or His_{ε}^{0}) to mimic the extracellular environment, thus generating twelve mutants. Six additional mutations were obtained by protonating the histidine (His^{+}) to simulate the endosomal environment. After energy minimization of these eighteen complexes, the amino acids on both the ligand and receptor within 10 Å of the mutation site

were examined for structural changes relative to the wild-type complex. The side chain orientations are given in Table 4.1 as angular deviations from the crystal structure coordinates along the carbon chain.

On average, a total of eight side chains on the ligand and receptor were included in a complex energy minimization. However, in each case, many side chains were unaffected by the mutation, as Table 4.1 shows only non-zero deviations. The deviation of the second angle of Tyr143 on GCSFR for the Glu20 mutations and Asp110 mutations is somewhat misleading, since this essentially results in a flip of the tyrosyl ring. Additionally, with the exception of Leu76 on GCSFR for the $D113H_{\delta}^{0}$ and $D113H^{+}$ complexes and Arg46 on GCSFR for the Gln120 mutant complexes, all deviations for the first two angles along the amino acid backbone are less than 50°.

In each case, control simulations were performed by allowing the same amino acids within 10 Å of the chosen mutation site to rearrange without making the substitution to histidine, thereby testing the ability of the energy function and search algorithms to return the wild-type configuration. These results are given in Table 4.2. With the exception of the Gln120 mutation site, all angular deviations along the side chain backbone are small, suggesting that the energy function and search algorithms closely rebuild the wild-type structure. Comparison of Tables 4.1 and 4.2 further reveals that the side chain rearrangements due to histidine mutations (and not due to the choice of energy function or search algorithms) are minimal and should therefore be structurally benign. Thus, these histidine mutations on the ligand should provide the desired electrostatic properties, without compromising the structural characteristics necessary for receptor recognition and activation.

ΔG_{elec} values for wild type and mutants

The electrostatic contributions of these same six side chains on GCSF were examined with respect to the free energy of receptor binding. However, here the goal was not to optimize the electrostatic affinity, but to generate a large differential in the free energy of binding between extracellular and endosomal pH values. The electrostatic free energies of binding (ΔG_{elec} values) were calculated for: the wild-type complex, the energy-minimized controls of the wild-type complex for each mutation site (which deviate from the wild-type complex only as shown in Table 4.2), complexes with hydrophobic isosteres of each of the

six side chains, complexes with single unprotonated histidine mutations, and these complexes with the histidine mutation protonated.

The energy-minimized controls have similar electrostatic free energies of binding to the wild-type complex (Figure 4.4). Additionally, for each mutation site considered, the original side chain was stripped of charge to assess the contribution of these charges in formation of the wild-type complex. As can be seen in Figure 4.4, it appears that the charges on Glu20 are critical for receptor recognition, consistent with experimental observations (Layton *et al.*, 1999; Reidhaar-Olson *et al.*, 1996). For the hydrophobic isosteres of Gln21, Asp110, Asp113, Thr117, and Gln120, the electrostatic binding free energy is either unchanged or reduced relative to wild type. Thus, for these five side chains, a mutation to an unprotonated histidine would not be expected to dramatically impact the electrostatics of the interaction between ligand and receptor.

The electrostatic free energies of binding for the His_δ^0, His_ε^0, and His^+ mutants are given in Figure 4.5. With the exception of E20H, the unprotonated histidine mutants all have similar electrostatic binding free energies (ranging from 24.7 to 28.9 kcal/mol) to wild type (26.4 kcal/mol). Interestingly, Q120H appears to have a reduced ΔG_{elec} compared to wild type, although the control simulation for Gln120 also resulted in a comparably lower ΔG_{elec} (see Figure 4.4). The protonated histidine mutants exhibit ΔG_{elec} values ranging from 25.5 to 37.8 kcal/mol. Since we are interested in the change in the electrostatic binding free energy along the endocytic pathway, we look at $\Delta\Delta G_{elec,His_\delta^0 \rightarrow His^+}$ and $\Delta\Delta G_{elec,His_\varepsilon^0 \rightarrow His^+}$ for each mutant. Glu20 has the largest impact ($\Delta\Delta G_{elec,His_\delta^0 \rightarrow His^+}$ = 11.3 kcal/mol and $\Delta\Delta G_{elec,His_\varepsilon^0 \rightarrow His^+}$ = 11.1 kcal/mol), although based on the result obtained for the Glu20 hydrophobic isostere and the ΔG_{elec} values for $E20H_\delta^0$ and $E20H_\varepsilon^0$, it is probable that the initial mutation to histidine disrupts interaction with the receptor. However, there are substantial changes in ΔG_{elec} upon protonation of the histidine for the two aspartate side chains, which do not appear to be as sensitive to the mutation. For Asp110, $\Delta\Delta G_{elec,His_\delta^0 \rightarrow His^+}$ = 4.7 kcal/mol and $\Delta\Delta G_{elec,His_\varepsilon^0 \rightarrow His^+}$ = 5.3 kcal/mol; for Asp113, $\Delta\Delta G_{elec,His_\delta^0 \rightarrow His^+}$ = 9.1 kcal/mol and $\Delta\Delta G_{elec,His_\varepsilon^0 \rightarrow His^+}$ = 8.5 kcal/mol. The differences in the electrostatic free energy of binding for protonated histidine substitutions of residues Gln21, Thr117, and

Gln120 compared to unprotonated histidines at the same positions are too small to be confident about the predictions.

Correlation between ΔG_{elec} and electrostatic potential

The net electrostatic potential for each of the histidine mutants (both protonated and unprotonated) of these six amino acids was also visualized using GRASP. Two examples are given in Figure 4.6 for comparison. It is visually evident that the His^+ mutants have worse electrostatic complementarity than wild type. However, without prior knowledge of the electrostatic binding free energies, it is not clear what the order of complementarity might be among wild type, $E20H_\delta^0$, and $D110H_\delta^0$, nor is it obvious whether $E20H^+$ or $D110H^+$ is worse. We have utilized a new measure of electrostatic complementarity, β, at an interfacial surface to allow for a more rigorous and quantitative analysis (see Materials and Methods). The parameter β is a function of the electrostatic potentials of the ligand and receptor at this interfacial surface. The function is defined such that a β of zero suggests ideal complementarity between two molecules; conversely, a value of two suggests that the two molecules have equal electrostatic potentials at the surface (see Materials and Methods).

β values for wild-type and mutant complexes were calculated as a quantitative measure of electrostatic complementarity (Table 4.3). For the wild-type complex, the complexes with hydrophobic isosteres of the side chains, and the complexes with unprotonated or protonated histidine mutations, β was plotted against ΔG_{elec} to examine whether this parameter could effectively correlate electrostatic potentials to electrostatic binding free energies. Figure 4.7 suggests that the degree of electrostatic complementarity, visualized in Figure 4.6, can be a strong indicator of the electrostatic free energy of binding through use of the parameter β, although the correlation is likely not fully linear since for β equal to zero, the electrostatic binding free energy should be negative (Kangas and Tidor, 1999).

We find that absolute β values for the unprotonated histidine mutants (excluding $E20H_\delta^0$ and $E20H_\varepsilon^0$, which are likely to disrupt electrostatic interaction with GCSFR based on Figures 4.4 and 4.5) range from 0.23 to 0.30, which suggests that the mutations themselves do not greatly disrupt the electrostatic complementarity seen in wild type (β_{WT} =

0.24). Addition of a single proton to each of these five histidine side chains leads to absolute β values ranging from 0.21 to 0.44, implying that some positions are unaffected by the protonation while others are significantly influenced. In particular, the $D110H^+$ and $D113H^+$ mutations resulted in β/β_{WT} values greater than 1.7, suggesting significant disruption of complementarity at endosomal pH.

Examining the ratio of β for the protonated histidine side chain (β_{His^+}) to β for the unprotonated side chains ($\beta_{His_\delta 0}$ and $\beta_{His_\varepsilon 0}$), we find that a histidine substitution at Glu20, Asp110, or Asp113 will significantly affect electrostatic complementarity in the context of cellular trafficking. By contrast, Q21H, Q120H, and T117H appear to have minimal changes, with Q120H and T117H showing slight improvements in electrostatic complementarity upon histidine protonation. While the electrostatic binding free energies should serve as the primary indicator of candidate histidine mutation sites, β provides a quantitative metric for electrostatic complementarity and further supports the trends seen with the electrostatic binding free energies of the mutants.

DISCUSSION

Importance of electrostatic interactions in cellular trafficking of complexes

For many ligands, electrostatic interactions can play a significant role in receptor recognition. An electrostatic analysis of growth hormone and interleukin-4 complexes revealed complementary potentials on the binding surfaces (Demchuk *et al.*, 1994). Additionally, these forces have been shown to play an important role in steering the ligand onto the proper site on the receptor, especially in the case of cytokines, many of which are therapeutically important (Cunningham and Wells, 1993). For surface complexes which are trafficked by cells, the electrostatic interactions are manipulated as the pH decreases along the endocytic pathway. A sorting decision is made when the complexes reach the endosomes.

Endosomal pH plays an essential role in many receptor-mediated processes, such as inducing the release of iron from the transferrin/transferrin receptor complex (Hopkins and Trowbridge, 1983) or the release of low-density lipoprotein from its receptor (Goldstein *et al.*, 1985). For signaling ligands, intact complexes in the endosomes are often sorted to

degradation to attenuate the generated signal. However, for cytokine/receptor systems in which complex numbers are relatively low, cell-level computational models predict that a decrease in binding affinity at endosomal pH can increase the fraction of recycled ligand, thereby allowing further rounds of binding and signaling (French and Lauffenburger, 1997). Since most ligand/receptor complexes are naturally sensitive to the acidic endosomal environment, the complex affinity is somewhat reduced as a result (Dunn and Hubbard, 1984). The findings in our study on GCSF suggest that the complex affinity can be more effectively weakened in the endosomes using the rational 'histidine switching' framework, thereby enhancing the cellular trafficking properties of the ligand.

Choosing a mutant with recycling potential

In designing a ligand with the possibility for enhanced recycling from the endosomes, we wish to find a mutant with poorer receptor recognition at endosomal pH than at extracellular pH. Additionally, we would like the receptor recognition of the mutant at extracellular pH to be similar to that of wild type. In this study, we have chosen histidine since the expected change in titration state of this amino acid along the endocytic pathway should negatively impact binding free energy and electrostatic complementarity. The two parameters that should provide insight into this are: $\Delta\Delta G_{elec,His^0 \rightarrow His^+}$ and $\beta_{His^+}/\beta_{His^0}$. As either of these parameters increase, the relative receptor recognition from the cell surface to the endosomes worsens. Therefore, we seek a mutant with either a high $\Delta\Delta G_{elec,His^0 \rightarrow His^+}$ or a high $\beta_{His^+}/\beta_{His^0}$. Of the GCSF mutants examined, E20H, D113H, and D110H best fit this description. However, E20H is not similar to wild type at extracellular pH ($\beta/\beta_{WT} = 1.5$), and ΔG_{elec} for this mutant suggests that initial receptor recognition would be very poor (Figure 4.5). Additionally, Figure 4.4 implicates the Glu20 charges in receptor recognition. As confirmation that this residue is likely critical to receptor binding and signaling, we have noticed in a cell proliferation assay that the analog E20A elicits essentially no response (see Chapter 2). Others have also shown Glu20 to be critical for receptor binding (Layton *et al.*, 1999; Reidhaar-Olson *et al.*, 1996).

$Q120H_\delta^0$ and $Q120H_\varepsilon^0$ are unusual in that they actually appear to have improved ΔG_{elec} values relative to wild type, with 1.7 kcal/mol and 1.2 kcal/mol decreases, respectively, in electrostatic binding free energy. However, the implication of this result is

clouded by the fact that the control simulation for Gln120, in which this amino acid and its neighbors were repacked, resulted in a 2.2-kcal/mol decrease in ΔG_{elec}. Additionally, we cannot be confident of the impact that the mutation to histidine may have on the endosomal sorting decision, since protonation of the histidine results in a much smaller increase in ΔG_{elec} (0.8 kcal/mol) than that seen for the Asp $\rightarrow$ His mutants. Nonetheless, it would be interesting to determine how the Q120H mutation would affect affinity for the receptor at both pH 7 and pH 5, and to find out how any potential differences might manifest themselves in terms of cellular trafficking and ligand potency.

The two candidates that appear most promising for further study with regard to enhanced endosomal recycling are D110H and D113H. These mutations provide similar properties to wild type at extracellular pH; namely, they have $\Delta\Delta G_{elec,WT\rightarrow His^0}$ close to zero and β/β_{WT} values close to unity. Additionally, comparison of $D110H^+$ and $D113H^+$ to their respective unprotonated analogs reveals large values of $\Delta\Delta G_{elec,His^0\rightarrow His^+}$ (> 4 kcal/mol) and $\beta_{His^+}/\beta_{His^0}$ values near 1.5. These mutations were proposed for experimental validation, and these experimental studies are the focus of the next chapter.

REFERENCES

Aritomi, M., Kunishima, N., Okamoto, T., Kuroki, R., Ota, Y. and Morikawa, K. (1999). Atomic structure of the GCSF-receptor complex showing a new cytokine-receptor recognition scheme. *Nature*. **401:** 713-717.

Berman, H.M., Westbrook, J., Feng, Z., Gilliland, G., Bhat, T.N., Weissig, H., Shindyalov, I.N. and Bourne, P.E. (2000). The Protein Data Bank. *Nucleic Acids Research*. **28:** 235-242.

Berndt, W.G., Chang, D.Z., Smith, K.A. and Ciardelli, T.L. (1994). Mutagenic analysis of a receptor contact site on interleukin-2: preparation of an IL-2 analog with increased potency. *Biochemistry*. **33:** 6571-6577.

Brooks, B.R., Bruccoleri, R.E., Olafson, B.D., States, D.J., Swaminathan, S. and Karplus, M. (1983). CHARMM: a program for macromolecular energy, minimization, and dynamics calculations. *Journal of Computational Chemistry*. **4:** 187-217.

Brünger, A.T. and Karplus, M. (1988). Polar hydrogen positions in proteins: empirical energy placement and neutron diffraction comparison. *Proteins: Structure, Function, and Genetics*. **4:** 148-156.

Cunningham, B.C. and Wells, J.A. (1993). Comparison of a structural and a functional epitope. *Journal of Molecular Biology*. **234:** 554-563.

Demchuk, E., Mueller, T., Oschkinat, H., Sebald, W. and Wade, R.C. (1994). Receptor binding properties of four-helix-bundle growth factors deduced from electrostatic analysis. *Protein Science*. **3:** 920-935.

Desmet, J., De Maeyer, M., Hazes, B. and Lasters, I. (1992). The dead-end elimination theorem and its use in protein side-chain positioning. *Nature*. **356:** 539-542.

Dunbrack, R.L. and Karplus, M. (1993). Backbone-dependent rotamer library for proteins: application to side-chain prediction. *Journal of Molecular Biology*. **230:** 543-574.

Dunn, W.A. and Hubbard, A.L. (1984). Receptor-mediated endocytosis of epidermal growth factor by hepatocytes in the perfused rat liver: ligand and receptor dynamics. *Journal of Cell Biology*. **98:** 2148-2159.

Fallon, E.M., Liparoto, S.F., Lee, K.J., Ciardelli, T.L. and Lauffenburger, D.A. (2000). Increased endosomal sorting of ligand to recycling enhances potency of an interleukin-2 analog. *Journal of Biological Chemistry*. **275:** 6790-6797.

French, A.R. and Lauffenburger, D.A. (1997). Controlling receptor/ligand trafficking: effects of cellular and molecular properties on endosomal sorting. *Annals of Biomedical Engineering*. **25:** 690-707.

French, A.R., Tadaki, D.K., Niyogi, S.K. and Lauffenburger, D.A. (1995). Intracellular trafficking of epidermal growth factor family ligands is directly influenced by the pH sensitivity of the receptor/ligand interaction. *Journal of Biological Chemistry*. **270:** 4334-4340.

Fukunaga, R., Ishizaka-Ikeda, E. and Nagata, S. (1993). Growth and differentiation signals mediated by different regions in the cytoplasmic domain of granulocyte colony-stimulating factor receptor. *Cell*. **74:** 1079-1087.

Fukunaga, R., Ishizaka-Ikeda, E., Pan, C.-X., Seto, Y. and Nagata, S. (1991). Functional domains of the granulocyte colony-stimulating factor receptor. *EMBO Journal*. **10:** 2855-2865.

Gilson, M.K., Sharp, K.A. and Honig, B.H. (1988). Calculating the electrostatic potential of molecules in solution: method and error assessment. *Journal of Computational Chemistry*. **9:** 327-335.

Goldstein, J.L., Brown, M.S., Anderson, R.G.W., Russell, D.W. and Schneider, W.J. (1985). Receptor-mediated endocytosis: concepts emerging from the LDL receptor system. *Annual Review of Cell Biology*. **1:** 1-39.

Goldstein, R.F. (1994). Efficient rotamer elimination applied to protein side-chains and related spin glasses. *Biophysical Journal*. **66:** 1335-1340.

Hart, P.E., Nilsson, N.J. and Raphael, B. (1968). A formal basis for the heuristic determination of minimum cost paths. *IEEE Transactions on Systems, Science, and Cybernetics*. **4:** 110-114.

Hopkins, C.R. and Trowbridge, I.S. (1983). Internalization and processing of transferrin and the transferrin receptor in human carcinoma A431 cells. *Journal of Cell Biology*. **97:** 508-521.

Horan, T., Wen, J., Narhi, L., Parker, V., Garcia, A., Arakawa, T. and Philo, J. (1996). Dimerization of the extracellular domain of granulocyte-colony stimulating factor receptor by ligand binding: a monovalent ligand induces 2:2 complexes. *Biochemistry*. **35:** 4886-4896.

Horan, T.P., Martin, F., Simonet, L., Arakawa, T. and Philo, J.S. (1997). Dimerization of granulocyte-colony stimulating factor receptor: the Ig plus CRH construct of granulocyte-colony stimulating factor receptor forms a 2:2 complex with a ligand. *Journal of Biochemistry*. **121:** 370-375.

Kangas, E. and Tidor, B. (1998). Optimizing electrostatic affinity in ligand-receptor binding: theory, computation, and ligand properties. *Journal of Chemical Physics*. **109:** 7522-7545.

Kangas, E. and Tidor, B. (1999). Charge optimization leads to favorable electrostatic binding free energy. *Physical Review E*. **59:** 5958-5961.

Lauffenburger, D.A., Fallon, E.M. and Haugh, J.M. (1998). Scratching the (cell) surface: cytokine engineering for improved ligand/receptor trafficking dynamics. *Chemistry & Biology*. **5:** R257-R263.

Layton, J.E., Hall, N.E., Connell, F., Venhorst, J. and Treutlein, H.R. (2001). Identification of ligand-binding site III on the immunoglobulin-like domain of the granulocyte colony-stimulating factor receptor. *Journal of Biological Chemistry*. **276:** 36779-36787.

Layton, J.E., Hockman, H., Sheridan, W.P. and Morstyn, G. (1989). Evidence for a novel in vivo control mechanism of granulopoiesis: mature cell-related control of a regulatory growth factor. *Blood*. **74:** 1303-1307.

Layton, J.E., Iaria, J., Smith, D.K. and Treutlein, H.R. (1997). Identification of a ligand-binding site on the granulocyte colony-stimulating factor receptor by molecular modeling and mutagenesis. *Journal of Biological Chemistry*. **272:** 29735-29741.

Layton, J.E., Shimamoto, G., Osslund, T., Hammacher, A., Smith, D.K., Treutlein, H.R. and Boone, T. (1999). Interaction of granulocyte colony-stimulating factor (G-CSF) with its receptor: evidence that Glu^{19} of G-CSF interacts with Arg^{288} of the receptor. *Journal of Biological Chemistry*. **274:** 17445-17451.

Leach, A.R. and Lemon, A.P. (1998). Exploring the conformational space of protein side chains using dead-end elimination and the A* algorithm. *Proteins: Structure, Function, and Genetics*. **33:** 227-239.

Morstyn, G., Dexter, T.M. and Foote, M. (1998). *Filgrastim (r-metHuG-CSF) in Clinical Practice*. Marcel Dekker, New York.

Nicholls, A. and Honig, B. (1991). A rapid finite difference algorithm, utilizing successive over-relaxation to solve the Poisson-Boltzmann equation. *Journal of Computational Chemistry*. **12:** 435-445.

Nicholls, A., Sharp, K.A. and Honig, B. (1991). Protein folding and association: insights from the interfacial and thermodynamic properties of hydrocarbons. *Proteins: Structure, Function, and Genetics*. **11:** 281-296.

Reddy, C.C., Niyogi, S.K., Wells, A., Wiley, H.S. and Lauffenburger, D.A. (1996). Engineering epidermal growth factor for enhanced mitogenic potency. *Nature Biotechnology*. **14:** 1696-1699.

Reidhaar-Olson, J.F., De Souza-Hart, J.A. and Selick, H.E. (1996). Identification of residues critical to the activity of human granulocyte colony-stimulating factor. *Biochemistry*. **35:** 9034-9041.

Sharp, K.A. and Honig, B. (1990). Calculating total electrostatic energies with the nonlinear Poisson-Boltzmann equation. *Journal of Physical Chemistry*. **94:** 7684-7692.

Sitkoff, D., Sharp, K.A. and Honig, B. (1994). Accurate calculation of hydration free energies using macroscopic solvent models. *Journal of Physical Chemistry*. **98:** 1978-1988.

Tanokura, M. (1983). ^{1}H-NMR study on the tautomerism of the imidazole ring of histidine residues. *Biochimica et Biophysica Acta*. **742:** 576-585.

Yang, A.-S. and Honig, B. (1993). On the pH dependence of protein stability. *Journal of Molecular Biology*. **231:** 459-474.

Table 4.1: Orientations for side chains on both ligand and receptor within 10 Å of each histidine mutation, excluding the mutation itself, expressed as positive deviations from angles in crystal structure along the side chain backbones. Only side chains with non-zero deviations are shown. H_δ^0 and H_ε^0 represent unprotonated tautomers of histidine; H^+ represents a protonated histidine.

Complex	GCSF	Angular Deviations (°)	GCSFR	Angular Deviations (°)
$E20H_\delta^0$	Leu16	0.43, 8.19	Tyr143	6.02, 179.46
$E20H_\varepsilon^0$	Leu16	0.43, 8.19	Tyr143	6.02, 179.46
$E20H^+$	Leu16 Arg23	0.43, 8.19 10.74, 0.09, 156.47, 67.24	Tyr143	6.02, 179.46
$Q21H_\delta^0$	Ile25 Asp113 Phe114	1.59, 5.79 8.28, 47.61 2.33, 13.28	–	–
$Q21H_\varepsilon^0$	Ile25 Asp113 Phe114	1.59, 5.79 8.28, 47.61 2.33, 13.28	–	–
$Q21H^+$	Ile25 Asp113 Phe114	1.59, 5.79 8.28, 47.61 2.33, 13.28	–	–
$D110H_\delta^0$	Asp28 Asp113	2.59, 30.15 8.28, 47.61	Tyr143	6.02, 179.46
$D110H_\varepsilon^0$	Asp28 Asp113	2.59, 30.15 8.28, 47.61	Tyr143	6.02, 179.46
$D110H^+$	Lys24 Asp28 Asp113	6.03, 8.34, 98.92, 130.30 2.59, 30.15 8.28, 47.61	Tyr143	6.02, 179.46

Table 4.1 (con't):

Complex	GCSF	Angular Deviations (°)	GCSFR	Angular Deviations (°)
$D113H_{\delta}^{0}$	Leu109 Thr117	17.15, 5.96 27.09	Leu76	38.71, 122.5
$D113H_{\varepsilon}^{0}$	Thr117	27.09	Arg72	23.75, 15.59, 73.52, 56.51
$D113H^{+}$	Leu109 Thr117	17.15, 5.96 27.09	Arg72 Leu76	23.75, 15.59, 73.52, 56.51 38.71, 122.46
$T117H_{\delta}^{0}$	Gln21 Gln121	8.01, 11.92, 33.11 2.57, 0.91, 149.62	Gln79	7.46, 24.41, 32.46
$T117H_{\varepsilon}^{0}$	Gln21 Gln121	8.01, 11.92, 33.11 2.57, 0.91, 149.62	Gln79	7.46, 24.41, 32.46
$T117H^{+}$	Lys17 Gln121	0.77, 3.37, 9.21, 121.13 2.57, 0.91, 149.62	Gln79	7.46, 24.41, 32.46
$Q120H_{\delta}^{0}$	Thr117 Glu123	27.09 9.53, 23.31, 16.23	Arg46 Tyr51 Leu76 Gln79	1.25, 72.91, 12.04, 162.52 6.84, 26.95 19.31, 2.86 7.46, 24.41, 32.46
$Q120H_{\varepsilon}^{0}$	Thr117 Glu123	27.09 9.53, 23.31, 16.23	Arg46 Tyr51 Leu76 Gln79	1.25, 72.91, 12.04, 162.52 6.84, 26.95 19.31, 2.86 7.46, 24.41, 32.46
$Q120H^{+}$	Thr117 Glu123	27.09 9.53, 23.31, 16.23	Arg46 Tyr51 Leu76 Gln79	1.25, 72.91, 12.04, 162.52 6.84, 26.95 19.31, 2.86 7.46, 24.41, 32.46

Table 4.2: Orientations for side chains on both ligand and receptor within 10 Å of each mutation site, without the mutation being made, expressed as positive deviations from angles in crystal structure along the side chain backbones. Only side chains with non-zero deviations are shown.

Mutation Site	GCSF	Angular Deviations (°)	GCSFR	Angular Deviations (°)
Glu20	Leu16	0.43, 8.19	Tyr143	6.02, 179.46
Gln21	Ile25 Asp113 Phe114	1.59, 5.79 8.28, 47.61 2.33, 13.28	–	–
Asp110	Asp28 Thr106 Asp113	2.59, 30.15 7.11 8.28, 47.61	Asn20 Tyr143	78.30, 93.07 6.02, 179.46
Asp113	Asp113 Thr117	8.28, 47.61 27.09	Leu76	38.71, 122.46
Thr117	Thr117 Gln121	27.09 2.57, 0.91, 149.62	Gln79	7.46, 24.41, 32.46
Gln120	Thr117 Gln120	27.09 10.03, 114.79, 38.44	Arg44 Arg46 Tyr51 Leu76 Gln79	99.00, 86.95, 94.31, 5.41 1.25, 72.91, 12.04, 162.52 6.84, 26.95 112.51, 106.44 100.44, 137.71, 29.56

Table 4.3: β values for wild-type and mutant complexes. H_δ^0 and H_ε^0 represent unprotonated tautomers of histidine; H^+ represents a protonated histidine.

	β	β/β_{WT}	$\beta_{His^+}/\beta_{His_\delta^0}$	$\beta_{His^+}/\beta_{His_\varepsilon^0}$
Wild type	0.2376	1.000	---	
$E20H_\delta^0$	0.3544	1.492	1.813	1.574
$E20H_\varepsilon^0$	0.4082	1.718		
$E20H^+$	0.6427	2.705		
$Q21H_\delta^0$	0.2431	1.023	1.026	1.103
$Q21H_\varepsilon^0$	0.2261	0.952		
$Q21H^+$	0.2493	1.049		
$D110H_\delta^0$	0.2819	1.186	1.565	1.733
$D110H_\varepsilon^0$	0.2544	1.071		
$D110H^+$	0.4411	1.856		
$D113H_\delta^0$	0.2766	1.164	1.497	1.833
$D113H_\varepsilon^0$	0.2258	0.950		
$D113H^+$	0.4140	1.742		
$T117H_\delta^0$	0.2804	1.180	0.894	0.845
$T117H_\varepsilon^0$	0.2969	1.250		
$T117H^+$	0.2508	1.056		
$Q120H_\delta^0$	0.2254	0.949	0.909	0.891
$Q120H_\varepsilon^0$	0.2300	0.968		
$Q120H^+$	0.2050	0.863		

Figure 4.1: 1:1 complex of GCSF (metallic blue) and GCSFR (pink), with residues considered for histidine mutagenesis in color. Color coding: Glu20 (orange), Gln21 (purple), Asp110 (blue), Asp113 (red), Thr117 (brown), and Gln120 (green).

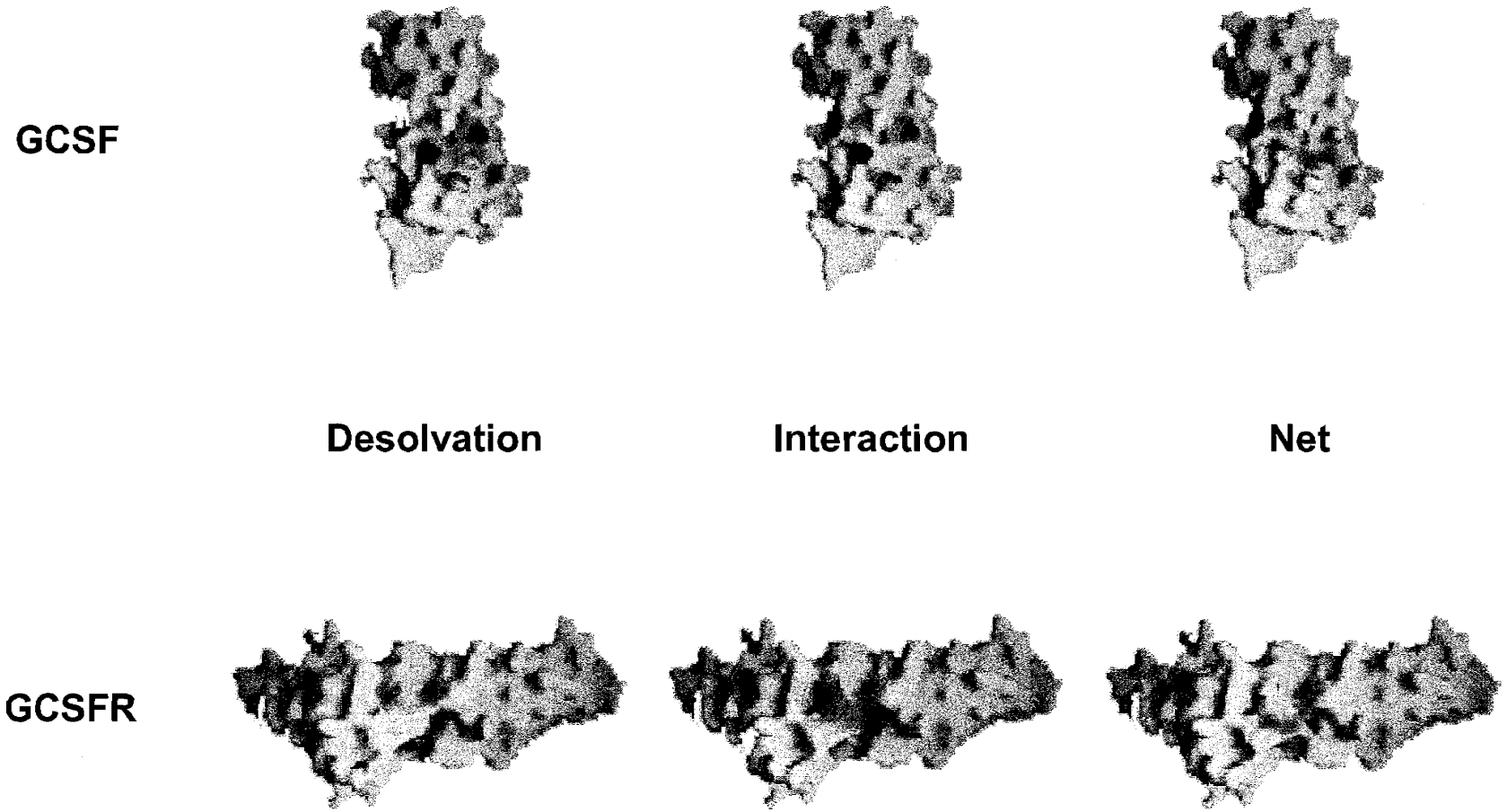

Figure 4.2: Desolvation, interaction, and net electrostatic potentials of GCSF (top) and GCSFR (bottom). Scale is $-40kT$ (dark red) to $40kT$ (dark blue). A white surface in the net column would indicate ideal electrostatic complementarity.

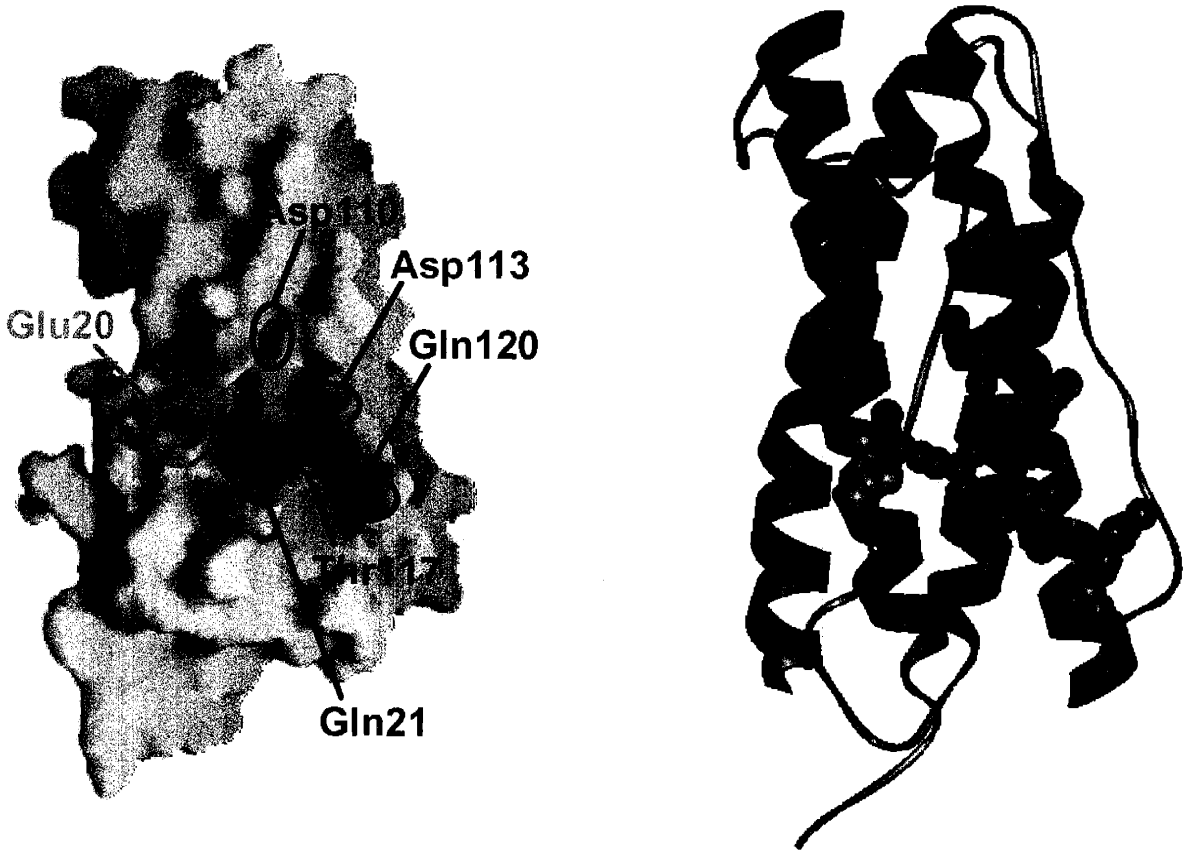

Figure 4.3: Net electrostatic potential on the surface of wild-type GCSF next to crystal structure showing residues on GCSF which contribute to the negative net electrostatic potential and which were considered for mutation to histidine. Color coding: Glu20 (orange), Gln21 (purple), Asp110 (blue), Asp113 (red), Thr117 (brown), and Gln120 (green).

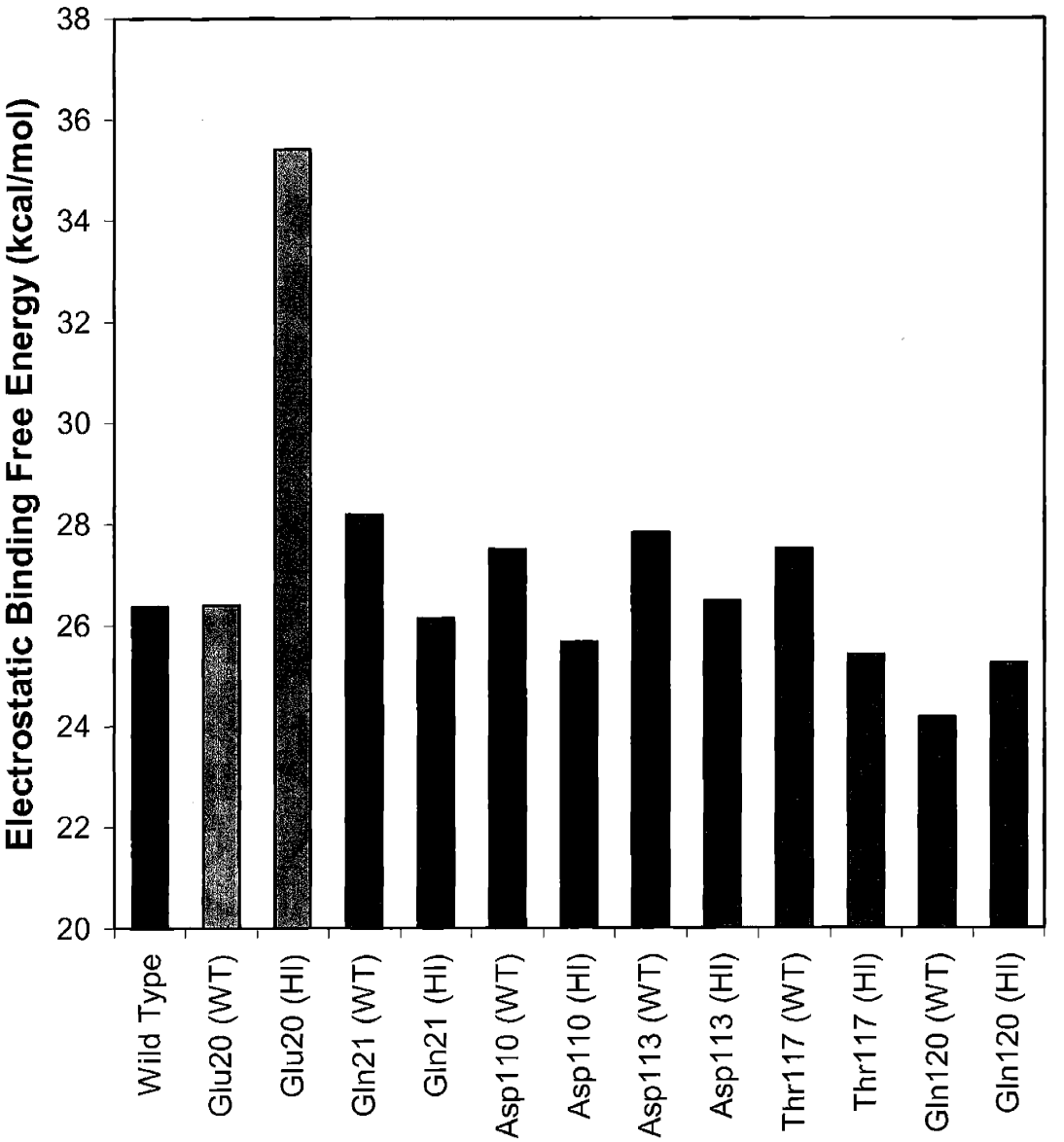

Figure 4.4: Electrostatic binding free energies of wild-type GCSF:GCSFR complex, complexes which were energy-minimized at each mutation site to rebuild the wild-type complex (denoted WT following the side chain), and complexes in which the side chain was stripped of charge, leaving its hydrophobic isostere (denoted HI following the side chain).

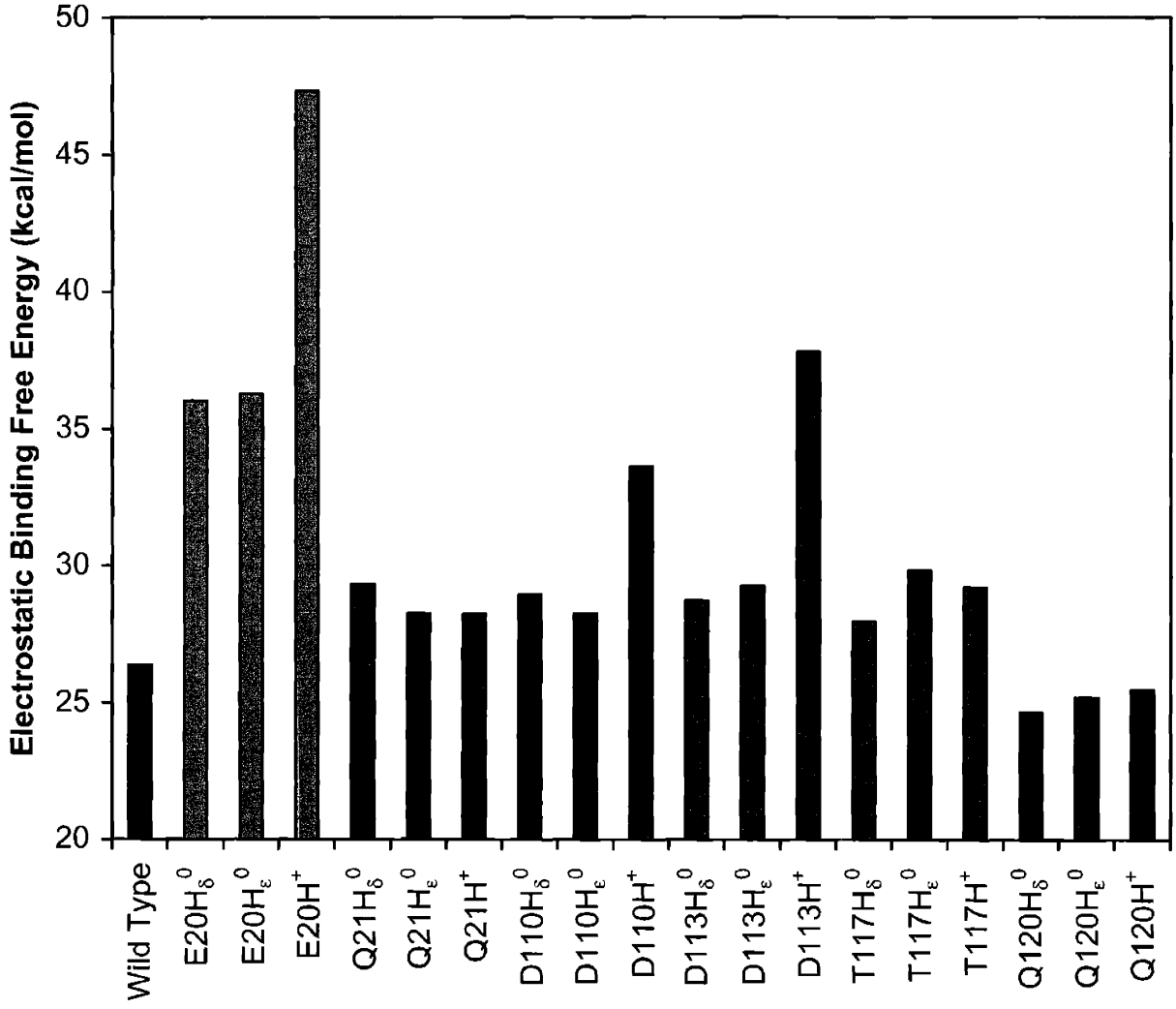

Figure 4.5: Electrostatic binding free energies of wild-type GCSF and mutants upon formation of 1:1 complex. H_δ^0 and H_ε^0 represent unprotonated tautomers of histidine; H^+ represents a protonated histidine.

A)

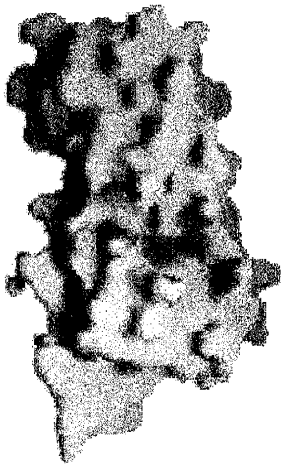

B)

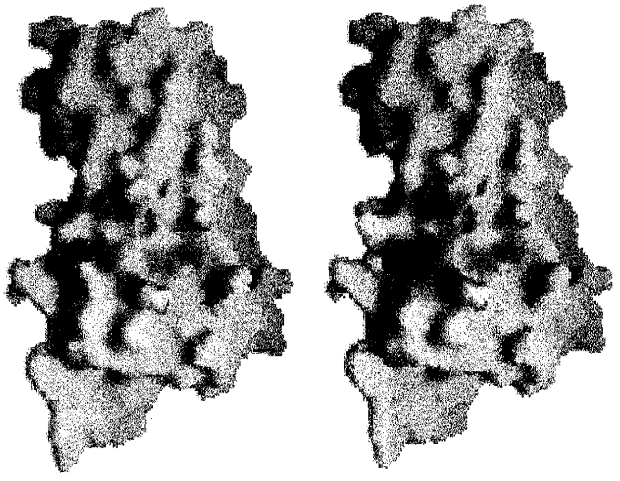

C)

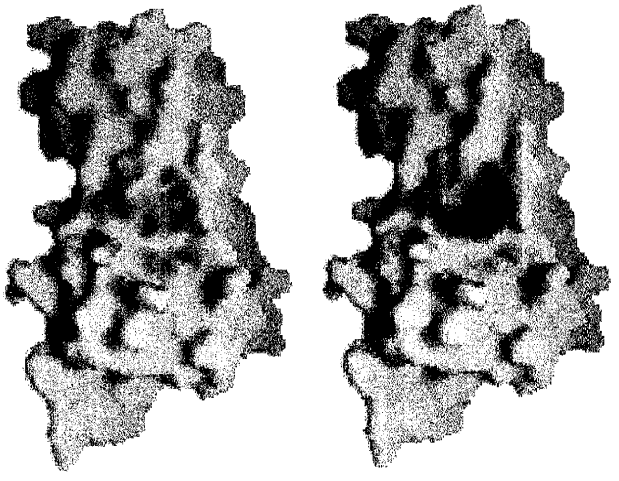

Figure 4.6: Net electrostatic potentials on the surfaces of A) wild-type GCSF, B) $E20H_{\delta}^{0}$ (left) & $E20H^{+}$ (right), and C) $D110H_{\delta}^{0}$ (left) & $D110H^{+}$ (right). These visualizations of net electrostatic potentials correlate with the β values given in Table 4.3.

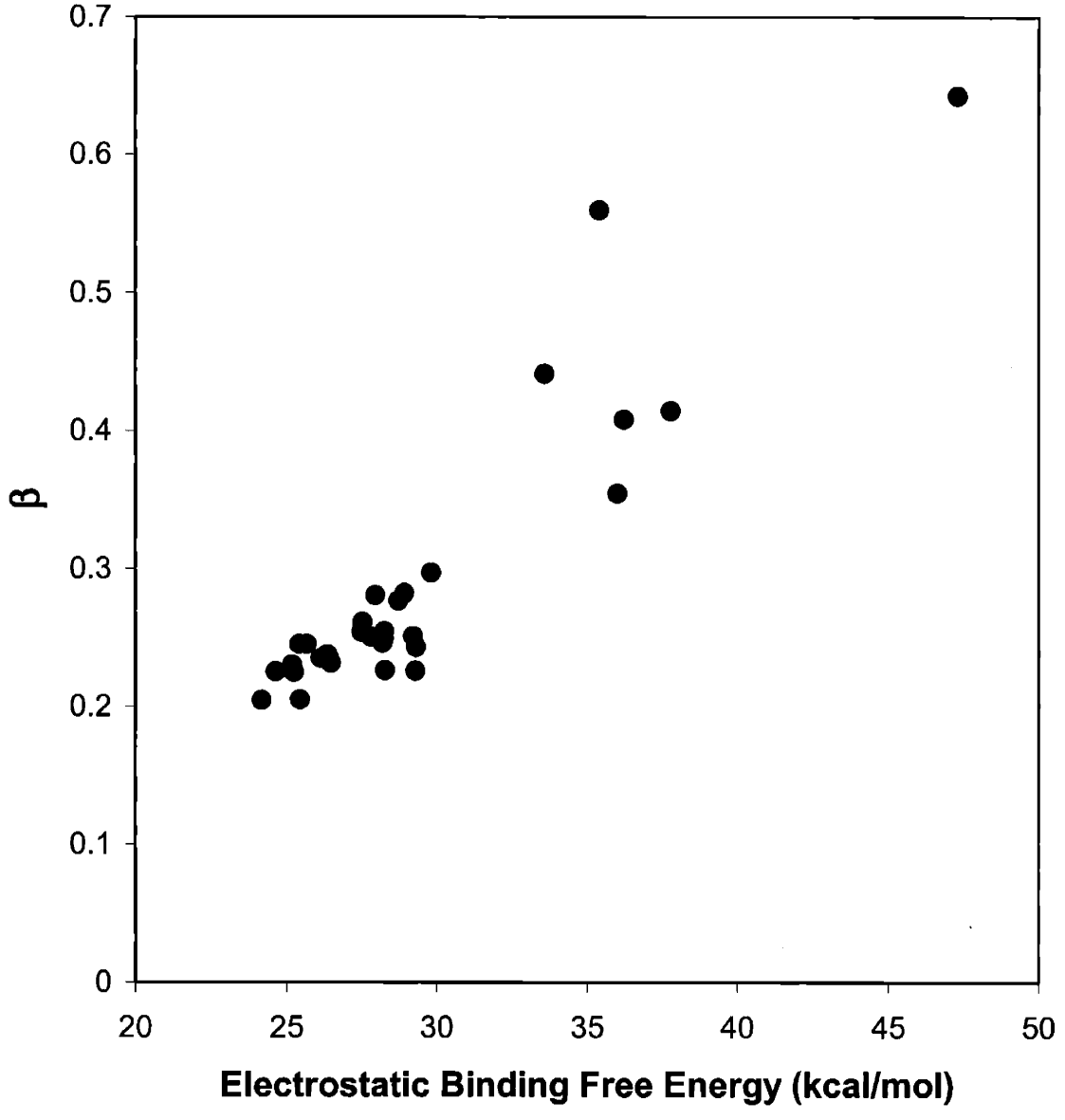

Figure 4.7: Correlation between electrostatic binding free energy and β for the mutations considered. The data are from the wild-type GCSF:GCSFR complex, the complexes with hydrophobic isosteres of the side chains, and the complexes with mutations to unprotonated and protonated histidines.

Chapter 5: Binding and Trafficking Studies on Histidine Analogs

We describe here experimental results on computationally designed analogs of granulocyte colony-stimulating factor (GCSF). The goal (see Chapter 4) was to predict amino acid substitutions in the ligand that would reduce binding affinity in intracellular endosomal compartments, since this biochemical design target is predicted to enhance ligand sorting to recycling and consequently result in a longer half-life in extracellular medium. The strategy was implemented using histidine substitutions to switch protonation states between cell-surface and endosomal pH, and two candidate single-histidine mutants of GCSF were identified. Experimental assays on these mutants demonstrate that each of these mutants indeed exhibits an order-of-magnitude increase in medium half-life, as well as greater potency, resulting from enhanced endosomal recycling compared to wild-type GCSF.

INTRODUCTION

Many naturally existing cytokines hold promise for clinical use, but the efficacy of these molecules observed *in vitro* does not typically translate into the desired *in vivo* potency. For those cytokines that do realize some therapeutic benefit, the drug often has to be administered multiple times and at abnormally high concentrations over the course of treatment to overcome *in vivo* pharmacokinetics and elicit the desired biological response. As discussed in Chapter 2, engineering the ligand to improve its trafficking properties may enhance pharmacodynamic potency and attenuate cell-based clearance mechanisms *in vivo*. A common practice in engineering a drug is to increase the affinity of the molecule for its *in vivo* target, since it is believed that this will increase the efficacy of the drug. However, for drugs such as cytokines that act as agonists for cell-surface receptors, a more global examination of the processes in which the ligand participates reveals that this approach is shortsighted, since the cytokine/receptor dynamics are more complex than a single cell-surface binding event.

Consideration of the additional endocytic trafficking dynamics led to the following non-intuitive design goal for cytokines: *decrease* the affinity of the ligand/receptor complex in the *endosomal* compartments. Cell-level computational modeling of the endosomal sorting process predicts that such a design would increase ligand recycling and improve

ligand half-life if the receptor expression level is low (French and Lauffenburger, 1997), as is often the case for cytokine receptors. This improvement in cellular trafficking dynamics may in turn enhance the pharmacodynamic and pharmacokinetic properties of the cytokine *in vivo*.

We implemented this design strategy computationally for granulocyte colony-stimulating factor (GCSF), using histidine substitutions in the ligand to serve as pH-activated switches to reduce the binding affinity for its receptor (GCSFR) in low-pH endosomes. This cytokine is already an important pharmaceutical agent but it suffers from a short lifespan *in vivo*, due in large part to receptor-mediated endocytosis and degradation by circulating neutrophils that express GCSFR (Morstyn *et al.*, 1998; Layton *et al.*, 1989). Thus, the efficacy of the drug is attenuated by this negative feedback mechanism, and consequently GCSF is commonly administered daily to maintain an adequate concentration *in vivo* (Morstyn *et al.*, 1998). Attempts to improve the potency of the cytokine by increasing its affinity for cell-surface GCSFR may actually be counterproductive, as they may augment receptor-mediated clearance of the drug by circulating neutrophils.

Here, we experimentally test two candidate single-histidine mutants proposed by our computational design strategy. Each mutant exhibits a half-life greater than wild type by an order of magnitude, as well as increased mitogenic potency, as a consequence of enhanced ligand recycling. These results confirm that it is possible to rationally design more effective cytokines for potential *in vitro* and *in vivo* applications using the 'histidine switching' approach.

MATERIALS AND METHODS

Materials and cell culture

Mutations of GCSF at Asp110 and Asp113 to histidine were made by oligo-directed mutagenesis using the polymerase chain reaction overlap extension method (Aiyar *et al.*, 1996). After confirming mutations by sequence analysis, each mutant was expressed in *Escherichia coli* K12, refolded, and purified as described previously (Lu *et al.*, 1992).

The GCSF-dependent suspension cell line OCI/AML1 was used for all experiments (Kelleher *et al.*, 1988). Minimum essential medium alpha (MEMα), L-glutamine, penicillin-streptomycin, fetal bovine serum (FBS), and phosphate-buffered saline were obtained from

Life Technologies (Frederick, MD). Isotonic solution for the Coulter counter (ISOTON II, Coulter Diagnostics, Hialeah, FL) was obtained from Curtin Matheson Scientific (Houston, TX). For routine passaging, cells were diluted to 10^5/mL in MEMα supplemented with 20% FBS, 200 mM L-glutamine, 100 units/mL penicillin, 100 μg/mL streptomycin, and 270 pM GCSF in a humidified atmosphere with 5% CO_2 at 37°C.

Equilibrium binding experiments

The equilibrium binding affinity between the soluble domain of GCSFR (Horan *et al.*, 1996) and each ligand at pH 7.4 was determined by surface plasmon resonance, using the BIAcore™ 2000 (BIAcore, Uppsala, Sweden). Wild-type and mutant GCSF, modified to include histidine tag $(His)_7$, were coupled to the BIAcore™ NTA chip in the presence of nickel. Binding of GCSFR to coupled GCSF was measured directly in eluent buffer (10 mM HEPES, 150 mM NaCl, 50 μM EDTA, 0.005% Surfactant P-20 (BIAcore, Uppsala, Sweden), pH 7.4). Varying concentrations of GCSFR were passed over a surface with 300 relative units (RU) of GCSF attached at a flow rate of 20 μL/min for 5 min. The binding curves were analyzed by BIAeval™ version 3.0 (BIAcore, Uppsala, Sweden), using a single-site binding model. A second method for measuring the equilibrium binding constants for the histidine mutants used the concentration of free receptor in equilibrium mixtures of GCSF and GCSFR. The rate of binding for various concentrations of GCSFR was determined in NTA buffer at a flow rate of 5 μL/min, with 1000 RU of $(His)_7$-GCSF attached to the surface, and a standard curve of receptor concentration *versus* binding was used to determine the concentration of free GCSFR. All samples were analyzed three times and all experiments were carried out in triplicate.

Once the absolute equilibrium binding affinity was determined for each ligand at pH 7.4, the ratio of equilibrium binding dissociation constants (K_D values) at pH 5.5 relative to pH 7.4 was measured for wild type, D110H, and D113H. Since $(His)_7$-GCSF could not be immobilized to the chip in the BIAcore™ at pH 5.5, these ratios were calculated using a cell receptor-binding assay. GCSF was labeled with ^{125}I (NEN Life Science Products, Boston, MA) by the Bolton-Hunter method and equilibrium binding experiments at both pH 5.5 and pH 7.4 were performed. To measure equilibrium binding, 2.5×10^7 cells were incubated for 3 h at 4°C in 1 mL of each of four subsaturating concentrations of radiolabeled ligand. The

binding of radiolabeled GCSF was saturable and specific (as determined by competition with unlabeled GCSF); therefore, the equilibrium binding affinity was calculated using a single-site binding model. For each experiment, identical ligand concentrations were used at both pH 7.4 and pH 5.5, and the K_D ratio at pH 7.4 relative to pH 5.5 was computed. Values for the absolute K_D values of the mutants at pH 7.4, as estimated from these cell-based assays, are also reported parenthetically in Table 5.1. The errors associated with the K_D ratios are standard deviations of at least two independent experiments.

Although there is no statistically significant difference in the K_D values for the three ligands at pH 7.4, any possible decrease in the surface binding affinity of the mutants relative to wild type only serves to further buttress validation of our theoretical predictions of reduced endosomal affinity, given the pH 5.5 to pH 7.4 K_D ratios. Thus, the primary effect of each histidine mutation is a reduction of the binding affinity at pH 5.5, without significant change in the binding affinity at pH 7.4.

Ligand depletion and cell proliferation experiments

Cells were passaged into supplemented MEMα medium without GCSF 24 h prior to the initiation of the ligand depletion and cell proliferation experiments, at which point parallel flasks of cells at a density of 10^5/mL were incubated in supplemented MEMα medium with a known concentration of wild-type GCSF, D110H, or D113H. For the depletion experiments, the initial ligand concentration was 125 pM, and the concentration in the medium supernatant was quantitated every 24 h over the time course using enzyme-linked immunosorbent assay (ELISA) kits obtained from R&D Systems (Minneapolis, MN). The errors associated with the ligand depletion results are standard deviations of at least two independent experiments. Wild-type GCSF depletion experiments performed using the YT-2C2 suspension cell line, which is GCSF-independent and does not express GCSFR, revealed nearly 80% intact ligand after six days (data not shown); therefore, ligand depletion from the medium indeed appears to be driven by receptor-mediated trafficking and not by differences in extracellular ligand stability. For the cell proliferation experiments, initial ligand concentrations were 25, 62, and 125 pM and OCI/AML1 cell growth in each flask was monitored every 24 h over the time course using a Coulter counter.

Internalization, recycling, and steady-state sorting experiments

Internalization experiments were performed over a time period of 5 min (4 time points), similarly to published work (Kuwabara *et al.*, 1996), and complex dissociation rates were fitted from these experiments. In brief, ^{125}I-labeled ligand was used to quantify the amount of surface-bound ligand and the rate of change in internalized ligand over time. An acetic acid strip, which removes only surface-bound ligand, was used to discriminate surface-bound and internal ligand at each time point. The internalization rate constants were calculated from these data. Internalized GCSF receptors have been found to be degraded, without any re-expression at the cell surface (Khwaja *et al.*, 1993); although this observation (*i.e.*, no GCSFR recycling) is for endocytosis induced by wild-type GCSF, any possible recycling of receptors internalized with the histidine analogs would actually serve to deplete these mutants from the extracellular medium to a greater extent than wild type. Our assumption that receptor sorting remains the same for the mutants is therefore a conservative one, so the focus of our recycling experiments is on ligand sorting. Indeed, it should be clear that reducing the endosomal binding affinity would enhance ligand recycling, particularly if receptor degradation is constitutive. Ligand recycling experiments were performed identically, except over a time period of 25 min (4 time points). Data from ligand recycling experiments were parameter fitted to obtain recycling rate constants. The errors associated with the dissociation, internalization, and recycling rate constants are standard deviations of at least three independent experiments. The recycling rate constants for the mutants were found to be greater than that for wild type with 95% confidence by two-sample *t*-test.

Steady-state sorting experiments are described in detail elsewhere (French *et al.*, 1994; Fallon *et al.*, 2000). Briefly, upon addition of saturating amounts of ^{125}I-labeled ligand, cells were incubated at 37°C for 3 h to bring the endocytic sorting process to steady state. Aliquots from the medium were then taken, and intact (recycled) ligand was separated from degraded ligand by gel filtration. The fraction of ligand recycled is the ratio of intact to total (intact + degraded). The errors associated with the ligand sorting fractions are standard deviations of the fractions recycled at three time points (5, 10, and 15 min).

RESULTS AND DISCUSSION

Experimental receptor binding properties of wild type and mutants

Since there are no native histidine residues in wild-type GCSF at the binding interface of interest, wild type should serve as an appropriate control in that it should show minimal sensitivity to binding affinity at endosomal pH relative to extracellular pH. To test whether our biochemical property targets were met, we performed equilibrium binding experiments for wild type and each of the Asp → His mutants at pH 7.4 and pH 5.5 (Table 5.1 and Figures 5.1A, 5.1B, and 5.1C). Both surface plasmon resonance and cell experiments demonstrate that there is no significant difference in binding affinity between the mutants and wild-type ligand at pH 7.4, consistent with our molecular modeling predictions. At the same time, the cell experiments demonstrate that the histidine mutants exhibit a significant decrease in binding affinity at pH 5.5 relative to pH 7.4, while wild-type binding remains largely insensitive to pH; this is also consistent with our computational modeling predictions. Since the mutants bind to GCSFR with significantly lower affinity than wild type under conditions representative of the endosomal compartments, we could then predict a cell-level result of increased ligand lifetime in the medium for the histidine analogs relative to native GCSF due to enhanced recycling.

Ligand depletion and cell proliferation results

We tested the first part of this cell-level prediction by comparing the behaviors of D110H and D113H to wild-type GCSF in ligand depletion and cell proliferation assays. Figure 5.2 shows that each mutant had a much greater half-life (> 500 h) than that of wild-type GCSF (~ 50 h). Additionally, neither mutant appears to have reduced potency relative to wild type over the first few days (Figures 5.3A, 5.3B, and 5.3C), suggesting no substantial loss of signaling competency despite the fact that both of the mutated residues lie at the receptor interface (see Figure 4.1). In fact, the mutants yield 50–100% enhancement in cell proliferation response relative to wild type after 6–8 days in culture, in a dose-dependent manner (Figures 5.3B and 5.3C). Maximal increases in cell proliferation for the mutants are seen at the intermediate initial ligand concentration (62 pM). The smaller relative effects observed for high initial ligand concentration are not unexpected, since ligand depletion is a

less significant factor under these conditions. Overall, these observations are consistent with the greater ligand availability over a longer period of time (Figure 5.2).

Comparison of cellular trafficking properties of wild type and mutants

Next, to test whether the mechanism underlying this increase in half-life and potency of both Asp → His mutants is specifically due to enhanced endosomal recycling we measured rates indicative of dissociation from the cell surface, internalization, and recycling. As seen in Table 5.2, we found no significant difference in the dissociation rate at the cell surface and all three ligands have roughly the same rate of internalization. In contrast, we find a greater than 50% increase in the recycling rate for the Asp → His mutants compared to wild type (Table 5.2). This result was confirmed by a complementary steady-state sorting assay, in which the fractions of internalized ligand sorted to recycling were measured to be approximately 45% for wild type and greater than 60% for the two mutants (Table 5.2). This enhancement of ligand recycling is precisely the goal we predicted and sought to achieve through our computational modeling.

While the experimentally measured increase in recycling is effectively from one round of internalization, the vast augmentation in mutant half-life (Figure 5.2) results from the compounded effect of internalization, recycling, re-internalization, and so on. The net increases in recycling (Table 5.2) and half-life (Figure 5.2) of the GCSF mutants are comparable to those seen for the library-screened IL-2 mutant (Fallon *et al.*, 2000), and kinetic modeling of IL-2 dynamics can quantitatively correlate endosomal affinity to ligand recycling and depletion (Fallon and Lauffenburger, 2000), thus supporting our results. A more detailed computational model correlating these GCSF trafficking dynamics to larger-scale cellular processes is presented in Chapter 6. The iterative effect of the recycling phenomenon can therefore greatly improve drug potency by increasing its lifetime *in vivo* and reducing the negative feedback propagated by the drug-induced expansion of cells expressing the target receptor. In particular, because receptor-mediated clearance of GCSF by peripheral neutrophils represents a bottleneck in drug efficacy (Layton *et al.*, 1989; Morstyn *et al.*, 1998), the *in vivo* potency of GCSF could be substantially enhanced by improving the trafficking properties of the ligand in the manner we have demonstrated.

Implications for drug design

The purpose of our work is to provide a rational strategy through which more potent analogs of certain protein therapeutics might be designed. In particular, cytokines such as GCSF, which have predominant cell-based clearance mechanisms (Layton *et al.*, 1989; Morstyn *et al.*, 1998), are prime candidates for mutagenesis to enhance trafficking properties. The use of histidine as a pH-activated switch to achieve our goal was not suggested by analysis of mutations in non-rationally screened agonists with increased ligand recycling (*e.g.*, the IL-2 double mutant, L18M/L19S). Rather, the choice of histidine in this application of cytokine design is in itself novel. Here, we only examined single substitutions to histidine to minimize any complications resulting from gross structural changes upon mutagenesis, yet these mutations appear sufficient to impact cellular trafficking in the necessary manner. While it may be possible to magnify the effect with multiple histidine substitutions, this minimalist approach may also be desirable in drug design to prevent possible immune complications upon administration. The methodology presented here should be generalizable to other systems. Given a crystal structure of a ligand/receptor complex, we believe this 'histidine switching' technique provides a framework for generating mutants with enhanced endosomal recycling of components of the trafficked complexes. To the best of our knowledge, this is the first work to demonstrate rational drug design in the context of a systems-level cellular trafficking analysis, rather than individual binding or signaling events *per se*.

REFERENCES

Aiyar, A., Xiang, Y. and Leis, J. (1996). Site-directed mutagenesis using overlap extension PCR. *Methods in Molecular Biology*. **57:** 177-191.

Fallon, E.M. and Lauffenburger, D.A. (2000). Computational model for effects of ligand/receptor binding properties on interleukin-2 trafficking dynamics and T cell proliferation response. *Biotechnology Progress*. **16:** 905-916.

Fallon, E.M., Liparoto, S.F., Lee, K.J., Ciardelli, T.L. and Lauffenburger, D.A. (2000). Increased endosomal sorting of ligand to recycling enhances potency of an interleukin-2 analog. *Journal of Biological Chemistry*. **275:** 6790-6797.

French, A.R. and Lauffenburger, D.A. (1997). Controlling receptor/ligand trafficking: effects of cellular and molecular properties on endosomal sorting. *Annals of Biomedical Engineering*. **25:** 690-707.

French, A.R., Sudlow, G.P., Wiley, H.S. and Lauffenburger, D.A. (1994). Postendocytic trafficking of epidermal growth factor receptor complexes is mediated through saturable and specific endosomal interactions. *Journal of Biological Chemistry*. **269:** 15749-15755.

Horan, T., Wen, J., Narhi, L., Parker, V., Garcia, A., Arakawa, T. and Philo, J. (1996). Dimerization of the extracellular domain of granulocyte-colony stimulating factor receptor by ligand binding: a monovalent ligand induces 2:2 complexes. *Biochemistry*. **35:** 4886-4896.

Kelleher, C.A., Wong, G.G., Clark, S.C., Schendel, P.F., Minden, M.D. and McCulloch, E.A. (1988). Binding of iodinated recombinant human GM-CSF to the blast cells of acute myeloblastic leukemia. *Leukemia*. **2:** 211-215.

Khwaja, A., Carver, J., Jones, H.M., Paterson, D. and Linch, D.C. (1993). Expression and dynamic modulation of the human granulocyte colony-stimulating factor receptor in immature and differentiated myeloid cells. *British Journal of Haematology*. **85:** 254-259.

Kuwabara, T., Kobayashi, S. and Sugiyama, Y. (1996). Kinetic analysis of receptor-mediated endocytosis of G-CSF derivative, nartograstim, in rat bone marrow cells. *American Journal of Physiology-Endocrinology and Metabolism*. **34:** E73-E84.

Layton, J.E., Hockman, H., Sheridan, W.P. and Morstyn, G. (1989). Evidence for a novel in vivo control mechanism of granulopoiesis: mature cell-related control of a regulatory growth factor. *Blood*. **74:** 1303-1307.

Lu, H.S., Clogston, C.L., Narhi, L.O., Merewether, L.A., Pearl, W.R. and Boone, T.C. (1992). Folding and oxidation of recombinant human granulocyte colony stimulating factor produced in *Escherichia coli*. *Journal of Biological Chemistry*. **267:** 8770-8777.

Morstyn, G., Dexter, T.M. and Foote, M. (1998). *Filgrastim (r-metHuG-CSF) in Clinical Practice*. Marcel Dekker, New York.

Table 5.1: Equilibrium dissociation constants for wild-type GCSF and histidine mutants at pH 7.4 and 5.5. The K_D values at pH 7.4 were determined by surface plasmon resonance measurements (Figure 5.1A) with parenthetical values calculated from cell experiments (Figure 5.1B). The K_D ratios showing the pH-dependence of receptor binding were measured using cell experiments (Figures 5.1B and 5.1C). Further details are provided in the Materials and Methods section.

	K_D, pH 7.4 (pM)	(K_D, pH 5.5)/(K_D, pH 7.4)
Wild Type	270 ± 90	1.7 ± 0.5
D110H	700 ± 400 (370 ± 150)	4.4 ± 0.8
D113H	400 ± 400 (320 ± 130)	6.8 ± 2.4

Table 5.2: Dissociation, internalization and recycling parameters for wild-type GCSF and histidine mutants. The dissociation, internalization, and recycling rate constants (k_{off}, k_{int}, and k_{rec}, respectively) and the ligand sorting fraction (fraction of internal ligand that is recycled intact) were determined as described in the Materials and Methods section.

	k_{off} (min^{-1})	k_{int} (min^{-1})	k_{rec} (min^{-1})	Ligand sorting fraction
Wild Type	0.030 ± 0.013	0.104 ± 0.016	0.020 ± 0.004	0.44 ± 0.08
D110H	0.038 ± 0.011	0.115 ± 0.003	0.032 ± 0.002	0.66 ± 0.02
D113H	0.020 ± 0.008	0.112 ± 0.004	0.048 ± 0.018	0.62 ± 0.02

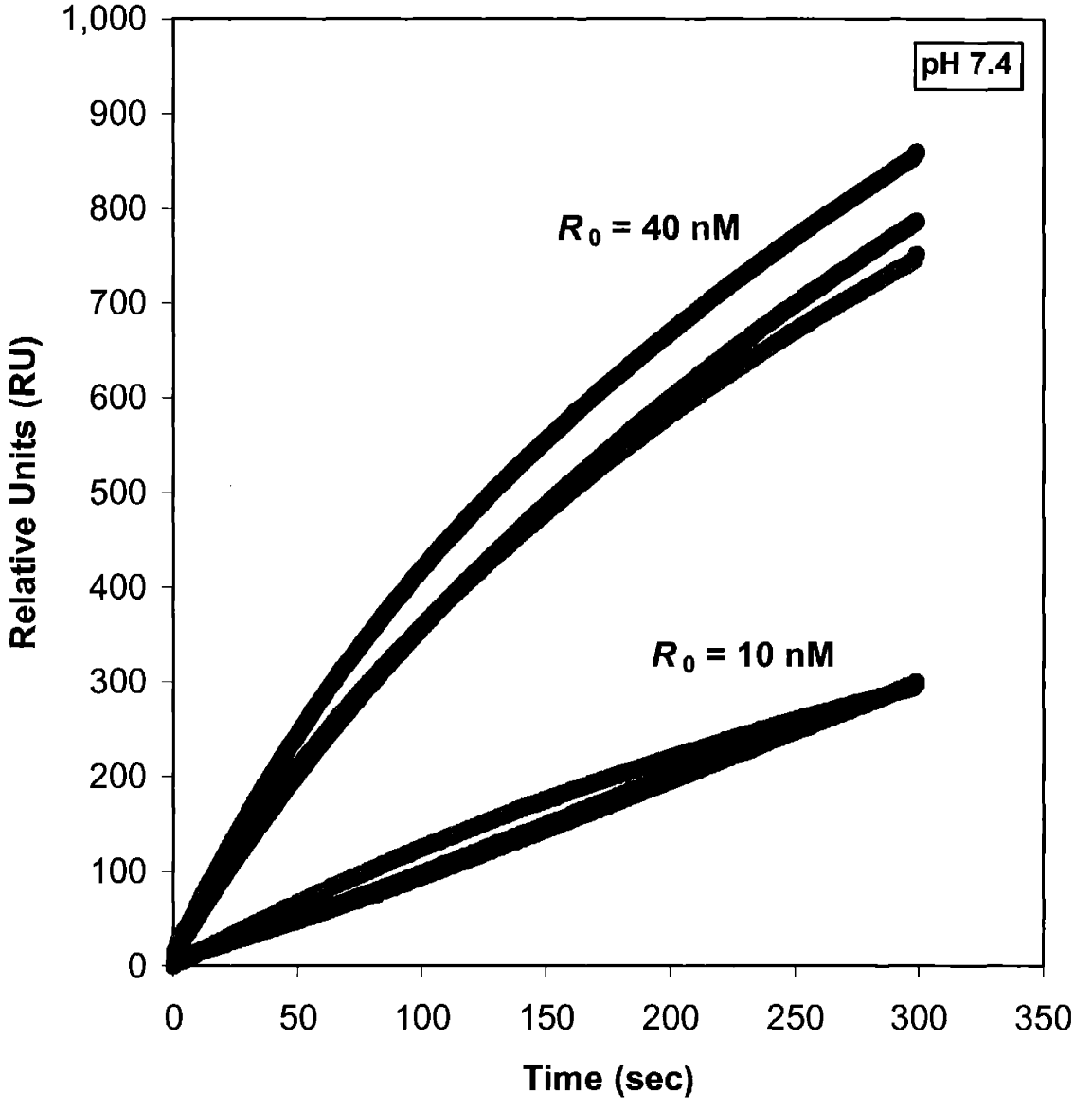

Figure 5.1A: Binding association curves for wild-type GCSF, D110H, and D113H from surface plasmon resonance measurements under two representative conditions at pH 7.4. In these experiments, soluble GCSFR (ranging from 10 nM to 300 nM) was flowed over immobilized ligand and K_D values were calculated from a single-site binding model. Color coding: wild type (black), D110H (blue), and D113H (red).

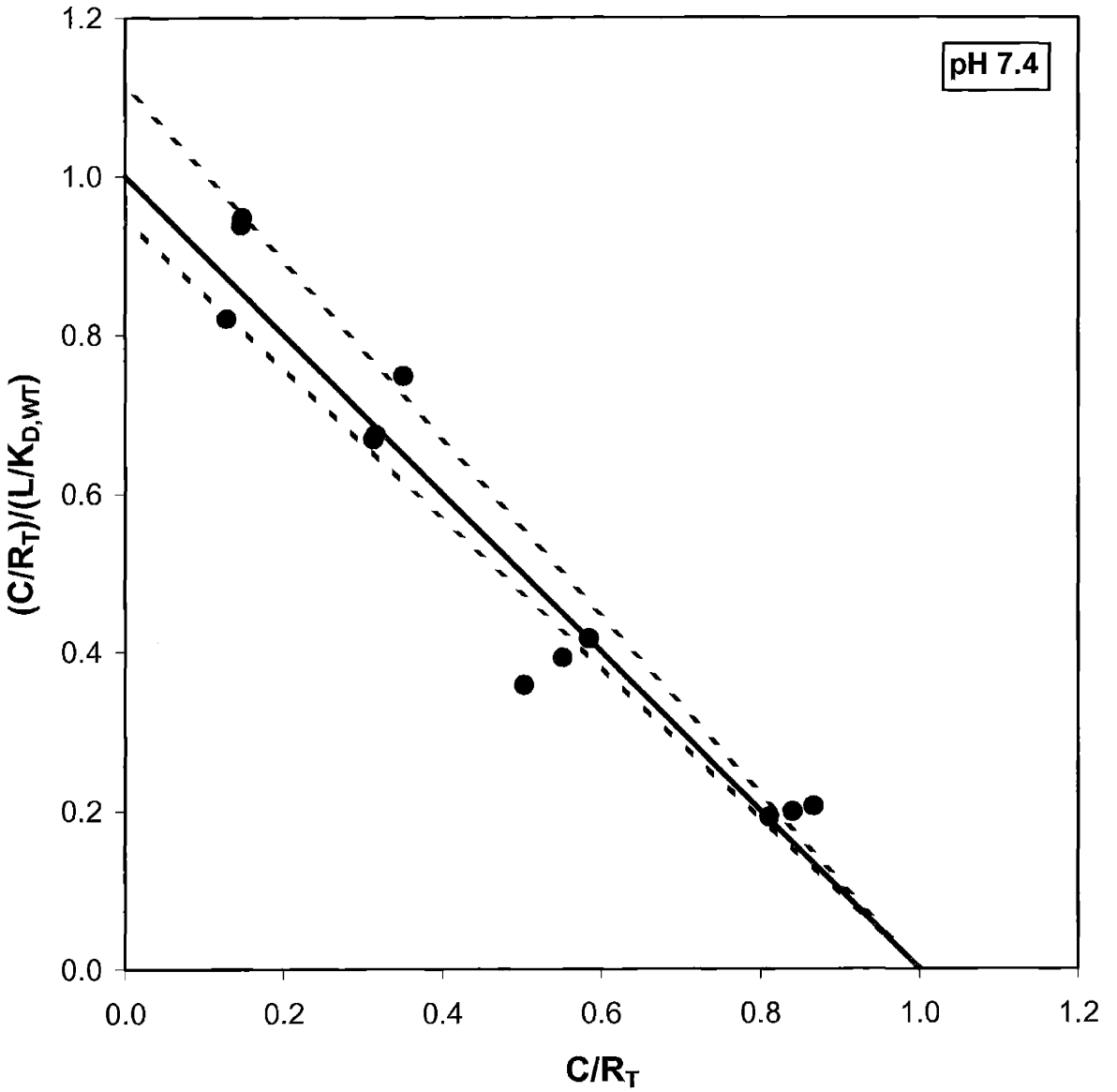

Figure 5.1B: Scatchard analysis of representative cell-binding assays for wild-type GCSF, D110H, and D113H at pH 7.4. Plotting $(C/R_T)/(L/K_{D,WT})$ versus C/R_T (where C/R_T is the fraction of bound receptors) should yield a straight line with slope –1 and y-intercept 1 for wild-type GCSF. The mutants also lie along this line, indicating that they have similar K_D values to wild type at pH 7.4. Color coding: wild type (black), D110H (blue), and D113H (red).

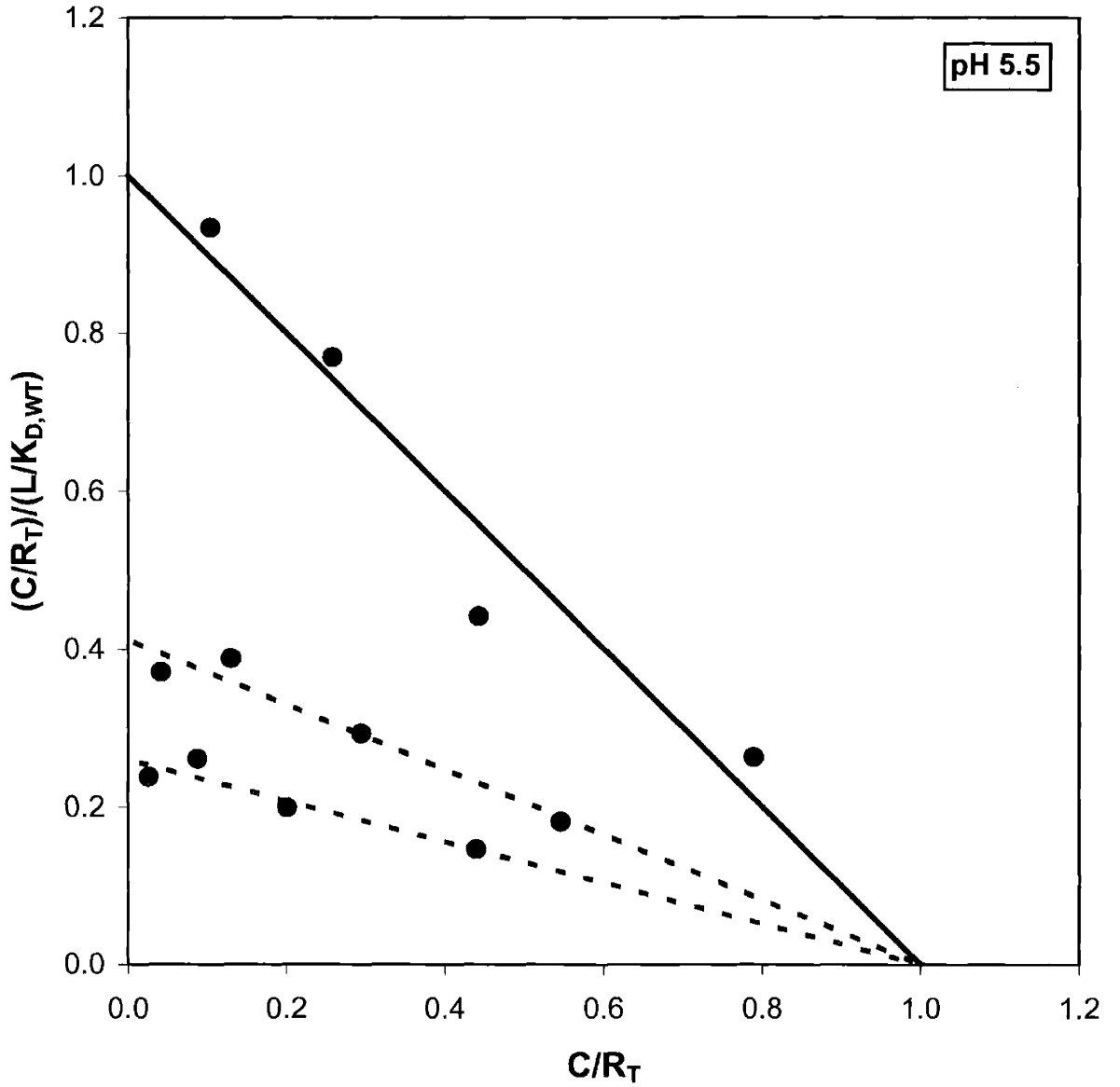

Figure 5.1C: Scatchard analysis of representative cell-binding assays for wild-type GCSF, D110H, and D113H at pH 5.5. Here, the mutants lie below the wild-type line and have less negative slopes, indicating that they have higher K_D values (lower affinities) than wild type at pH 5.5. Color coding: wild type (black), D110H (blue), and D113H (red).

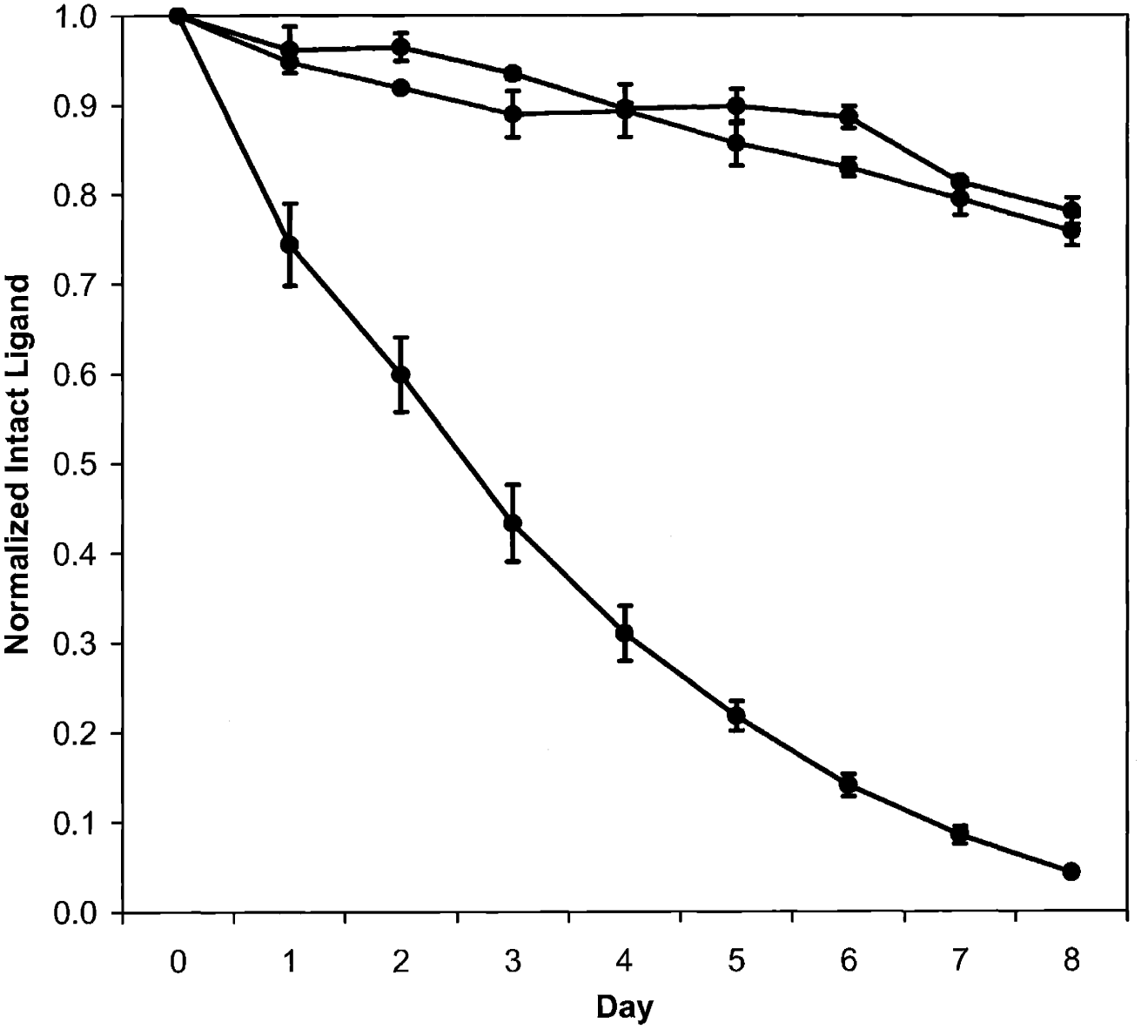

Figure 5.2: Normalized ligand depletion over time in response to an initial bolus of wild-type GCSF, D110H, or D113H. The initial ligand concentration was 125 pM and the initial cell density was 10^5/mL. The concentration in the medium supernatant over time was quantified using enzyme-linked immunosorbent assays. Color coding: wild type (black), D110H (blue), and D113H (red).

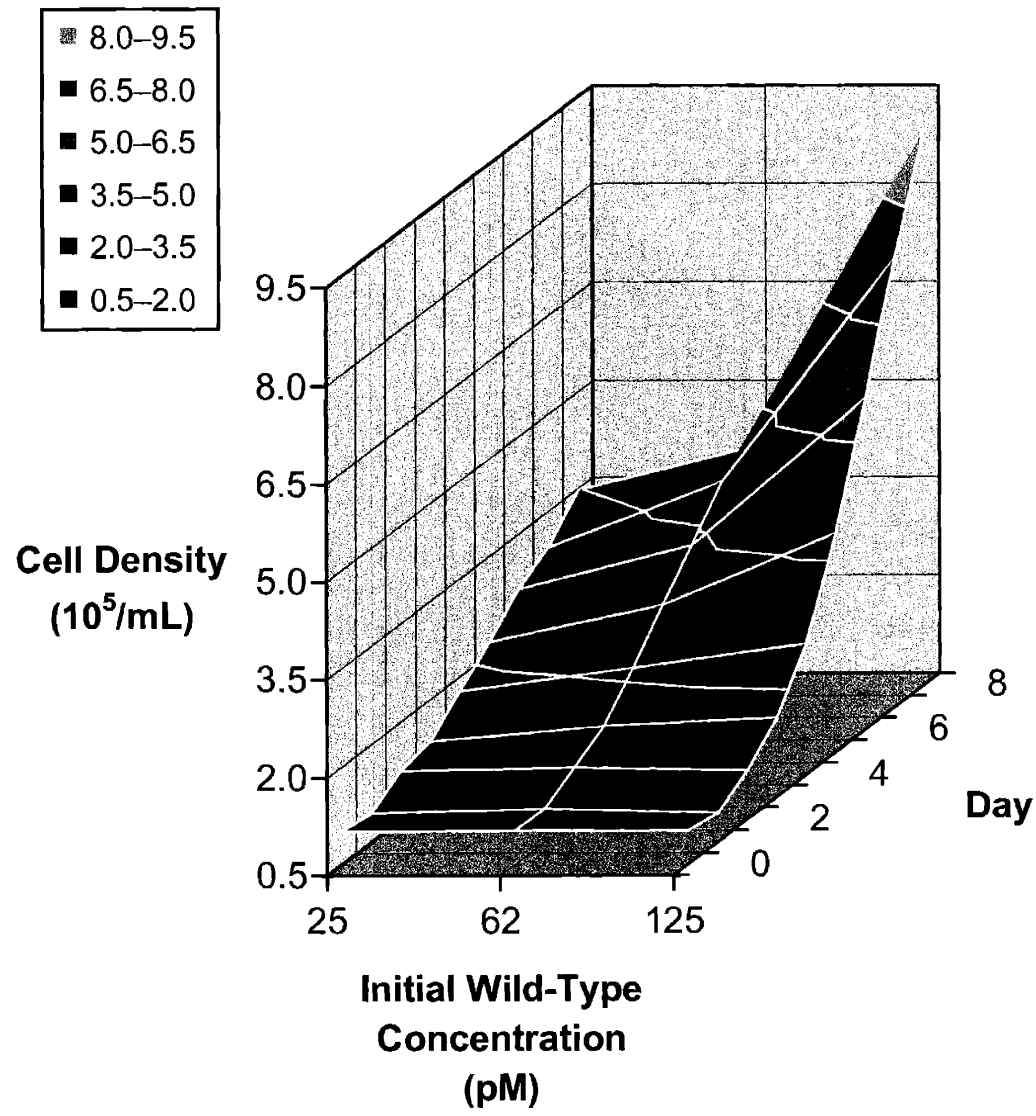

Figure 5.3A: Cell proliferation over time in response to wild-type GCSF. Initial cell density was 10^5/mL and initial ligand concentrations were 25, 62, and 125 pM. Cell growth was monitored using a Coulter counter.

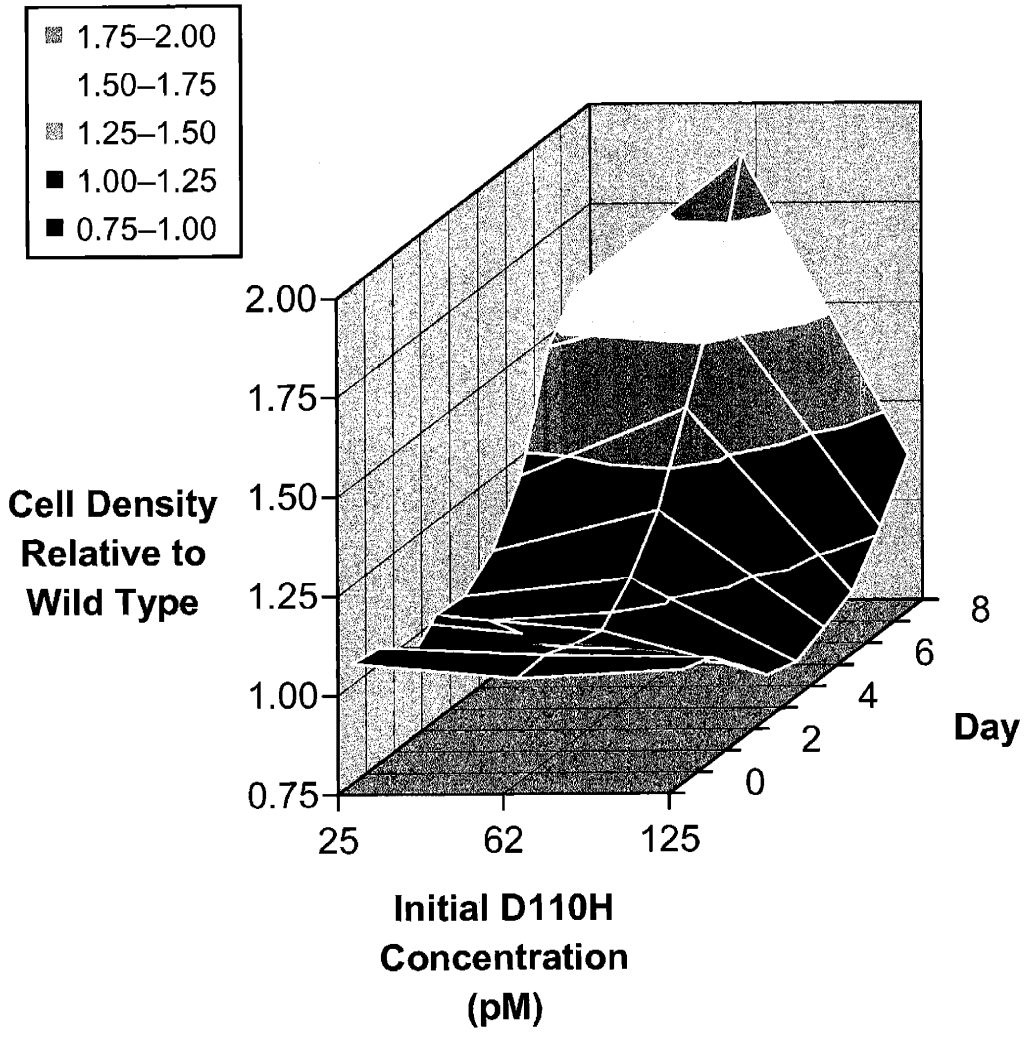

Figure 5.3B: Cell proliferation over time in response to D110H, normalized to wild type. Initial cell density was 10^5/mL and initial ligand concentrations were 25, 62, and 125 pM. Cell growth was monitored using a Coulter counter.

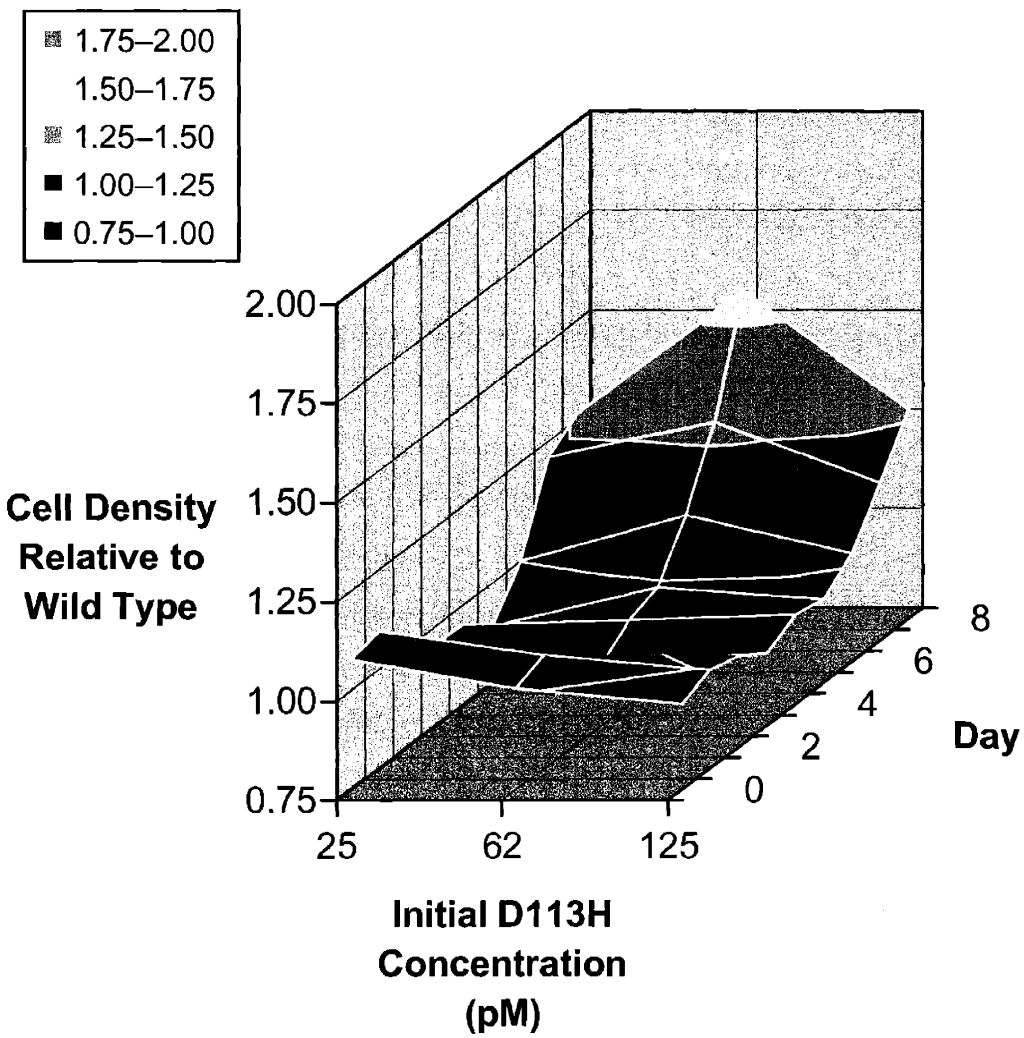

Figure 5.3C: Cell proliferation over time in response to D113H, normalized to wild type. Initial cell density was 10^5/mL and initial ligand concentrations were 25, 62, and 125 pM. Cell growth was monitored using a Coulter counter.

APPENDIX

We have shown that the 'histidine switching' strategy works for the two most promising mutations, D110H and D113H. However, the selection of all candidate ligands was done prior to any experimental testing, and to improve the chances that at least one of the mutations would prove more potent than wild-type GCSF, we also proposed that the Q120H mutation be made. The rationale for choosing this mutant was as follows. Based upon the computed electrostatic binding free energies (Figure 4.5), the D110H and D113H mutants were predicted to exhibit the desirable pH-sensitivity of binding; however, this figure also suggests that $D110H^0$ and $D113H^0$ may not bind as well as wild type at extracellular pH. If cell-surface receptor recognition were too poor, these mutants would not exhibit superagonism, even if their trafficking properties were improved. While subsequent experimental measurements showed that this was not a concern, at the time of candidate selection we wanted to choose another analog that would be most likely to maintain cell-surface receptor binding affinity. The only mutant that was predicted (based upon Figure 4.5) to bind GCSFR as well as wild type – in fact, it was predicted to bind more tightly – was Q120H. This ligand should also exhibit some pH-sensitivity to binding, although the difference in the electrostatic binding free energies for $Q120H^+$ and $Q120H^0$ is only about 0.8 kcal/mol. Thus, this mutant would not be expected to exhibit a pH-sensitivity to binding as great as that for D110H or D113H.

The equilibrium binding experiments showed no significant difference in binding affinity between Q120H and wild type at pH 7.4 (Table 5A.1). While the prediction from Figure 4.5 was that this mutant would bind more tightly, an examination of Figure 4.4 reveals that the control simulation for Gln120, in which the mutation was not made but the local side chains were allowed to rearrange, results in an electrostatic binding free energy lower than the original crystal structure and comparable to the simulation for $Q120H^0$. This is not observed with any of the other control simulations (see Figure 4.4), and possibly results from artifacts in side chain rearrangement (see Table 4.2). However, when the simulation for $Q120H^0$ is properly normalized to this control simulation for Gln120, molecular modeling does predict a comparable affinity to wild type at pH 7.4. The computed increase in the electrostatic binding free energy for $Q120H^+$ (0.8 kcal/mol) corresponds to at most a 3.9-fold decrease in affinity compared to $Q120H^0$ under the simulation conditions. Thus, the

predicted decrease in endosomal affinity for Q120H is more modest than those for D110H and D113H. Indeed, the Q120H mutant displays a pH-sensitivity to binding greater than that for wild type but less than that for the Asp → His mutants (Table 5A.1).

In ligand depletion and cell proliferation experiments, Q120H had a longer half-life than wild type, and was more potent (Figures 5A.1 and 5A.2). In fact, whereas neither D110H nor D113H displayed superagonist properties up to 4 days in culture (see Figures 5.3B and 5.3C), Q120H exhibited approximately a 50% increase in cell density after 4 days (Figure 5A.2), suggesting that this ligand results in enhanced cell signaling through an increase in the intrinsic signal per complex (since the binding affinities in Table 5A.1 imply that Q120H would not form more cell-surface signaling complexes than wild type). Furthermore, the difference in specific growth rates for wild type and Q120H in Figure 5A.2 increases with time, implying that cell proliferation in response to the mutant cannot only be explained by enhanced signaling, but rather improved trafficking is implicated as well at longer times. This is also supported by the ligand depletion profiles in Figure 5A.1.

As mentioned, the Q120H mutant displays a pH-sensitivity to binding in between that for wild type and the Asp → His mutants, and this correspondingly results in intermediate values for the recycling rate constant and ligand sorting fraction (Table 5A.2). The dissociation and internalization rate constants are not significantly different from wild type. Similar to the observations for D110H and D113H, the improvements in Q120H trafficking can augment half-life in culture, as seen in Figure 5A.1.

Thus, Q120H also appears to be a more potent ligand than wild type. However, based on our results, the superagonist properties likely arise from a combination of enhanced signaling and trafficking properties, rather than modifications in trafficking alone. More detailed experiments would be required to quantify the contribution of signaling to the superagonism of this mutant. Nonetheless, the 'histidine switching' framework was successfully employed to select three mutations of GCSF with improved trafficking properties and enhanced potencies compared to the native cytokine.

Table 5.A1: Comparison of Q120H binding properties to wild-type GCSF and Asp → His mutants. The K_D values at pH 7.4 were determined by surface plasmon resonance measurements and the K_D ratios showing the pH-dependence of receptor binding were measured using cell experiments, as described in the Materials and Methods section of this chapter.

	K_D, pH 7.4 (pM)	(K_D, pH 5.5)/(K_D, pH 7.4)
Wild Type	270 ± 90	1.7 ± 0.5
D110H	700 ± 400	4.4 ± 0.8
D113H	400 ± 400	6.8 ± 2.4
Q120H	400 ± 200	3.5 ± 0.4

Table 5.A2: Comparison of Q120H trafficking properties to wild-type GCSF and Asp → His mutants. The dissociation, internalization, and recycling rate constants (k_{off}, k_{int}, and k_{rec}, respectively) and the ligand sorting fraction (fraction of internal ligand that is recycled intact) were determined as described in the Materials and Methods section of this chapter.

	k_{off} (min^{-1})	k_{int} (min^{-1})	k_{rec} (min^{-1})	Ligand sorting fraction
Wild Type	0.030 ± 0.013	0.104 ± 0.016	0.020 ± 0.004	0.44 ± 0.08
D110H	0.038 ± 0.011	0.115 ± 0.003	0.032 ± 0.002	0.66 ± 0.02
D113H	0.020 ± 0.008	0.112 ± 0.004	0.048 ± 0.018	0.62 ± 0.02
Q120H	0.027 ± 0.019	0.108 ± 0.014	0.029 ± 0.010	0.58 ± 0.07

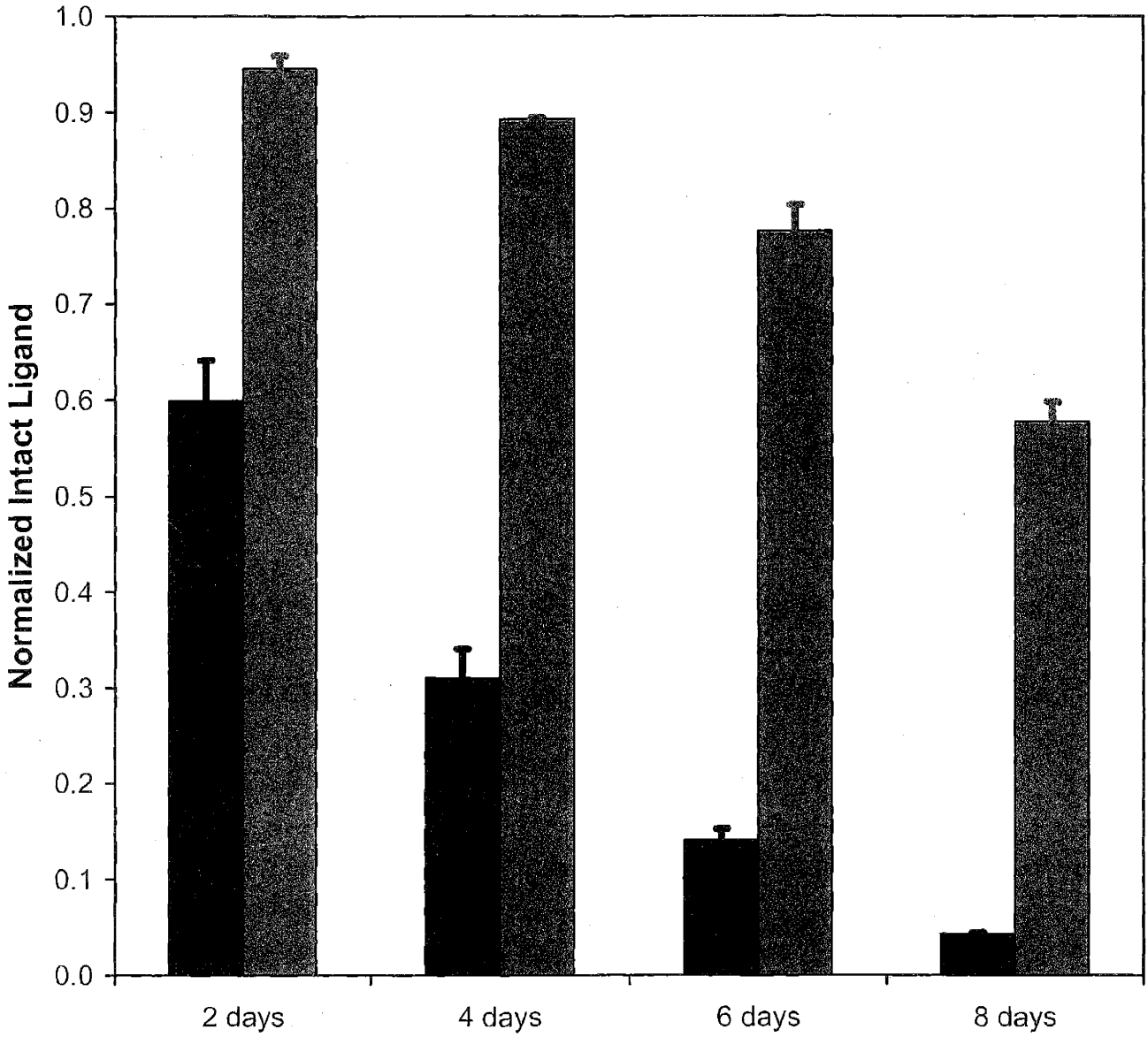

Figure 5A.1: Normalized ligand depletion over time in response to an initial bolus of wild-type GCSF or Q120H. The initial ligand concentration was 125 pM and the initial cell density was 10^5/mL. The concentration in the medium supernatant over time was quantitated using enzyme-linked immunosorbent assays. Color coding: wild type (black) and Q120H (green).

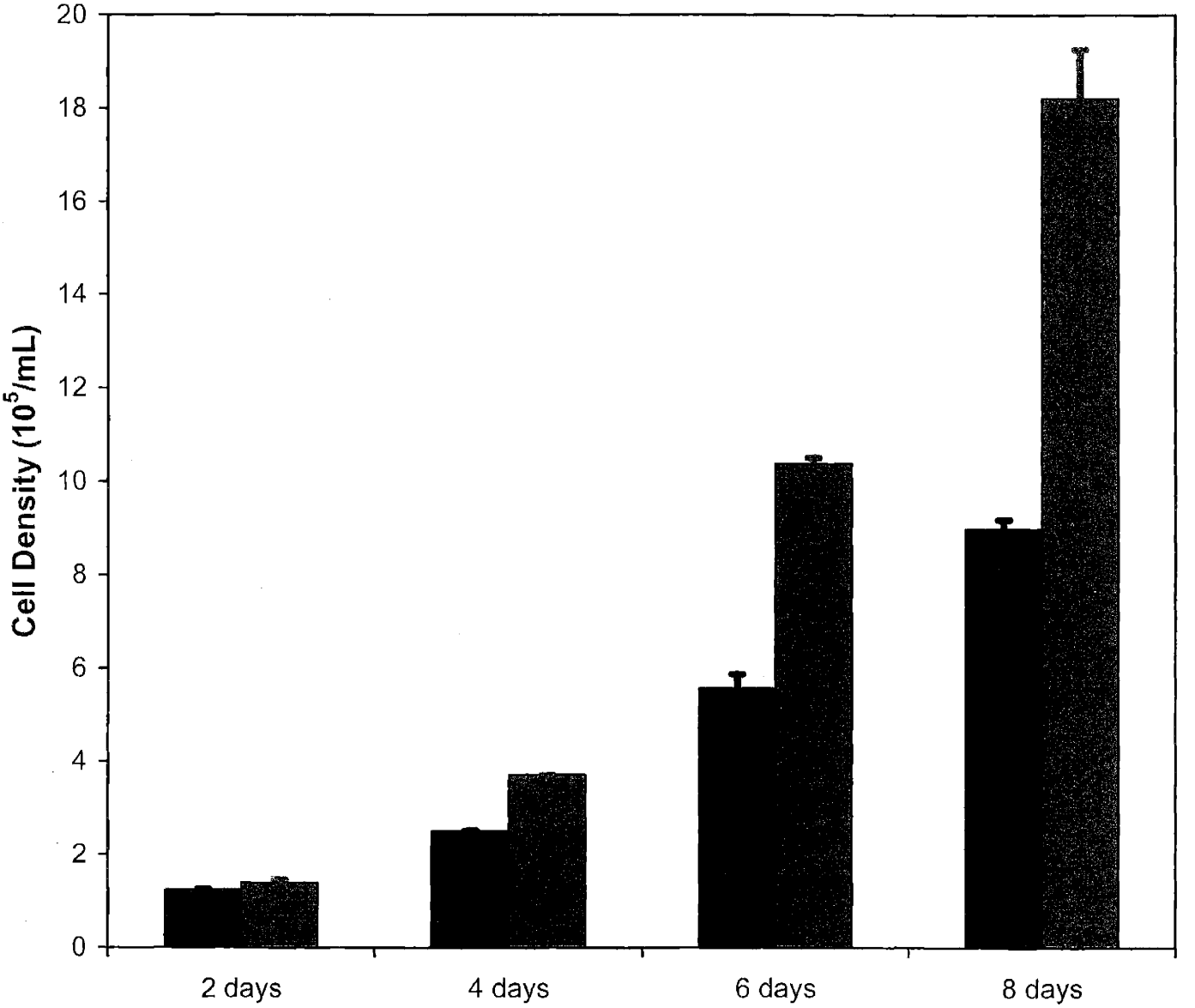

Figure 5A.2: Cell proliferation over time in response to wild-type GCSF or Q120H. Initial cell density was 10^5/mL and initial ligand concentration was 125 pM. Cell growth was monitored using a Coulter counter. Color coding: wild type (black) and Q120H (green).

Chapter 6: Mathematical Modeling of Cellular Trafficking Processes

The cytokine granulocyte colony-stimulating factor (GCSF) is of great clinical importance, with one of its major applications to rapidly elevate the peripheral neutrophil levels of cancer patients undergoing chemotherapy and other patients with neutropenia, primarily through accelerated granulopoiesis. However, these mature neutrophils express the GCSF receptor (GCSFR); therefore, as they enter the bloodstream, they present a significant and specific clearance mechanism of GCSF that increases with time. Here, we formulate a mathematical model that describes these cell-level GCSF/GCSFR dynamics, and correlate the effect of these endocytic trafficking processes to ligand depletion in an *in vitro* culture. We further incorporate this cell-level model into an existing pharmacokinetic/ pharmacodynamic (PK/PD) model, to gain insight into the effects that specific cellular parameters may have on overall PK/PD effects *in vivo*. Our cell-level model suggests that ligand depletion may be reduced *in vitro* by decreasing the endosomal affinity of endocytosed GCSF/GCSFR complexes, consistent with experimental findings. Additionally, our modified PK/PD model suggests that a GCSF analog with a modification that effectively eliminates renal clearance should have a significantly longer half-life *in vivo* and should therefore improve peripheral neutrophil counts. This is consistent with clinical studies on a polyethylene glycol chemical conjugate of GCSF called SD/01. We further explore the sensitivities of extracellular and endosomal receptor-binding properties on PK/PD behavior. The model predicts that a GCSF analog that eliminates renal clearance and has reduced endosomal binding affinity may result in an even longer ligand half-life and increased neutrophil counts at a lower dose than either wild-type GCSF or SD/01. More generally, this type of hierarchical model provides a correlation between the molecular and pharmacological properties of a drug, and may help to elucidate design goals for such protein therapeutics.

INTRODUCTION

Currently, the design and development of a therapeutic drug takes around 12 years and costs upwards of $800 million. Of this total cost, approximately one-third is spent on drugs and experiments that fail in the laboratory. In addition, once a candidate drug makes it

into clinical trials, the success rate is still less than 20%. One of the major problems in the development of a successful drug is the inability to correlate the effects of a molecular perturbation in the drug to the resulting effects in efficacy and half-life *in vivo*. This correlation can be particularly non-intuitive for protein therapeutics, such as hematopoietic cytokines, that act as agonists for cell-surface receptors.

The pharmacodynamic properties of such an agonist depend not only on receptor binding affinity, but subsequent intracellular signaling cascades and endocytic trafficking of the cell-surface cytokine/receptor complexes (see Chapters 2 and 5). Endocytic trafficking often serves to attenuate the generated signals, resulting in ligand depletion and receptor downregulation, which in turn reduces the pharmacodynamic potency of the drug over time. Furthermore, the pharmacokinetic profile of such a cytokine is often determined not only by non-specific renal and hepatic clearance mechanisms, but also through specific endocytosis and degradation by local and systemic cell populations expressing the target receptor (Layton *et al.*, 1989). Thus, optimization of cell-surface binding and endocytic trafficking properties could improve both the pharmacodynamic and pharmacokinetic properties of the drug. An understanding of the molecular properties that govern cytokine/receptor dynamics in the context of these cellular processes may help to optimize the design of the therapeutic protein.

An important instance in which altered trafficking of the ligand may have a significant impact on these *in vivo* properties is the cytokine granulocyte colony-stimulating factor (GCSF). GCSF is indicated for a wide range of clinical applications, primarily for cancer patients undergoing chemotherapy and other neutropenic patients (Morstyn *et al.*, 1998). The drug is typically administered subcutaneously or intravenously; once it has entered the bloodstream, it diffuses into the bone marrow, where it binds to its receptor (GCSFR) on precursor cells, inducing them to proliferate and differentiate into mature neutrophils. These mature neutrophils then enter the bloodstream. In this manner, the cytokine rapidly elevates peripheral neutrophil counts in these immuno-compromised patients so that they are less susceptible to serious complications from infection. However, the bone marrow precursor cells internalize and degrade the ligand – a negative feedback mechanism that can reduce its pharmacodynamic potency. Additionally, the mature neutrophils also express GCSFR, and they bind, internalize, and degrade the drug from the bloodstream. Thus, given the large number of these neutrophils, there exists a substantial

second negative feedback loop that operates through much larger space *in vivo* and reduces the pharmacokinetic properties of the drug.

Here, we have developed a mathematical model that relates extracellular ligand depletion to the molecular properties of GCSF and cells expressing the GCSF receptor. We have further integrated this cell-level model to a physiologically relevant pharmacokinetic/ pharmacodynamic (PK/PD) model. Currently, there is little mechanistic understanding as to how the various levels of biological complexity – from molecular interactions to cellular function to tissue organization and beyond – are integrated. The hierarchical model described here attempts to tie together these various biological levels and, for the specific case of GCSF, the model provides some insight into the molecular parameters of the therapeutic protein that should be varied in order to improve clinical efficacy.

MODEL DESCRIPTION

Our cell-level mathematical model describes the fate of extracellular ligand and cell receptors over time. These molecules form complexes at the cell surface, become internalized into endosomal compartments, and undergo sorting to either recycling or degradation (Figure 6.1). The model variables, parameters, and equations that describe these processes are given in Tables 6.1, 6.2, and 6.3, respectively. While not treating every step explicitly, this model attempts to capture the salient features of ligand/receptor trafficking dynamics that may have predictive value.

The cell-level model simulates the time-progression of the following variables: extracellular ligand concentration (L), free surface receptors per cell (R_s), surface complexes per cell (C_s), intracellular ligand concentration per cell (L_i), free intracellular receptors per cell (R_i), intracellular complexes per cell (C_i), and degraded ligand per cell (L_d) over the course of several days during which the cell density (N) is increasing. We can then use this kinetic model to simulate ligand depletion and endosomal sorting after an initial bolus of ligand into the extracellular medium, and compare these to experimental results that were obtained using a GCSF-dependent cell line, OCI/AML1. In the absence of ligand, L, C_s, L_i, C_i, and L_d are zero and N is time-invariant. Then, as is clear from Equation 6.1 in Table 6.3, the number of steady-state surface receptors per cell (R_s) is determined from a balance between constitutive receptor endocytosis (k_{eR}) and receptor synthesis (V_s). Likewise, from

Equation 6.4, the number of steady-state intracellular receptors per cell (R_i) is set by the degradation rate constant (k_{deg}) and the receptor synthesis rate (V_s). These values serve as initial conditions for the cell-surface and intracellular receptors in simulations performed with non-zero initial extracellular ligand.

An extracellular ligand molecule can bind reversibly to a surface receptor (with the forward rate constant, k_f, linked to the reverse rate constant, k_r, through the equilibrium dissociation constant, $K_D = k_r/k_f$). These surface complexes are then internalized (k_{eC}) into endosomal compartments, which have a volume V_e per cell. Under these intracellular conditions, the ligand/receptor dynamic can be significantly different (k_{fi}, k_{ri}, and $K_{Di} = k_{ri}/k_{fi}$), and therefore intracellular receptor occupancy may also vary from that seen on the cell surface. From the endosomes, the molecules are either recycled back to the cell membrane and extracellular medium intact or degraded in lysosomal compartments. There is evidence that GCSF receptors and similar cytokine receptors are degraded upon internalization (Khwaja *et al.*, 1993), and intracellular complexes and intracellular receptors are therefore routed to degradation (k_{deg}). Conversely, we allow ligand molecules that dissociate from intracellular receptors to recycle back out of the cell intact (k_{rec}).

Thus, in tracking the ligand throughout these cellular processes, there is a ligand molecule associated with L, L_i, L_d, C_s, and C_i. As a consistency check, a mass balance on the five equations for these species reveals that the total ligand in the system (intact + degraded) is indeed conserved:

$$\frac{dL_{total}}{dt} = \frac{d\left(L + NL_iV_e + \left(C_s + C_i + L_d\right)\cdot\frac{N}{N_A}\right)}{dt} = 0 \qquad (6.11)$$

The intention in developing this model was to see whether it could capture the gross features seen experimentally, both in ligand depletion and endosomal sorting studies. Our experimental results in Chapter 5 showed differential depletion and sorting properties for wild-type GCSF and two single Asp → His mutants, D110H and D113H. The two mutants were found to bind the cell-surface receptor with the same affinity as wild type and they also internalized at the same rate. However, the mutants bound with lower affinity to the receptor than wild type at endosomal pH, resulting in enhanced ligand recycling and ligand half-life.

The parameters for the cell-level model were either measured experimentally or taken from the literature. While the actual values were obtained from heterogeneous cell types, the trends observed from model simulations are largely insensitive to a change in any particular constant that is less than an order of magnitude. The receptor synthesis rate was chosen so that the steady-state number of surface receptors (5,000) would be comparable to the values reported in the literature (Morikawa *et al.*, 1996; El-Sonbaty *et al.*, 1995a; El-Sonbaty *et al.*, 1995b). The equilibrium endosomal affinity for wild-type GCSF was the only fitted parameter in the model. The affinity of wild-type GCSF was measured to be 1.7-fold lower at pH 5.5 than at pH 7.4 (see Chapter 5); however, the pH difference alone does not necessarily provide a true indication of the endosomal environment. Therefore, the experimental value (1.7) was multiplied by a factor of 50 to account for these potential environmental differences ($K_{Di} = 85K_D$ for wild type). The experimentally measured endosomal affinities of the mutants (4.4-fold lower for D110H and 6.8-fold lower for D113H) were also multiplied by this same scaling factor for the model ($K_{Di} = 220K_D$ for D110H and $K_{Di} = 340K_D$ for D113H); they were *not* fitted separately to match the results from their respective endosomal sorting and ligand depletion experiments. The model does not directly account for a sorting time of 5–10 min prior to recycling or degradation (Lauffenburger and Linderman, 1993); we therefore accelerate the endosomal kinetics to allow this sorting to occur without introducing a lag time into the model. Nonetheless, the model is largely insensitive to the actual values of k_{fi} and k_{ri} for a given K_{Di}. Because wild-type GCSF is prone to aggregation at neutral pH, an additional term was included that accounts for this loss ($k_{l,WT}$) over time. This rate constant was determined from experimental measurements in which approximately 75% of GCSF remained intact after 6 days in culture with a YT-2C2 cell line that does not express GCSFR. Interestingly, at least one of these aspartate residues is implicated in neutral-pH aggregation (David Brems, personal communication), so no k_l term is included for the mutants.

Model simulations were run on MATLAB using the *ode15s* subroutine. Ligand depletion was simulated over a period of 8 days with an initial ligand concentration of 125 pM, the same conditions as in experiments. Cell density was expressed as an exponential function that matched experimental data with an initial density of 10^8 cells/L. For endosomal sorting simulations, cells were exposed to a bolus of extracellular ligand for 180 min, after

which time the values for R_s, R_i, C_i, and L_i were recorded. These values were then used as initial conditions in a second simulation, in which the initial ligand concentration and k_f were set to zero; k_f was set to zero to prevent recycled ligand from rebinding to cell-surface receptors. Then, the values for L (intact) and L_d (degraded) were recorded for 15 min. The computational sorting fraction was then calculated from the average of three time points (5, 10, 15 min), as was done experimentally. This procedure was done for wild-type GCSF and both mutants, with the mutants having reduced endosomal binding affinities, as described above.

The full pharmacokinetic/pharmacodynamic (PK/PD) model is shown schematically in Figure 6.2, and can be described by the more complete set of equations in Table 6.3, which are adapted from a previous model (Wang *et al.*, 2001) to incorporate the cell-level model. The intent here is not to fully reproduce the original PK/PD model proposed by Wang *et al.*, but rather to take the salient features of that model and combine it with the cell-level model to generate a modified PK/PD model that explicitly includes molecular and cellular parameters.

In the original PK/PD model, two different doses of GCSF (750 μg and 375 μg) were administered subcutaneously to patients to generate experimental data for fitting the model parameters (Wang *et al.*, 2001). The dosing was best fit by a bisegmental absorption model, treating the fractional bioavailability of the total dose as two theoretically separate dose sites (n_1 and n_2). These doses then enter the bloodstream (main compartment concentration, L), where they can be cleared by renal, hepatic, and other non-specific clearance mechanisms (lumped parameter, η). In the original model, a saturable clearance mechanism was also included, but since this likely represents the receptor-mediated clearance by peripheral neutrophils, this implicit mechanism was replaced by the explicit cell-level model. The data is best fit by a two-compartment model, and the concentration of the drug in the second compartment (L_4) is driven by the interchange (Q) between the two compartments. Finally, in the original PK/PD model, the concentration of drug in the main compartment indirectly augments neutrophil production above basal levels (k_{in}) through a saturable mechanism (E_{max}, EC_{50}) with cooperativity, γ (Wang *et al.*, 2001):

$$production = k_{in} \cdot \left(1 + \frac{E_{max} L^{\gamma}}{EC_{50}{}^{\gamma} + L^{\gamma}}\right) \tag{6.12}$$

While this effect is expressed as a function of absolute drug concentration (L), it is likely more important to consider the number of complexes that the drug can form on the surface of bone marrow precursor cells (as an initial approximation), since it is the complexes that generate the signals to proliferate and differentiate into mature neutrophils (Fallon and Lauffenburger, 2000). In other words, if we designed an analog of the drug that had lower binding affinity for the receptor, it could reduce receptor-mediated clearance in the bloodstream, but it may also have reduced potency in generating such signals on the time scale of interest. A more relevant value to consider is L/K_D, and we have therefore substituted ($L \cdot K_{D,WT}/K_D$) for L in describing neutrophil production (see Table 6.3).

RESULTS

Comparison of cell-level (*in vitro*) model predictions to experimental results

The cell-level model is intended to simulate endosomal sorting and extracellular depletion of ligand. In Chapter 5, we determined the endosomal sorting fraction of wild-type GCSF experimentally using a GCSF-dependent human suspension cell line, OCI/AML1. We have also used this cell line to quantify the extracellular depletion of wild type over a time course of 8 days, during which the cell density was increasing. Additionally, we have measured the endosomal sorting fractions and ligand depletion profiles for two single mutants of GCSF, D110H and D113H. These analogs were rationally designed to maintain similar trafficking properties to wild-type GCSF, with the exception that the histidine residues would contribute to lower-affinity binding at endosomal pH. This, in turn, was predicted to enhance endosomal sorting to recycling, and therefore decrease extracellular ligand depletion.

Wild-type experiments were simulated using the base parameter values given in Table 6.2. The trials for the histidine mutants were performed identically, except the endosomal affinity (K_{Di}) was proportionally changed to match experimental measurements ($K_{Di} = 220K_D$ for D110H and $K_{Di} = 340K_D$ for D113H). For endosomal sorting simulations, cells were exposed to a bolus of extracellular ligand for 180 min, after which time the values

for R_s, R_i, C_i, and L_i were recorded. These values were then used as initial conditions in a second simulation, in which the initial ligand concentration and k_f were set to zero; k_f was set to zero to prevent recycled ligand from rebinding to cell-surface receptors. Then, the values for L (intact) and L_d (degraded) were recorded for 15 min. The computational sorting fraction was then calculated from the average of three time points (5, 10, 15 min), as was done experimentally. The computational endosomal sorting fraction was insensitive to the initial bolus of extracellular ligand. This procedure was done for wild-type GCSF and both mutants, with the mutants having reduced endosomal binding affinities, as described above. For the experiments and simulations of each analog, the average and standard deviation of these three time points are reported in Table 6.4.

The ligand depletion experiments were simulated over 8 days with an initial cell density of 10^8/L and an initial extracellular ligand concentration of 125 pM to match the experimental conditions. Since the cell line used is GCSF-dependent, exponential growth (specific growth rate = 0.277 day^{-1}) was included to account for changing cell density, $N(t)$. The fraction of intact ligand in the extracellular medium after this time period is reported in Table 6.4.

The results in Table 6.4 indicate that the model, even with lumped parameters from heterogeneous sources, can effectively capture the cellular trafficking dynamics observed experimentally. We have therefore integrated this cell-level model into an existing pharmacokinetic/pharmacodynamic (PK/PD) model to understand how the parameters in this full model might impact the efficacy of the drug in an *in vivo* setting. The remaining results focus on observations from this modified PK/PD model, with results showing the sensitivities of $L(t)$ and $N(t)$ to changes in model parameters.

In vivo predictions on ligand depletion and neutrophil counts from modified PK/PD model

The modified PK/PD model, in which we have omitted the saturable clearance mechanism and integrated the cell-level model (Figure 6.2), suggests that neutrophil production – the desired result from GCSF therapy – is correlated to the concentration of ligand in the bloodstream (compartment 3). Therefore, mechanisms that deplete the ligand would reduce neutrophil production. To understand the extent to which the parameters in the

model affect ligand depletion and neutrophil counts, we have monitored these two variables in response to the sensitivity of certain model parameters. In most cases, the sensitivities were simulated with two different amounts of subcutaneously injected ligand (375 μg or 750 μg). The absolute neutrophil count (ANC) at the beginning of the simulation was fixed by the basal rate of production (k_{in}) and the rate of decay (k_{out}).

Effects of non-specific clearance, η

Most therapeutics are administered at levels that are far above the concentrations needed to elicit the appropriate response *in vivo*. Often, this has to be done because of rapid non-specific clearance mechanisms in the body that make it difficult to sustain the physiologically normal levels over extended periods of time. In the case of wild-type GCSF, primarily renal clearance limits the half-life of the drug to several hours, while the time course of therapy is often several days (Morstyn *et al.*, 1998). Therefore, treatment necessitates multiple, artificially high doses of GCSF to the patient. Because these non-specific clearance mechanisms can depend significantly on molecular dimensions, artificially increasing the size of the molecule may help to reduce these clearance mechanisms. This can often be achieved by covalently attaching a bulky, inert moiety to the drug. Typically, polyethylene glycol (PEG) is chosen since it is known to be bioinert and the chemistry can be well controlled (Delgado *et al.*, 1992). This approach has shown promise in studies of many growth factors and cytokines, including interleukin-6, megakaryocyte growth and development factor, and interleukin-2 (Harris *et al.*, 2001).

Recently, the Food and Drug Administration approved a PEG-conjugated GCSF molecule (termed SD/01) for therapeutic use. The PEG moiety is 20 kDa in size, and is attached to the N-terminus of GCSF, which alone is only approximately 19 kDa. The PEG modification effectively eliminates renal clearance of the drug (Johnston *et al.*, 2000); therefore, depletion is essentially mediated by receptor-mediated uptake and degradation. The experimentally measured lifetime of SD/01 is dose dependent, but is on the order of 4 to 5 days in rats (Morstyn *et al.*, 2001).

We determined the effects of the non-specific clearance on ligand concentration, L (from compartment 3), and the absolute neutrophil count, N. The parameter η was varied from the base value to zero, and the resulting ligand concentration and ANC profiles were

recorded (Figure 6.3). This figure shows increases in ligand half-life that correspond well with experimental observations with SD/01. Furthermore, the neutrophil counts achieve a greater peak values and also maintain higher levels for longer periods of time as η is decreased.

Effects of endosomal binding affinity, K_{Di}

Since it was clear from our *in vitro* studies and from the cell-level model that decreasing the endosomal binding affinity (K_{Di}) could improve the ligand sorting fraction and enhance ligand half-life, we wanted to determine the effect of this parameter on ligand depletion and neutrophil counts in the PK/PD model. As seen in Figure 6.4, there is a small increase in GCSF concentration as the endosomal affinity is decreased; however, this still expands the neutrophil profile by up to one day. This can be explained by the fact that the K_D for GCSF is approximately 150 pM, whereas the subcutaneous doses are resulting in ligand concentrations in the nanomolar range. Thus, the apparently small increase in intact ligand between days 1 and 2 is sufficient to elicit a significant improvement in neutrophil production. Given these artificially high doses, it is more desirable to have a small amount of ligand available for a long period of time than to have a large initial dose of ligand that is rapidly depleted.

Effects of extracellular binding affinity, K_D, *in the absence of non-specific clearance*

Since it is possible to eliminate renal clearance of GCSF through PEG-modification (Johnston *et al.*, 2000), we focus on the effects of specific cellular parameters on the modified PK/PD model in the absence of non-specific clearance ($\eta = 0$). Under these conditions, the only mechanism by which ligand can be cleared in the model is through specific receptor-mediated endocytosis and degradation. One mechanism for reducing this depletion would be to decrease the flux of ligand molecules into the cell. This could be achieved in two ways: decreasing the internalization rate constant or decreasing the extracellular binding affinity. Since at present we do not know how to manipulate the ligand in a way that would decrease the internalization rate constant, we focus on the effect of extracellular binding affinity on ligand depletion and neutrophil enhancement. While it is clear that decreasing the extracellular binding affinity should increase ligand half-life,

Equation 6.8 in Table 6.3 suggests that this would also decrease the positive influence of ligand concentration on the neutrophil production rate. This tradeoff may explain why greatly increasing the binding affinity of a drug may not improve its efficacy and why greatly decreasing its affinity may also not result in enhanced effectiveness; there is likely an optimal binding affinity for a particular therapeutic application.

Figure 6.5 shows the GCSF concentration and neutrophil profiles for four hypothetical PEG-GCSF molecules (K_D = 50, 150, 450, 1350 pM). While ligand depletion is not significant at the higher dose (Figures 6.5C and 6.5D), the neutrophil counts show some interesting behaviors at the lower dose (Figure 6.5B). For the first 3 days, the neutrophil counts increase as the ligand binding affinity increases. However, the higher-affinity ligands are depleted more rapidly (Figure 6.5A), and this results in somewhat inverted neutrophil profiles at longer times. While three of the curves maintain relatively similar neutrophil counts over the first three days (K_D = 50, 150, 450 pM), the 50-pM and 150-pM binders have rapidly decaying profiles, whereas the 450-pM binder maintains neutrophil counts at a high level over the entire time course. Thus, the ligand with the 450 pM receptor-binding affinity appears to be the best in this application.

Interestingly, while SD/01 was developed to eliminate renal clearance, we have shown that it does not maintain wild-type affinity to the receptor. We have previously measured the receptor-binding affinity of SD/01 to be about 450 pM (see Chapter 2). This suggests that SD/01 may be optimized in multiple ways.

Effects of extracellular binding kinetics in the absence of non-specific clearance

We further examined the effects of binding by simulating hypothetical variants of SD/01 with altered extracellular binding kinetics. None of these molecules had non-specific clearance (η = 0) and they all had the same extracellular binding affinity (K_D = 450 pM). The kinetics for each hypothetical molecule were altered by increasing or decreasing the extracellular association (k_f) and dissociation (k_r) rate constants by the same percentage, thus maintaining the equilibrium binding affinity. Figure 6.6 shows that the kinetics have a minimal effect on ligand concentration and neutrophil counts, although at long times the neutrophil counts are slightly improved for lower k_r.

At short times, the ligand concentration is much greater than the K_D, and the system is therefore saturated. However, as the ligand concentration gets closer to the K_D, the kinetics of binding become more important and can change the efficacy of the drug. The results in Figure 6.6 suggest that depletion is driven more by ligand association than by the lack of ligand dissociation, since ligand depletion is reduced for slower association. If depletion were driven more by the lack of ligand dissociation, then faster dissociation would save more ligand molecules from internalization. Thus, if GCSF were dosed at concentrations near the K_D, it could be more effective to administer an analog with slower binding kinetics.

Effects of endosomal binding affinity, K_{Di}, in the absence of non-specific clearance

While decreasing the extracellular binding affinity is a way to decrease ligand depletion (Figure 6.5), there is a possible tradeoff of reduced pharmacodynamic potency because fewer signaling complexes are formed on the surface of the target cells in the timeframe of interest. This is the manifested to a first approximation in Equation 6.8 in Table 6.3. However, an alternate way to decrease the amount of ligand depleted without altering surface binding properties is to route the internal ligand to recycling instead of degradation. We have shown that, for GCSF, the amount of ligand recycled (instead of degraded) can be enhanced by decreasing the endosomal affinity of the complex, and we have captured this effect in our cell-level model (Table 6.4). This has also been shown for other ligand/receptor systems (French *et al.*, 1995; Fallon *et al.*, 2000), suggesting that this may be an important strategy for designing such ligands for therapeutic applications.

To determine the effects of endosomal binding affinity on ligand concentration and neutrophil counts in the PK/PD model, we simulated several theoretical SD/01-like molecules with reduced endosomal binding affinity. It is conceivable that this could be achieved in practice by adding a PEG-modification to one of the histidine mutants, D110H or D113H.

As seen in Figure 6.7A, decreasing the endosomal affinity can greatly increase the ligand half-life. Furthermore, the effect on neutrophil counts is even more dramatic (Figure 6.7B). The neutrophil counts for the ligand with the highest endosomal affinity return to baseline after 8 days, whereas the counts for the ligand with the lowest endosomal affinity stay at the maximal value even at 8 days. A comparison of Figures 6.5B and 6.7B shows that

decreasing the extracellular binding affinity can reduce potency at short times, whereas that is not observed in the simulations where only the endosomal binding affinity is decreased. While this is a result of our formulation of Equation 6.8 in Table 6.3, it is likely that this would be observed experimentally as well.

Comparison of two theoretical doses of GCSF analogs to wild type

In these simulations, we have observed that artificially high doses are required to sustain some level of therapeutic efficacy over a desirable time period. Often, even a single injection of such a large dose is insufficient for the entire treatment time, and multiple doses become necessary. The doses used in this work (375 μg and 750 μg, subcutaneous) were chosen from the PK/PD model formulated by Wang *et al.*, since our model incorporates many of those model parameters, including the bioavailability and bisegmental absorption parameters for these two doses. Since the simulations indicate that an SD/01-like molecule and an SD/01-like analog with decreased endosomal binding affinity would have improved efficacy compared to wild-type GCSF, we tested whether they could be equally effective at lower doses. This would be beneficial to the patient, the supplier, and the medical support staff.

The bisegmental absorption of the 750 μg dose gave initial conditions of n_{10} = 9.5×10^{-9} mol and n_{20} = 19.3×10^{-9} mol (a total of 28.8×10^{-9} mol) (Wang *et al.*, 2001). We simulated wild-type GCSF with this initial dose. We then simulated both SD/01 and an SD/01-like ligand with 5-fold lower endosomal affinity than normal (possibly a PEG-modified histidine mutant of GCSF) with much lower hypothetical doses, $n_{10} = 2.5\times10^{-9}$ mol and $n_{20} = 2.5\times10^{-9}$ mol. This total available dose is only about 17% that available from the 750 μg dose for wild-type GCSF.

The results for these three simulations are given in Figure 6.8. Figure 6.8A shows a rapid and large increase in the wild-type concentration, but the ligand is then completely consumed in less than 2 days. By contrast, the maximum peak of SD/01 is lower but the ligand is sustained for about 6 days. The SD/01-like ligand with reduced endosomal affinity is not fully depleted during the time course. The impact on neutrophil counts are shown in Figure 6.8B. The counts return to baseline after about 5 days for wild type, and they return to baseline after about 8 days for SD/01. However, the counts are more than 6-fold higher

than baseline for the SD/01 analog with reduced endosomal affinity at the end of the time course.

DISCUSSION

We have described here a hierarchical model that integrates a cell-level mathematical model of GCSF/GCSFR trafficking with a traditional pharmacokinetic/pharmacodynamic (PK/PD) model. We have made predictions on *in vivo* behavior based on the sensitivities of parameters representing physiological processes, including molecular and cellular parameters in the subset of equations representing the cell-level model.

The base value of the parameter for non-specific clearance, η, was fitted in a PK/PD model based upon clinical data (Wang *et al.*, 2001). Incremental reduction of this parameter in our simulations led to greater ligand sustenance and enhanced neutrophil counts over time. In the presence of non-specific clearance, decreases in the endosomal affinity were predicted to result in small increases in ligand concentration, with neutrophil profiles extended by up to one day. Our model likely underpredicts the magnitude of this effect, as other clinical data show a much more significant contribution of cell-mediated clearance in the presence of non-specific clearance mechanisms leading to significant nonlinear pharmacokinetics (Layton *et al.*, 1989; Morstyn *et al.*, 1998). These nonlinearities are not seen at the extremes of high GCSF dosage (when receptor-mediated clearance would be saturated) or severe neutropenia (when the number of cells participating in receptor-mediated clearance would be very low) (Layton *et al.*, 1989; Morstyn *et al.*, 1998). Any additional weight on the receptor-mediated clearance pathway would only lend more credence to our conjecture that molecular and cellular parameters can significantly impact the potency of therapeutic proteins such as hematopoietic cytokines.

Many of the simulations focus on *in vivo* behavior in the absence of non-specific clearance. SD/01, a GCSF analog with a 20-kDa polyethylene glycol (PEG) moiety at the N-terminus, is essentially depleted by only specific cell-mediated clearance (Johnston *et al.*, 2000). Interestingly, in the absence of these non-specific clearance mechanisms, it has been suggested that SD/01 is self-regulating *in vivo* (Johnston *et al.*, 2000). Part of this regulation is likely due to the negative feedback loop depicted in Figure 6.2. As neutrophil counts increase, the drug is then depleted to a greater extent, which in turn attenuates the increase in

neutrophil production. Based upon our model results, we propose that this regulation can be further tuned by also altering the molecular-level properties of the drug.

For example, SD/01 has a 3-fold lower affinity for GCSFR than wild-type GCSF. This slight reduction in extracellular binding affinity increases ligand concentration over time while maintaining neutrophil counts over a longer period of time in comparison to a hypothetical SD/01-like ligand with wild-type binding affinity (Figures 6.5A and 6.5B). The proposed self-regulation could be further improved by reducing the endosomal affinity of SD/01 (Figure 6.7). We have rationally designed GCSF mutants (D110H and D113H) whose receptor-binding properties are more pH-sensitive than wild type. These mutants bind with lower affinities than wild type at endosomal pH, and are therefore recycled to a much greater extent. If the effects of PEG-conjugation were superimposable upon the effects of one of these histidine mutants, the resulting PEG-conjugated analog (*e.g.*, PEG-D110H or PEG-D113H) could have even more desirable therapeutic properties than either wild-type GCSF or SD/01 (Figure 6.8). These could include greater stability (by substitution of the aspartate involved in neutral pH aggregation), lower dosing amounts which could reduce toxicity and side effects, and less frequent dosing.

To the best of our knowledge, this is the first attempt to develop a hierarchical PK/PD model that provides a link between molecular parameters and physiological response. We believe that such a model can have great value in determining which parameters play important roles in the pharmacokinetics and pharmacodynamics of a drug, and may thus provide insights and design goals for developing next-generation therapeutics.

REFERENCES

Delgado, C., Francis, G.E. and Fisher, D. (1992). The uses and properties of PEG-linked proteins. *Critical Reviews in Therapeutic Drug Carrier Systems*. **9:** 249-304.

El-Sonbaty, S.S., Tsuchiya, H., Watanabe, M., Hochito, K., Kunisada, T., Shimosaka, A. and Matsuda, I. (1995a). Exogenous expression of human granulocyte colony-stimulating factor receptor in a B-lineage acute lymphoblastic leukemia cell line: a possible model for mixed lineage leukemia. *Leukemia Research*. **19:** 249-256.

El-Sonbaty, S.S., Watanabe, M., Hochito, K., Yamaguchi, K., Matsuda, I. and Tsuchiya, H. (1995b). Exogenously expressed granulocyte colony stimulating factor (G-CSF) receptor on K562 cells can transduce G-CSF triggered growth and differentiation signals. *International Journal of Hematology*. **61:** 61-68.

Fallon, E.M. and Lauffenburger, D.A. (2000). Computational model for effects of ligand/receptor binding properties on interleukin-2 trafficking dynamics and T cell proliferation response. *Biotechnology Progress*. **16:** 905-916.

Fallon, E.M., Liparoto, S.F., Lee, K.J., Ciardelli, T.L. and Lauffenburger, D.A. (2000). Increased endosomal sorting of ligand to recycling enhances potency of an interleukin-2 analog. *Journal of Biological Chemistry*. **275:** 6790-6797.

French, A.R., Tadaki, D.K., Niyogi, S.K. and Lauffenburger, D.A. (1995). Intracellular trafficking of epidermal growth factor family ligands is directly influenced by the pH sensitivity of the receptor/ligand interaction. *Journal of Biological Chemistry*. **270:** 4334-4340.

Ghosh, R.N., Gelman, D.L. and Maxfield, F.R. (1994). Quantification of low-density lipoprotein and transferrin endocytic sorting in HEP2 cells using confocal microscopy. *Journal of Cell Science*. **107:** 2177-2189.

Harris, J.M., Martin, N.E. and Modi, M. (2001). Pegylation: a novel process for modifying pharmacokinetics. *Clinical Pharmacokinetics*. **40:** 539-551.

Johnston, E., Crawford, J., Blackwell, S., Bjurstrom, T., Lockbaum, P., Roskos, L., Yang, B.B., Gardner, S., Miller-Messana, M.A., Shoemaker, D., Garst, J. and Schwab, G. (2000). Randomized, dose-escalation study of SD/01 compared with daily filgrastim in patients receiving chemotherapy. *Journal of Clinical Oncology*. **18:** 2522-2528.

Khwaja, A., Carver, J., Jones, H.M., Paterson, D. and Linch, D.C. (1993). Expression and dynamic modulation of the human granulocyte colony-stimulating factor receptor in immature and differentiated myeloid cells. *British Journal of Haematology*. **85:** 254-259.

Kuwabara, T., Kobayashi, S. and Sugiyama, Y. (1996). Kinetic analysis of receptor-mediated endocytosis of G-CSF derivative, nartograstim, in rat bone marrow cells. *American Journal of Physiology-Endocrinology and Metabolism*. **34:** E73-E84.

Lauffenburger, D.A. and Linderman, J.J. (1993). *Receptors: Models for Binding, Trafficking, and Signaling*. Oxford University Press, New York.

Layton, J.E., Hockman, H., Sheridan, W.P. and Morstyn, G. (1989). Evidence for a novel in vivo control mechanism of granulopoiesis: mature cell-related control of a regulatory growth factor. *Blood*. **74:** 1303-1307.

Morikawa, K., Morikawa, S., Miyawaki, T., Nagasaki, M., Torii, I. and Imai, K. (1996). Constitutive expression of granulocyte colony-stimulating factor receptor on a human B-lymphoblastoid cell line. *British Journal of Haematology*. **94:** 250-257.

Morstyn, G., Dexter, T.M. and Foote, M. (1998). *Filgrastim (r-metHuG-CSF) in Clinical Practice*. Marcel Dekker, New York.

Morstyn, G., Foote, M.A., Walker, T. and Molineux, G. (2001). Filgrastim (r-metHuG-CSF) in the 21st century: SD/01. *Acta Haematologica*. **105:** 151-155.

Wang, B., Ludden, T.M., Cheung, E.N., Schwab, G.G. and Roskos, L.K. (2001). Population pharmacokinetic-pharmacodynamic modeling of Filgrastim (r-metHuG-CSF) in healthy volunteers. *Journal of Pharmacokinetics and Pharmacodynamics*. **28:** 321-342.

Table 6.1: Model variables.

Cell-level model variables	Description
N	cell density, #/L
R_s	cell-surface receptors, #/cell
C_s	cell-surface complexes, #/cell
L_i	intracellular ligand, M
R_i	intracellular receptors, #/cell
C_i	intracellular complexes, #/cell
L	extracellular ligand (or main compartment ligand), M
L_d	degraded ligand, #/L
Additional PK/PD model variables	**Description**
L_4	ligand in second compartment, M
n_1	bisegmental adsorption site 1 from subcutaneous dose, mol
n_2	bisegmental adsorption site 2 from subcutaneous dose, mol

Table 6.2: Model parameters.

Cell-level model parameters	Base value	Description
K_D	150×10^{-12} M	extracellular equilibrium dissociation constant, see Chapter 2
k_r	0.03 min^{-1}	extracellular dissociation rate constant, see Chapter 5
k_f	k_r/K_D	extracellular association rate constant
K_{Di}	$85K_D$	intracellular equilibrium dissociation constant, see Model Description
k_{ri}	$100k_r$	intracellular dissociation rate constant, see Model Description
k_{fi}	k_{ri}/K_{Di}	intracellular association rate constant
k_{eR}	0.005 min^{-1}	constitutive receptor endocytosis rate constant, (Kuwabara *et al.*, 1996)
V_s	25 min^{-1}	receptor synthesis rate, see Model Description
k_{eC}	0.10 min^{-1}	complex endocytosis rate constant, see Chapter 5
V_e	10^{-14} L	endosomal volume, (French *et al.*, 1995)
N_A	6.02×10^{23} molec/mol	Avogadro's number
k_{rec}	0.15 min^{-1}	recycling rate constant, (Ghosh *et al.*, 1994)
k_{deg}	0.059 min^{-1}	degradation rate constant, (Kuwabara *et al.*, 1996)
$k_{l,WT}$	4.17×10^{-5} min^{-1}	rate constant for loss of functional wild type from medium, unpublished

Additional PK/PD model parameters	Base value	Description, all taken from Wang *et al.* (2001)
V_3	1.81 L	volume of main compartment
k_{13}	0.0044 min^{-1}	absorption rate constant from site 1 to main compartment
k_{23}	0.0033 min^{-1}	absorption rate constant from site 2 to main compartment
η	0.0049 L/min	rate constant for non-specific clearance of L
Q	4.65×10^{-4} L/min	rate of interchange between main and secondary compartments
V_4	0.249 L	volume of secondary compartment
k_{in}	3.13×10^{6} cells/L/min	basal neutrophil production rate
E_{max}	12.7	maximal fold increase in basal neutrophil production rate
EC_{50}	2.53×10^{-10} M	concentration eliciting half-maximal response in absence of cooperativity
γ	1.34	Hill coefficient
k_{out}	7.57×10^{-4} min^{-1}	neutrophil decay rate constant

Table 6.3: Model equations.

Cell-level model		PK/PD model	
$\frac{d(NR_s)}{dt} = \left(-k_f LR_s + k_r C_s - k_{eR} R_s + V_s\right) \cdot N$			(6.1)
$\frac{d(NC_s)}{dt} = \left(k_f LR_s - k_r C_s - k_{eC} C_s\right) \cdot N$			(6.2)
$\frac{d(NL_i)}{dt} = \left(\left(-k_{fi} L_i R_i + k_{ri} C_i\right) \cdot \frac{1}{N_A V_e} - k_{rec} L_i\right) \cdot N$			(6.3)
$\frac{d(NR_i)}{dt} = \left(-k_{fi} L_i R_i + k_{ri} C_i + k_{eR} R_s - k_{deg} R_i\right) \cdot N$			(6.4)
$\frac{d(NC_i)}{dt} = \left(k_{fi} L_i R_i - k_{ri} C_i + k_{eC} C_s - k_{deg} C_i\right) \cdot N$			(6.5)
$\frac{dL}{dt} = \left(-k_f LR_s + k_r C_s + k_{recL} L_i V_e N_A\right) \cdot \frac{N}{N_A} - k_{l,WT} L$	(6.6')	$\frac{dL}{dt} = \frac{1}{V_3} \cdot \left(k_{13} n_1 + k_{23} n_2 - \eta L + Q \cdot \left(L_4 - L\right)\right) + \left(-k_f LR_s + k_r C_s + k_{rec} L_i V_e N_A\right) \cdot \frac{N}{N_A}$	(6.6)
$\frac{d(NL_d)}{dt} = \left(k_{deg} C_i\right) \cdot N$	(6.7')		
		$\frac{dL_4}{dt} = \frac{Q}{V_4} \cdot \left(L - L_4\right)$	(6.7)
		$\frac{dN}{dt} = k_{in} \cdot \left(1 + \frac{E_{max} \left(\frac{LK_{D,WT}}{K_D}\right)^{\gamma}}{EC_{50}{}^{\gamma} + \left(\frac{LK_{D,WT}}{K_D}\right)^{\gamma}}\right) - k_{out} N$	(6.8)
		$\frac{dn_1}{dt} = -k_{13} n_1$	(6.9)
		$\frac{dn_2}{dt} = -k_{23} n_2$	(6.10)

Table 6.4: Comparison of cell-level model and cell-based experiments.

	Ligand sorting fraction (experiment)	Ligand sorting fraction (model)	Fraction of ligand intact after 8 days (experiment)	Fraction of ligand intact after 8 days (model)
Wild Type	0.44 ± 0.08	0.45 ± 0.04	0.04 ± 0.00	0.20 ± 0.03
D110H	0.66 ± 0.02	0.63 ± 0.03	0.78 ± 0.01	0.59 ± 0.03
D113H	0.62 ± 0.02	0.70 ± 0.04	0.76 ± 0.02	0.67 ± 0.06

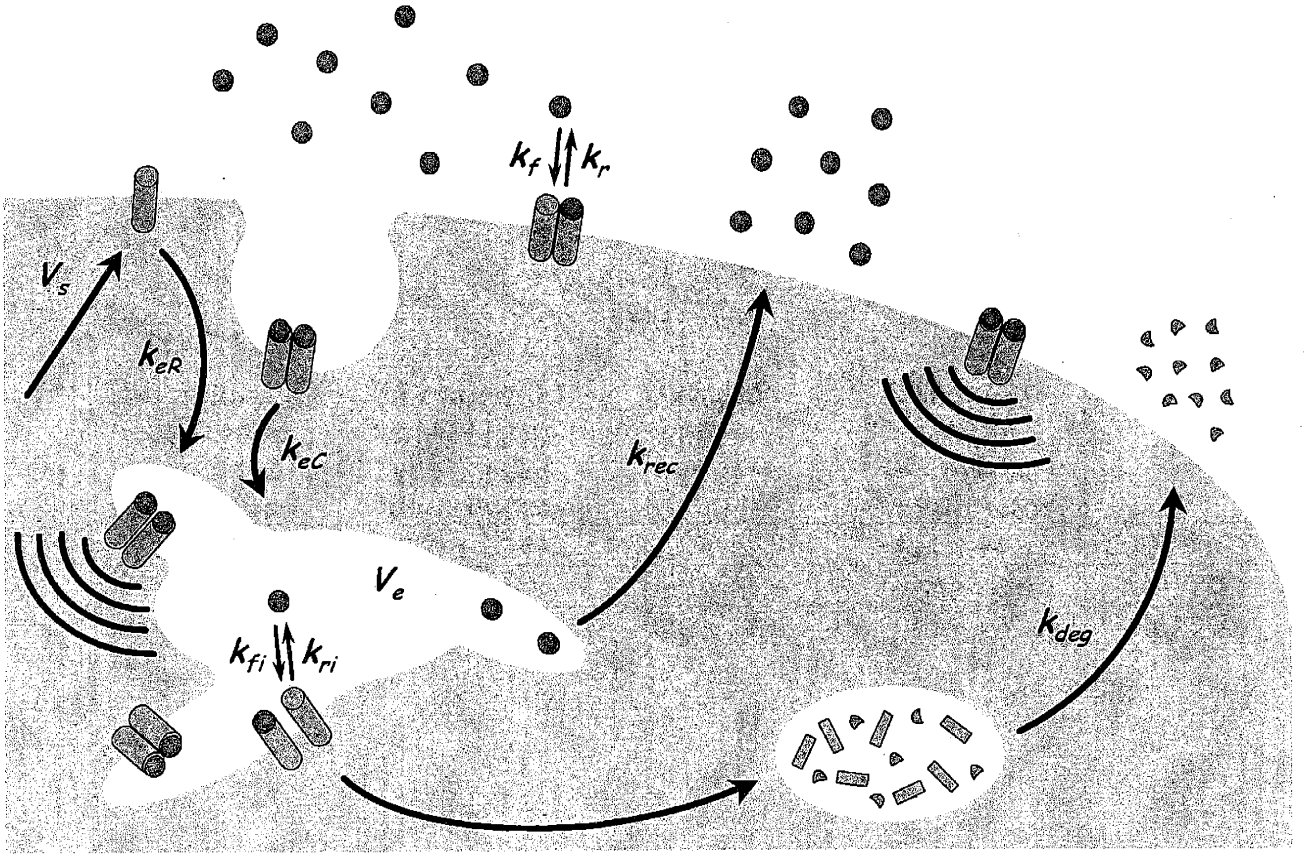

Figure 6.1: Cell-level trafficking model for the GCSF/GCSFR system. Model parameters are defined in Table 6.2, and the corresponding equations are given in Table 6.3.

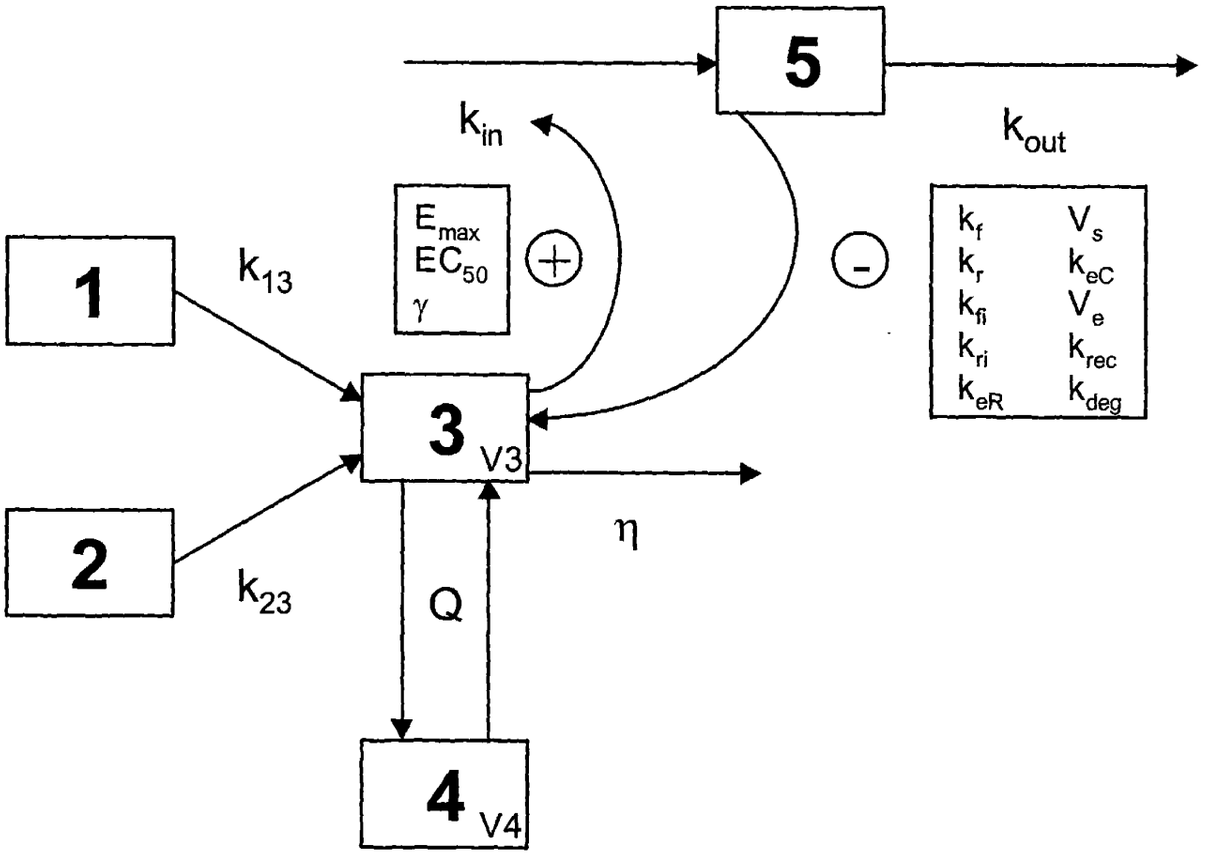

Figure 6.2: Modified PK/PD model incorporating cell-level model. 1, 2 = bisegmental absorption sites; 3 = main ligand compartment; 4 = secondary ligand compartment; 5 = absolute neutrophil counts. Neutrophil production is indirectly stimulated by the amount of ligand in compartment 3; depletion of ligand in compartment 3 is accelerated by neutrophils through receptor-mediated uptake and degradation (as implemented by the cell-level model, Figure 6.1). The corresponding equations are given in Table 6.3.

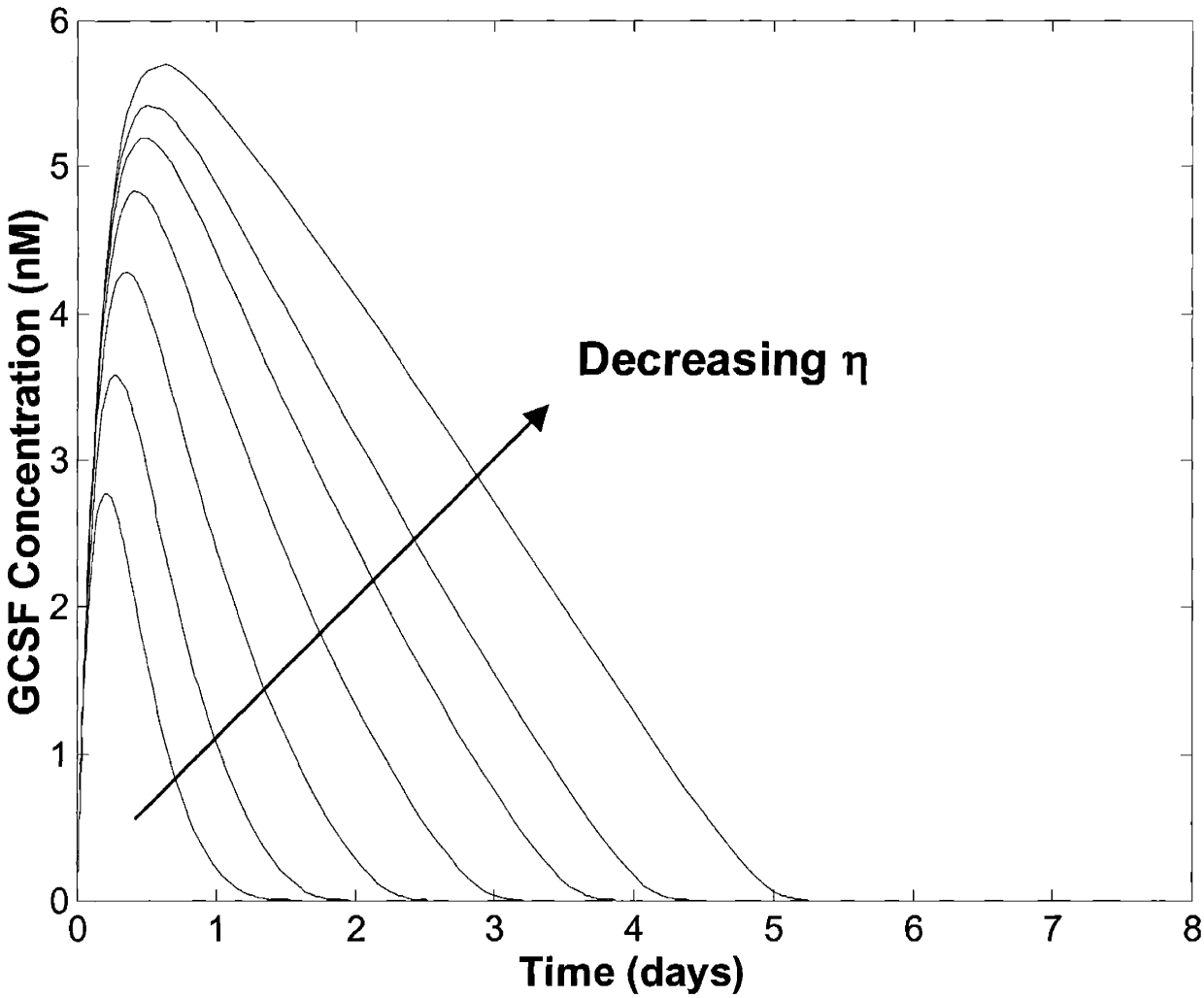

Figure 6.3A: Sensitivity of GCSF concentration to non-specific clearance, η, after initial subcutaneous injection of 375 μg dose; $\eta = 0.0049\times(1, 1/2, 1/4, 1/8, 1/16, 1/32, 0)$ L/min.

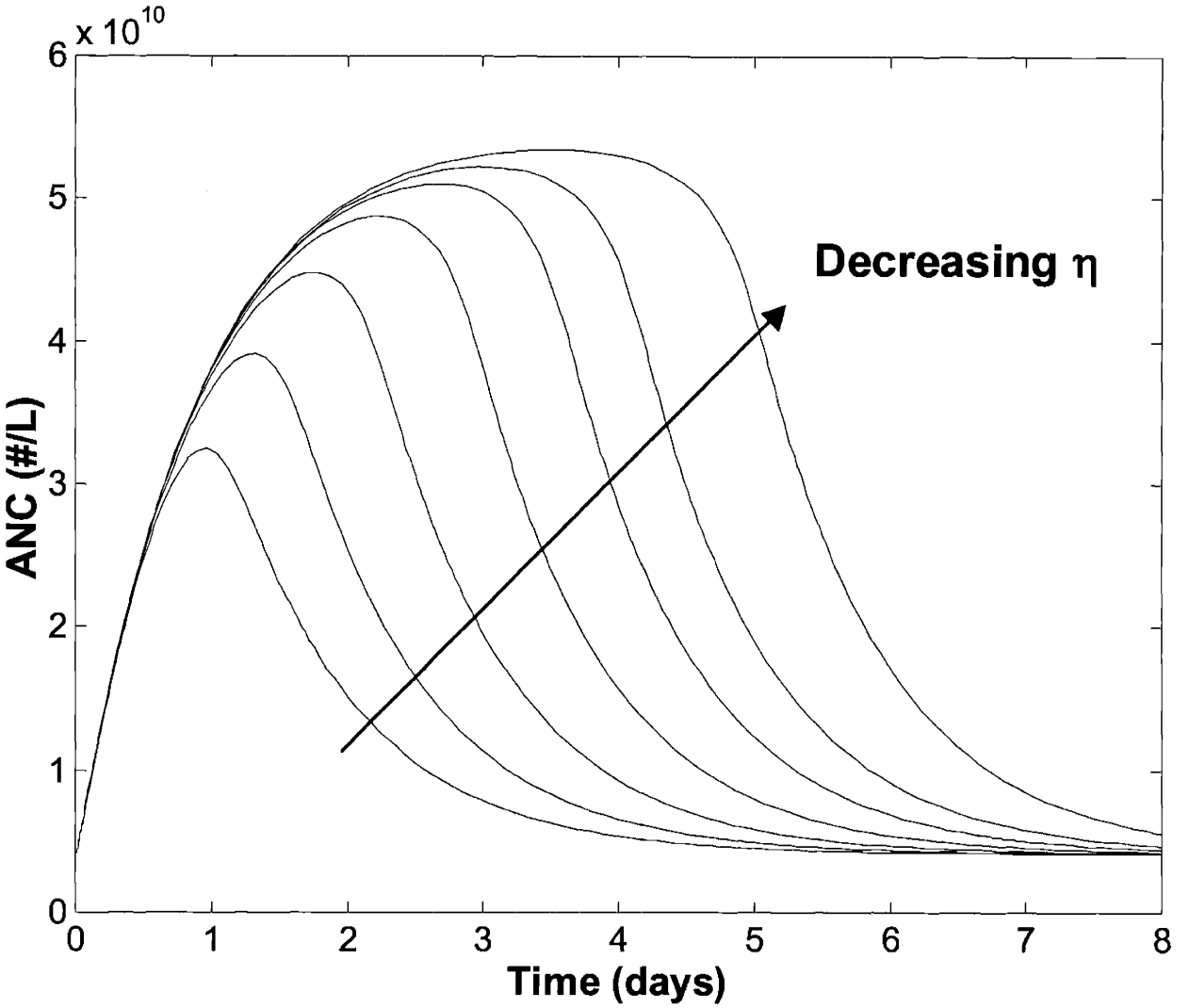

Figure 6.3B: Sensitivity of absolute neutrophil counts (ANC) to non-specific clearance, η, after initial subcutaneous injection of 375 μg dose; $\eta = 0.0049\times(1, 1/2, 1/4, 1/8, 1/16, 1/32, 0)$ L/min.

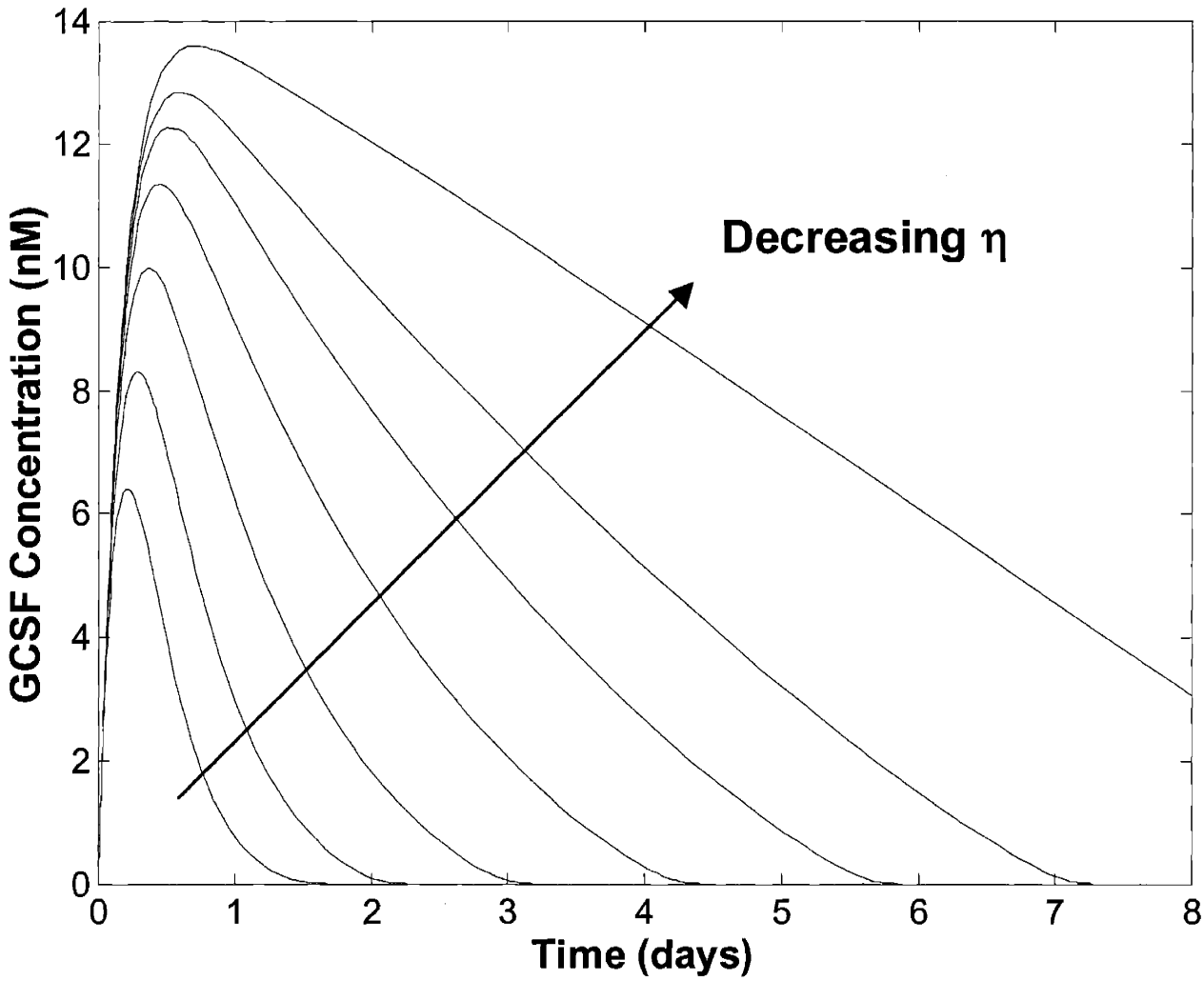

Figure 6.3C: Sensitivity of GCSF concentration to non-specific clearance, η, after initial subcutaneous injection of 750 μg dose; $\eta = 0.0049\times(1, 1/2, 1/4, 1/8, 1/16, 1/32, 0)$ L/min.

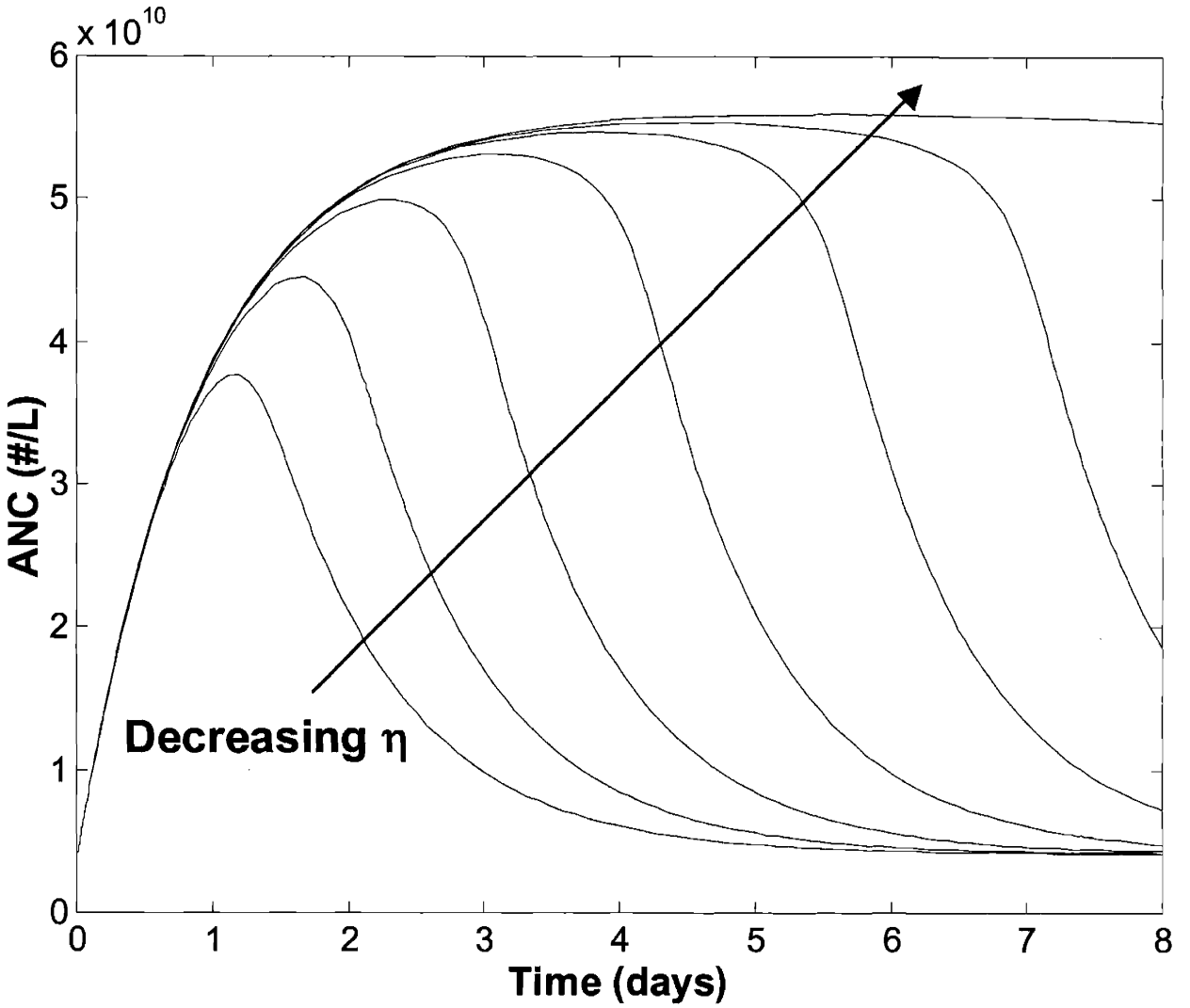

Figure 6.3D: Sensitivity of absolute neutrophil counts (ANC) to non-specific clearance, η, after initial subcutaneous injection of 750 μg dose; $\eta = 0.0049\times(1, 1/2, 1/4, 1/8, 1/16, 1/32, 0)$ L/min.

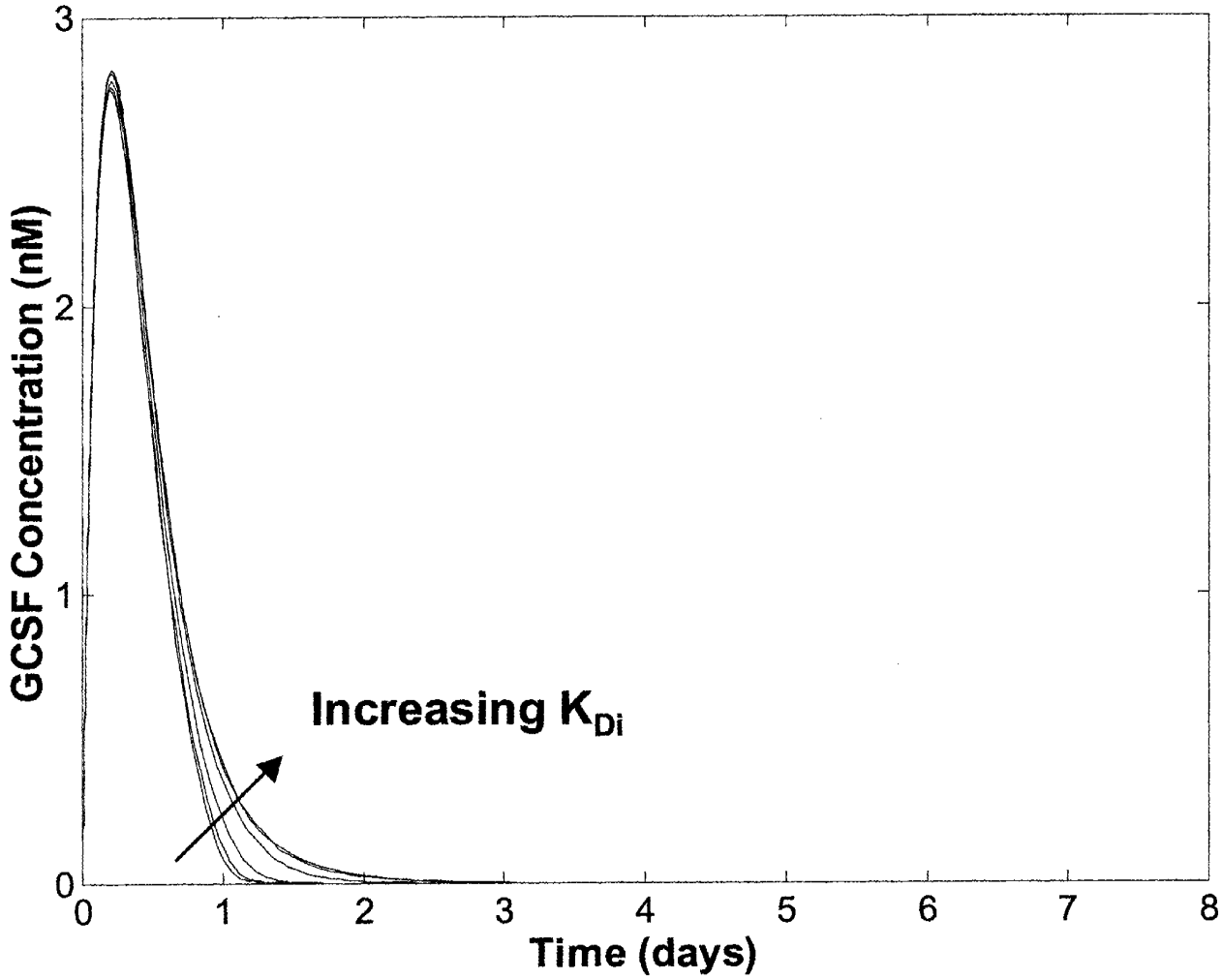

Figure 6.4A: Sensitivity of GCSF concentration to endosomal binding affinity, K_{Di}, after initial subcutaneous injection of 375 μg dose; $K_{Di} = 85K_D \times (0.01, 0.1, 1, 10, 100, \infty)$ pM.

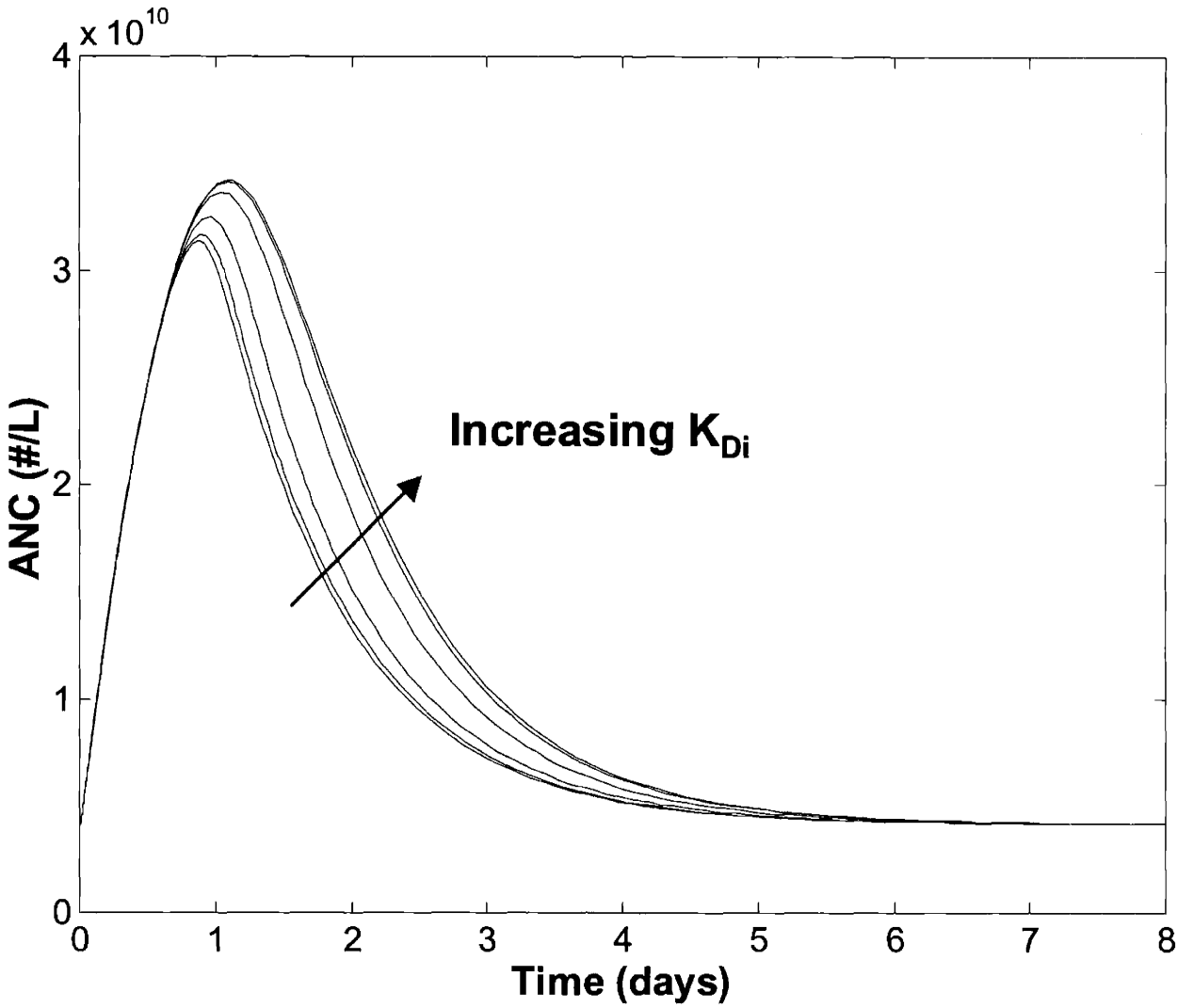

Figure 6.4B: Sensitivity of absolute neutrophil counts (ANC) to endosomal binding affinity, K_{Di}, after initial subcutaneous injection of 375 μg dose; $K_{Di} = 85K_D \times (0.01, 0.1, 1, 10, 100, \infty)$ pM.

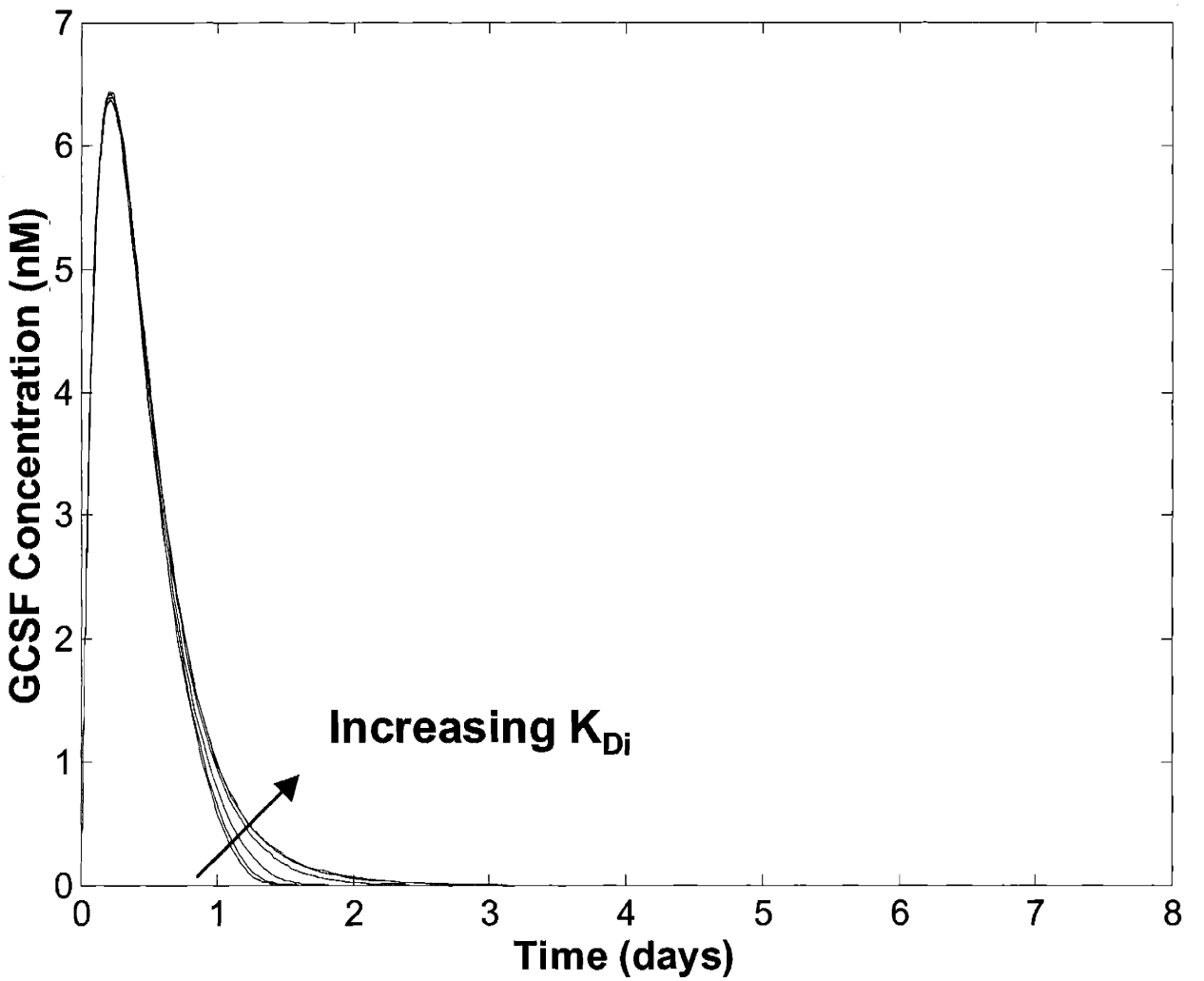

Figure 6.4C: Sensitivity of GCSF concentration to endosomal binding affinity, K_{Di}, after initial subcutaneous injection of 750 μg dose; $K_{Di} = 85K_D \times (0.01, 0.1, 1, 10, 100, \infty)$ pM.

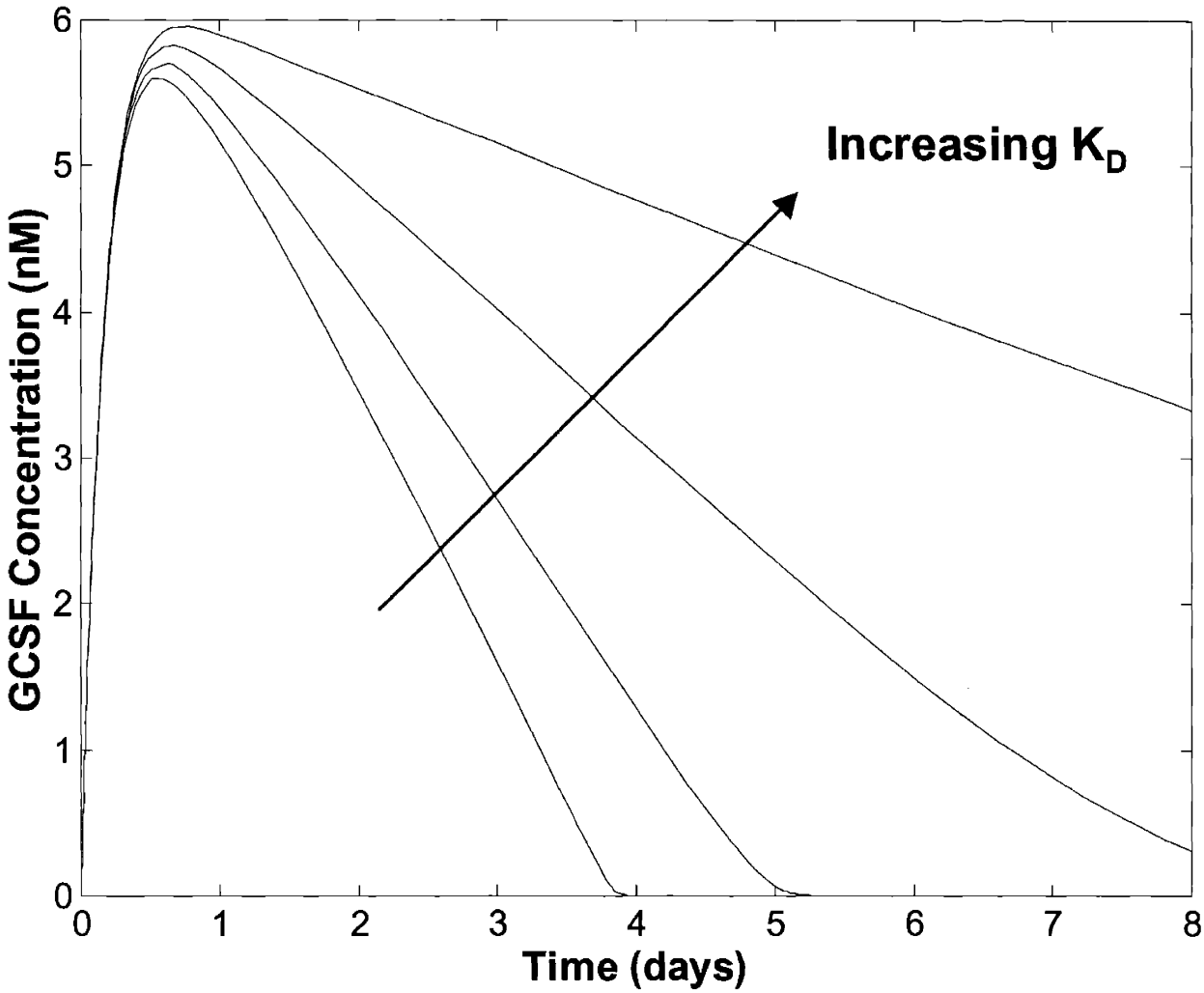

Figure 6.5A: Sensitivity of GCSF concentration to extracellular receptor binding affinity, K_D, in the absence of non-specific clearance ($\eta = 0$) after initial subcutaneous injection of 375 μg dose; K_D = 50, 150, 450, 1350 pM.

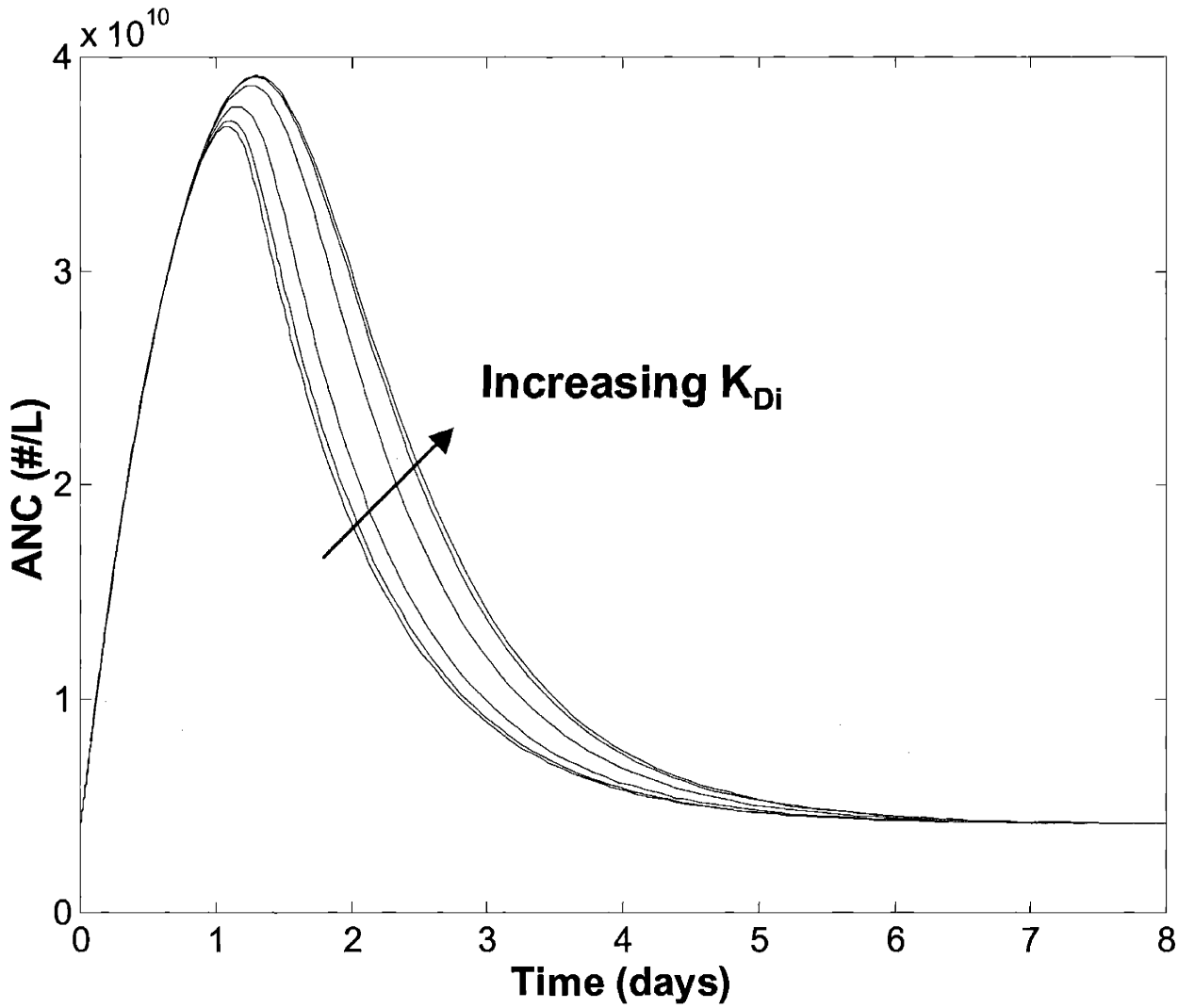

Figure 6.4D: Sensitivity of absolute neutrophil counts (ANC) to endosomal binding affinity, K_{Di}, after initial subcutaneous injection of 750 μg dose; $K_{Di} = 85K_D \times (0.01, 0.1, 1, 10, 100, \infty)$ pM.

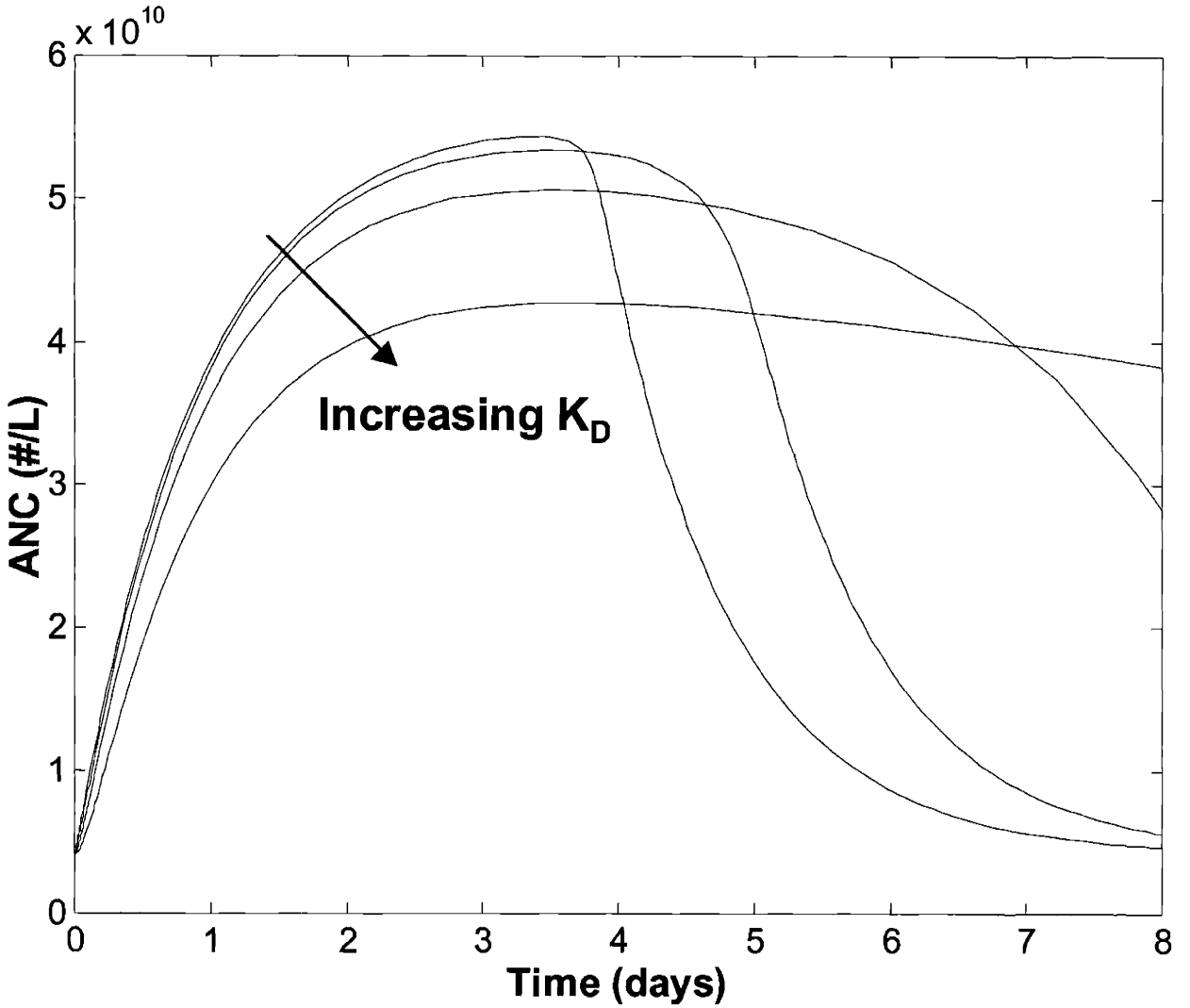

Figure 6.5B: Sensitivity of absolute neutrophil counts (ANC) to extracellular receptor binding affinity, K_D, in the absence of non-specific clearance (η = 0) after initial subcutaneous injection of 375 μg dose; K_D = 50, 150, 450, 1350 pM.

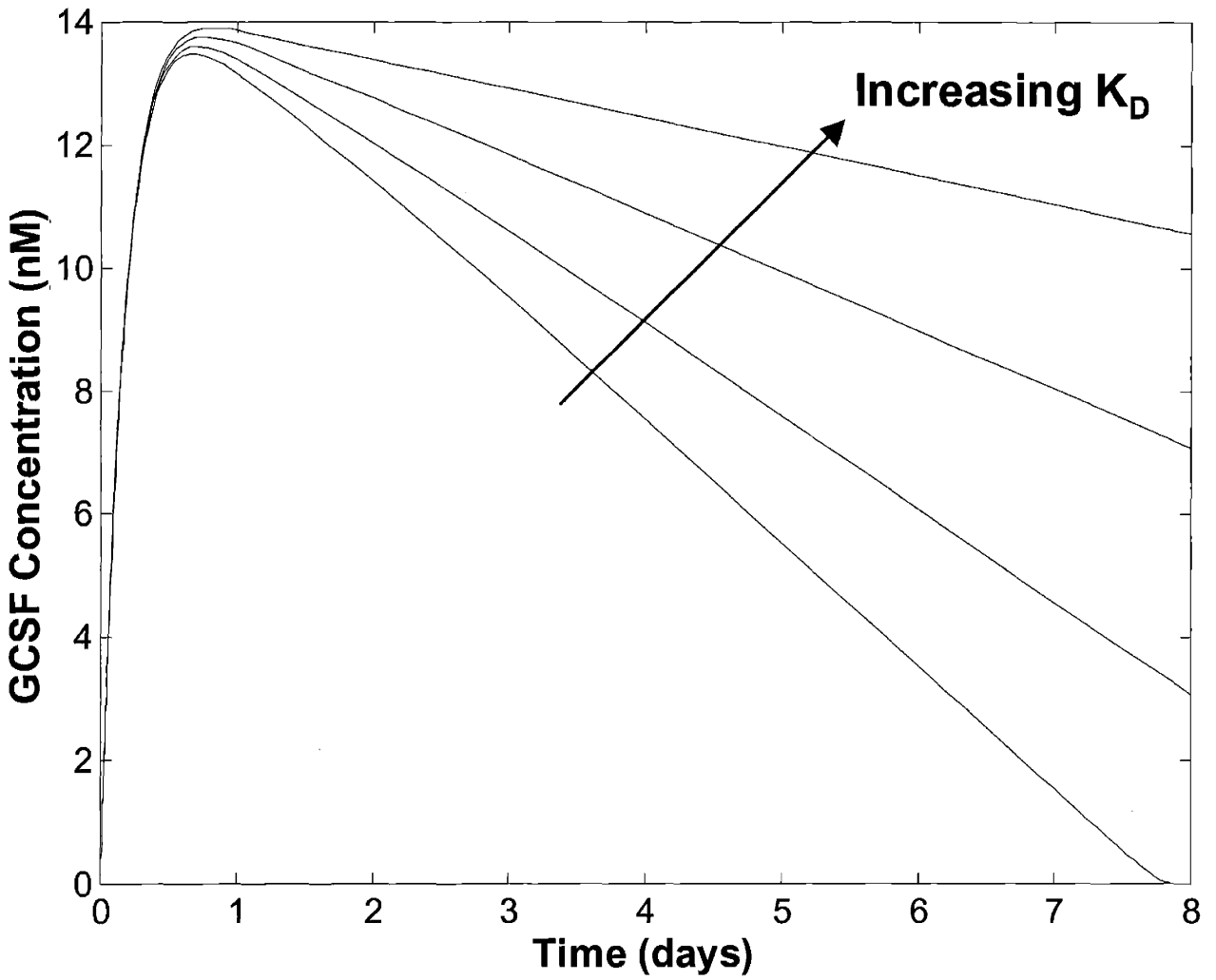

Figure 6.5C: Sensitivity of GCSF concentration to extracellular receptor binding affinity, K_D, in the absence of non-specific clearance ($\eta = 0$) after initial subcutaneous injection of 750 μg dose; K_D = 50, 150, 450, 1350 pM.

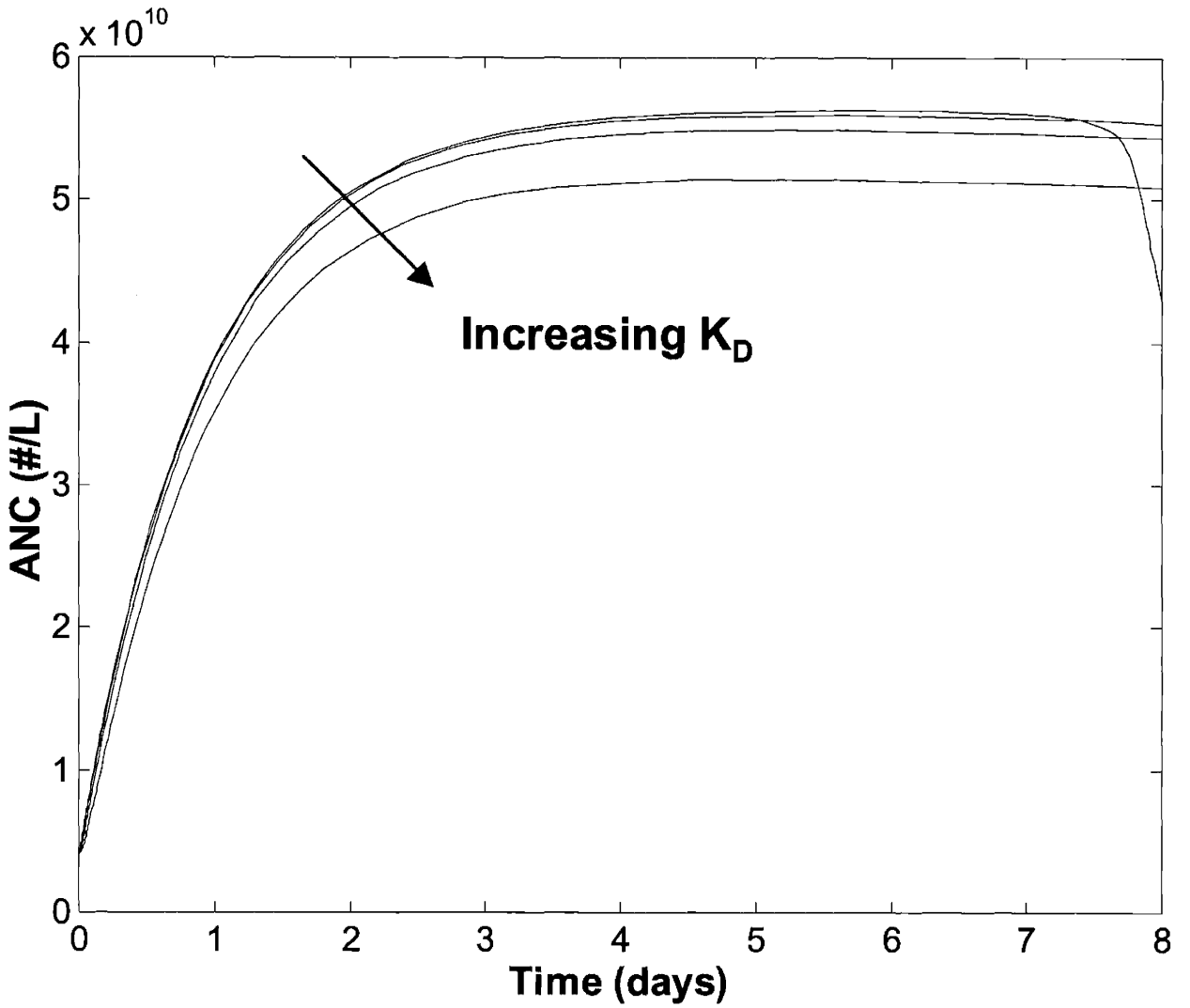

Figure 6.5D: Sensitivity of absolute neutrophil counts (ANC) to extracellular receptor binding affinity, K_D, in the absence of non-specific clearance (η = 0) after initial subcutaneous injection of 750 μg dose; K_D = 50, 150, 450, 1350 pM.

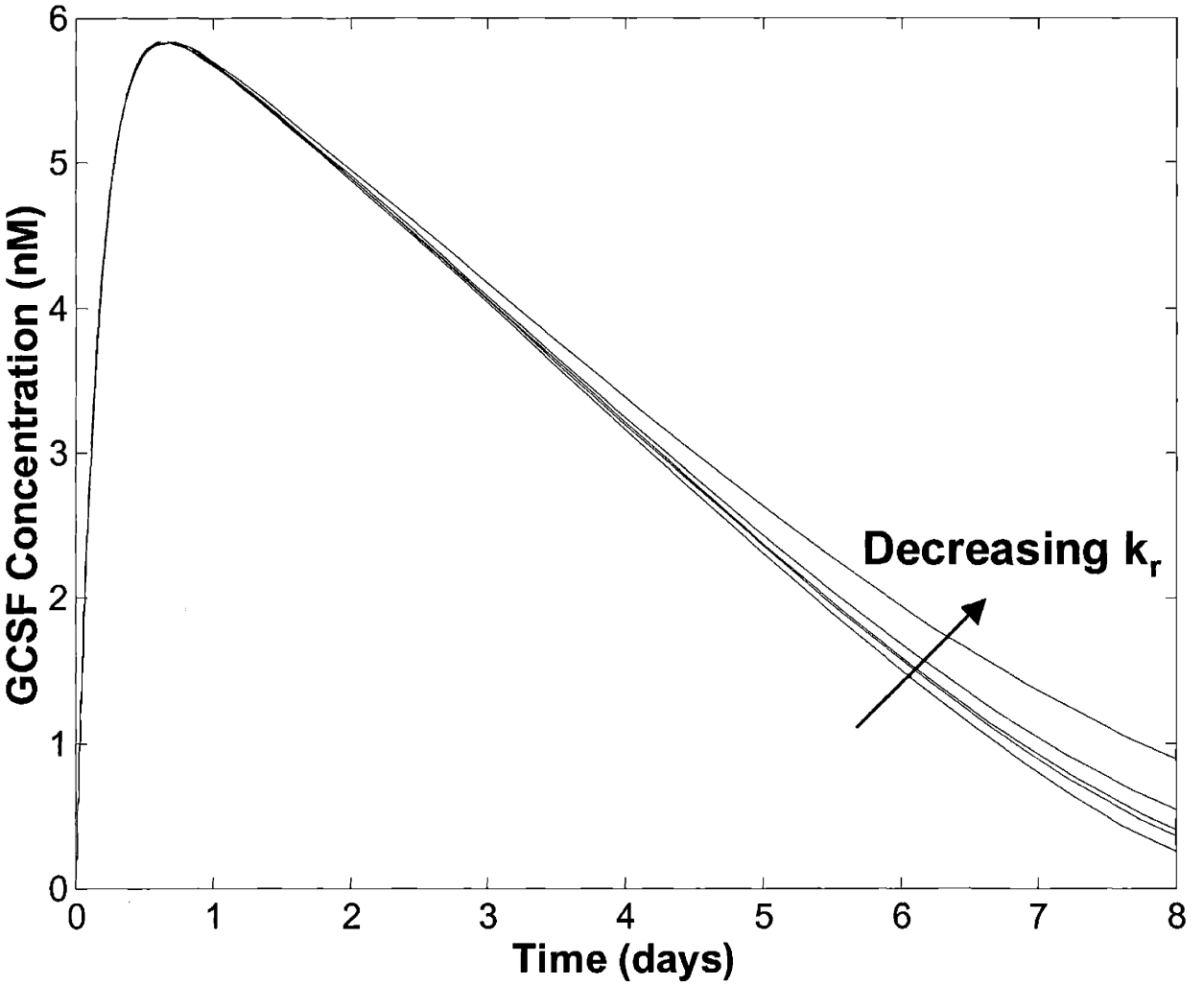

Figure 6.6A: Sensitivity of GCSF concentration to extracellular binding kinetics, k_r and k_f, in the absence of non-specific clearance ($\eta = 0$) after initial subcutaneous injection of 375 μg dose; $k_r = 0.03\times(1/10, 1/3, 1, 3, 10)$ min^{-1}. The K_D is held constant by varying both k_r and k_f by the same percentage.

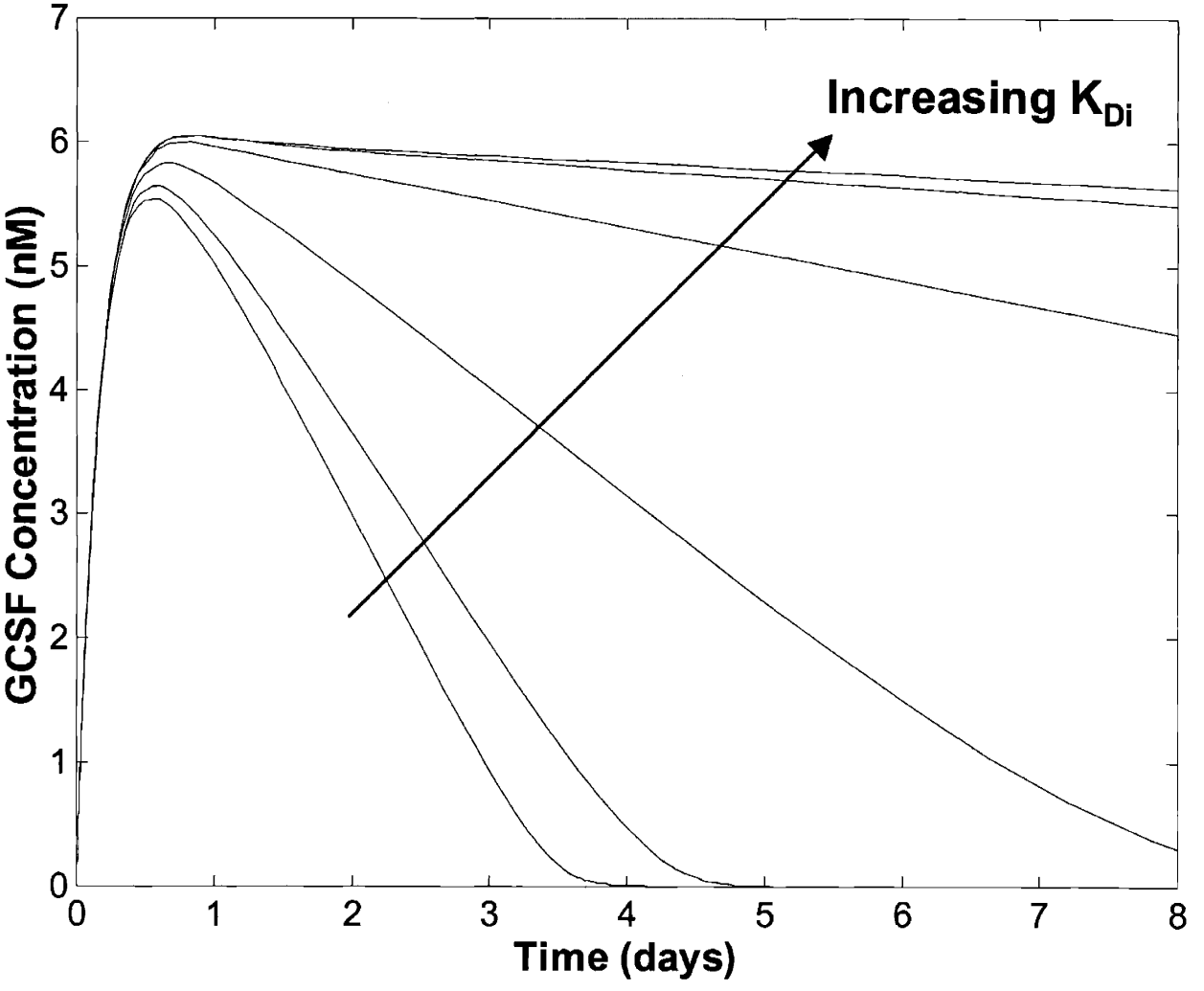

Figure 6.7A: Sensitivity of GCSF concentration to endosomal binding affinity, K_{Di}, in the absence of non-specific clearance ($\eta = 0$) after initial subcutaneous injection of 375 μg dose; $K_{Di} = 85K_{D,SD/01} \times (0.01, 0.1, 1, 10, 100, \infty)$ pM.

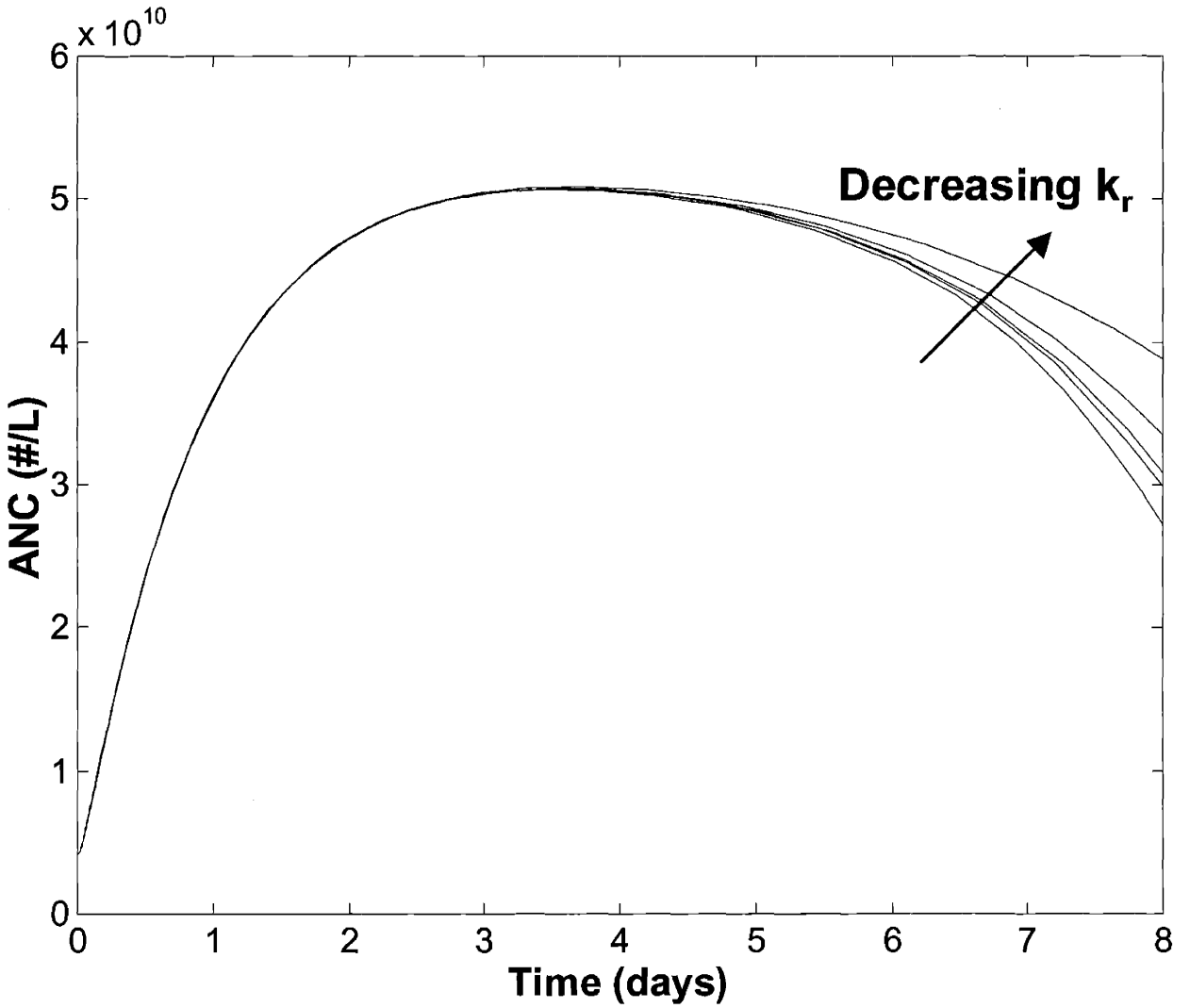

Figure 6.6B: Sensitivity of absolute neutrophil counts (ANC) to extracellular binding kinetics, k_r and k_f, in the absence of non-specific clearance ($\eta = 0$) after initial subcutaneous injection of 375 μg dose; $k_r = 0.03\times(1/10, 1/3, 1, 3, 10)$ min^{-1}. The K_D is held constant by varying both k_r and k_f by the same percentage.

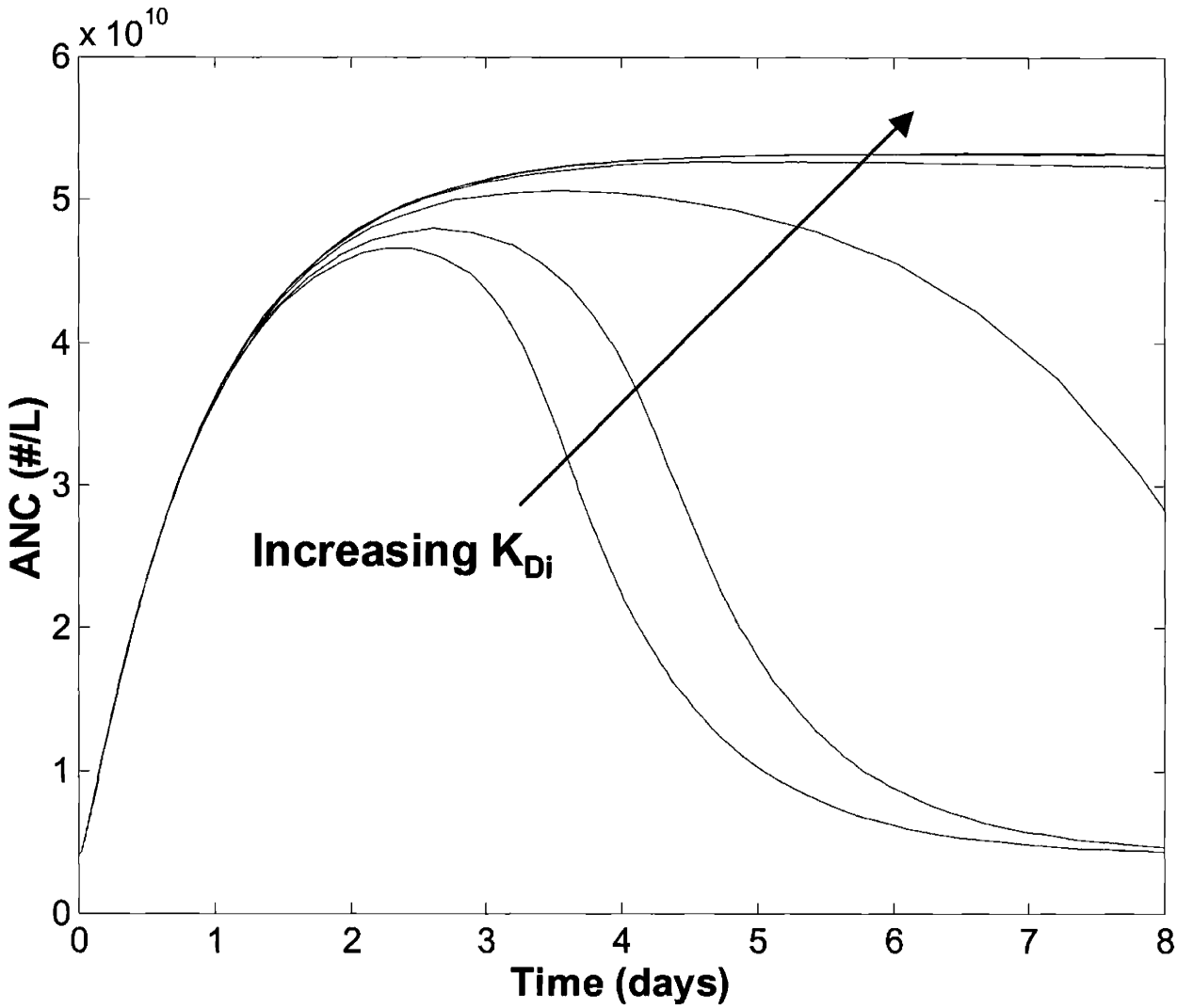

Figure 6.7B: Sensitivity of absolute neutrophil counts (ANC) to endosomal binding affinity, K_{Di}, in the absence of non-specific clearance ($\eta = 0$) after initial subcutaneous injection of 375 μg dose; $K_{Di} = 85K_{D,SD/01} \times (0.01, 0.1, 1, 10, 100, \infty)$ pM.

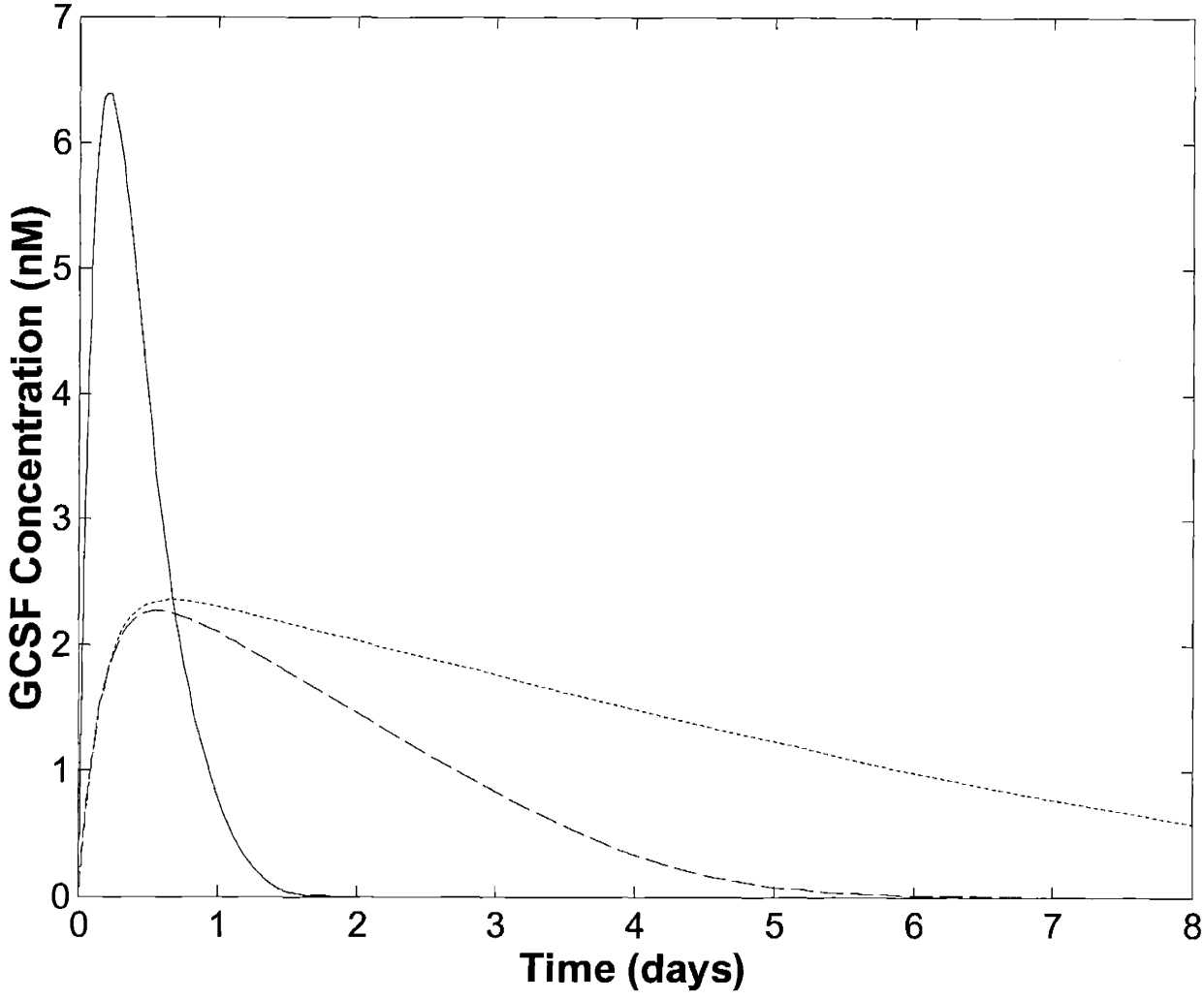

Figure 6.8A: Concentration profiles for wild type (750 μg, n_{10} = 9.5×10^{-9} mol and n_{20} = 19.3×10^{-9} mol, solid), SD/01 (hypothetical dose, n_{10} = 2.5×10^{-9} mol and n_{20} = 2.5×10^{-9} mol, dashed), and an SD/01-like molecule with 5-fold lower endosomal binding affinity (K_{Di} = 5×85$K_{D,SD/01}$; hypothetical dose, n_{10} = 2.5×10^{-9} mol and n_{20} = 2.5×10^{-9} mol, dotted). The hypothetical dose for each of the latter two molecules is about 17% of that for wild type in these simulations.

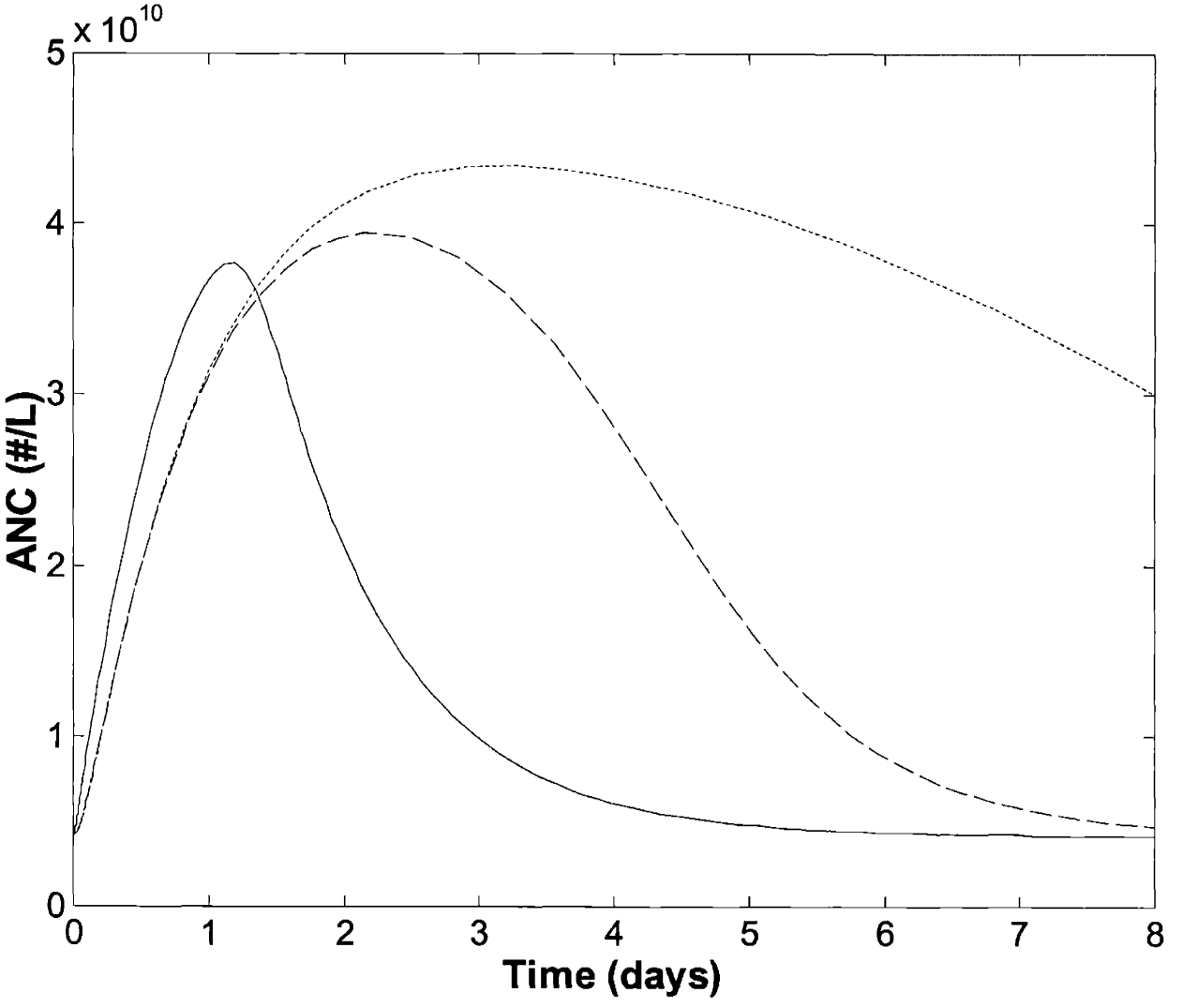

Figure 6.8B: Absolute neutrophil counts (ANC) for wild type (750 μg, $n_{10} = 9.5\times10^{-9}$ mol and $n_{20} = 19.3\times10^{-9}$ mol, solid), SD/01 (hypothetical dose, $n_{10} = 2.5\times10^{-9}$ mol and $n_{20} = 2.5\times10^{-9}$ mol, dashed), and an SD/01-like molecule with 5-fold lower endosomal binding affinity ($K_{Di} = 5\times85K_{D,SD/01}$; hypothetical dose, $n_{10} = 2.5\times10^{-9}$ mol and $n_{20} = 2.5\times10^{-9}$ mol, dotted). The hypothetical dose for each of the latter two molecules is about 17% of that for wild type in these simulations.

Chapter 7: Conclusions and Future Directions

The research described in this thesis provides insights into cytokine engineering from several perspectives using the GCSF/GCSFR system: ligand screening beyond binding affinity for hypothesis generation (Chapter 2), mutagenesis for control of structural stability and possibly endocytic trafficking (Chapter 3), molecular modeling for rational incorporation of desired molecular properties (Chapter 4), cellular trafficking studies to correlate molecular interactions to cellular processes (Chapter 5), and mathematical modeling to correlate molecular and cellular parameters to pharmacokinetic and pharmacodynamic properties (Chapter 6).

The results of these various studies provide some guiding principles for cytokine design in the context of ligand/receptor dynamics. Often, these principles can be non-intuitive and only become clear through systems analysis or computational modeling. Additionally, it is important to understand how the various time and length scales are integrated: from molecular interactions to cellular processes to systemic responses *in vivo*.

In the case of GCSF, we have successfully engineered two single-histidine mutants (D110H and D113H) that have significantly enhanced cell-level pharmacokinetics and pharmacodynamics in an *in vitro* culture, resulting from reduced endosomal binding affinity and enhanced ligand recycling. Through mathematical modeling, we can closely reproduce the *in vivo* behavior of a polyethylene glycol (PEG) conjugate of GCSF (SD/01). SD/01 is believed to have a longer half-life and greater efficacy than native GCSF *in vivo*, because the PEG conjugation essentially eliminates renal clearance. The model further predicts that the 3-fold reduction in receptor-binding affinity caused by the addition of the PEG moiety is actually desirable because it reduces receptor-mediated clearance by bloodstream neutrophils.

In designing even more potent analogs of GCSF, there are several avenues that may be explored. For *in vitro* cultures, it may be possible to improve ligand recycling to a greater extent by combining the histidine mutations (*e.g.*, D110H/D113H). An alternative to the rational 'histidine switching' framework is a 'histidine scanning' strategy, where histidine would simply substituted at each position (or multiple positions) at the binding interface, and each analog could then be tested for pH-sensitive binding properties. It is possible that non-

histidine mutations could also meet the molecular design criteria; these might be generated from combinatorial libraries of GCSF mutants through appropriate screening procedures. For enhanced *in vivo* efficacy, it would be desirable to have a molecule that is not susceptible to renal clearance and also has enhanced ligand recycling. Our modified pharmacokinetic/pharmacodynamic model suggests that such a molecule would be even more potent than SD/01. The synthesis of such a molecule may be as straightforward as conjugating the same PEG moiety used in SD/01 to one of the histidine mutants of GCSF (*e.g.*, PEG-D110H or PEG-D113H).

The techniques and principles outlined in this thesis may be applicable to other cytokine/receptor systems, given the similarities that exist within the cytokine superfamily. More generally, it is the quantitative analysis of dynamic systems that led to many of the results presented here, and such an approach may often be beneficial, even necessary, in engineering the properties of proteins such as therapeutic cytokines.

Curriculum Vitae

Casim A. Sarkar

Education

Massachusetts Institute of Technology (MIT) Cambridge, MA
PhD in Chemical Engineering, Summer 2002
Thesis title: Cytokine engineering through ligand/receptor dynamics: a study on granulocyte colony-stimulating factor
Thesis advisor: Prof. Douglas A. Lauffenburger (Chemical Engineering/Bioengineering, MIT)
In collaboration with Prof. Bruce Tidor (Electrical Engineering/Bioengineering, MIT) and Dr. David N. Brems (Pharmaceutics, Amgen)
GPA: 4.9/5.0
Minor in Computational Biology

The University of Texas Austin, TX
BS in Chemical Engineering, May 1997
Research title: Characterization of affinity and selectivity resulting from mutations in the 26-10 scFv antibody binding pocket
Research advisor: Prof. George Georgiou
GPA: 4.0/4.0

Selected Distinctions

Fannie and John Hertz Graduate Fellowship *(1997 – 2002)*
Was also offered Howard Hughes, National Science Foundation, and Whitaker Foundation Graduate Fellowships *(1997)*
MIT $50K Entrepreneurship Competition Semifinalist *(1999)*
NSPE – Ashland Oil Scholarship; only one was awarded nationwide *(1993 – 1997)*

Research Experience

University of Zürich Zürich, Switzerland
Post-doctoral research, starting September 2002, ~ 2 years
In the laboratory of Prof. Andreas Plückthun (Biochemistry), I plan to learn techniques for directed evolution approaches to protein engineering.

The University of Texas Austin, TX
Undergraduate research, 1996 – 1997
The cardiac glycoside digoxin is used to treat congestive heart failure, although it can be fatal when present in excess quantities. The anti-digoxin monoclonal antibody 26-10 can be used to monitor these levels, but antibodies with greater affinity for the antigen would be more useful. My project focused on mutations of the heavy chain tyrosine 50 in the single-chain fragment-variable region of 26-10. Using site-directed mutagenesis to generate variants at this position, I found that this tyrosine is important for antigen binding. As predicted, the most tolerated of all tested analogs was a mutation to phenylalanine, given its structural similarity to tyrosine.

Teaching Experience

Massachusetts Institute of Technology Cambridge, MA
Spring 2000
Teaching assistant for BE.420, Biomolecular Kinetics and Cell Dynamics
Instructors: Profs. K.D. Wittrup, D.A. Lauffenburger, and J. Sherley
The initial offering of a core graduate course required for all doctoral students in the Biological Engineering Division. Topics included equilibrium binding relationships, kinetics of protein-protein interactions, system stability dynamics, combinatorial library screening, cell cycle regulation and proliferation, bioreactor design, and pharmacokinetic modeling.

Industrial Experience

Amgen Thousand Oaks, CA
Summer 2000
I performed structural studies (spectrophotometry, circular dichroism, and intrinsic fluorescence) on granulocyte colony-stimulating factor and several mutants of this protein to determine structural stability.

Procter & Gamble Cincinnati, OH
Summer 1996
I performed experimental studies aimed toward a fundamental understanding of nucleation and crystal growth of a fluid product in a scraped-wall heat exchanger.

Patents

Two patents filed, each entitled "G-CSF analog compositions and methods." Nos. PCT/US01/28602 and PCT/US01/28828. *(2001)*

Publications

Sarkar, C.A, K. Lowenhaupt, T. Horan, T.C. Boone, B. Tidor, and D.A. Lauffenburger. "Rational cytokine design for increased lifetime and enhanced potency using pH-activated 'histidine switching.'" *Nature Biotechnology*, in press.

Sarkar, C.A., K. Lowenhaupt, P.J. Wang, T. Horan, and D.A. Lauffenburger. "Pharmacodynamic quadrant plot analysis of mechanisms regulating mitogenic potency of granulocyte colony-stimulating factor analogs." Under review.

Sarkar, C.A. and D.A. Lauffenburger. "Cell-level pharmacokinetic model of granulocyte colony-stimulating factor: implications for ligand lifetime and potency *in vivo*." Submitted for publication.

Sarkar, C.A., B. Tidor, and D.A. Lauffenburger. "Optimizing ligand design for receptor interactions: molecular engineering in the context of cellular processes." Invited review to *Annual Review of Biophysics and Biomolecular Structure*, in preparation.

Ricci, M.S., C.A. Sarkar, E.M. Fallon, E. Bancroft, D.A. Lauffenburger, and D.N. Brems. "pH dependence of structural stability of interleukin-2 and granulocyte colony-stimulating factor." In preparation.

Presentations

"A rational approach to improving cytokine-receptor binding properties in the context of cellular trafficking dynamics." American Chemical Society, National Meeting, Orlando, FL. Invited platform. *(2002)*

"A novel systems engineering approach to rational cytokine design." Pacific Symposium on Biocomputing, Annual Meeting, Kauai, HI. Poster. *(2002)*

"Histidine switching: a new approach to rational cytokine design for enhanced potency." American Institute of Chemical Engineers, Annual Meeting, Reno, NV. Platform. *(2001)*

"Increased structural stability of 4-helix cytokines at low pH." American Institute of Chemical Engineers, Annual Meeting, Reno, NV. Platform. *(2001)*

"Histidine switching: a new approach to rational cytokine design for enhanced potency." Biomedical Engineering Society, Annual Meeting, Durham, NC. Platform. *(2001)*

"Implication of trafficking mechanisms in enhanced potency of granulocyte colony-stimulating factor." American Institute of Chemical Engineers, Annual Meeting, Los Angeles, CA. Platform. *(2000)*

"Enhanced potency of covalently modified granulocyte colony-stimulating factor." Biomedical Engineering Society, Annual Meeting, Seattle, WA. Poster. *(2000)*

"Structural basis for altered trafficking of granulocyte colony-stimulating factor mutants." Amgen, Pharmaceutics Department, Thousand Oaks, CA. Invited seminar. *(2000)*

"Differential ligand depletion and cell proliferation responses with granulocyte colony-stimulating factor conjugated with polyethylene glycol." American Society for Cell Biology, Annual Meeting, Washington D.C. Poster. *(1999)*

Skills

Mammalian cell culture
Ligand/receptor binding and trafficking assays
Molecular modeling of proteins (CHARMM, DelPhi, GRASP, Insight II, and Quanta)
Spectrophotometry, circular dichroism, and intrinsic fluorescence measurements of proteins
Fluorescence-activated cell sorting
Polymerase chain reaction techniques
Protein radiolabeling
Experience with ASPEN, Maple, Mathematica, and MATLAB
Working knowledge of HTML and UNIX

Activities

Violin
Basketball, football, ice hockey, softball, tennis, and volleyball
Sailing